AD-A154 652 VLF (VERY LOW FREQUENCY) WORKSHOP: HELD AT SAN DIEGO CALIFORNIA ON 24-25..(U) SCRIPPS INSTITUTION OF OCEANOGRAPHY LA JOLLA CA MARINE PHYSIC.. W S HODGKISS 1/3

UNCLASSIFIED 1985 MPL-U-11/85 N00014-80-C-0220 F/G 5/1 NL

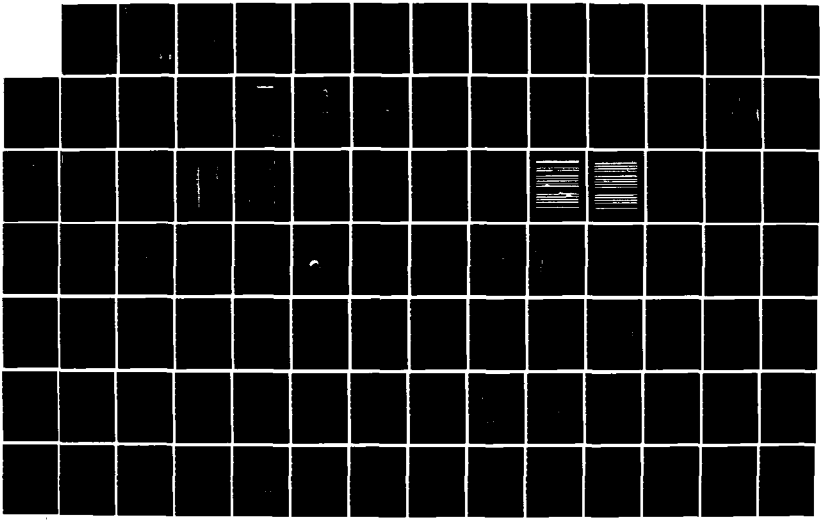

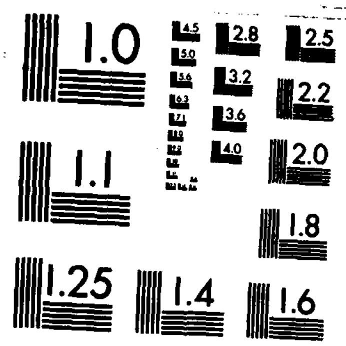

MICROCOPY RESOLUTION TEST CHART
NATIONAL BUREAU OF STANDARDS-1963-A

(2)

AD-A154 652

MPL TECHNICAL MEMORANDUM 376

VLF Workshop: 24-25 January 1985

W.S. Hodgkiss

Office of Naval Research
N00014-80-C-0220
N00014-79-C-0472

Document cleared for public release;
distribution unlimited.

15 April 1985

MPL-U-11/85

DTIC FILE COPY

DTIC
ELECTE
JUN 6 1985
S D
E

MARINE PHYSICAL LABORATORY
of the Scripps Institution of Oceanography
San Diego, California 92152

85 05 10 001

SECURITY CLASSIFICATION OF THIS PAGE (When Data Entered)

REPORT DOCUMENTATION PAGE

READ INSTRUCTIONS BEFORE COMPLETING FORM

1. REPORT NUMBER: MPL-U-11/85	2. GOVT ACCESSION NO.
3. RECIPIENT'S CATALOG NUMBER	
4. TITLE (and Subtitle): VLF WORKSHOP: 24-25 January 1985	5. TYPE OF REPORT & PERIOD COVERED: Technical Memorandum
	6. PERFORMING ORG. REPORT NUMBER: MPL TM-376
7. AUTHOR(s): W. S. Hodgkiss	8. CONTRACT OR GRANT NUMBER(s): N00014-80-C-0220 N00014-79-C-0472
9. PERFORMING ORGANIZATION NAME AND ADDRESS: University of California, San Diego, Marine Physical Laboratory of the Scripps Institution of Oceanography, San Diego, CA 92152	10. PROGRAM ELEMENT, PROJECT, TASK AREA & WORK UNIT NUMBERS
11. CONTROLLING OFFICE NAME AND ADDRESS: Office of Naval Research, Department of the Navy, 800 North Quincy Street, Arlington, Virginia 22209	12. REPORT DATE: 1985
	13. NUMBER OF PAGES
14. MONITORING AGENCY NAME & ADDRESS(if different from Controlling Office)	15. SECURITY CLASS. (of this report): Unclassified
	15a. DECLASSIFICATION/DOWNGRADING SCHEDULE

16. DISTRIBUTION STATEMENT (of this Report)

Document cleared for public release; distribution unlimited.

17. DISTRIBUTION STATEMENT (of the abstract entered in Block 20, if different from Report)

Accession For	
NTIS GRA&I	☒
DTIC TAB	☐
Unannounced	☐
Justification	
By	
Distribution/	
Availability Codes	
Dist	Avail and/or Special
A/1	

18. SUPPLEMENTARY NOTES

19. KEY WORDS (Continue on reverse side if necessary and identify by block number)

very low frequency, workshop

20. ABSTRACT (Continue on reverse side if necessary and identify by block number)

The focus of this classified workshop was on the frequency region 1-30 Hz. The program included presentations by the participants followed by a discussion covering areas of potential Navy interest and future research objectives. A summary of the presentations and discussion is contained in this report.

DD FORM 1 JAN 73 1473 EDITION OF 1 NOV 65 IS OBSOLETE

S/N 0102-LF-014-6601

SECURITY CLASSIFICATION OF THIS PAGE (When Data Entered)

VLF Workshop: 24-25 January 1985

Marine Physical Laboratory
Scripps Institution of Oceanography
San Diego, CA

I. Introduction

The focus of this classified workshop was on the frequency region 1-30 Hz. The program included presentations by the participants followed by a discussion covering areas of potential Navy interest and future research objectives. A summary of the presentations and discussion is contained in this report.

II. Participants

The following is a roster of those people who participated in the VLF Workshop. Full addresses and telephone numbers are provided in Appendix A.

ONR

Dr. Mike McKisic
Dr. Gerry Morris

NAVELEX

LT Bradley Ogg
Mr. Tom Higby

NRL

Dr. Ralph Baer
Mr. John Perkins

NORDA

Dr. Wm. Carey
Dr. Thomas Tunnell
Dr. Ron Wagstaff
Mr. Don Del Balzo

NOSC

Mr. David Keir
Mr. David Edelblute
Dr. Randy Moore
Mr. Mike Morrison
Dr. Homer Bucker
Dr. Ed Hamilton

NADC

Mr. James McEachern

Naval Postgraduate School

Dr. Rudolph Nichols

APL/JH

Dr. Julius Bowen
Mr. Joe Lombardo
Mr. Ross Rottier

ARL/UT

Dr. Robert Koch

MIT/WHOI

Dr. Arthur Baggeroer
Mr. John Ewing

SIO

Dr. LeRoy Dorman
Dr. John Orcutt
Dr. Peter Worcester

MPL/SIO

Dr. Wm. Hodgkiss
Dr. Victor Anderson
Dr. Fred Fisher
Mr. Lee Culver
Mr. Chris Nickles
Mr. Greg Edmonds

PSI

Dr. Marshall Bradley

BBN

Mr. Mike Sullivan
Mr. Dale Green
Mr. Alan Ma

Polar Research, Inc.

Dr. James Wilson

III. Presentations

The presentations covered the following broad areas: (1) ambient noise, (2) propagation, and (3) system implications. Summaries of the presentations (i.e. abstract and copies of the vu-graphs) are contained either in Appendix B of this report or in a companion classified MPL technical report. The presentations were given in the following order.

Ambient Noise

1. W.S. Hodgkiss and V.C. Anderson, "Infrasonic Acoustic Ambient Noise"
2. Art Baggeroer (for Ira Dyer), "Arctic Ambient Noise"
3. Marshall Bradley, "VLF Ambient Noise"
4. Jim Wilson, "Active Ice Ridge Ambient Noise Levels"
5. John Orcutt, "Noise Characteristics and Wave Propagation at Low Frequencies"

Propagation

1. John Orcutt, "Noise Characteristics and Wave Propagation at Low Frequencies" (continued)
2. LeRoy Dorman, "The Seafloor Sound Channel and Stoneley Waves as Observed Using Seafloor Explosions and Ocean Bottom Seismographs"
3. Jim Wilson, "Buck/Wilson Deep Water Arctic Transmission Loss Model"
4. Art Baggeroer, "Energy Partitioning for Long Range, Low Frequency Propagation in the Arctic Ocean"
5. John Ewing, "VLF Propagation in the Oceanic Crust and Upper Mantle"
6. Art Baggeroer, "On the Relative Amplitudes between Primary and Multiple Signals from Seismic Refractions in Oceanic Crust"
7. Ralph Baer, "A Three-Dimensional Model for Bathymetric Scattering with VLF Applications"
8. Tom Tunnell, "Modeling Support for Cape Fear VLF Exercise"

System Implications

1. Jim McEachern, "NADC Infrasonic Sonobuoy Program - A Brief Summary" *
2. Victor C. Anderson, "Comments on Nearfield VLF Surveillance"
3. Julius Bowen, "Effect of Submarine Speed on Comparative Detectability of Blade and Machinery Tones" *
4. Ross Rottier, "Transmission Loss to a Seismometer in Oceanic Basement"
5. Richard Koch, "VLF Propagation Modeling to an Ocean Borehole Receiver"
6. Joe Lombardo, "Applications of Ocean Seismometers to ASW" **
7. Wm. Carey, "VLF Borehole Surveillance Program Requirements" *
8. Mike Morrison, "Arctic Remote Sensing" *
9. Randy Moore, "Soviet Submarine Source Levels" *
10. Mike Sullivan, "Implications of VLF Clutter on Performance Prediction" *

* All or a subset of the vu-graphs are contained in a companion classified MPL technical report.

** Vu-graphs not available.

IV. Summary

The last half day of the workshop was devoted to reviewing and summarizing what had been said during the course of the presentations. In general, the discussion was a blend of the three broad areas covered in the workshop: (1) ambient noise, (2) propagation, and (3) system implications.

A. *Ambient Noise*

Based on available data and current models, the characteristics of ambient noise in the VLF region appear to be dominated by a microseism peak in the region of 0.1 Hz with shipping noise being the dominant contributor above 3-4 Hz. More needs to be understood regarding ambient noise levels generated due to atmospheric pressure fluctuations, surface wave motion, and turbulence. Future ambient noise measurement programs should acquire a substantial amount of environmental data to aid in isolating the various contributing mechanisms (meterological, water column, and bottom properties). Additional array studies are needed to characterize the frequency/wavenumber content of VLF noise in order to better understand where the noise is coming from and what propagation paths are important.

B. *Propagation*

At VLF frequencies, bottom interaction is a significant aspect of the propagation problem. There is a strong need to have available range-dependent propagation models for use in investigating the significant pathways of energy transfer. For example, future models based on modal formalisms must have the capability of properly accounting for the coupling of energy between modes in order to explain existing observations. High quality array studies at these low frequencies are needed to accurately measure amplitudes, phase velocities, and angles of approach of propagating energy. Many complex wave propagation phenomena can be adequately modeled with algorithms which simply take into account all multiples. Nevertheless, strong evidence exists to support an important role for scattering at these low frequencies although the incorporation of a useful theory in the advanced propagation formalisms remains an unsolved problem.

C. *System Implications*

A better understanding of the origin and magnitude of VLF ambient noise coupled with measured/predicted source levels and new propagation models will aid in ascertaining the usefulness of the VLF band for surveillance purposes. The trade-offs between the various types of sensors (geophone/hydrophone) and their placement (water column, bottom mounted, or buried) need to be better understood. Sensor design to reduce flow-induced self-noise and the decoupling of tethered sensors from the contaminating effects of mechanical linkages (strumming) are areas of continuing interest. Over what aperture the coherent processing of data from an array of VLF sensors is viable (coherence length) and whether the array should be vertical or horizontal are important system-related issues.

Appendix A

This appendix contains the full addresses and telephone numbers of the VLF Workshop participants.

Dr. Victor Anderson
Marine Physical Laboratory
Scripps Inst. of Oceanog.
San Diego, CA 92152

(619) 294-5578

Dr. Ralph Baer
Code 5160
Naval Research Laboratory
Washington, DC 20375-5000

(202) 767-3173

Dr. Arthur Baggeroer
Rm. 5-204
Massachusetts Inst. of Technology
Cambridge, MA 02139

(617) 253-4336

Dr. Julius Bowen
Applied Physics Laboratory
The Johns Hopkins University
Johns Hopkins Rd
Laurel, MD 20707

(301) 953-5000 (x4562)

Dr. Marshall Bradley
Planning Systems Inc.
Suite 204
1508 Gause Blvd.
Slidell, LA 70458

(504) 649-0450

Dr. Homer Bucker
Code 541
Naval Ocean Systems Center
San Diego, CA 92152

(619) 225-7618

Dr. Wm. Carey
Code NLO
Office of Naval Research
800 N. Quincy St.
Arlington, VA 22217

(202) 696-4951

Mr. Lee Culver
Marine Physical Laboratory
Scripps Inst. of Oceanog.
San Diego, CA 92152

(619) 294-3651

Mr. Don Del Balzo
Code 200
NSTL Station, MS 39529

(601) 688-5734

Dr. LeRoy Dorman
Geological Research Division (A-015)
Scripps Inst. of Oceanog.
La Jolla, CA 92093

(619) 452-2406

Mr. David Edelblute
Code 71
Naval Ocean Systems Center
San Diego, CA 92152

(619) 225-6511

Mr. Greg Edmonds
Marine Physical Laboratory
Scripps Inst. of Oceanog.
San Diego, CA 92152

(619) 294-3652

Mr. John Ewing
Woods Hole Oceanographic Inst.
Woods Hole, MA 02543

(617) 548-1400 (x2609)

Dr. Fred Fisher
Marine Physical Laboratory
Scripps Inst. of Oceanog.
San Diego, CA 92152

(619) 294-5589

Mr. Dale Green
Bolt, Beranek, and Newman, Inc.
4015 Hancock St., Suite #101
San Diego, CA 92110

(619) 224-3243

Dr. Ed Hamilton
Code 541

Naval Ocean Systems Center
San Diego, CA 92152

(619) 225-6309

Mr. Thomas Higby
Code 612
NAVELEX
2511 Jefferson Davis Hwy
Arlington, VA 22202

(202) 692-4781

Dr. Wm. Hodgkiss
Marine Physical Laboratory
Scripps Inst. of Oceanog.
San Diego, CA 92152

(619) 294-3658

Mr. David L. Keir
Code 71
Naval Ocean Systems Center
San Diego, CA 92152

(619) 225-2261

Dr. Robert Koch
Applied Research Laboratories,
University of Texas at Austin
P.O. Box 8029
Austin, TX 78713-8029

(512) 835-3498

Mr. Joe Lombardo
Applied Physics Laboratory
The Johns Hopkins University
Johns Hopkins Rd
Laurel, MD 20707

(301) 953-5000 (x4283)

Mr. Alan Ma
Bolt, Beranek, and Newman, Inc.
4015 Hancock St., Suite #101
San Diego, CA 92110

(619) 224-3240

Mr. James McEachern
Code 3043
Naval Air Development Center
Warminster, PA 18974

(215) 441-1777

Dr. Mike McKisic
Code 420
Office of Naval Research
800 N. Quincy St.
Arlington, VA 22217

(202) 696-4204

Dr. Randall Moore
Code 7303
Naval Ocean Systems Center
San Diego, CA 92152

(619) 225-6501

Dr. Gerald Morris
Code 425-GG
Office of Naval Research
NSTL Station, MS 39529

(601) 688-4168

Mr. Mike Morrison
Code 541
Naval Ocean Systems Center
San Diego, CA 92152

(619) 225-6309

Dr. Rudolph H. Nichols
Physics Department
Naval Postgraduate School
Monterey, CA 93943

(408) 646-2648

Mr. Chris Nickles
Marine Physical Laboratory
Scripps Inst. of Oceanog.
San Diego, CA 92152

(619) 294-3677

LT Brad Ogg
Code 6124
NAVELEX
2511 Jefferson Davis Hwy
Arlington, VA 22202

(202) 692-4781

Dr. John Orcutt

IGPP (A-025)
Scripps Inst. of Oceanog.
La Jolla, CA 92093

(619) 452-2887

Mr. John Perkins
Code 5160
Naval Research Laboratory
Washington, DC 20375

(202) 767-3173

Mr. Ross Rottier
Applied Physics Laboratory
The Johns Hopkins University
Johns Hopkins Rd
Laurel, MD 20707

(301) 953-5000

Mr. Mike Sullivan
Bolt, Beranek, and Newman, Inc.
4015 Hancock St., Suite #101
San Diego, CA 92110

(619) 224-3243

Dr. Thomas Tunnell
Code 240
NORDA
NSTL Station, MS 39529

(601) 688-5233

Dr. Ron Wagstaff
Code 245
NORDA
NSTL Station, MS 39529

(601) 688-4751

Dr. James H. Wilson
16333 Keeler Dr.
Granada Hills, CA 91344

(818) 709-5615

Dr. Peter Worcester
IGPP (A-025)
Scripps Inst. of Oceanog.
La Jolla, CA 92093

(619) 452-4688

Appendix B

This appendix contains summaries (i.e. abstracts and vu-graphs) of most of the presentations. As indicated earlier, summaries of a few of the presentations are contained in a companion classified MPL technical report.

Infrasonic Acoustic Ambient Noise

W.S. Hodgkiss and V.C. Anderson

Marine Physical Laboratory
Scripps Institution of Oceanography
San Diego, CA 92152

(619) 294-3658/5578

(2)

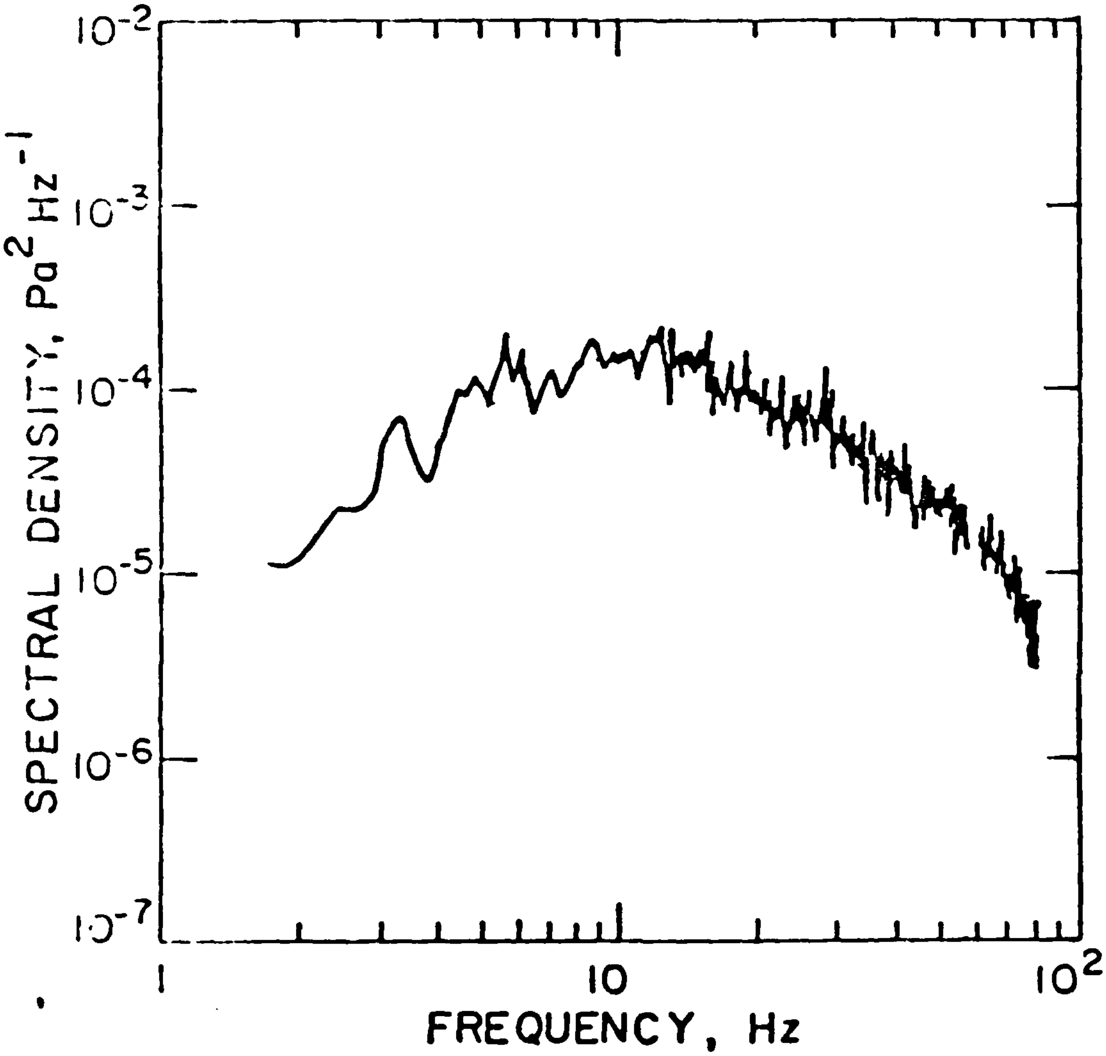

SPECTRAL DENSITY, $Pa^2 Hz^{-1}$
10^{-2}
10^{-3}
10^{-4}
10^{-5}
10^{-6}
10^{-7}
1
10
10^2
FREQUENCY, Hz

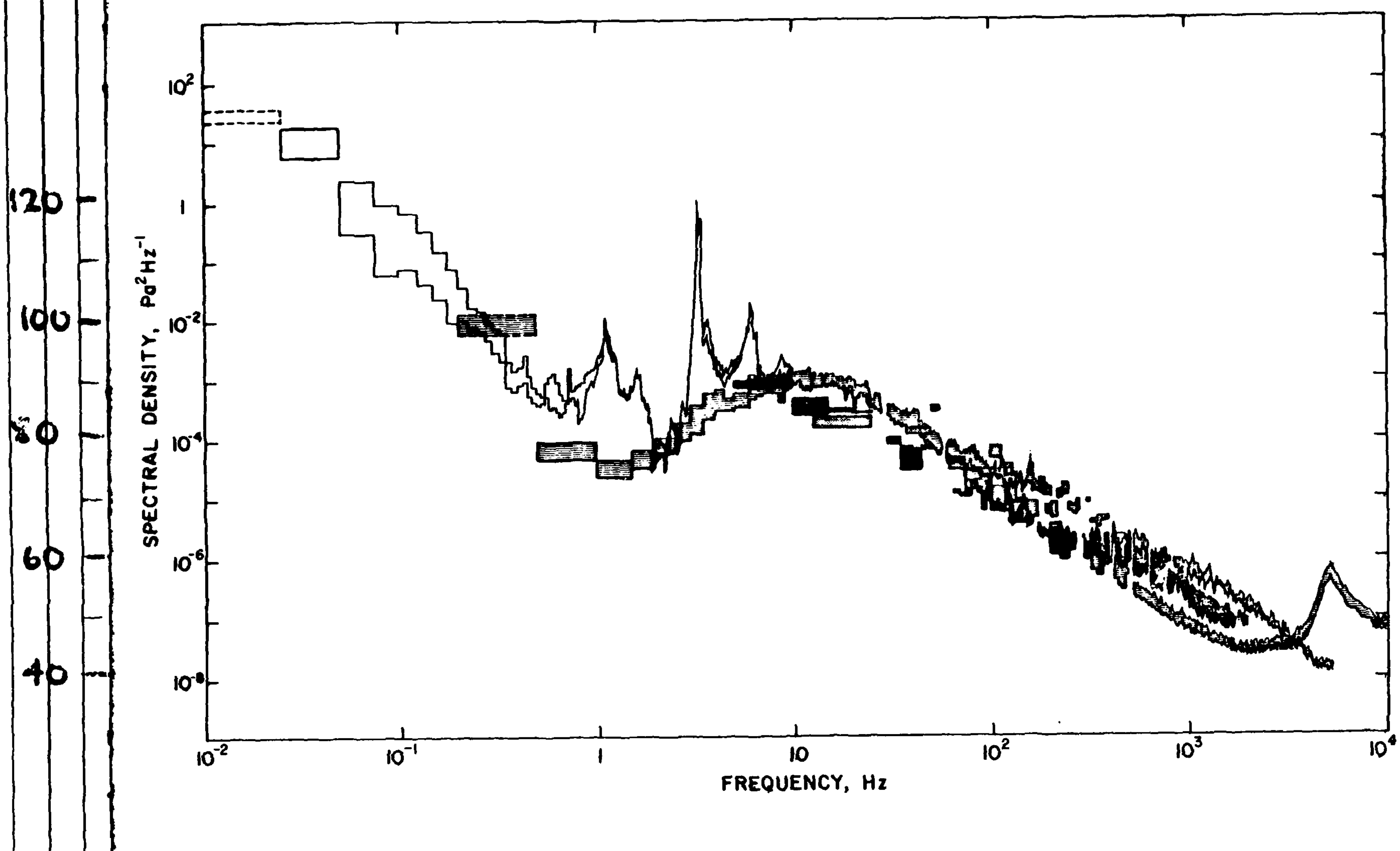

120
100
80
60
40
SPECTRAL DENSITY, Pa^2Hz^{-1}
10^2
1
10^{-2}
10^{-4}
10^{-6}
10^{-8}
10^{-2}
10^{-1}
1
10
10^2
10^3
10^4
FREQUENCY, Hz

(1)

AVCOM

Fig. 7

This spectrogram shows, among other things, a 77 Hz ice event lasting for more than 20 minutes. It is influenced by the increased ice stress caused by the helicopter landing at time 7 minutes, and by the decreased ice stress caused by the underwater air gun at 16 minutes.

FIG. 1

Composite of ambient noise typical of the central Arctic under moderate noise conditions. Measurements made at a depth of 90 m below the ice. The frequency characteristic below 1 Hz is not yet explained, but hypotheses include nonlinear surface wave noise from the open ocean, pseudosound from the planetary boundary layer turbulence interacting with the hydrophone, and radiation from the seismic noise in the earth's crust and mantle. Peaks from 1-10 Hz are caused by hydrophone cable strum, which is quite variable even under similar cable and current conditions. The broad peak centered on about 15 Hz is most likely caused by a large number of independent ice cracking events.

Fig. 2

This shows in clearer form the broad peak centered at about 15 Hz mentioned in Fig. 1. A 60 Hz tone due to line frequency pick up has been eliminated.

Fig. 3

A time series of noise (pressure magnitude in the 10-20 Hz band) is shown for a 10 day period in the central Arctic. (Noise magnitude is sampled once per hour in a 10 minute window.)

Fig. 4

Inferred ice stress for the same 10 day period as in Fig. 3. This ice stress is the horizontal normal stress in the ice determined as a consequence of force balance among wind loads, current loads, coriolis forces, and pressure gradient forces. This inferred internal ice stress is followed closely by the time series of Fig. 3. (Ice stress is sampled once per hour in a 10 minute window.)

Fig. 5

Cross-correlation of the time series of Figs. 3 and 4, indicating that horizontal internal ice stress is a good predictor of acoustic noise. Other data show that the noise is created by the large number of independent ice cracking events, with the most likely mechanism being flexural failure of the ice. These ice cracking events are individually on the order of a few 100 msecs in duration.

Fig. 6

A pathological observation in the marginal ice zone and often seen as well in the central Arctic. This pathology represents a very long time narrow band event lasting at times for minutes to hours. They are hypothesized to be caused by slip-stick oscillations of adjacent floes in shear deformation.

Art Baggeroer (for Ira Dyer)

Arctic Ambient Noise

SF #3 : July 1983
Offset = 13 hrs, Duration = 40.96 sec, FFT = 5.12 sec

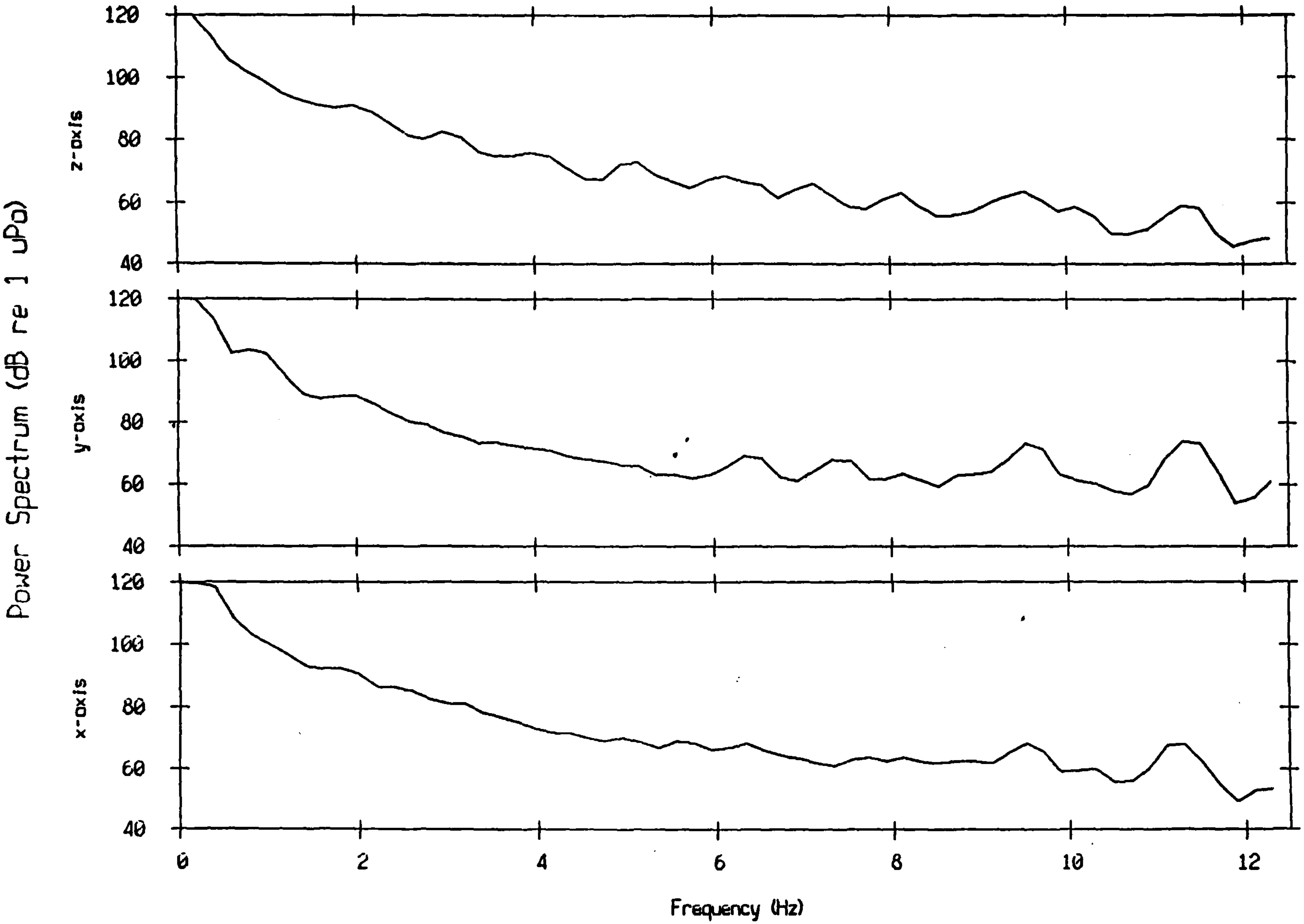

SF #3 : July 1983
Offset = 9hrs, Duration = 40.96 sec, FFT = 5.12 sec

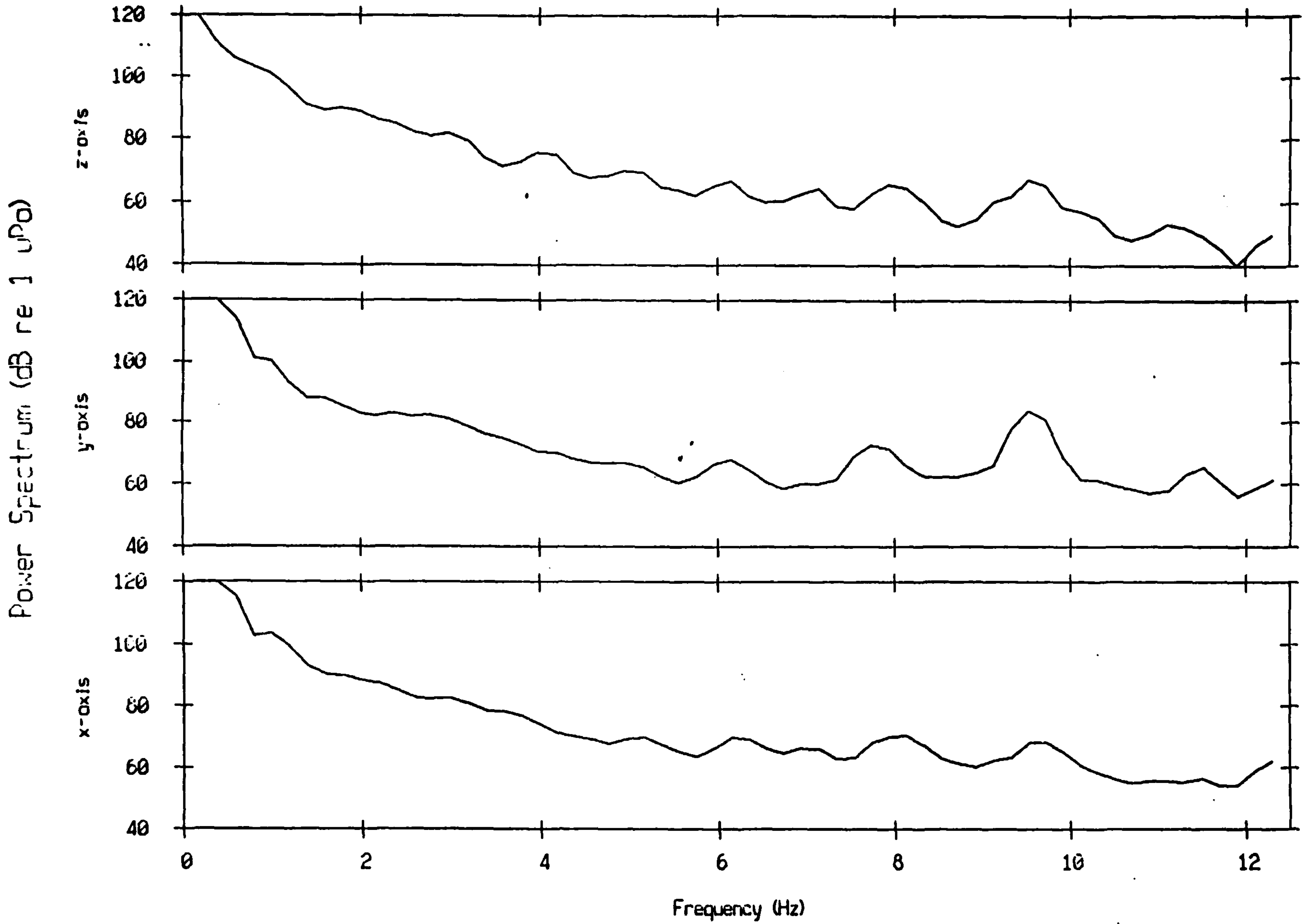

SF #3: July 1983

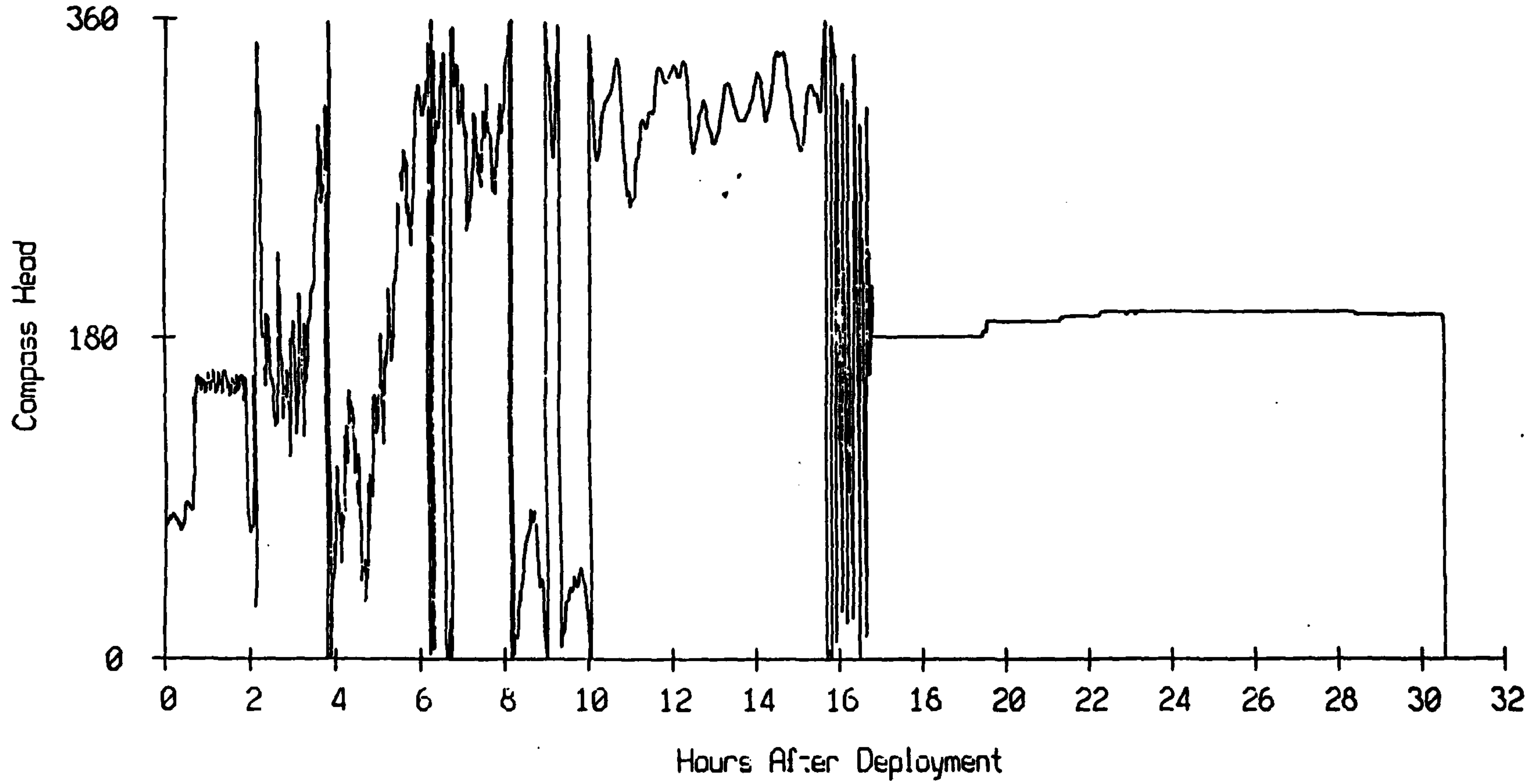

083

ACKNOWLEDGMENT

The authors wish to acknowledge beneficial discussions with Dr. F. N. Spiess, Marine Physical Laboratory, during the course of this work. Other recent contributors to this program from the Marine Physical Laboratory include J. C. Nickles, G. L. Edmonds, and R. Hawes. Initial fabrication of the prototype Swallow float was carried out by W. Whitney and S. Lai.

REFERENCES

[1] J. R. McGrath, "Infrasonic sea noise measurements and experimental problems," *Acustica*, vol. 38, pp. 324–327, 1977.

[2] "Proc. ONR Workshop Seismic Propagation Shallow Water," July 6–7, 1978.

[3] M. Strasberg, "Nonacoustic noise interference in measurements of infrasonic ambient noise," *J. Acoust. Soc. Amer.*, vol. 66, no. 5, pp. 1487–1493, 1979.

[4] J. H. Wilson, "Very low frequency (VLF) wind-generated noise produced by turbulent pressure fluctuations in the atmosphere near the ocean surface," *J. Acoust. Soc. Amer.*, vol. 66, no. 5, pp. 1499–1518, 1979.

[5] B. M. Buch and C. R. Greene, "A two-hydrophone method of eliminating the effects of nonacoustic noise interference in measurements of infrasonic ambient noise levels," *J. Acoust. Soc. Amer.*, vol. 68, no. 5, pp. 1306–1308, 1980.

[6] R. H. Nichols, "Infrasonic ambient ocean noise measurements: Eleuthera," *J. Acoust. Soc. Amer.*, vol. 69, no. 4, pp. 974–981, 1981.

[7] J. McGrath, O. Griffin, and R. Finger, "Infrasonic flow-noise measurements using an H-58 omnidirectional cylindrical hydrophone," *J. Acoust. Soc. Amer.*, vol. 61, no. 2, pp. 390–396, 1977.

[8] W. Lawson and J. McGrath, "A buoy to record infrasonic and low-frequency sea-noise," in *Proc. 1977 IEEE Int. Conf. Acoust., Speech, Signal Processing*, Hartford, CT, pp. 142–143, May 9–11, 1977.

[9] R. Martin and A. Perrone, "Geographical variation of ambient noise in the ocean for the frequency range from 1 Hz to 5 kHz," in *Proc. Int. Workshop Low-Frequency Propagation and Noise*, vol. 2, Woods Hole, MA, pp. 817–841, Oct. 14–19, 1974.

[10] W. S. Hodgkiss and V. C. Anderson, "Hardware dynamic beamforming," *J. Acoust. Soc. Amer.*, vol. 69, no. 4, pp. 1075–1083, 1981.

[11] B. Widrow *et al.*, "Adaptive noise cancelling: principles and applications," *Proc. IEEE*, vol. 63, no. 12, pp. 1692–1716, 1975.

[12] C. D. Lowenstein and J. D. Mudie, "On the optimization of transponder spacing for range-range navigation," *J. Ocean Tech.*, vol. 1, no. 2, pp. 29–31, 1967.

[13] B. D. Steinberg, *Principles of Aperture and Array System Design*. New York: Wiley, 1976.

★

William S. Hodgkiss, Jr. (S'68–M'75) was born in Bellefonte, PA, on August 20, 1950. He received the B.S.E.E. degree from Bucknell University, Lewisburg, PA, in 1972, and the M.S. and Ph.D. degrees from Duke University, Durham, NC, in 1973 and 1975, respectively.

From 1975 to 1977 he worked with the Naval Ocean Systems Center, San Diego, CA. From 1977 to 1978 he was a faculty member in the Electrical Engineering Department, Bucknell University, Lewisburg, PA. Since 1978 he has been a member of the faculty of the Scripps Institution of Oceanography and on the staff of the Marine Physical Laboratory, University of California, San Diego. His present research interests are in the areas of adaptive digital signal processing, adaptive array processing, application of these to underwater acoustics, and the statistical properties of ambient ocean noise.

★

Victor C. Anderson (SM'56) was born in Shanghai, China, on March 31, 1922. He received the A.B. degree from the University of Redlands, 1943 and the Ph.D. degree from the University of California, Los Angeles, in 1953.

From 1947 to present he has worked with the Marine Physical Laboratory, San Diego, CA and has held the position of Research Physicist. He is also a Professor of Applied Physics and Information Science at the University of California, San Diego. His fields of interest are in reverberation and scattering acoustic energy in the ocean, oceanic measurement of acoustical noise background statistics, digital signal processing, hardware development for underwater acoustics application, and remotely operating sea floor vehicles. He is Deputy Director of the Marine Physical Laboratory, Scripps Institution of Oceanography.

Dr. Anderson is a Fellow of the Acoustical Society of America and member of the Naval Studies Board.

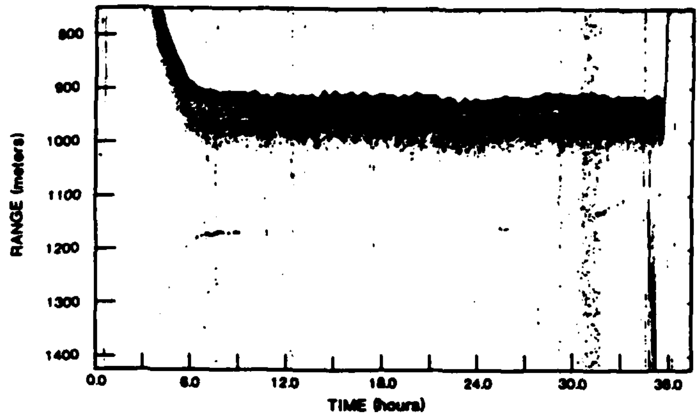

Fig. 3. Surface echo data: July 27, 1982. (Edge detection algorithm input.)

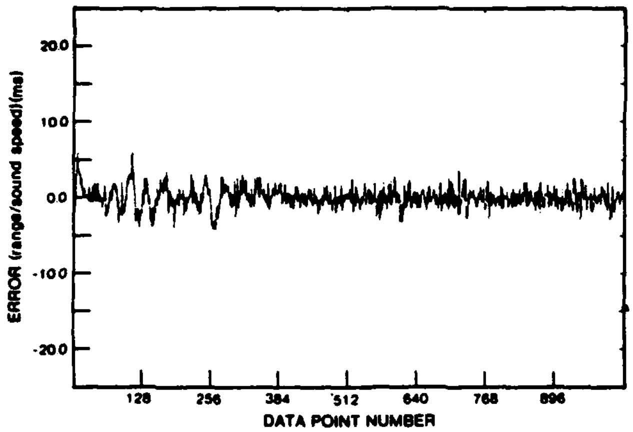

Fig. 4. Error time series: July 27, 1982. (Edge detection algorithm output.)

this observation. The resulting windowed-edge detection time series of sea surface range corresponding roughly to 8–33 h in Fig. 3 is shown in Fig. 5 (1.5 min/sample). A 1024-point FFT of that time series is provided in Fig. 6. Period (inverse frequency) is displayed along the horizontal axis for convenience. The broad band of power from approximately 120 to 30 min in period corresponds to internal wave activity. Note that the spectrum has dropped off to being essentially flat beyond 15 min in period. Thus localizing the array elements at least as often as every 7.5 min would capture the significant dynamics of array motion.

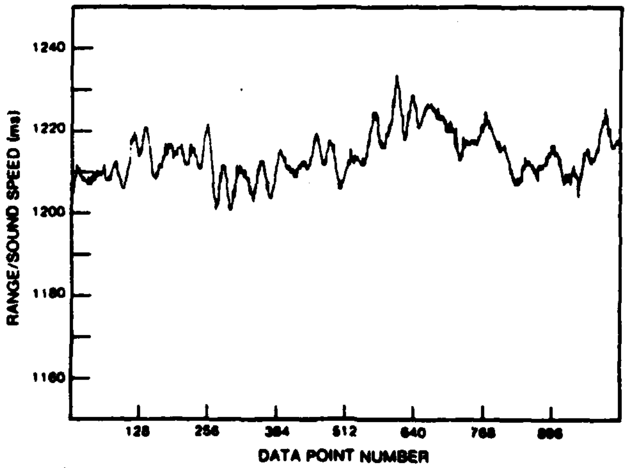

Fig. 5. Surface range time series: July 27, 1982. (Edge detection algorithm output.)

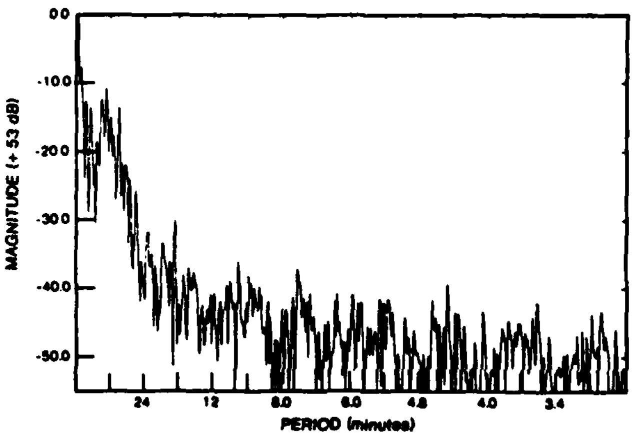

Fig. 6. FFT of surface range time series: July 27, 1982. (Edge detection algorithm output.)

IV. CONCLUSIONS

Surface echo data from a recent sea test of the prototype element of a freely drifting infrasonic measurement system has been used to illustrate the type of pulse processing which will be implemented as a first step in the localization procedure. For the surface echo data set processed, an arrival time error of 1.3-ms rms was indicated by the edge detection algorithm. Since this represents an uncertainty of approximately 0.1 λ at 10 Hz, we can expect our overall rms positioning error for the full array to be less than 0.1 λ [12]. Such random positioning errors lead to a maximum array signal gain degradation of less than 2 dB [13].

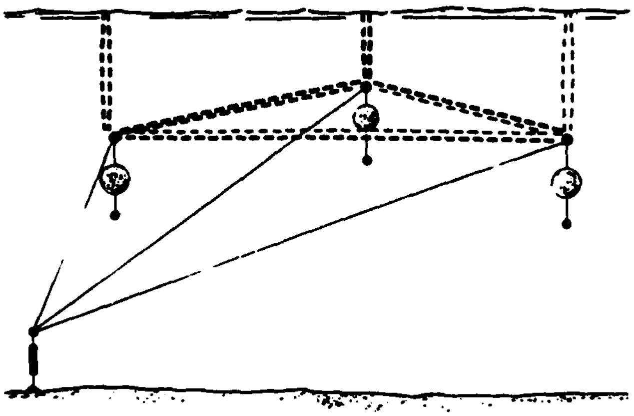

Fig. 2. Array element localization.

depicted in Fig. 2. This 8-kHz system has a maximum range of approximately 15 km and a nominal resolution of ±0.75 m based on a 1-ms sampling interval at the output of the pulse detection circuit. A different buoy pings every 1.5 min until each Swallow float has transmitted. The sequence then repeats. Since each buoy maintains an internal time base (clock), deciphering which buoy transmitted any given received pulse is not difficult. Synchronization of the clocks is possible due to the occurrence of reciprocal transmission paths between buoys. All floats (including the transmitter listening to its own sea surface reflection) internally record arrival time of the transmission on magnetic tape. These tapes then will be read at the completion of a deployment and the arrival times at all buoys from each ping will be combined algorithmically to yield the relative three-dimensional positions of the array elements as a function of time. An absolute coordinate system can be established with the addition of external receivers and/or transmitters of known position (e.g., a ship positioned via satellite navigation and a bottom-tethered buoy at a known location, as shown in Fig. 2).

III. TIME-OF-ARRIVAL ESTIMATION

Within each buoy, the arrival times of the received pings must be estimated as a first step in the localization process. The pulse-detection circuit is of a fairly common design. It consists of two filters in cascade. Both pass the localization pulse which is centered at 8 kHz and is 6 ms in duration. The first filter is rather broad band (2-kHz bandwidth centered at 10.5 kHz). The output of this filter is hard limited yielding a constant power time series. The second filter is narrow band (0.2-kHz bandwidth centered at 8 kHz). The power spectrum of ambient noise passed on to the second filter predominately lies outside its bandwidth and thus yields a small output. In contrast, the power spectrum of an 8-kHz pulse received on the skirt of the first filter mostly lies inside the bandwidth of the second filter and thus yields a large output. The envelope-detected output of the second filter is compared against a threshold and generates a pulse present-absent decision. The decision output [1, 0] of the sonar is sampled at a 1-kHz rate. That bit stream is not recorded directly, but is first operated on by data-compression logic. The bit stream is inspected in blocks of 8 bits. If a 1 (pulse present) is observed, the block of 8 bits is recorded as one byte along with its associated time (2 bytes). Otherwise, nothing is recorded. Up to 85 3-byte groups can be recorded for each 1.5-min period.

Both ocean-ambient noise and gross-data gaps make the raw sonar data unusable as a continuous record of pulse time of arrival. Accurate arrival time measurements are required by array-element localization and tracking algorithms. Thus it is necessary to preprocess the raw detector output to provide usable inputs to these algorithms. We have had several opportunities to test our prototype self-contained Swallow float at sea. These tests have provided experimental data sets representative of those which will be recorded by the acoustic localization system. Using one of these data sets, we have investigated candidate algorithms for the preprocessing operation.

As mentioned previously, each buoy not only listens for transmissions from the other elements of the array, but for the sea surface reflection of its own pulse as well. Raw sonar surface echo data from a recent sea trip is shown in Fig. 3. Time delay after transmission is displayed positive downward in terms of range. The closest edge of the dark band represents the shortest path to the surface from the Swallow float. Hence, the problem of distinguishing the surface echo from other returns and noise becomes a problem of detecting this edge.

Several edge detection algorithms have been tried. The following approach, which makes use of an adaptive linear predictor directing the search for an edge in a narrow range window, has been the most successful.

First, range is predicted using a 16-weight one-step linear predictor incorporating the least mean-squares (LMS) adaptive algorithm [11]. Then, the detector proceeds through four modes until a range is decided.

1) If no data record is present, the predicted range is used.
2) If a data record is present, a search is made for an edge in a small window plus and minus two standard deviations of the error (i.e., rms error) from the predicted range.
3) If no edge is found in the small window, a larger window representing the maximum physically possible movement is searched.
4) If the large window search fails, the predicted range is used.

After a range is determined, the edge detector calculates the error and the adaptive predictor is iterated.

The use of a small window is based on the assumption that the range will not deviate much from the predicted value. By using a multiple of the rms error for the width of the small window, the window is allowed to adapt to increasing or decreasing noise in the data. The large window allows any physically reasonable movement to be accepted, even though it might not be predictable.

When used with a small window of two standard deviations, a large window of 10 ms, and the July 27, 1982 data set, the edge detector remained in mode 2 most of the time, indicating the predictor was predicting the range well. As shown in Fig. 4, the small error signal (rms error of 1.3 ms) confirmed

Acoustic Positioning for an Array of Freely Drifting Infrasonic Sensors

WILLIAM S. HODGKISS, JR., MEMBER, IEEE, AND VICTOR C. ANDERSON, SENIOR MEMBER, IEEE

(Invited Paper)

***Abstract*—Initial testing of the prototype element of a freely drifting infrasonic sensor array is described. The intent of this measurement system is to gather wide aperture data sets which will be used both to characterize ambient noise in the region 1–10 Hz and to assess the gains possible from beam forming utilizing a collection of very low frequency (VLF) sensors. Coherent processing (beam forming) of the infrasonic sensor data is made possible by relative position measurements derived from mutual acoustic interrogation of the elements at a higher frequency. Surface echo data from a recent sea test of the prototype buoy are used to illustrate the type of pulse processing which will be implemented as a first step in the localization procedure.**

I. INTRODUCTION

ONE PROJECT at the Marine Physical Laboratory (MPL) is the development of an array to study infrasonic acoustic background noise in the ocean. In general, self-noise limits an accurate assessment of the true nature of this ambient acoustic noise field. Cable strumming, flow noise, and the local pressure and velocity fields due to turbulence are all difficulties associated with measurements in the region 1-10 Hz when using an array which requires some form of tethering or mechanical linkage [1]-[9]. Even for deep sensors near or on the sea floor, the flow noise associated with very slow currents can significantly contaminate the local pressure or particle velocity field.

The approach taken in this project is to develop an autonomous buoy capable of recording the components of particle velocity in the 1-10-Hz band and which is also able to both generate and receive high-frequency acoustic-positioning signals. The buoy is a neutrally buoyant Swallow float which is stable at midwater depths and, drifting freely, is not subject to any flow disturbance. The acoustic-positioning capability will be used to monitor the relative geometry of a set of these buoys in a freely drifting infrasonic array, so that data from the individual elements can be combined coherently off-line by use of the MPL dynamic beamformer [10].

A prototype buoy has been designed, built, and deployed at sea. The performance of the acoustic-positioning system in this prototype buoy, in measuring the time delay to the first surface echo, provides insight into the localization accuracy that can be expected for a multi-element array system. Satisfactory performance of the acoustic-positioning system is a key factor in the success of the project.

Manuscript received December 29, 1982; revised April 20, 1983. This work was supported by the Office of Naval Research under Contract N00014-80-C-0220. Contribution of the Scripps Institution of Oceanography, new series.

The authors are with the Marine Physical Laboratory, Scripps Institution of Oceanography, San Diego, CA 92152.

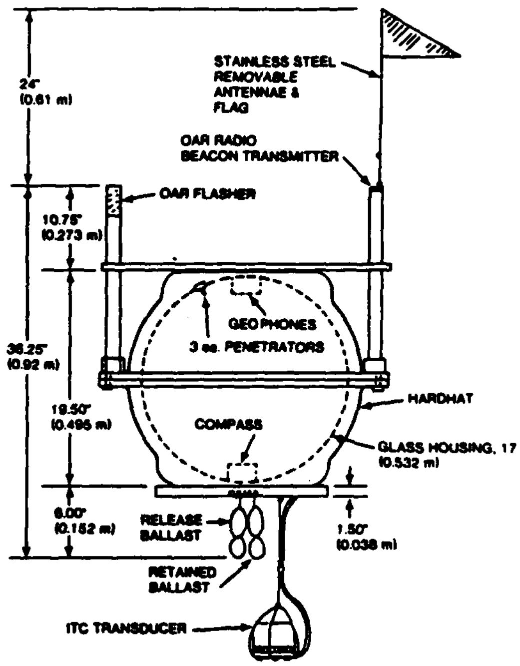

Fig. 1. MPL Swallow float.

II. THE INFRASONIC SENSOR BUOY AND ARRAY

The element of the Swallow float array is a spherical glass Swallow float which contains three geophones that measure the three components of particle velocity in the 1-10-Hz band: a compass for buoy heading; an acoustic transponder for localization; a solid-state memory-data buffer; a digital-tape data recorder; and an acoustically actuated ballast release. The general configuration of hardware in our prototype unit is shown in Fig. 1. The floats are neutrally buoyant and can be ballasted for a desired depth. Limited by tape recorder capacity, the maximum submergence period of the floats is on the order of 60 h. Each buoy continuously fills an 8-kB buffer memory, then periodically writes this buffer out to tape. The information contained in the buffer includes compass heading, acoustic localization pulse arrival times, and three channels of geophone data sampled at 25 Hz. Currently, the buffer is written out to tape in a burst mode every 1.5 min. During this 1-s procedure, no data are sampled.

Several of these elements can be deployed in a random configuration to create a spatially distributed array. Their relative three-dimensional position as a function of time are obtained via an acoustic pulse mutual interrogation system as

Potential Sources of Measurement Contamination

- Cable Strumming
- Flow Noise
- Turbulence-Related Pressure Fluctuations

Motivating Questions

- What is the temporal and spatial structure of ambient ocean noise in the 1-10 Hz frequency region?

- How do the results from different sensor types compare (e.g. VLF sonobuoys, bottom tethered hydrophones, and bottom mounted hydrophones)?

VAX/VMS *** PENPLOT 13-FEB-1984 16:22:29.06 RES1:[P2542.NICHOLAS]HDCOPY.PLT;61 NICHOLAS *** VAX/VMS

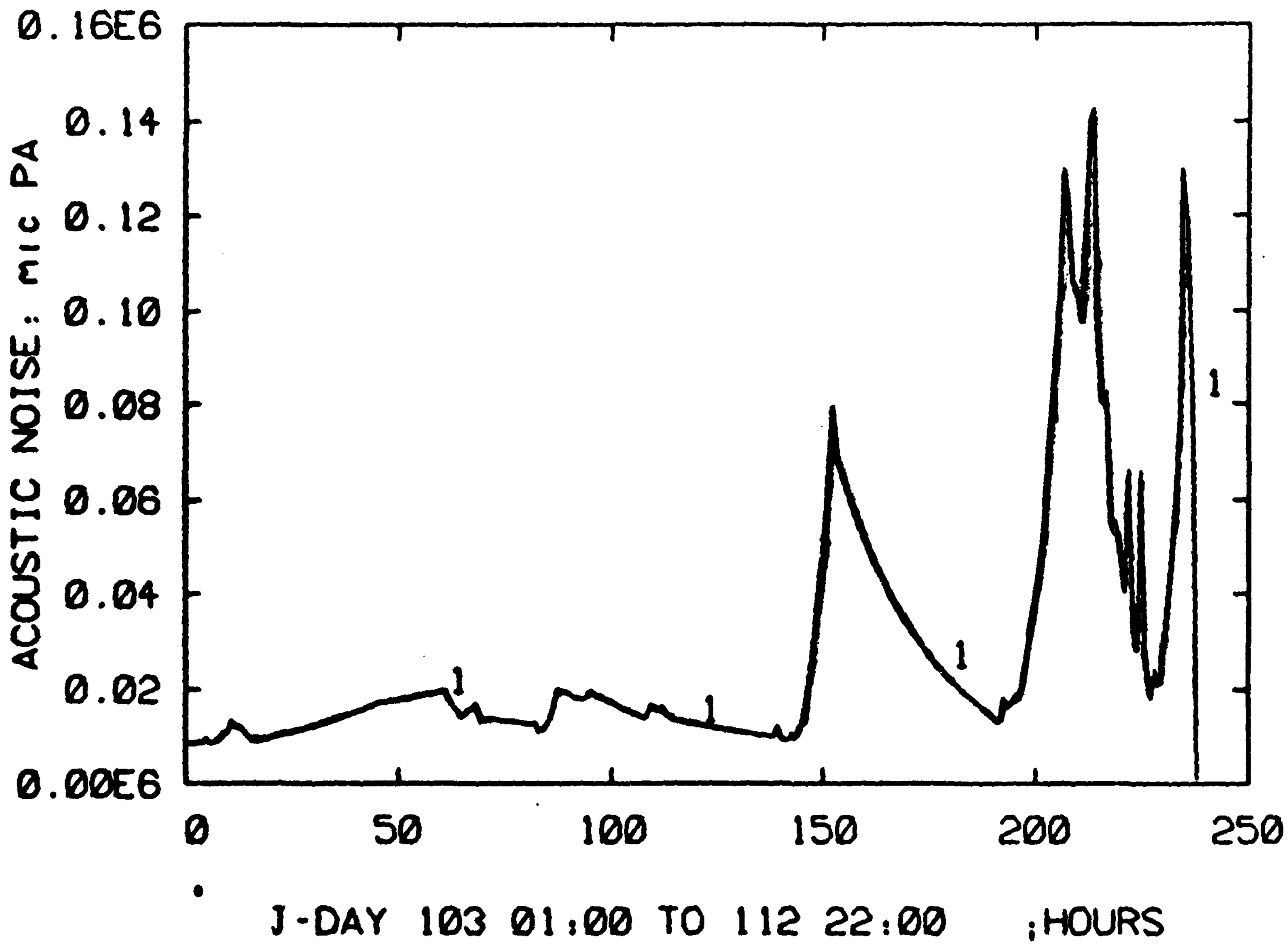

In one hour averages.

VAX/VMS *** PENPLOT 11-JUN-1984 14:04:48.30 RES1:[P3842.NICHOLAS]HDCOPY.PLT;69 NICHOLAS *** VAX/VMS

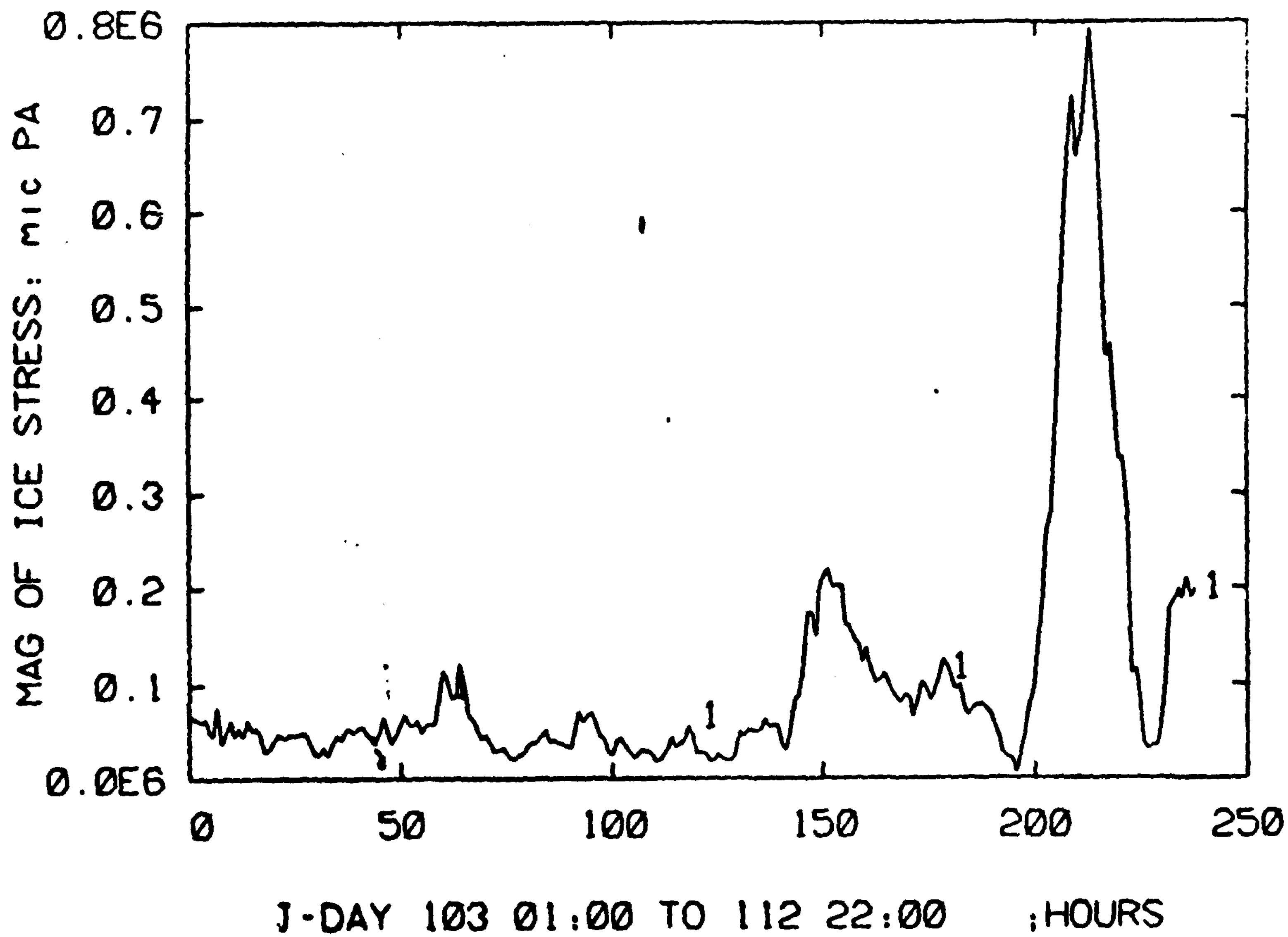

(4)

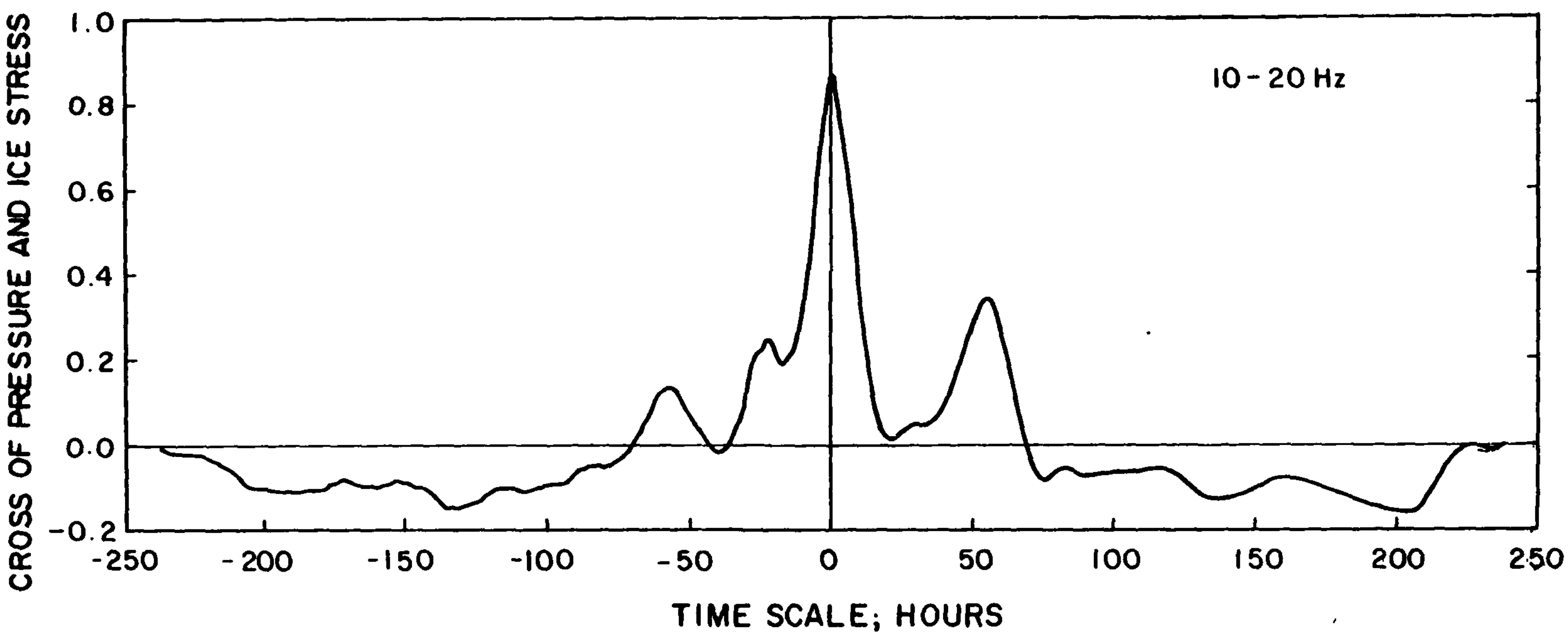
10-20 Hz
CROSS OF PRESSURE AND ICE STRESS
1.0
0.8
0.6
0.4
0.2
0.0
-0.2
-250
-200
-150
-100
-50
0
50
100
150
200
250
TIME SCALE; HOURS

D6

28 June 84 Ship up

1341

40 KH
to this
14½ Hz
tone
burst
real?

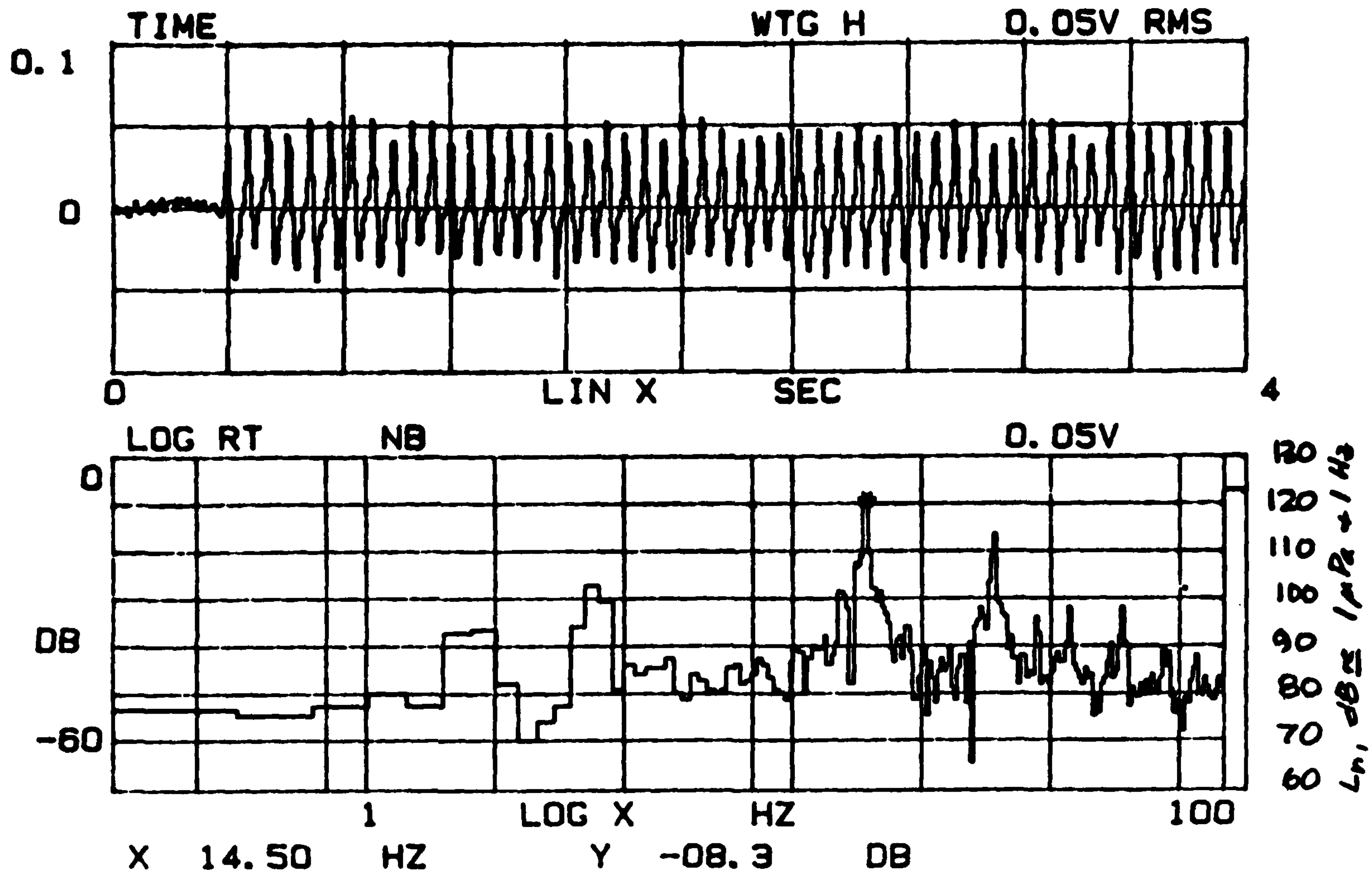

6

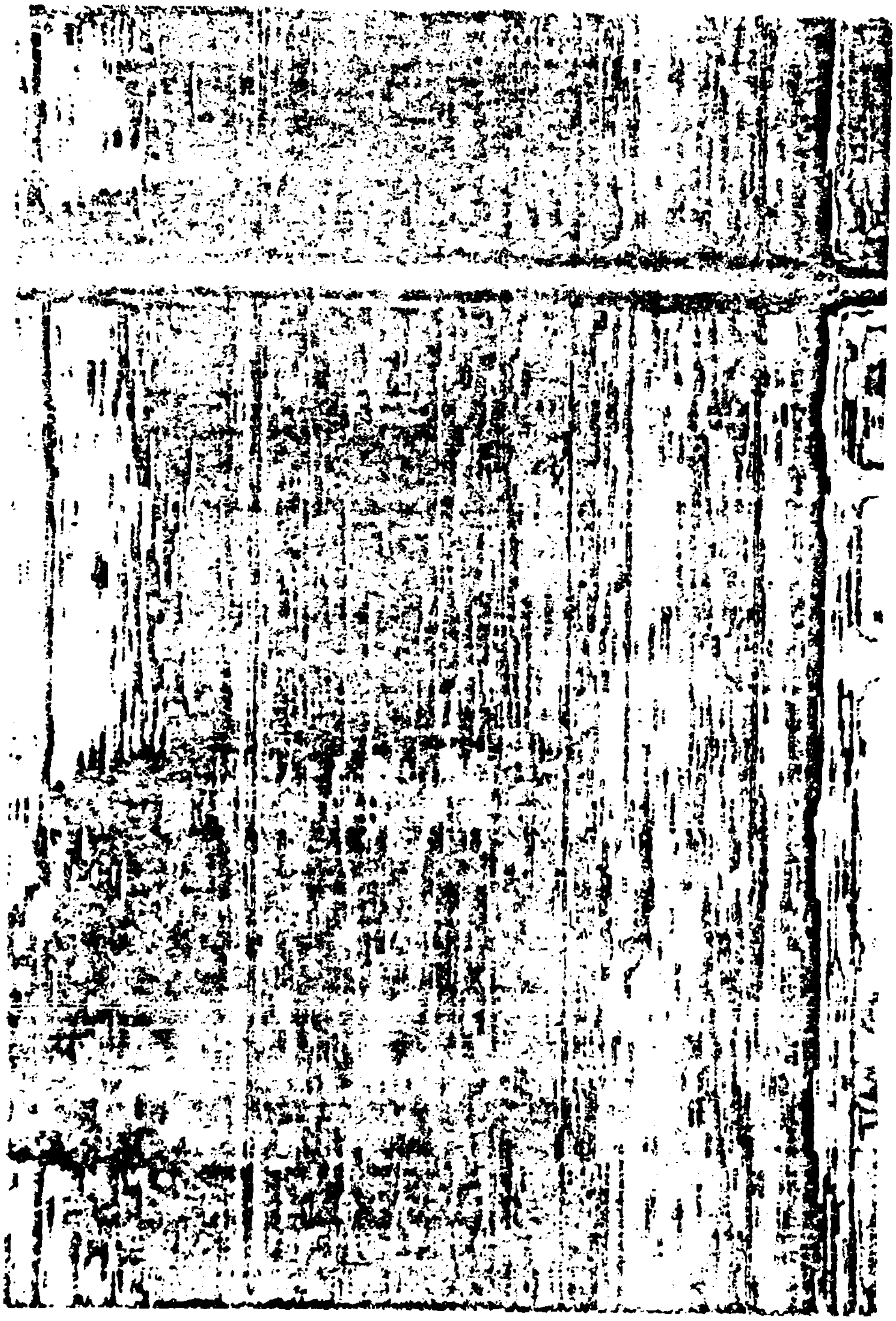

VLF AMBIENT NOISE

January 1985

Marshall R. Bradley
Planning Systems Incorporated
Slidell, Louisiana

INTRODUCTION

- Lack of quality VLF data
- No generally accepted theory for the non shipping noise component near 10 Hz
- No routine predictive capability
- Great potential for simple hydrophones being self noise limited
- Hydrophones mounted on cables are likely to be contaminated by strum noise

SOVIET NUCLEAR SUBMARINES
from 1984 edition of Jane's Fighting Ships

	Name	No.	Displacement (tons dived)	Dimensions (ft)	Shafts	Shaft Horse Power	Speed (kt)
SSGN	OSCAR	2+1	14 000	469 x 60 x 36	?	40 000	30
	PAPA	1	7 000	358 x 38 x 25	2	50 000	35+
	CHARLIE II	6	5 500	338 x 33 x 26	1	20 000	25
	CHARLIE I	11	5 000	308 x 33 x 25	1	20 000	28
	ECHO II	29	5 800	385 x 30 x 26	2	30 000	25
SSN	SIERRA	1+?	6 500	345 x 36 x 24	?	?	32
	MIKE	1+?	9 700	?	?	?	?
	ALFA	6	3 800	260 x 33 x 25	1	45 000	42+
	VICTOR III	18+?	6 000	341 x 33 x 24	1[a]	30 000	30
	VICTOR II	7	5 800	328 x 33 x 24	1[a]	30 000	31
	VICTOR I	16	5 200	308 x 33 x 24	1[a]	30 000	32
	ECHO I	5	5 200	374 x 30 x 24	2	30 000	28
	NOVEMBER	12	5 000	360 x 30 x 22	2	30 000	30
SSBN	TYPHOON	2+?	30 000	558 x 75 x ?	2	80 000	24?
	DELTA III	14+2-3	11 000	508 x 39 x 30	2	30 000	24
	DELTA II	4	11 000	508 x 39 x 30	2	30 000	26
	DELTA I	18	10 000	446 x 39 x 30	2	30 000	26
	YANKEE	24	9 300	426 x 38 x 26	2	30 000	28
	HOTEL III	1	5 500	377 x 30 x 25	2	30 000	24
	HOTEL II	3	5 500	377 x 30 x 25	2	30 000	26

[a] Two auxiliary props.

SOURCES OF VLF AMBIENT NOISE

Seismic Sources

Microseisms

Shipping

Wind $\left\{ \begin{array}{l} \text{Surface Waves} \\ \text{Wave Turbulence Interaction with Surface Waves} \\ \text{Wind Turbulence} \end{array} \right.$

Current $\left\{ \text{Turbulent Pressure Fluctuations} \right.$

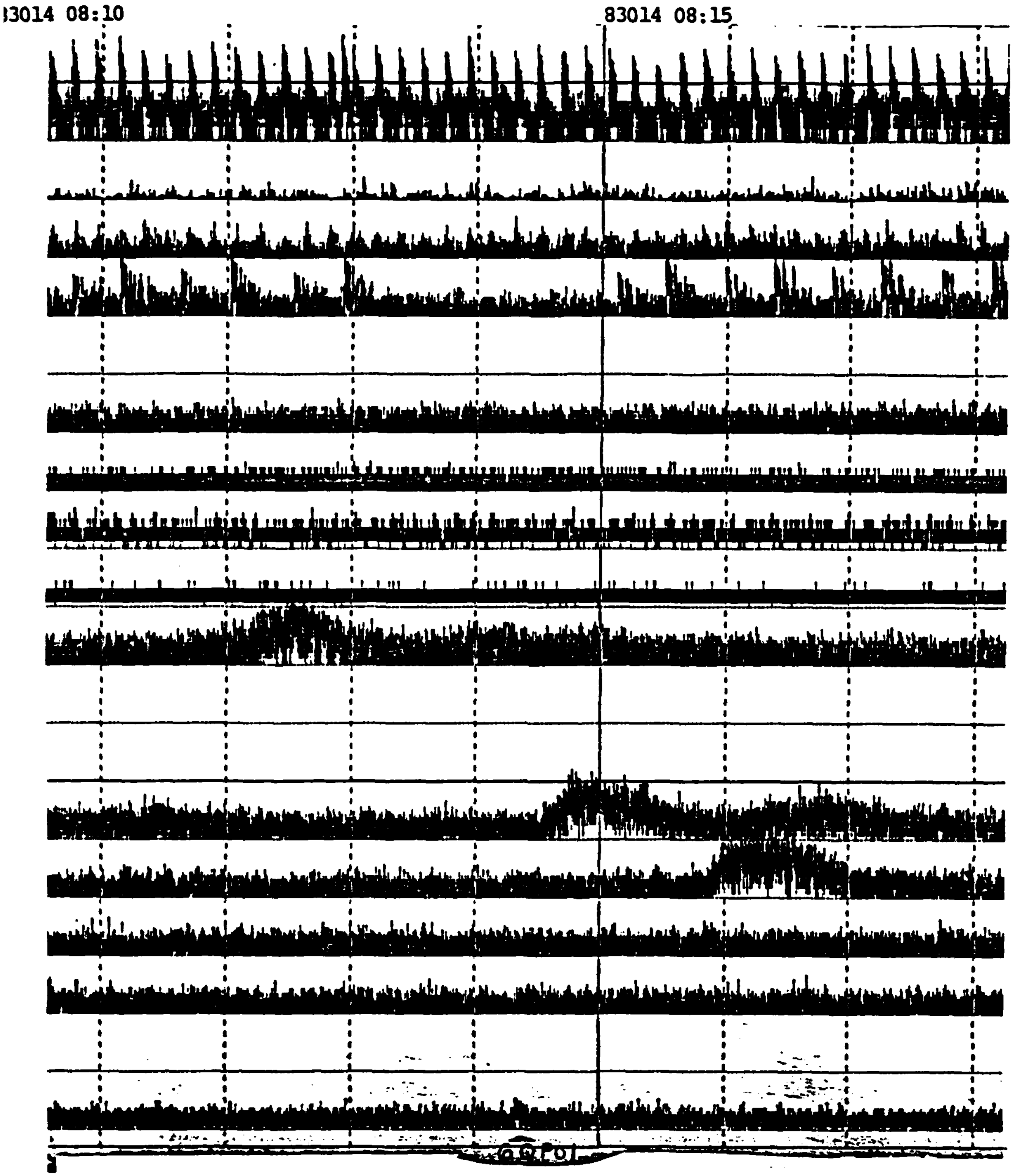

Seismic interference in the VLF band

- Seismic profiling - Channel 1
- T-Phase - Channel 9, 10, 11

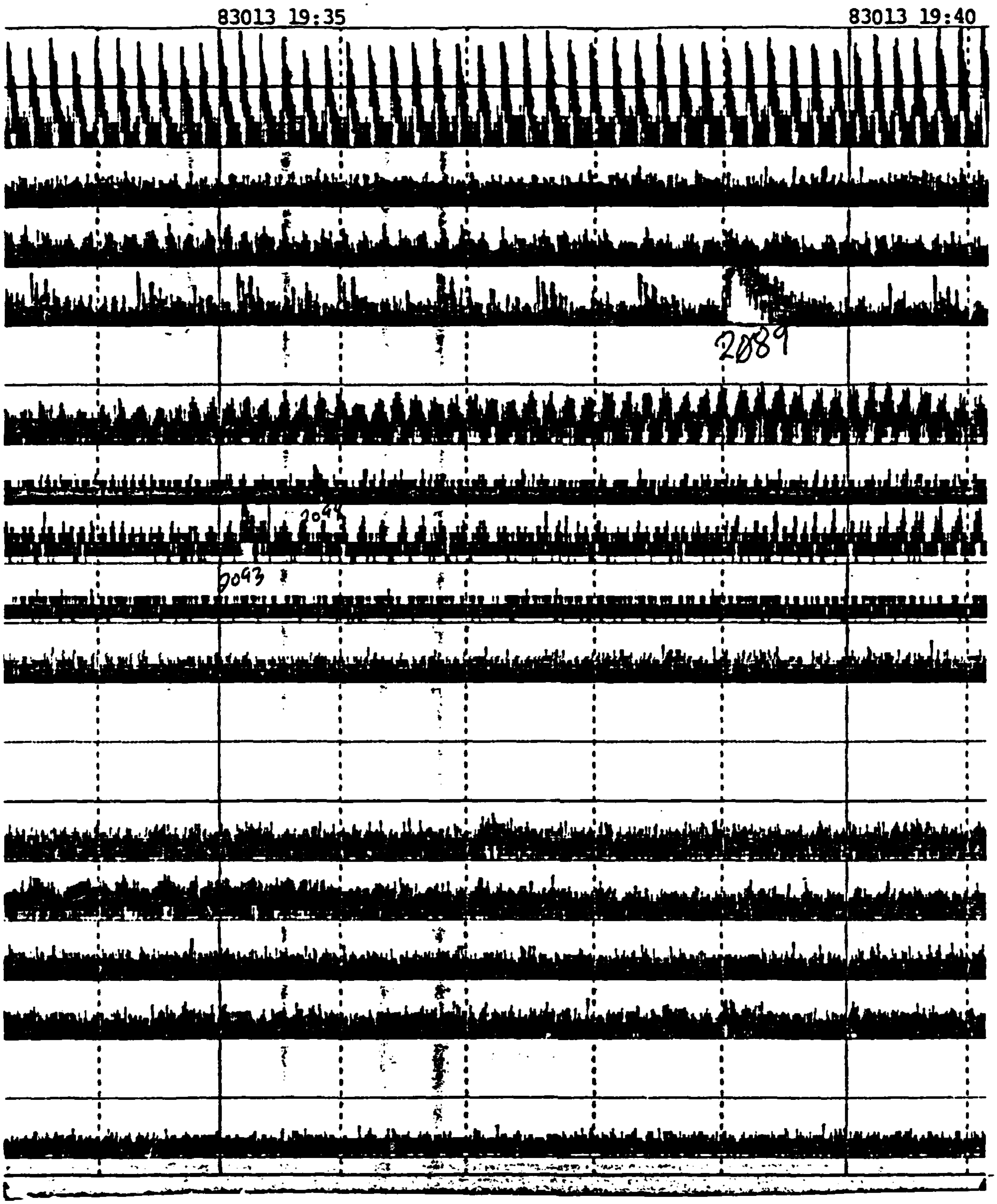

Seismic interference in the VLF band

- Seismic profiling - Channel 1, 5
- Signals - Channel 4, 6, 7

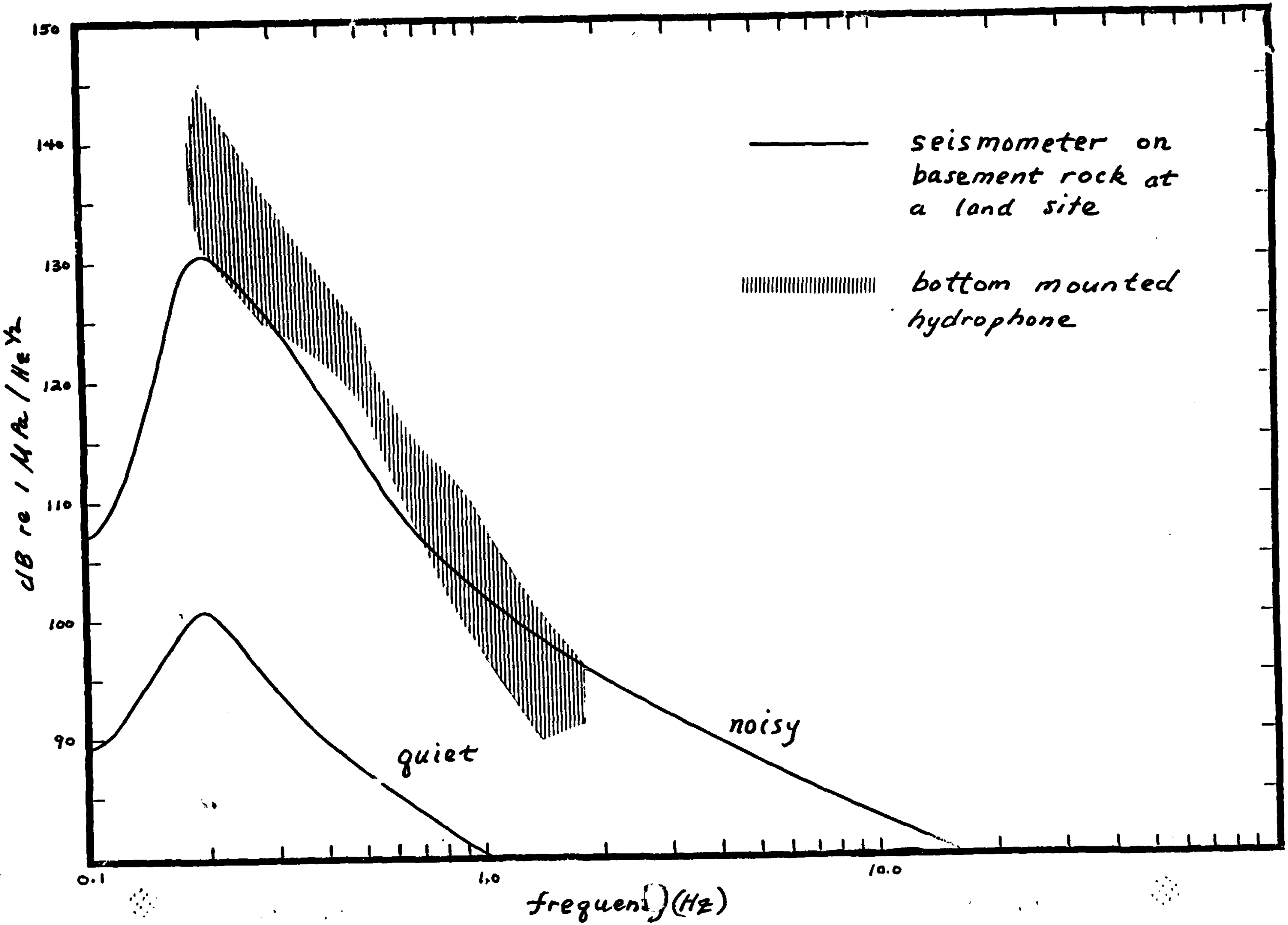
seismometer on basement rock at a land site
bottom mounted hydrophone
noisy
quiet
150
140
130
120
110
100
90
dB re 1 µPa / Hz½
0.1
1.0
10.0
frequency (Hz)

VLF Sound Radiation by Merchant Ships

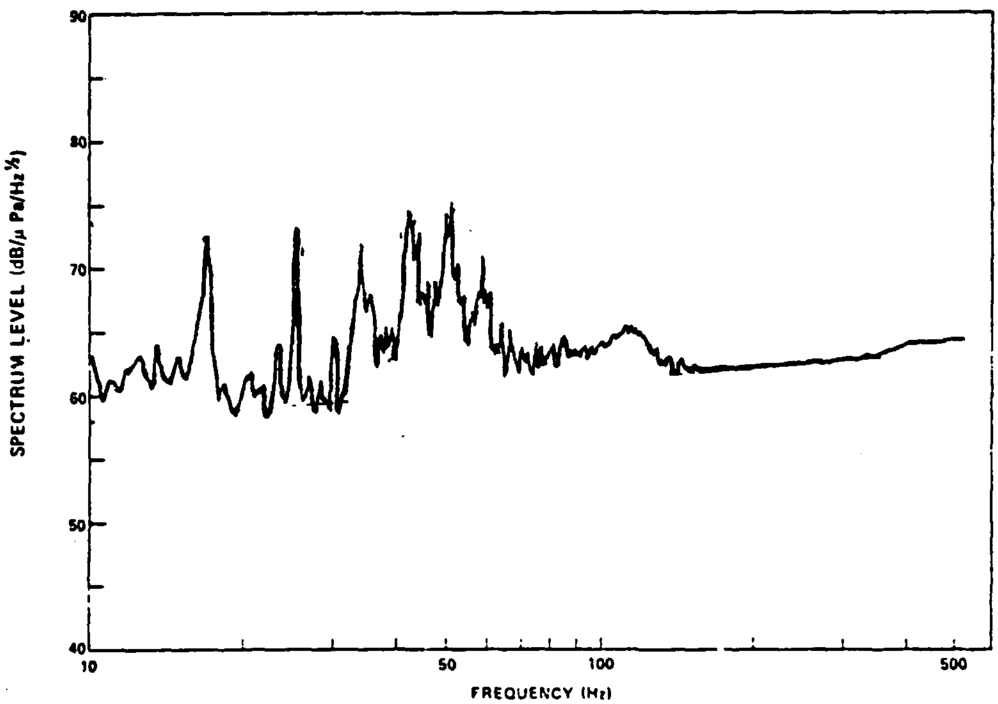

Received levels at 100 miles due to the freighter ADOLF LEONHARDT (22,000 tons, 10,600 bhp) moving at 15 knots (from Wittenborn, 1976).

VLF Sound Radiation by Merchant Ships

Estimated source levels (from Wittenborn, 1976).

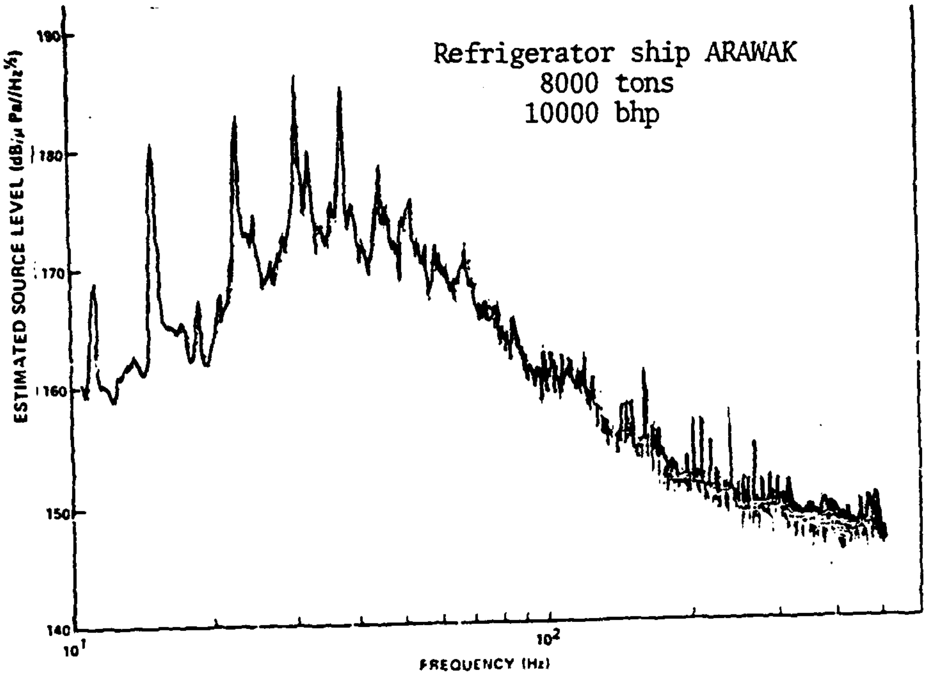

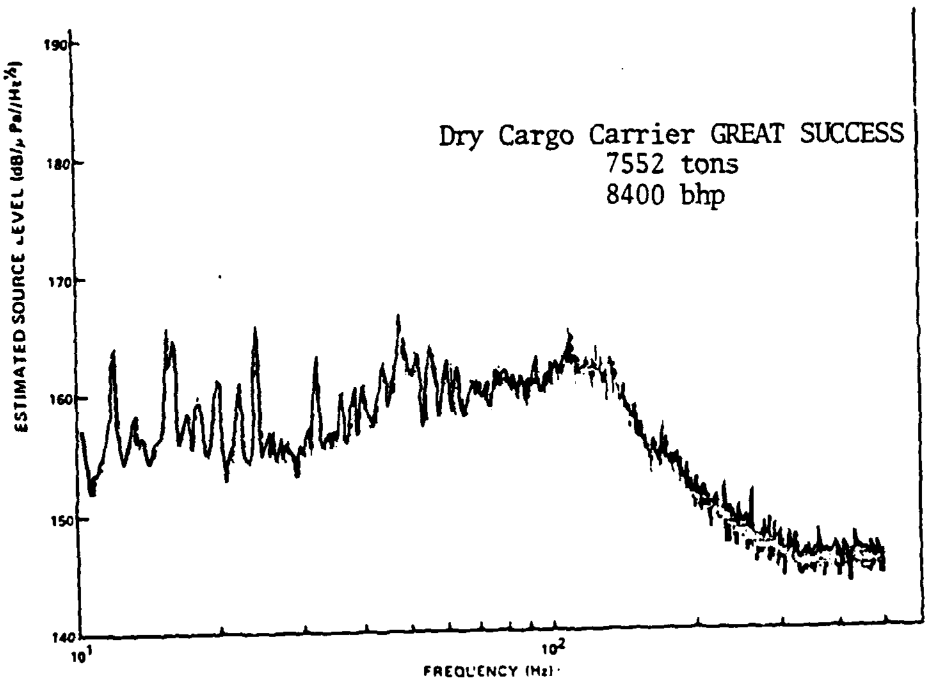

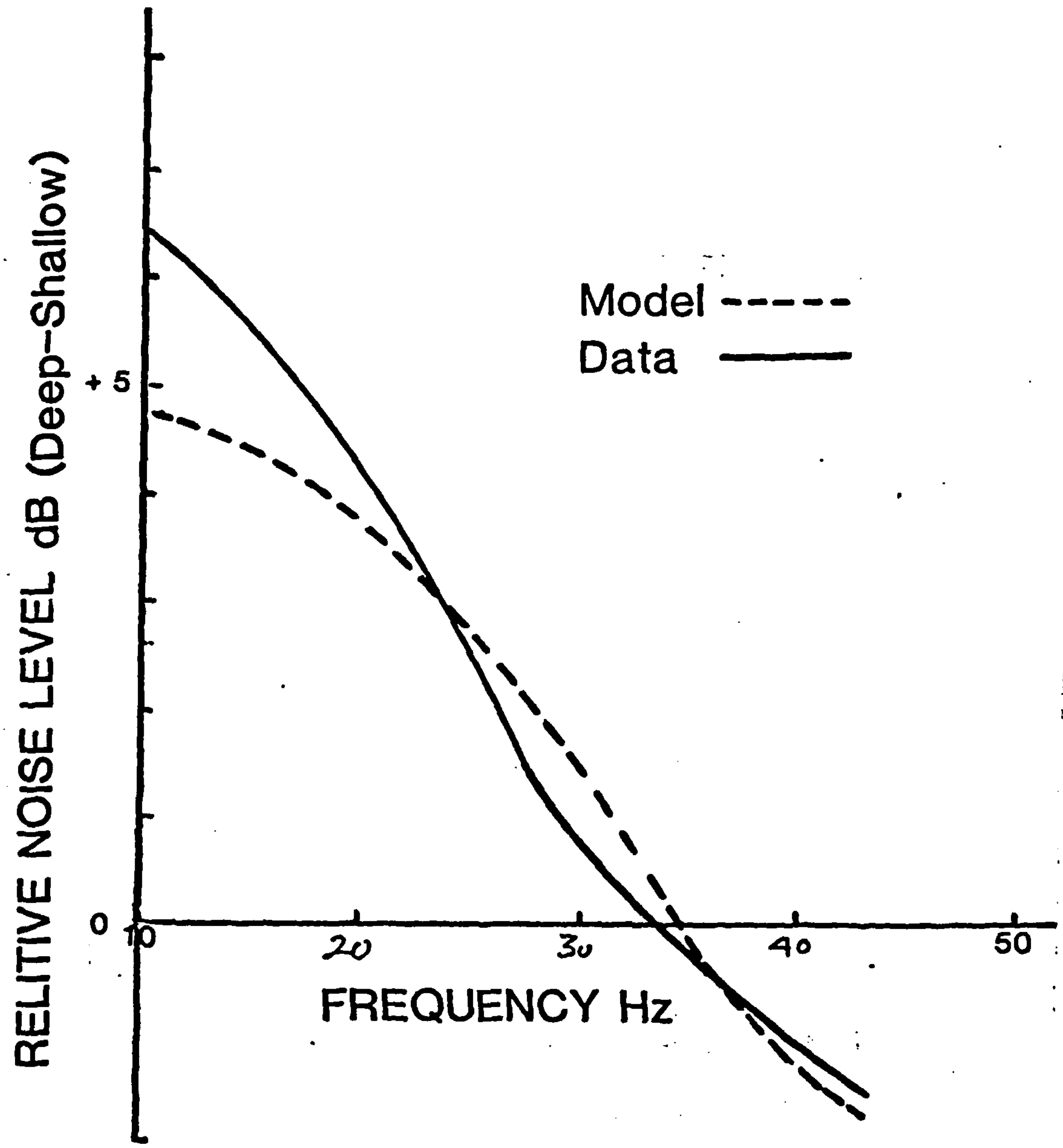

Figure 7 - Measured vs Modeled Receiver Depth Dependence of Near Field Pressure Ridge Noise.

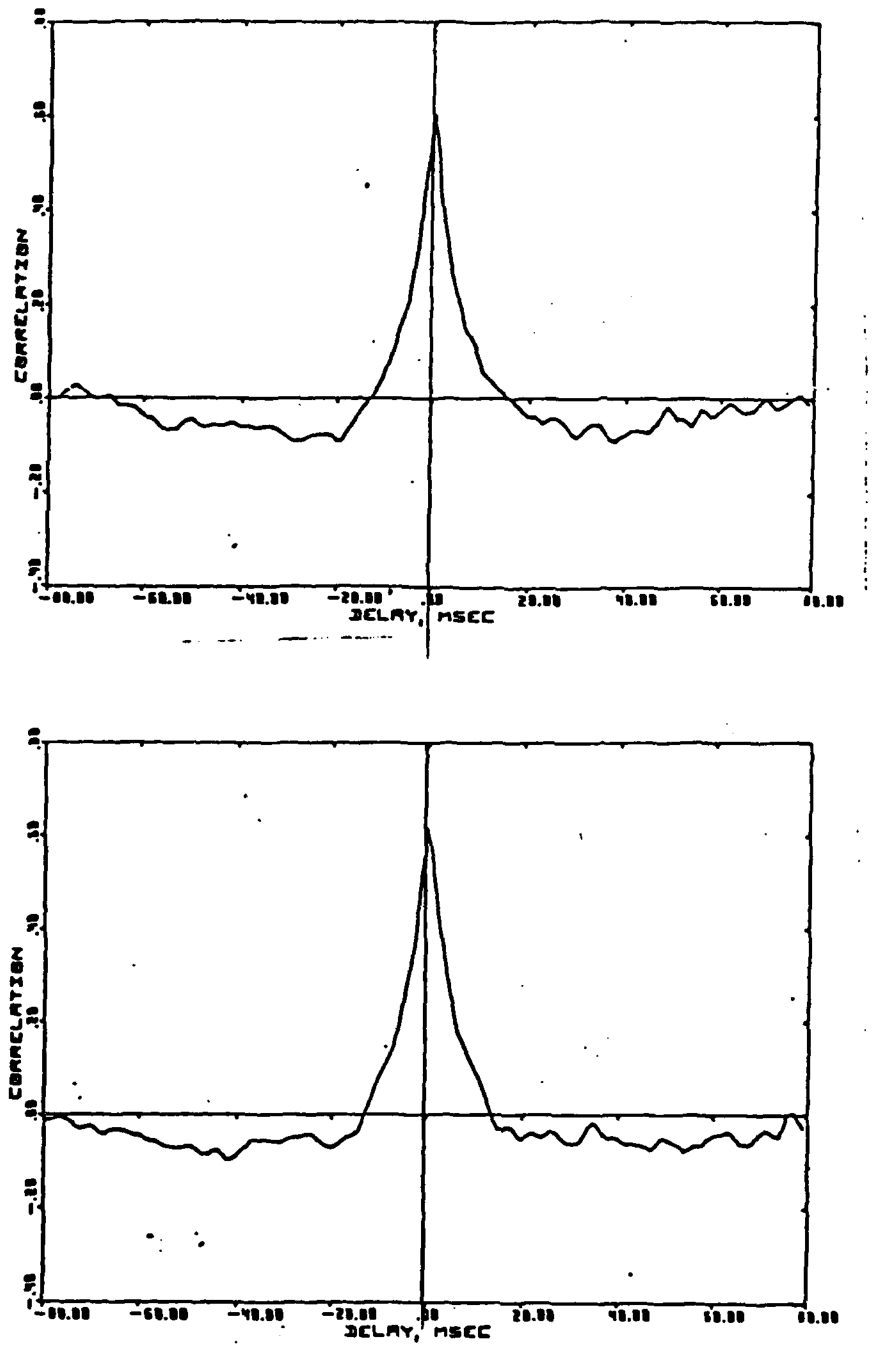

Figure 6 – Horizontal Spatial Cross-Correlation of Active Ice Ridge Noise

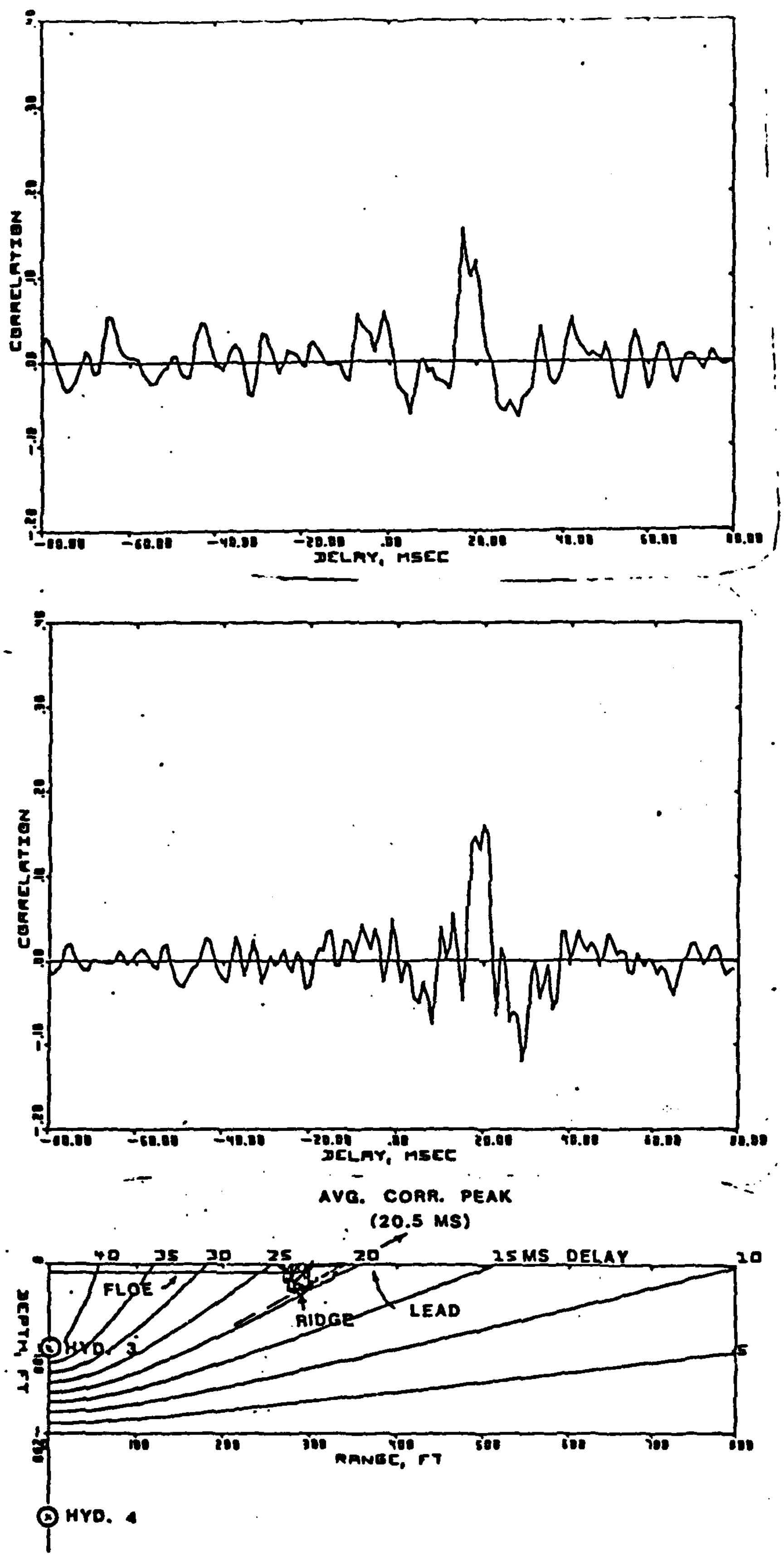

Figure 5 – Vertical Cross Correlation of Active Ice Ridge Noise

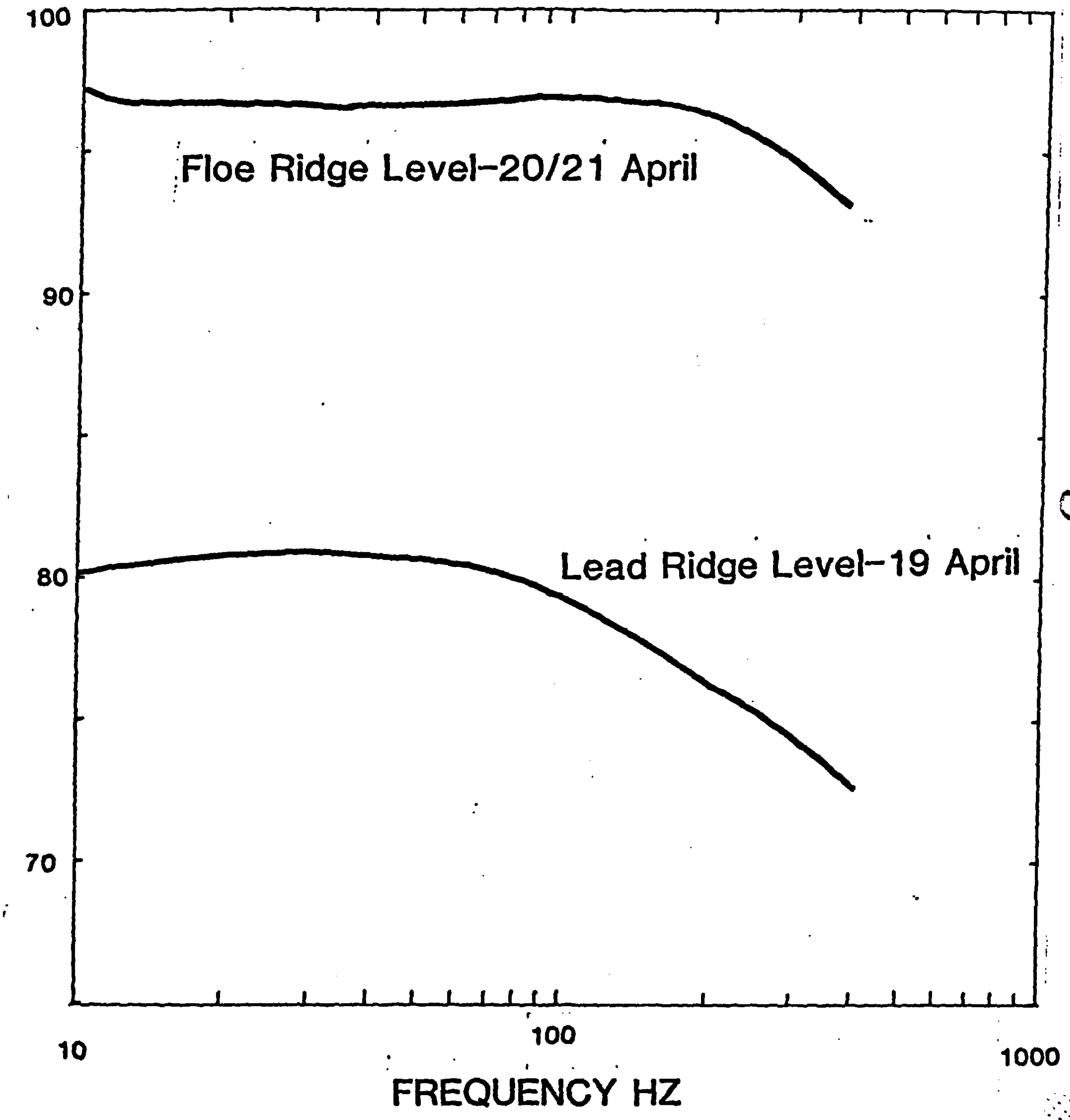

Figure 4 - Active Ice Ridge Ambient Noise Levels Measured Over a Three Day Period.

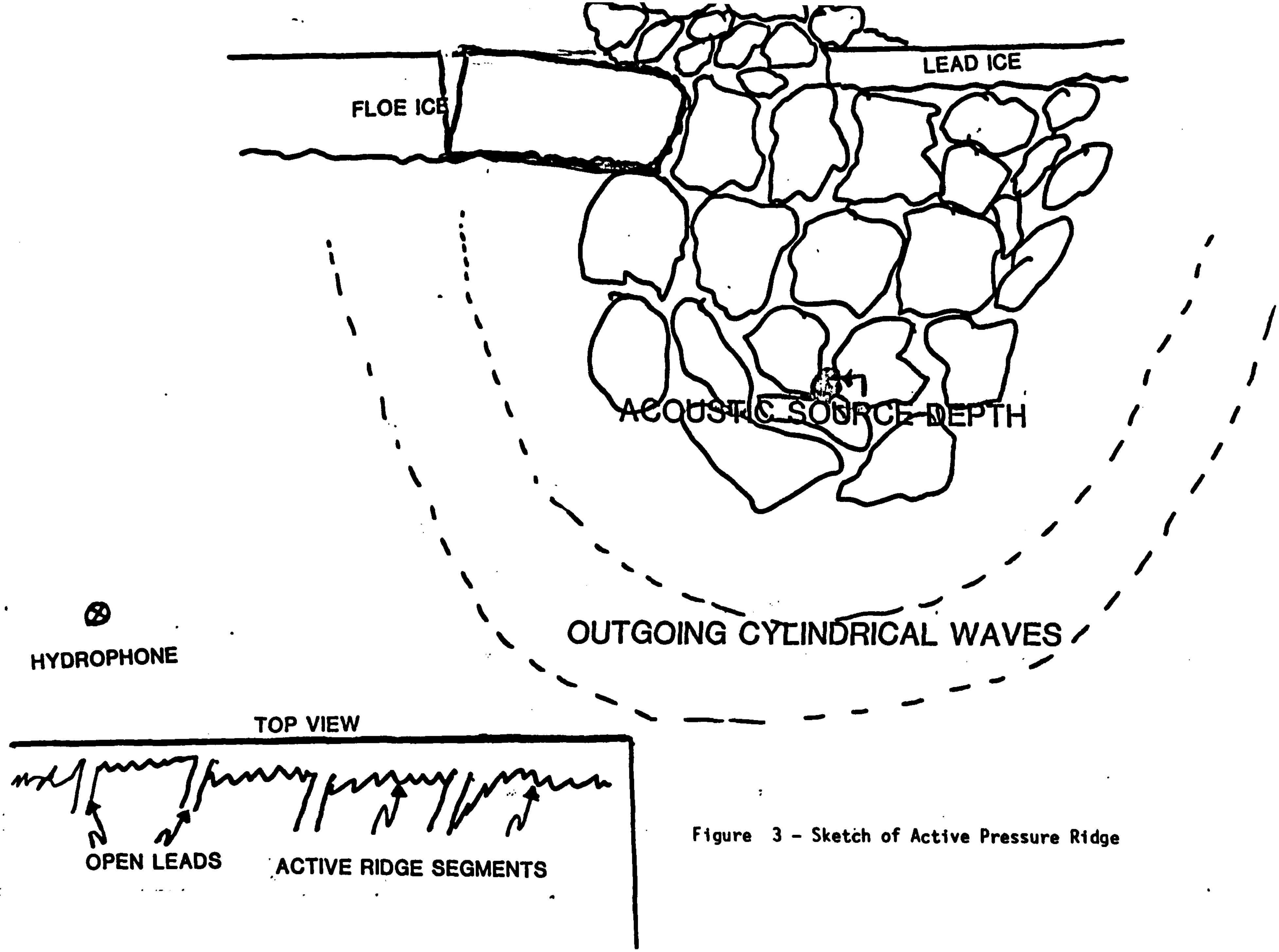

Figure 3 - Sketch of Active Pressure Ridge

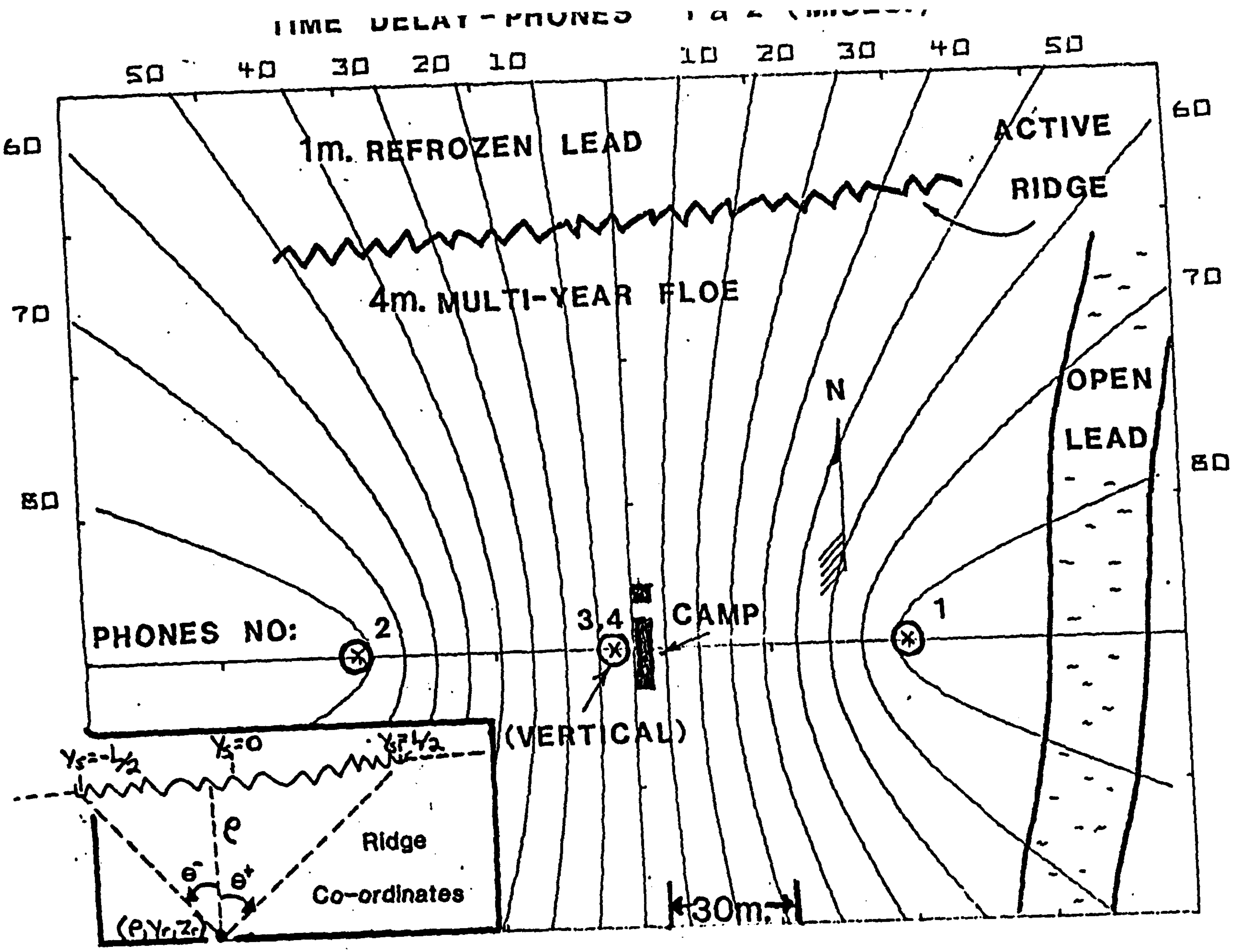

Figure 2 - Plan View of the Experiment

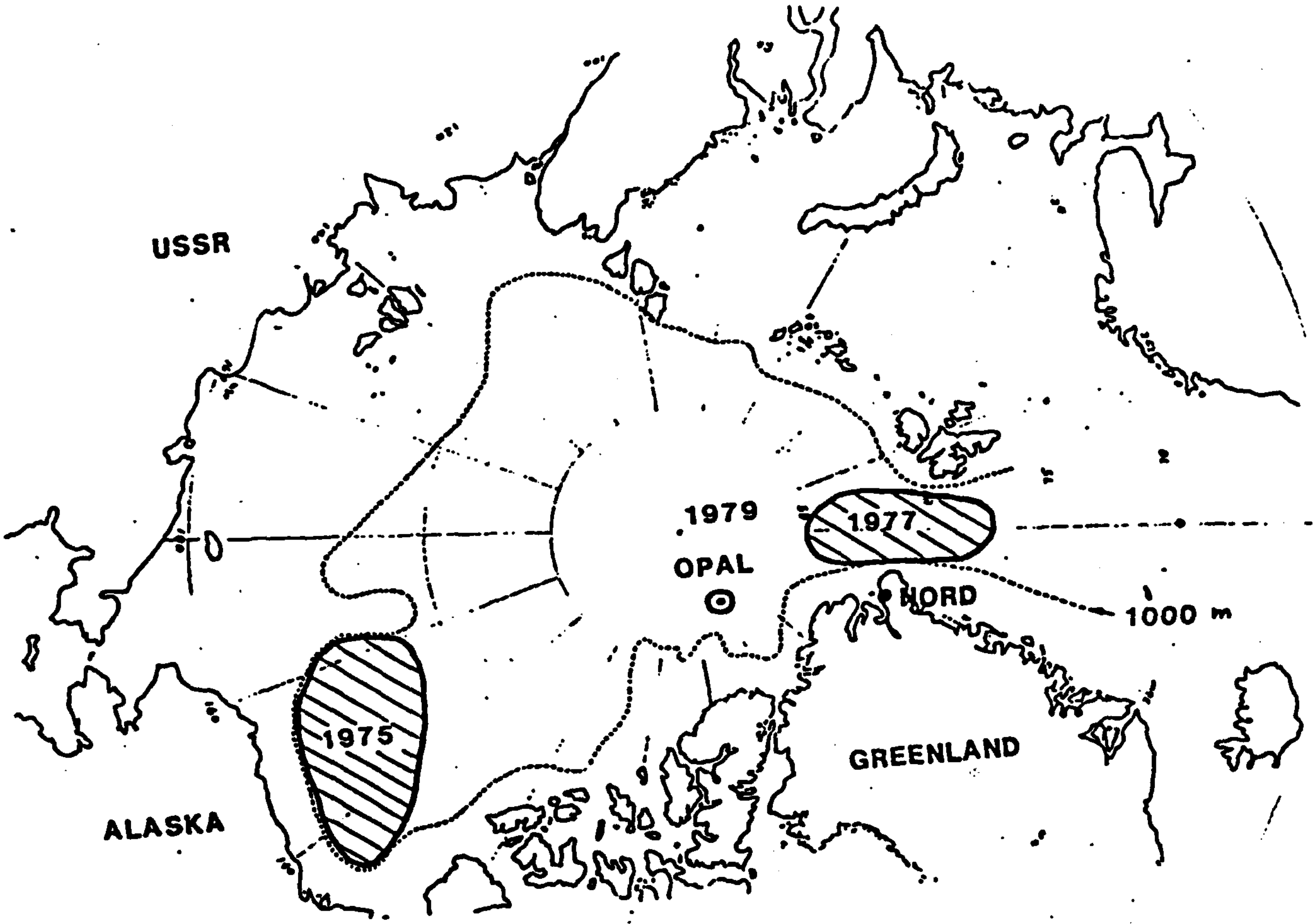

Figure 1 - Ice Camp Location

Jim Wilson

Active Ice Ridge Ambient Noise Levels

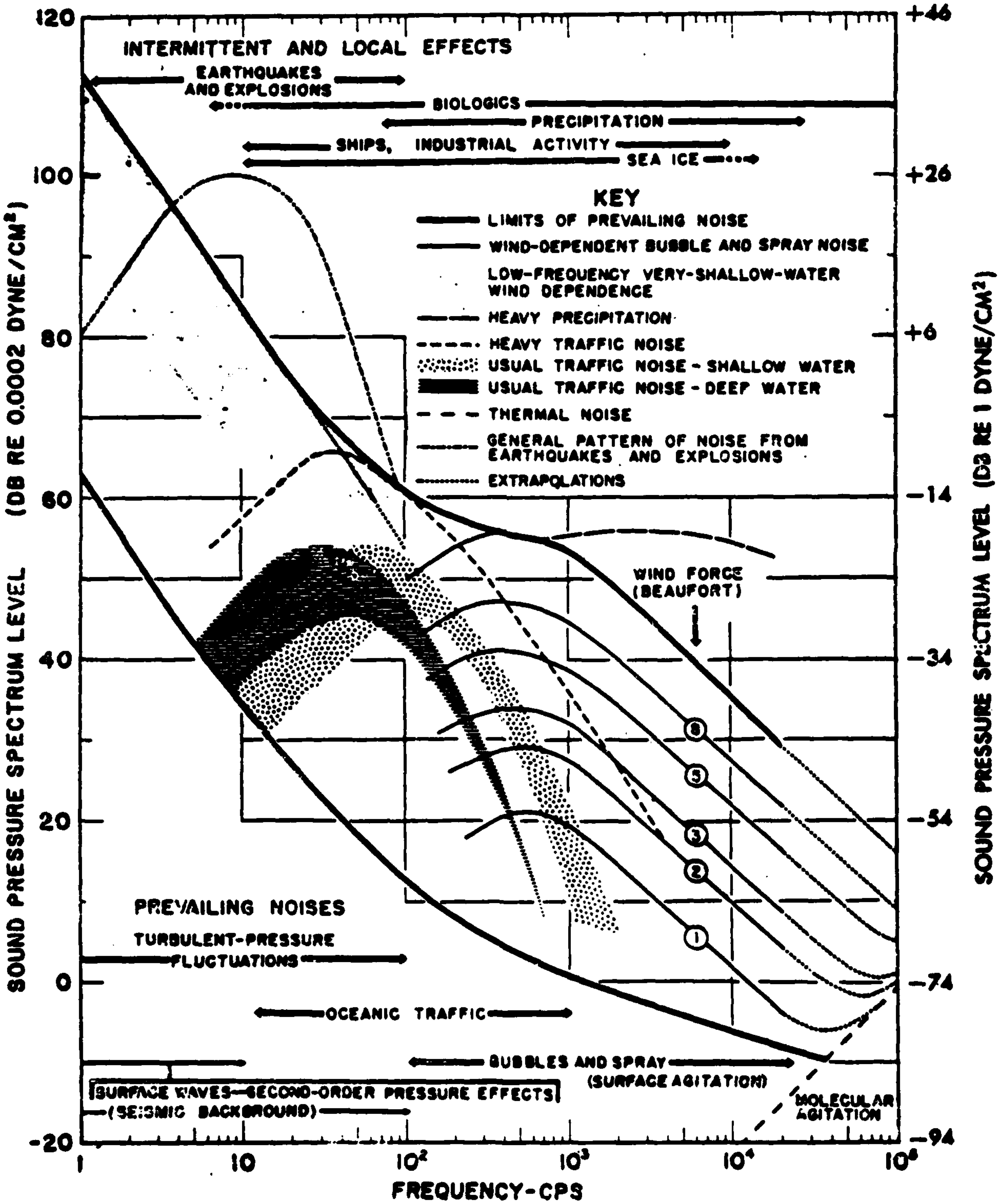
INTERMITTENT AND LOCAL EFFECTS
EARTHQUAKES AND EXPLOSIONS
BIOLOGICS
PRECIPITATION
SHIPS, INDUSTRIAL ACTIVITY
SEA ICE
KEY
LIMITS OF PREVAILING NOISE
WIND-DEPENDENT BUBBLE AND SPRAY NOISE
LOW-FREQUENCY VERY-SHALLOW-WATER WIND DEPENDENCE
HEAVY PRECIPITATION
HEAVY TRAFFIC NOISE
USUAL TRAFFIC NOISE - SHALLOW WATER
USUAL TRAFFIC NOISE - DEEP WATER
THERMAL NOISE
GENERAL PATTERN OF NOISE FROM EARTHQUAKES AND EXPLOSIONS
EXTRAPOLATIONS
WIND FORCE (BEAUFORT)
8
5
3
2
1
PREVAILING NOISES
TURBULENT-PRESSURE FLUCTUATIONS
OCEANIC TRAFFIC
BUBBLES AND SPRAY (SURFACE AGITATION)
SURFACE WAVES—SECOND-ORDER PRESSURE EFFECTS
(SEISMIC BACKGROUND)
MOLECULAR AGITATION
SOUND PRESSURE SPECTRUM LEVEL (DB RE 0.0002 DYNE/CM²)
SOUND PRESSURE SPECTRUM LEVEL (DB RE 1 DYNE/CM²)
FREQUENCY-CPS
120
100
80
60
40
20
0
-20
+46
+26
+6
-14
-34
-54
-74
-94
1
10
10²
10³
10⁴
10⁵

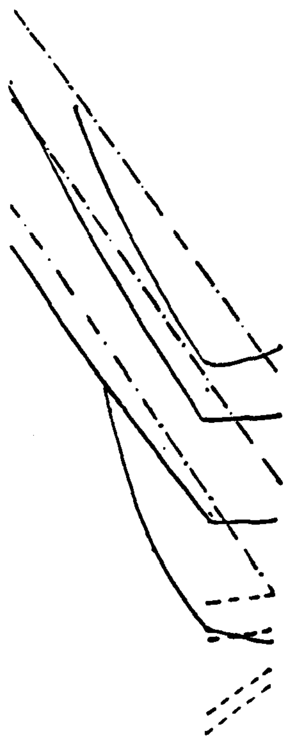

CONCLUSIONS

- In deep water areas shipping is usually dominant in the 10-20 Hz band
- Below about 4 Hz the sharp increase in noise levels appears to be caused by microseisms
- Difficult to assign generation mechanisms for the hydrodynamic component of VLF noise
- No convincing comparisons between measurement and theory
- Noise levels in the 4-10 Hz band are comparable to levels in the 10-20 Hz band
- No predictive capability

Nonacoustic Noise Interference in Measurements of Infrasonic Ambient Noise (Strassberg, 1979).

Mechanisms

Hydrophone response to temperature inhomogeneities

Turbulence generated by flow past hydrophone

- Interaction between hydrophone and turbulence

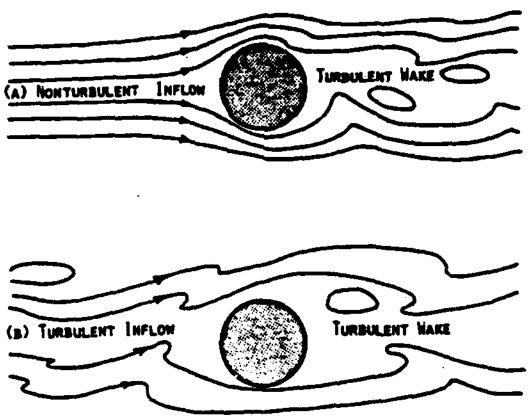

$$L(f) = 119 + 37\log_{10}U_0 - 27\log_{10}f$$

$$U_0(\mathrm{kt}),\ f(\mathrm{Hz})$$

Wind Component of VLF Noise

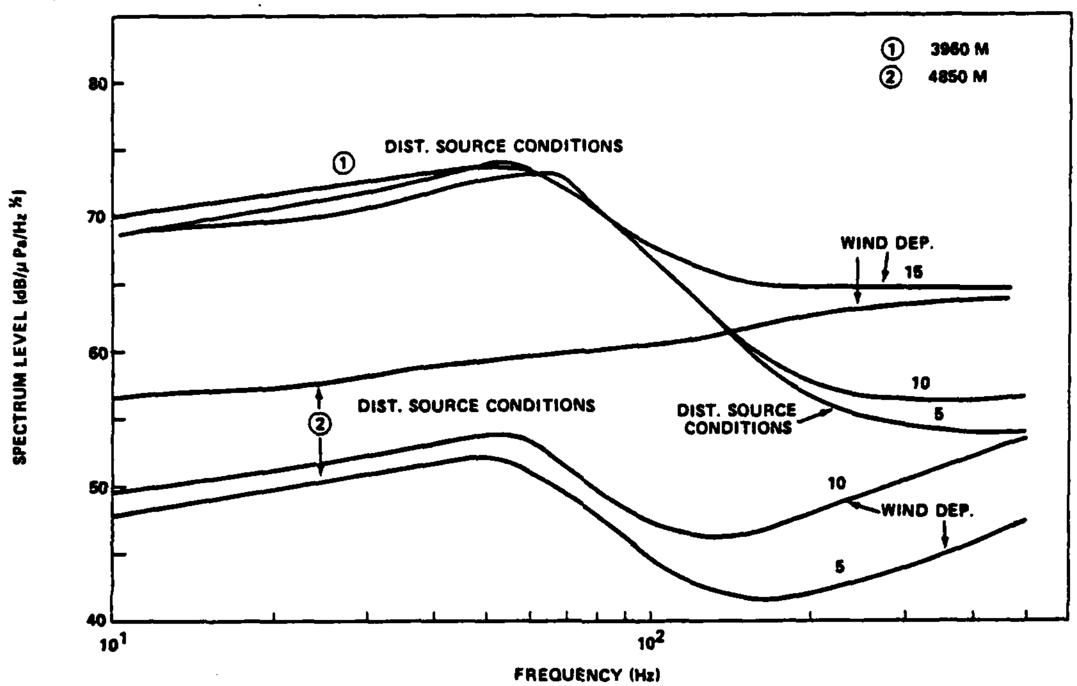

Dependence of the non-shipping component of VLF ambient noise upon wind speed (from Wittenborn, 1976).

VLF Sound Radiation by Merchant Ships

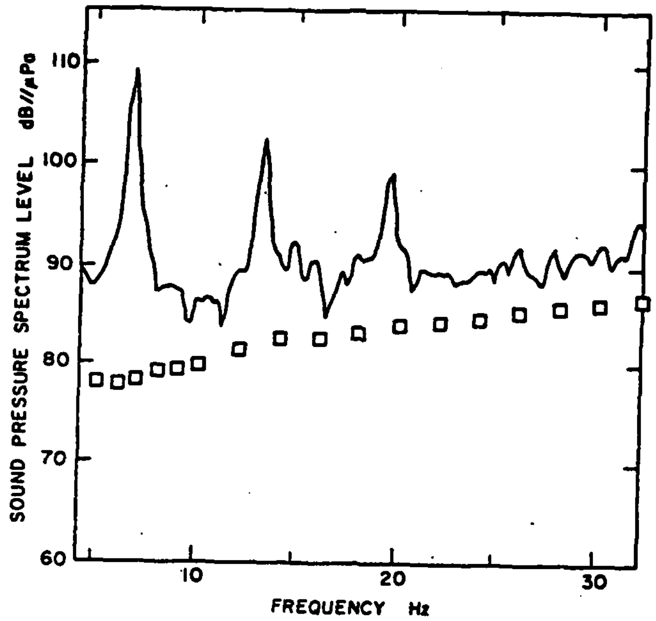

Radiated noise spectrum of the HAYES (from McGrath, 1976).

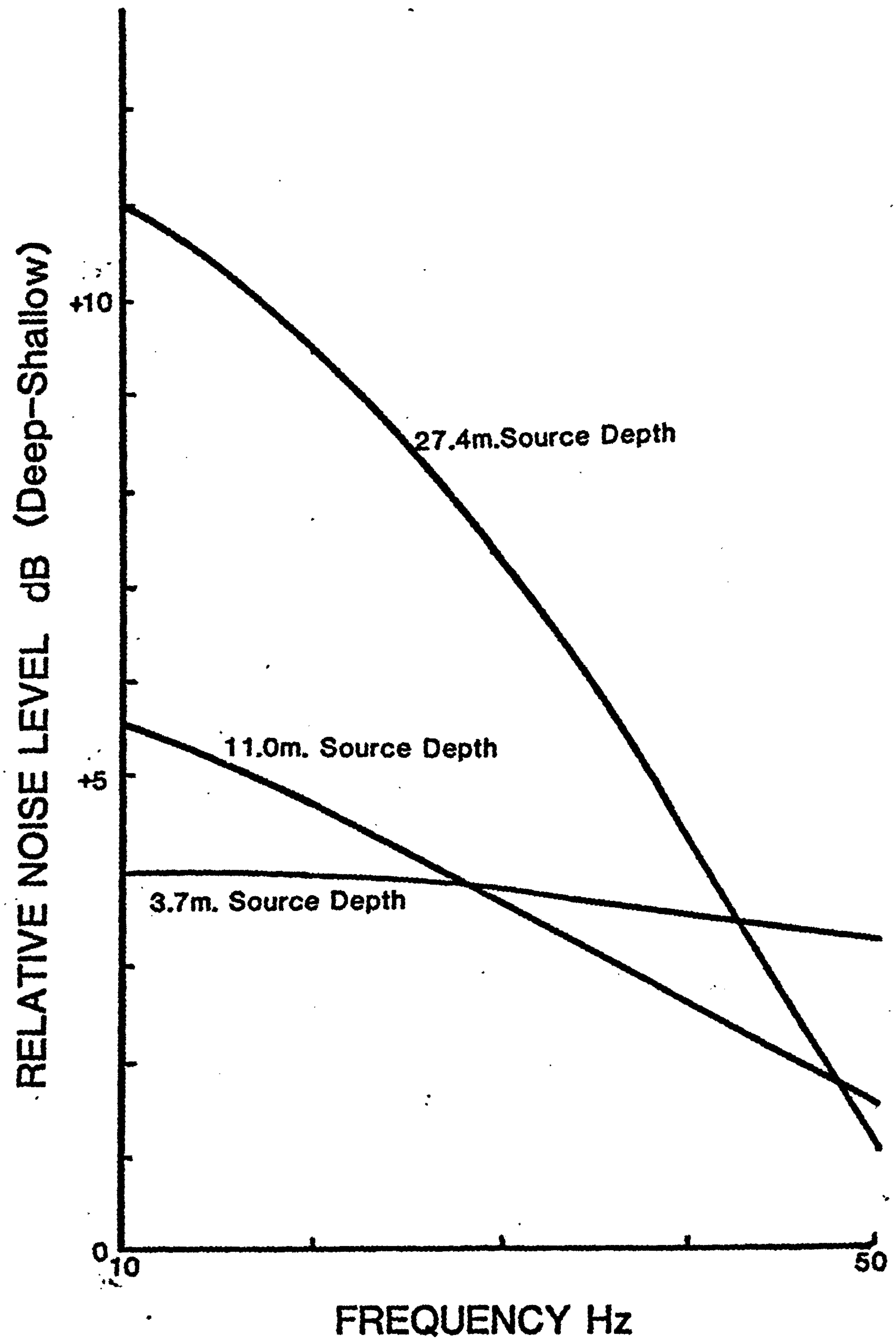

Figure 8 - Receiver Depth Dependence Predicted by FACT for Various Source Depths.

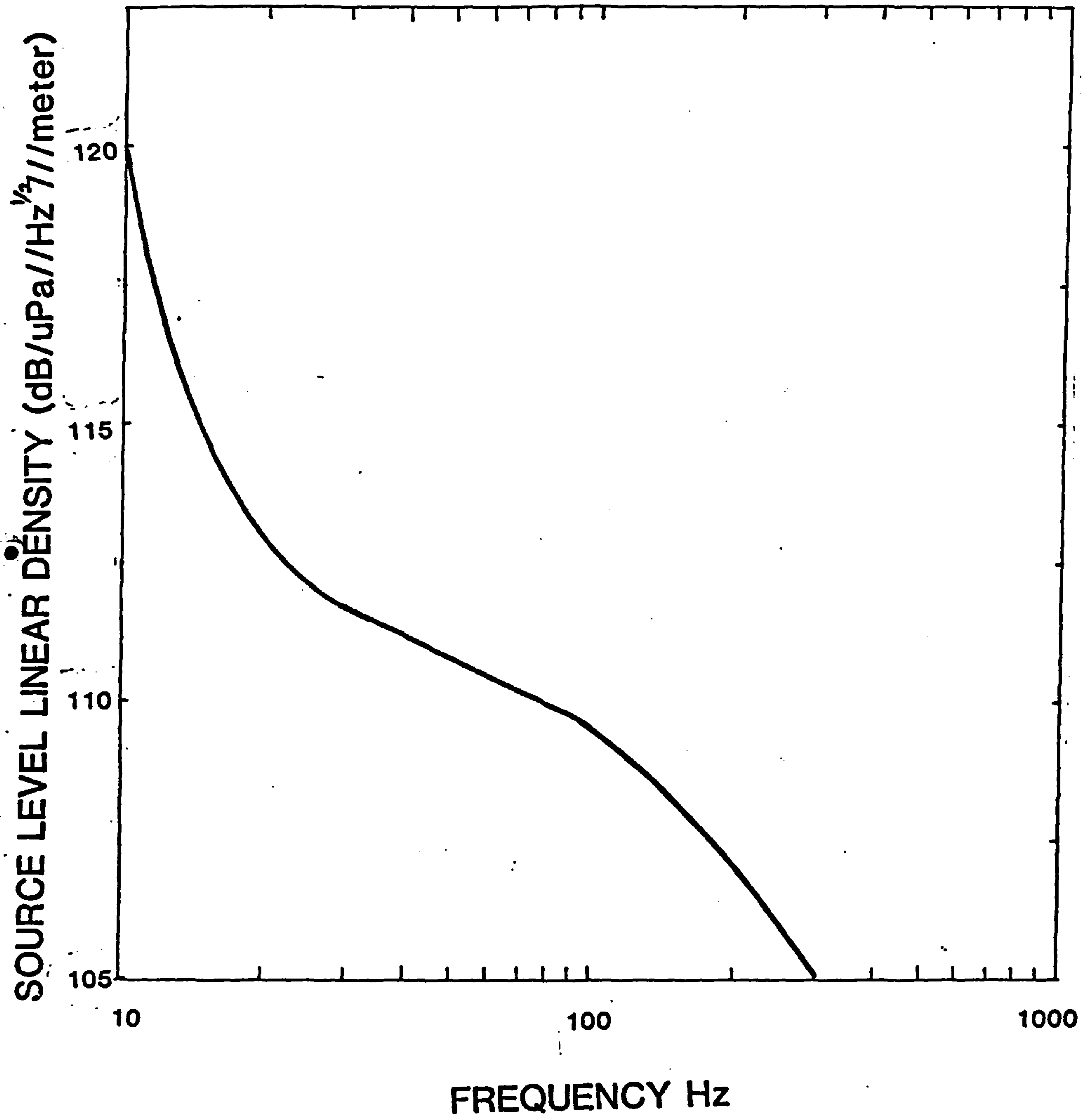

Figure 9 - Source Level Linear Density for an Active Pressure Ridge.

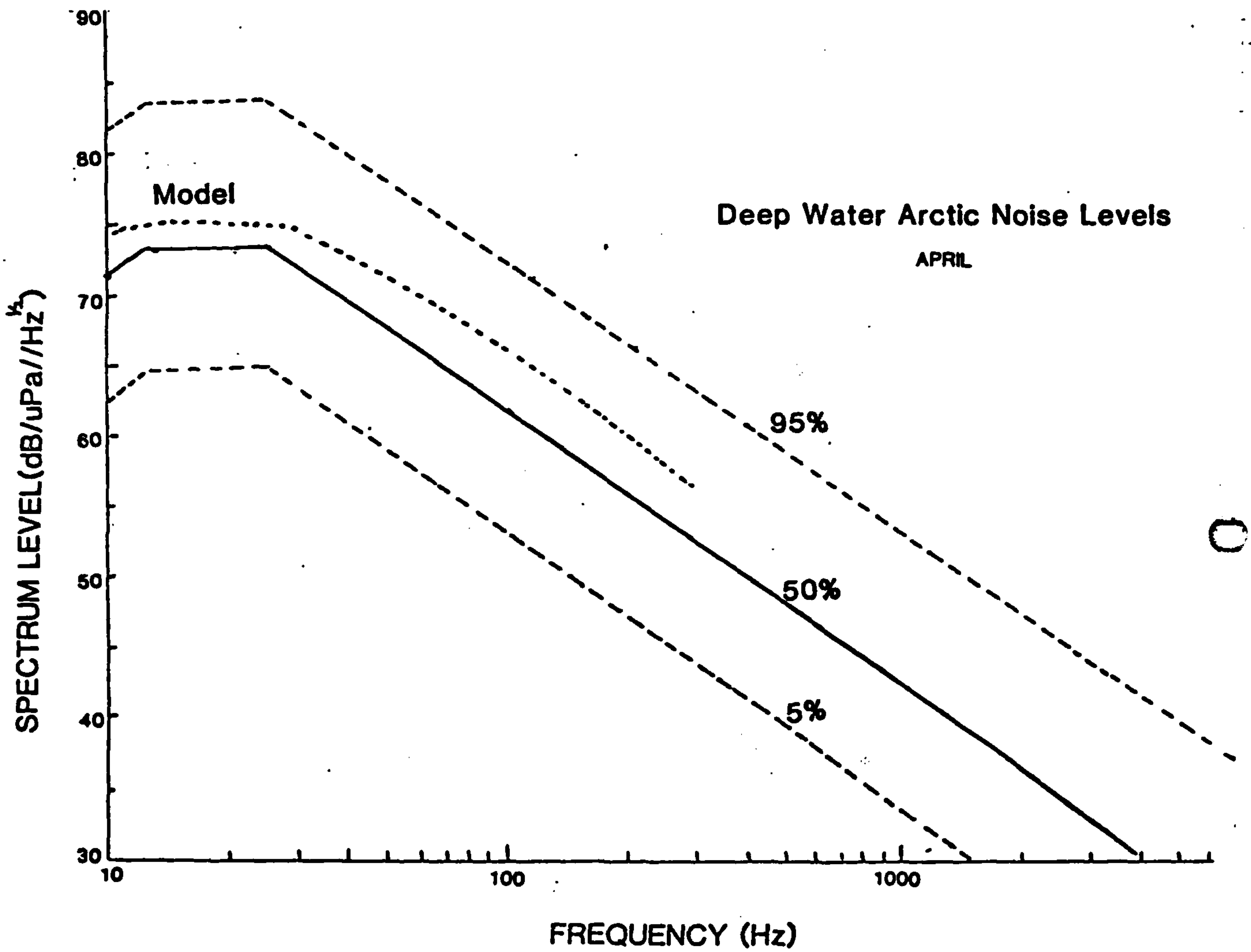

Figure 10 - Comparison of Estimated Noise Spectra and Measured Noise Spectra in the Beaufort Sea

VLF WORKSHOP
24,25 JANUARY 1985

John Orcutt
Rick Adair
Tom Sereno
Peter Shearer

- Seafloor and subseafloor noise
- Signal comparisons on seafloor and subseafloor inertial and hydrophone instruments at various phase velocities
- Propagation of seismic/acoustic signals over large ranges (P_n, S_n, T)

RESULTS

- Subseafloor noise levels as much as 20 db lower than seafloor noise levels.

- Seafloor noise levels consistent with many previous acoustics measurements.

- Seafloor noise at low frequencies, and high frequencies in the presence of shipping, is coherent over baselines of at least 700 m.

- Seafloor noise dominated, to 4-5 Hz, by interaction of surface gravity waves.

- Seafloor noise above 5 Hz likely controlled by shipping.

- Horizontal noise at seafloor generally greater than vertical noise. The levels are equal at subseafloor receivers.

- Signal levels at subseafloor sites are comparable in size to seafloor sites. Signal to noise ratios increase with burial of sensor.

- P_n, S_n, T phases can be synthesized by wave propagation in a laterally homogeneous medium with no inter-lithosphere waveguides.

- Slow decay of P_n, S_n, T phases with range depends upon the high Q ocean and not upon a high Q within the crust and lithosphere.

- Scattering plays a minor role in the formation of long P_n, S_n, T wavetrains.

- The character of the P_n, S_n, T wavetrain is controlled by the thickness of the water and sediment columns.

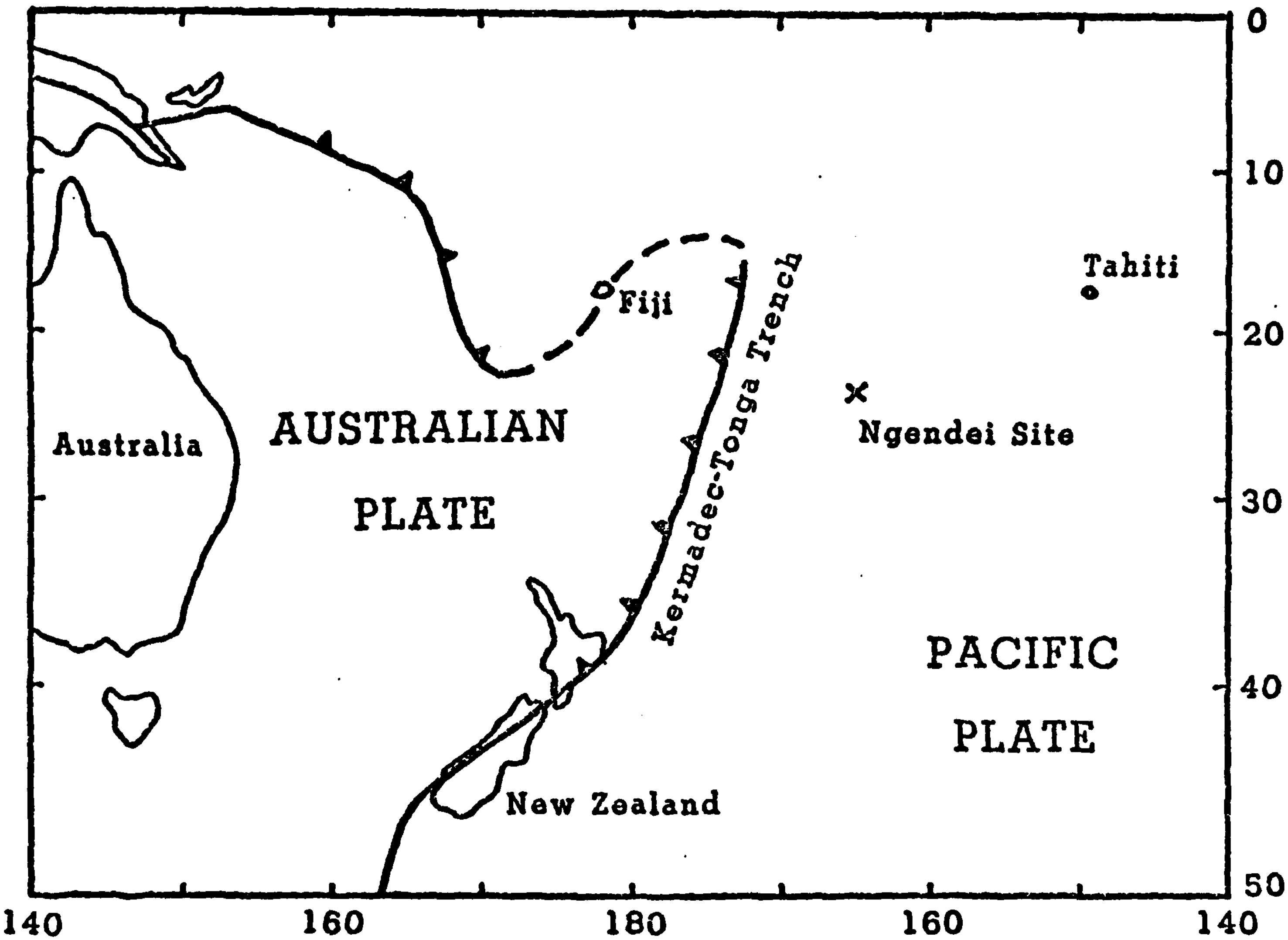

0
10
20
30
40
50
140
160
180
160
140
Tahiti
Fiji
Ngendei Site
Kermadec-Tonga Trench
AUSTRALIAN
PLATE
Australia
PACIFIC
PLATE
New Zealand

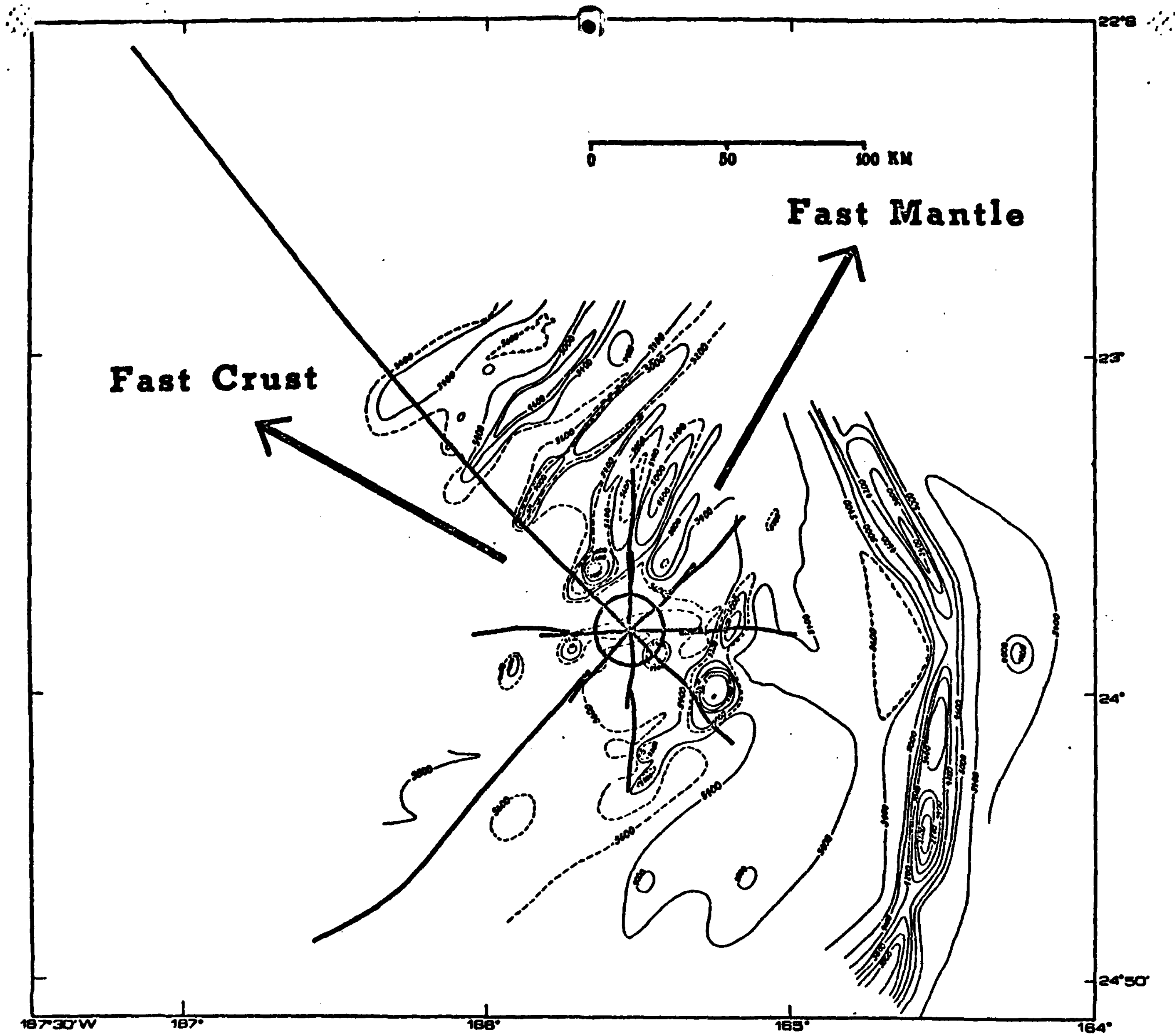
Fast Mantle
Fast Crust
0
50
100 KM
22°8
23°
24°
24°50'
167°30'W
167°
166°
165°
164°

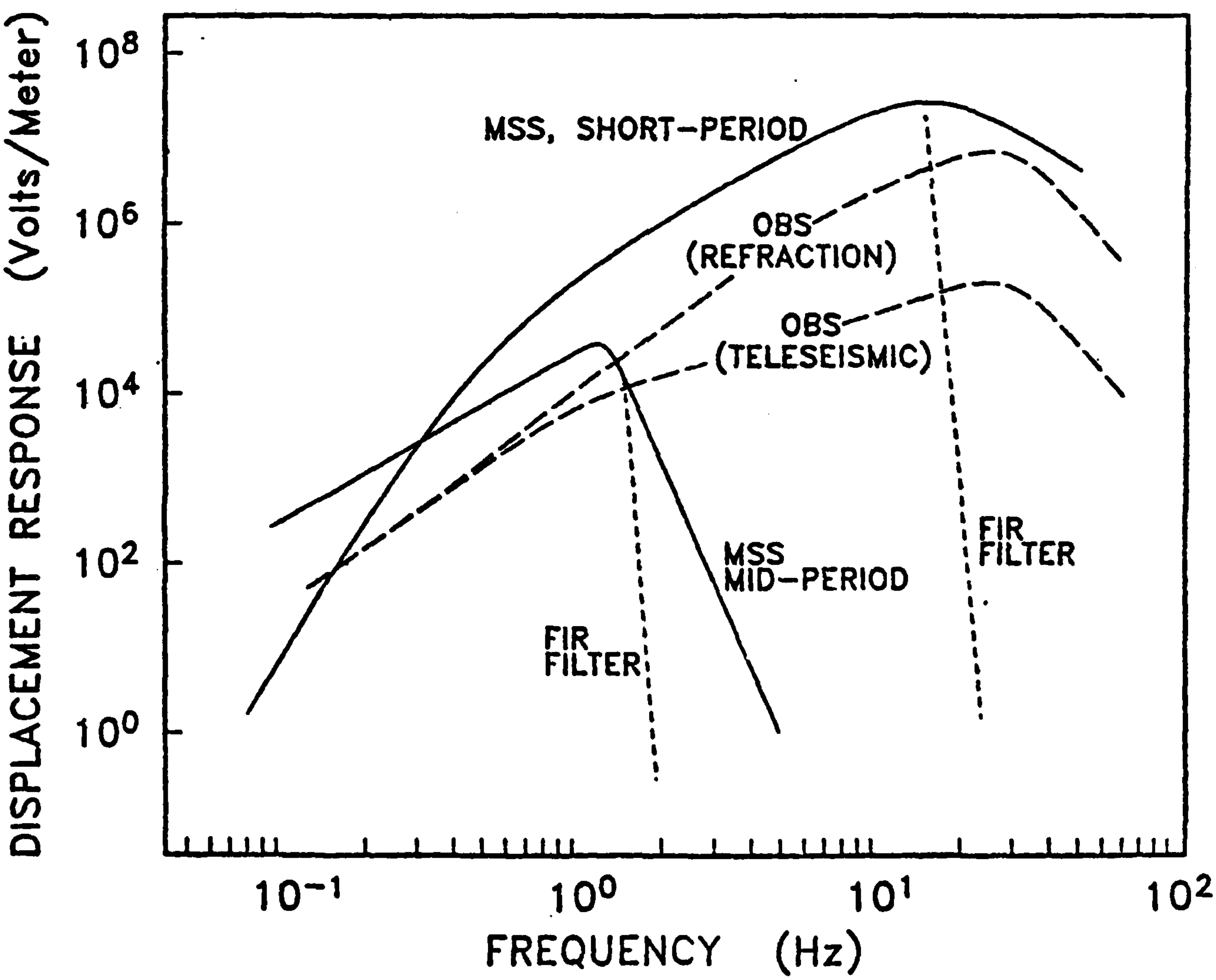

DISPLACEMENT RESPONSE (Volts/Meter)
10^8
10^6
10^4
10^2
10^0
MSS, SHORT-PERIOD
OBS (REFRACTION)
OBS (TELESEISMIC)
MSS MID-PERIOD
FIR FILTER
FIR FILTER
10^{-1}
10^0
10^1
10^2
FREQUENCY (Hz)

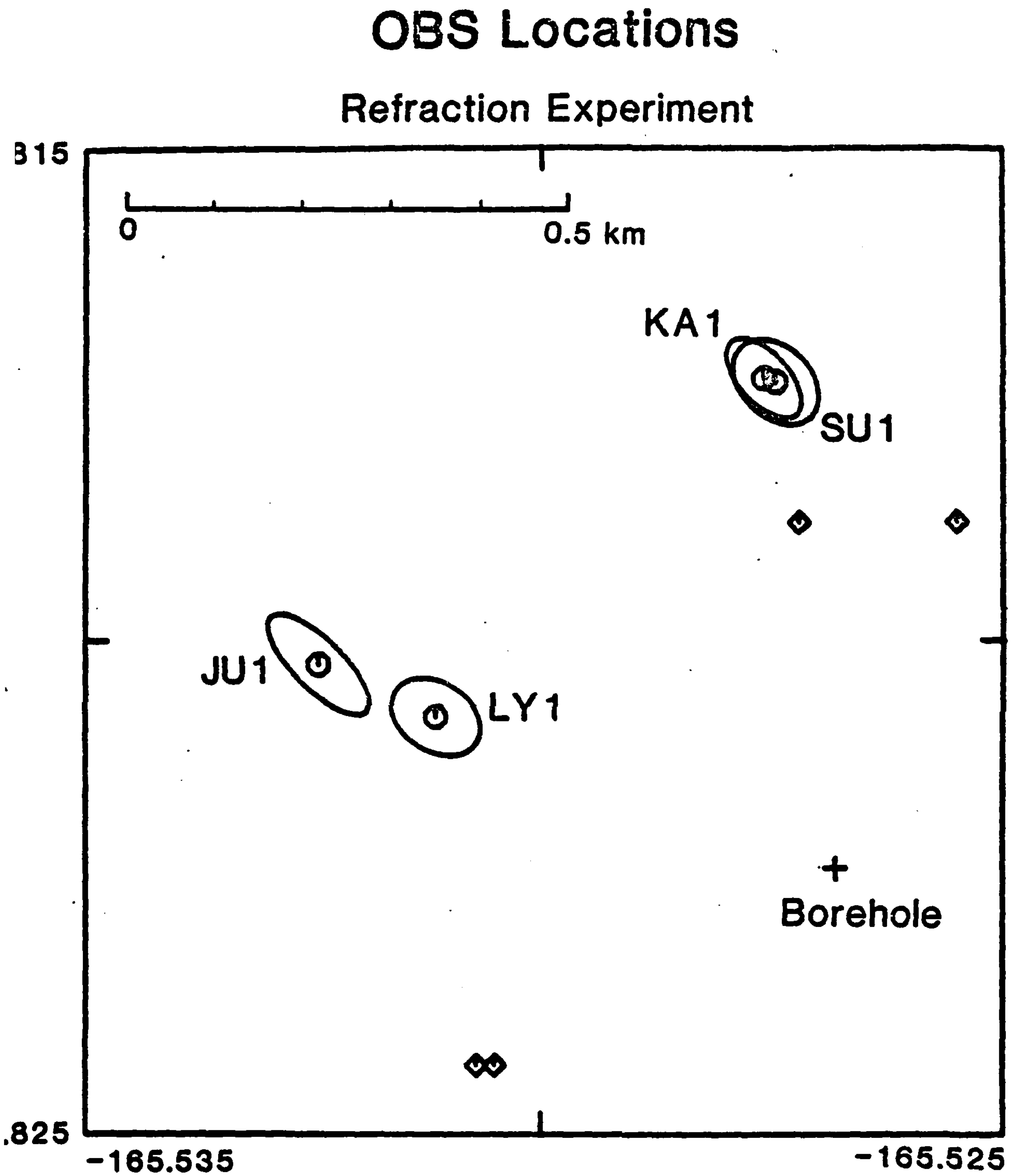

OBS Locations
Refraction Experiment
815
.825
0
0.5 km
KA1
SU1
JU1
LY1
Borehole
-165.535
-165.525

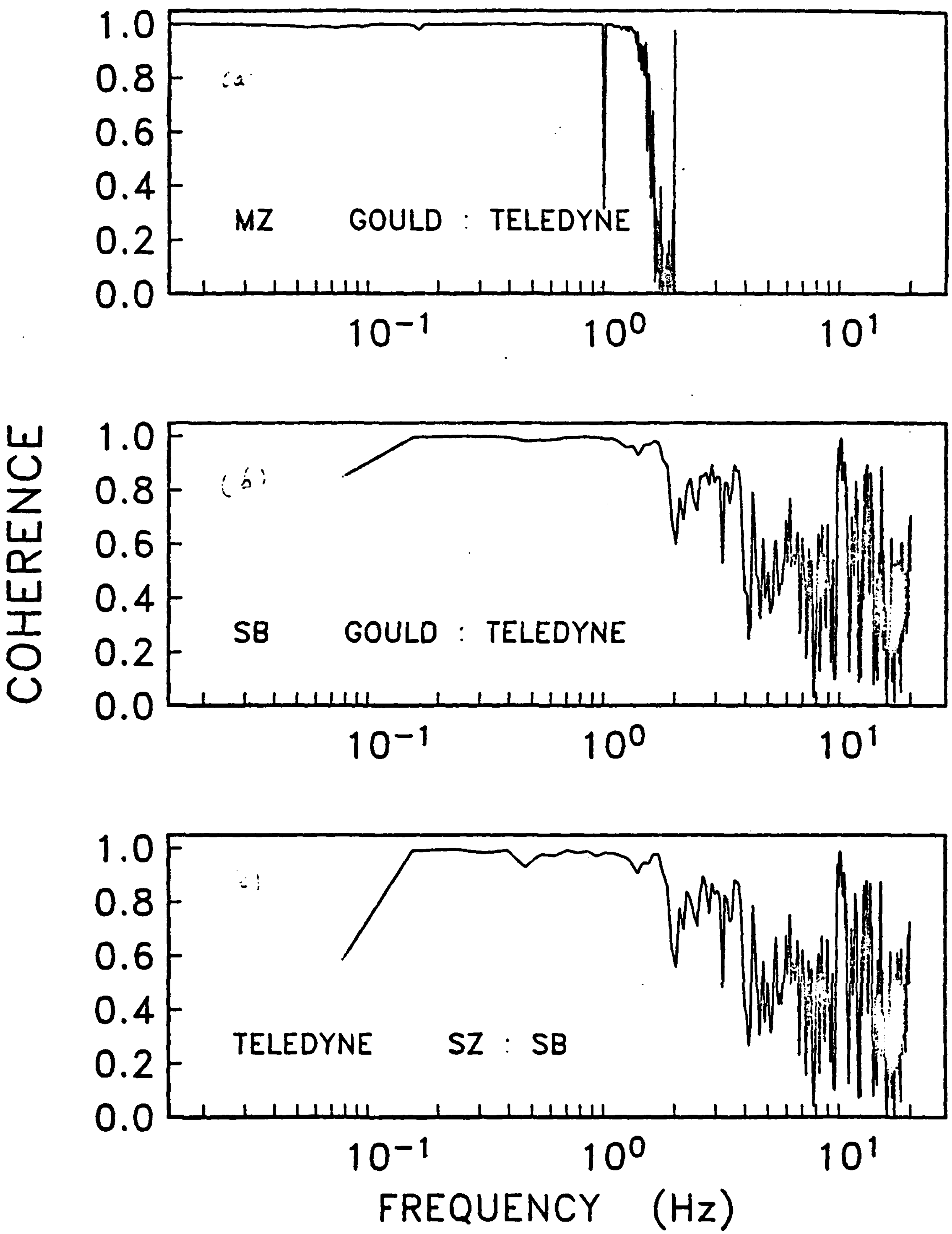

COHERENCE
1.0
0.8
0.6
0.4
0.2
0.0
(a)
MZ GOULD : TELEDYNE
(b)
SB GOULD : TELEDYNE
(c)
TELEDYNE SZ : SB
10^{-1}
10^{0}
10^{1}
FREQUENCY (Hz)

SHIP NOISE

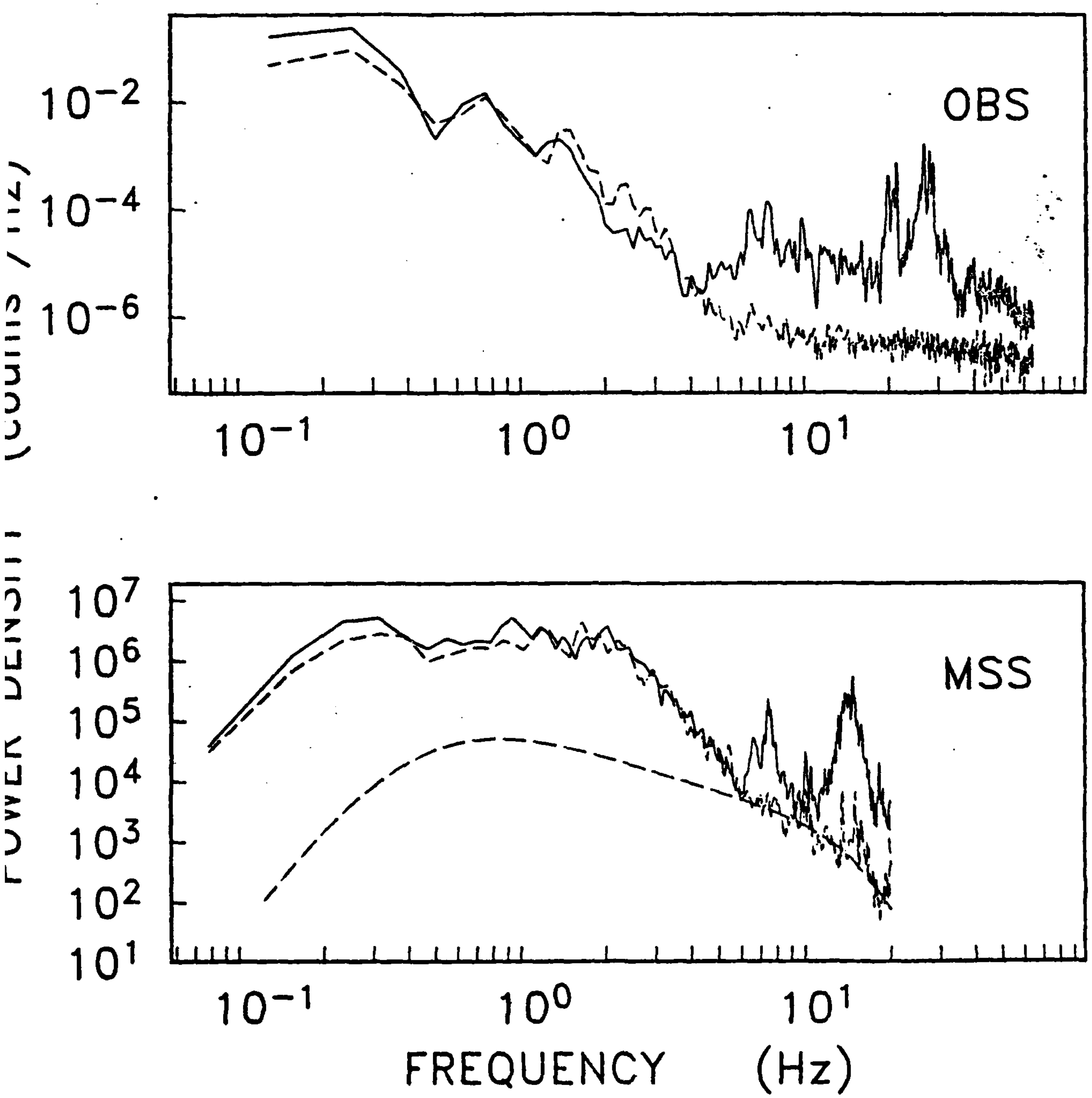

OBS
MSS
10−2
10−4
10−6
10⁷
10⁶
10⁵
10⁴
10³
10²
10¹
10−1
10⁰
10¹
FREQUENCY (Hz)

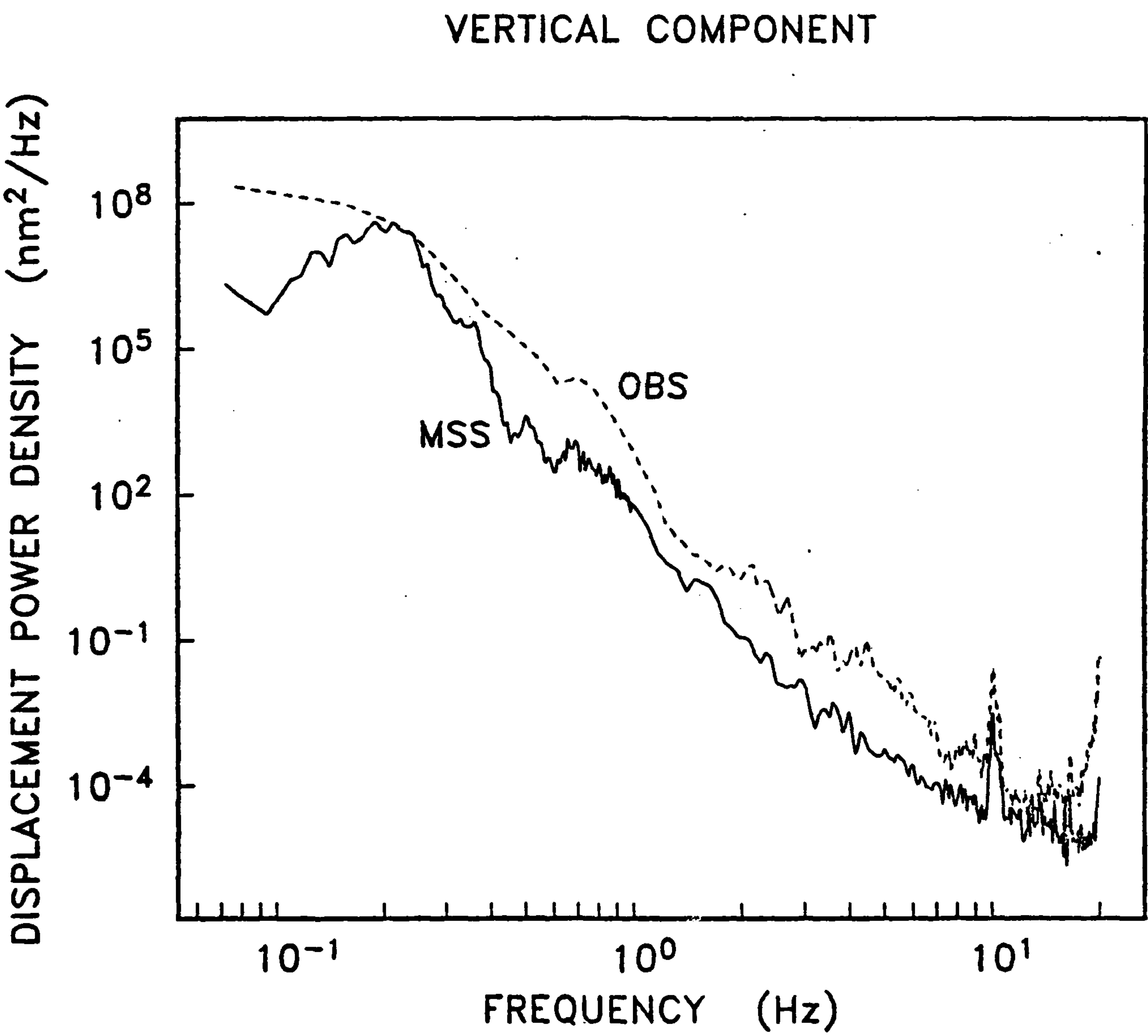
VERTICAL COMPONENT
DISPLACEMENT POWER DENSITY (nm²/Hz)
10⁸
10⁵
10²
10⁻¹
10⁻⁴
OBS
MSS
10⁻¹
10⁰
10¹
FREQUENCY (Hz)

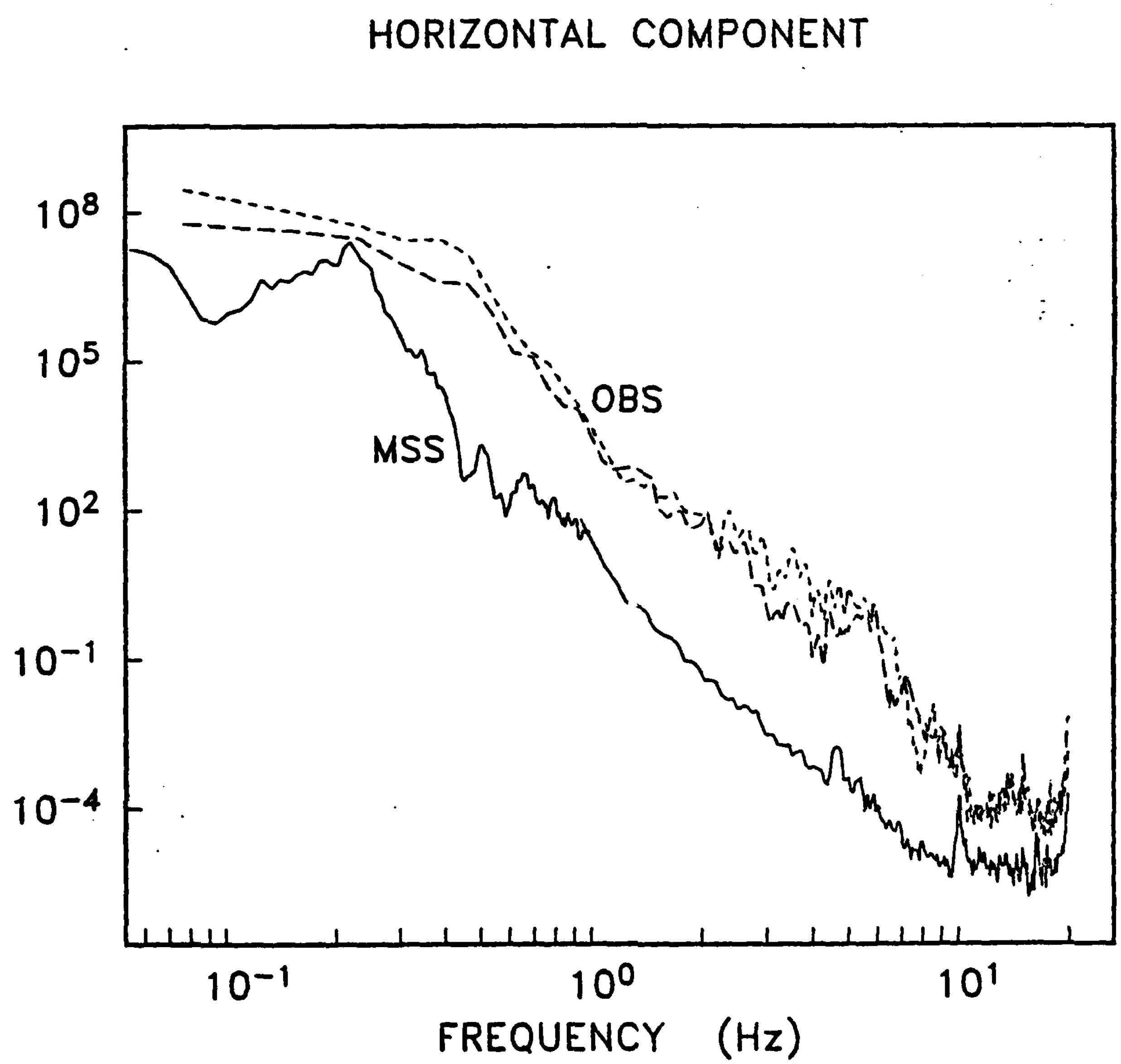
HORIZONTAL COMPONENT
10^8
10^5
10^2
10^{-1}
10^{-4}
OBS
MSS
10^{-1}
10^0
10^1
FREQUENCY (Hz)

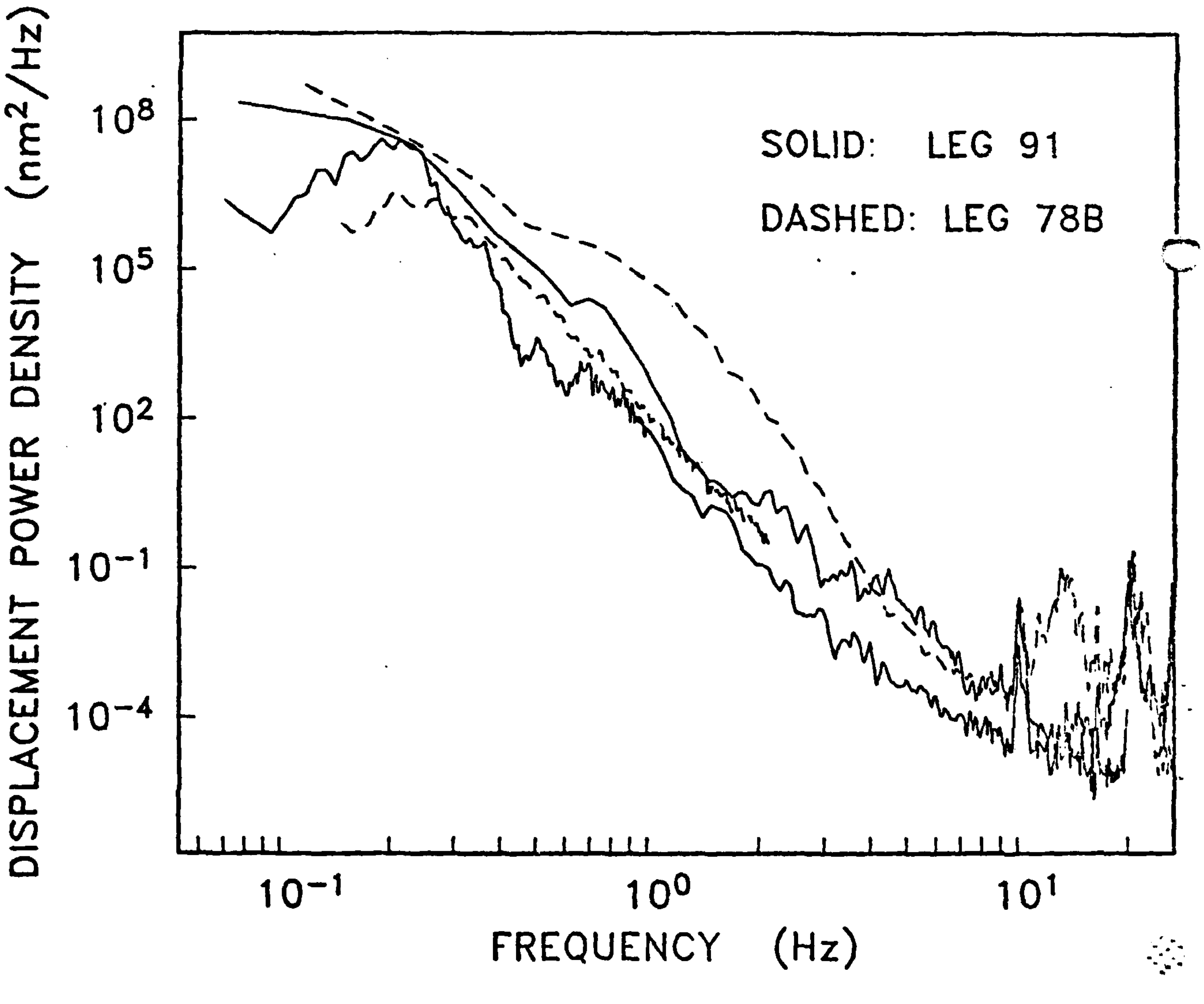

DISPLACEMENT POWER DENSITY (nm²/Hz)
10^8
10^5
10^2
10^{-1}
10^{-4}
SOLID: LEG 91
DASHED: LEG 78B
10^{-1}
10^0
10^1
FREQUENCY (Hz)

MSS (dashed) vs. OBS (solid)

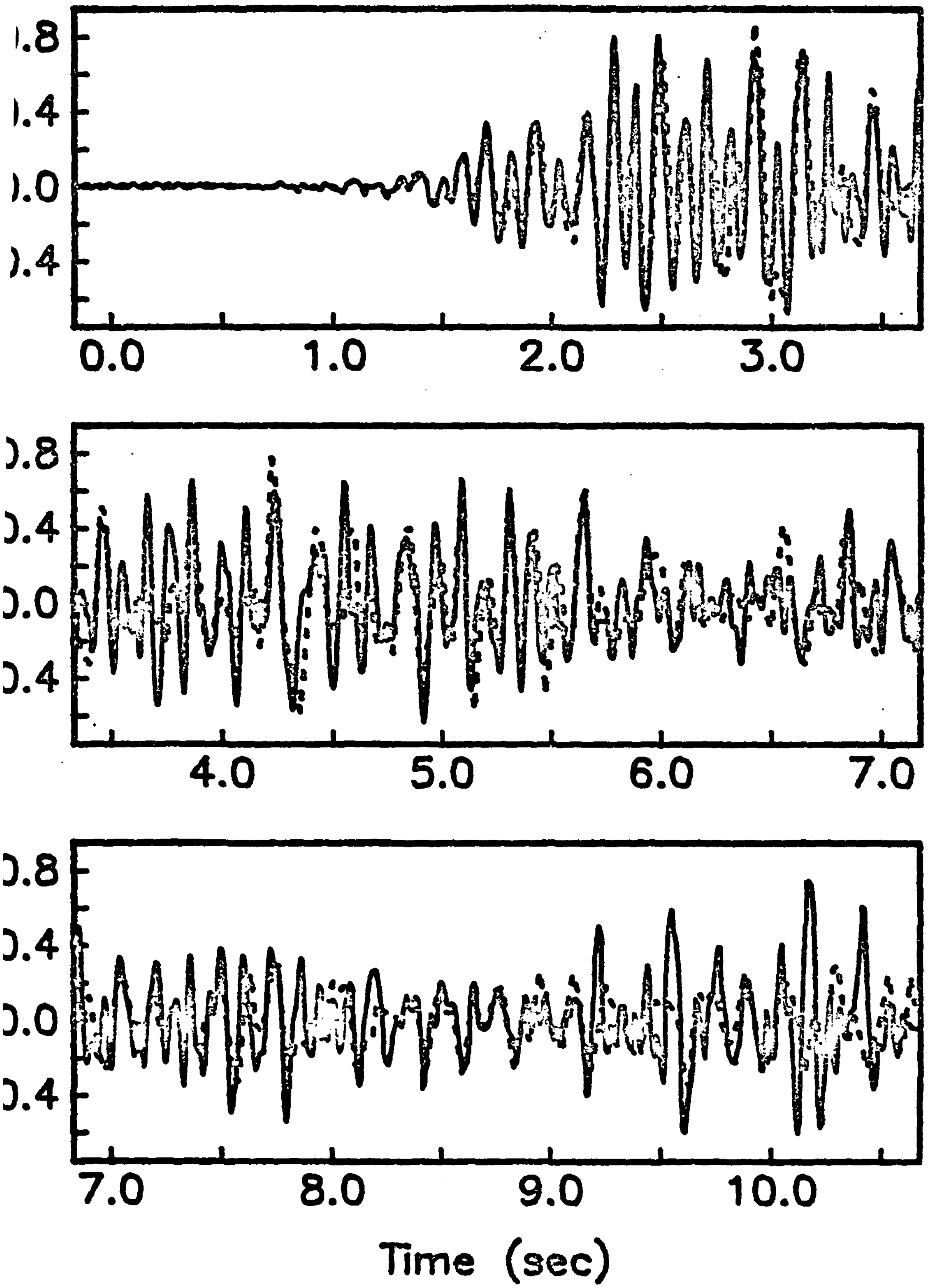

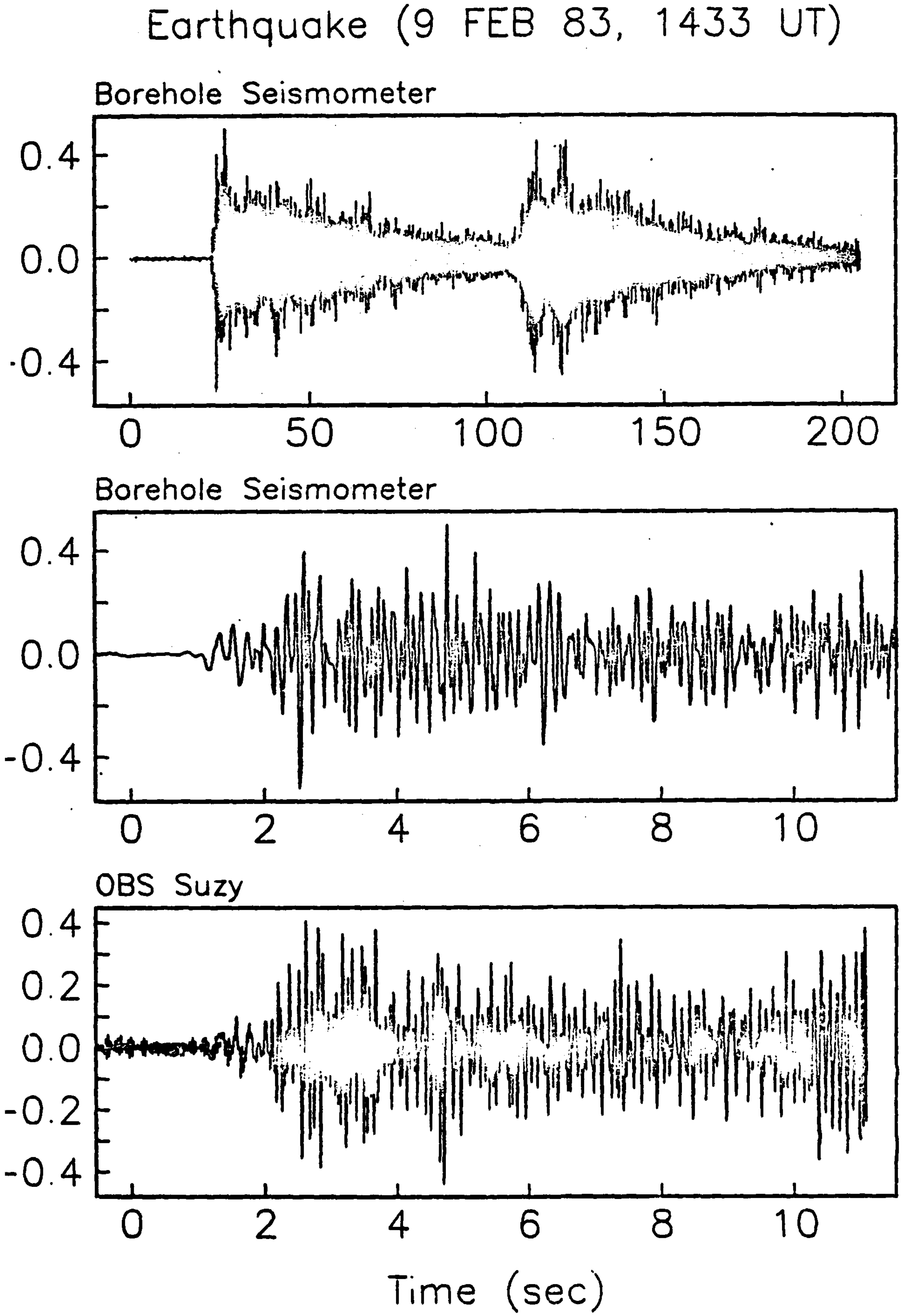

Earthquake (9 FEB 83, 1433 UT)
Borehole Seismometer
0.4
0.0
-0.4
0
50
100
150
200
Borehole Seismometer
0.4
0.0
-0.4
0
2
4
6
8
10
OBS Suzy
0.4
0.2
0.0
-0.2
-0.4
0
2
4
6
8
10
Time (sec)

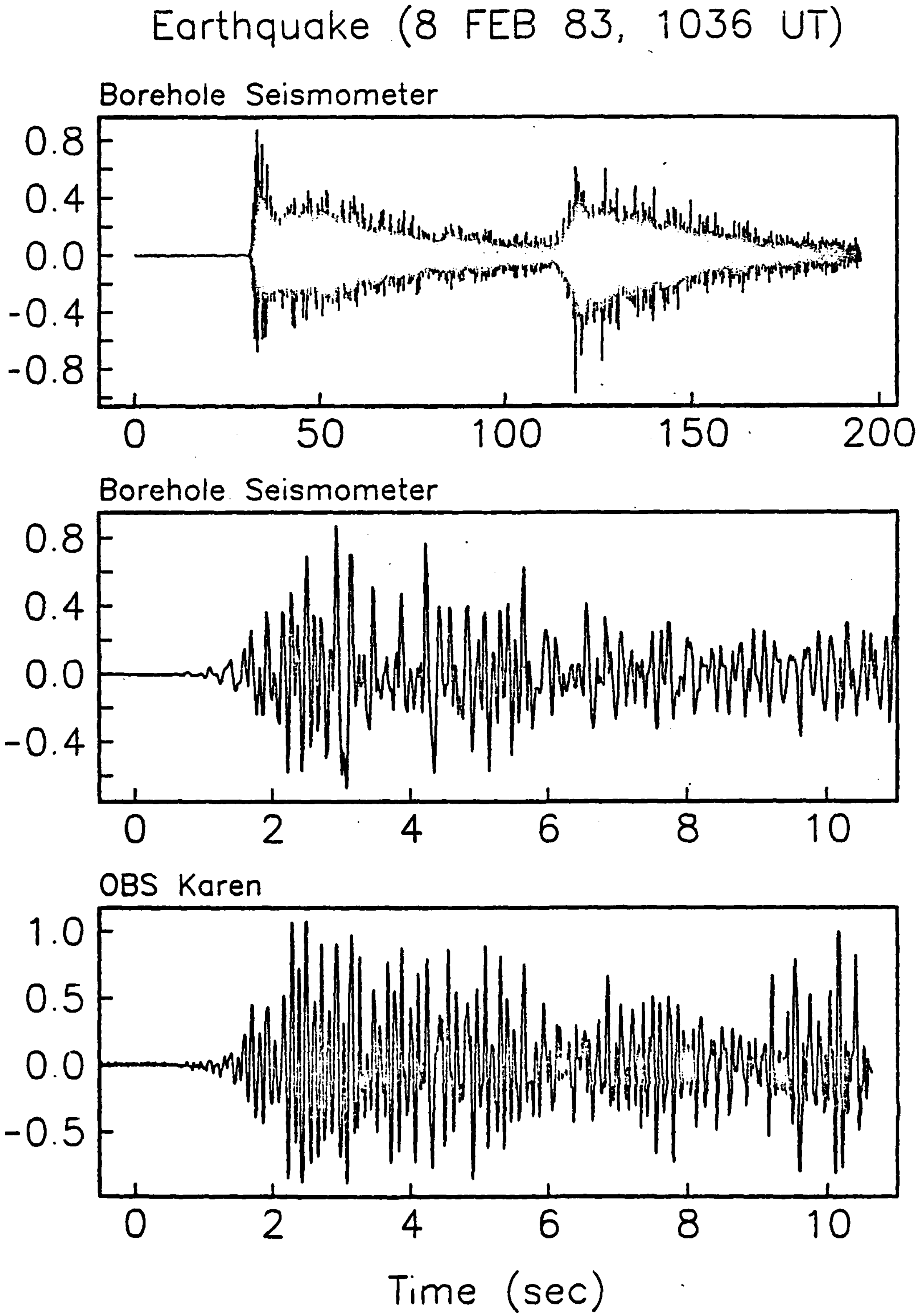

Earthquake (8 FEB 83, 1036 UT)
Borehole Seismometer
0.8
0.4
0.0
-0.4
-0.8
0
50
100
150
200
Borehole Seismometer
0.8
0.4
0.0
-0.4
0
2
4
6
8
10
OBS Karen
1.0
0.5
0.0
-0.5
0
2
4
6
8
10
Time (sec)

OBS Karen (solid) vs. MSS (dashed)

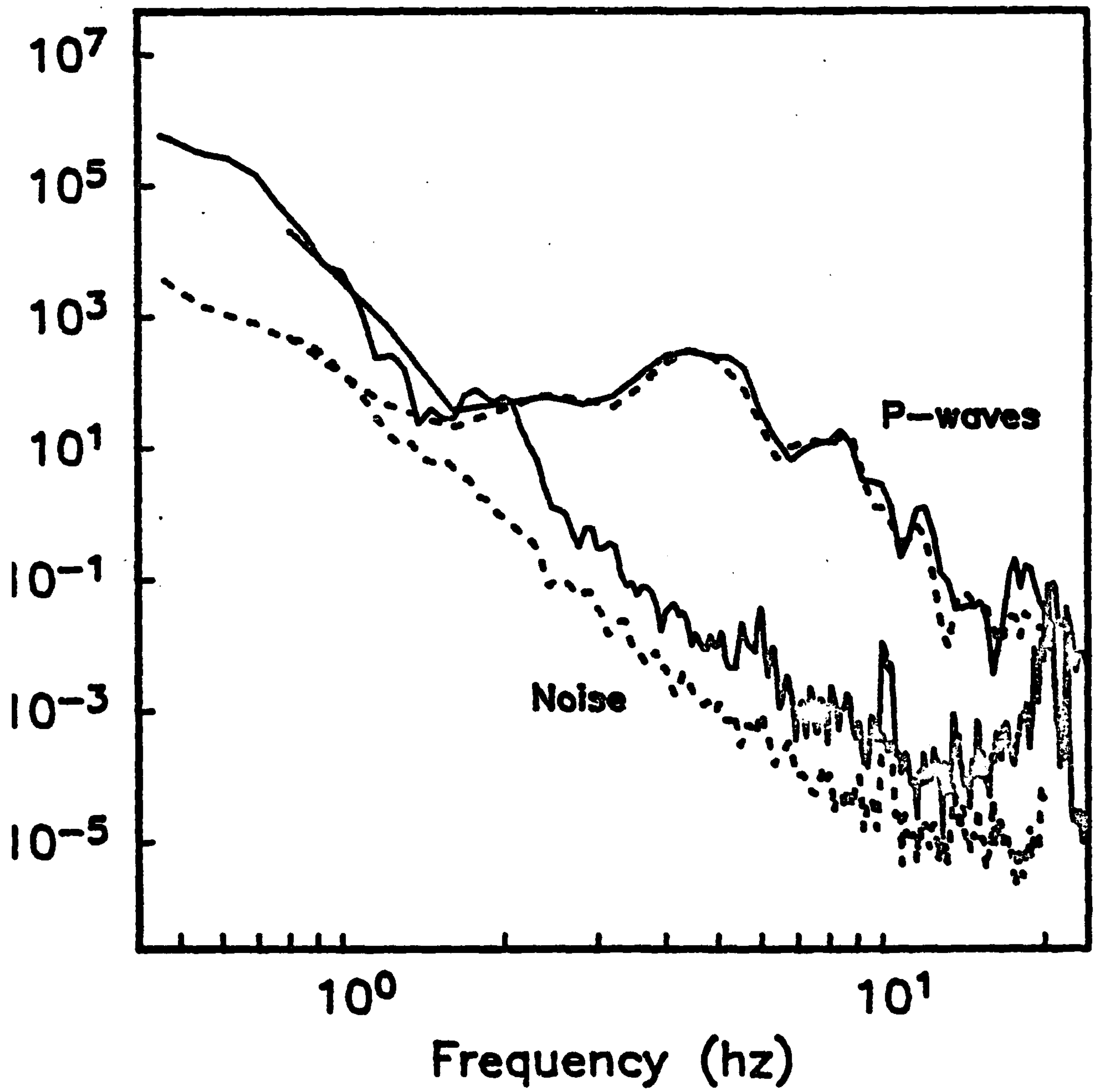

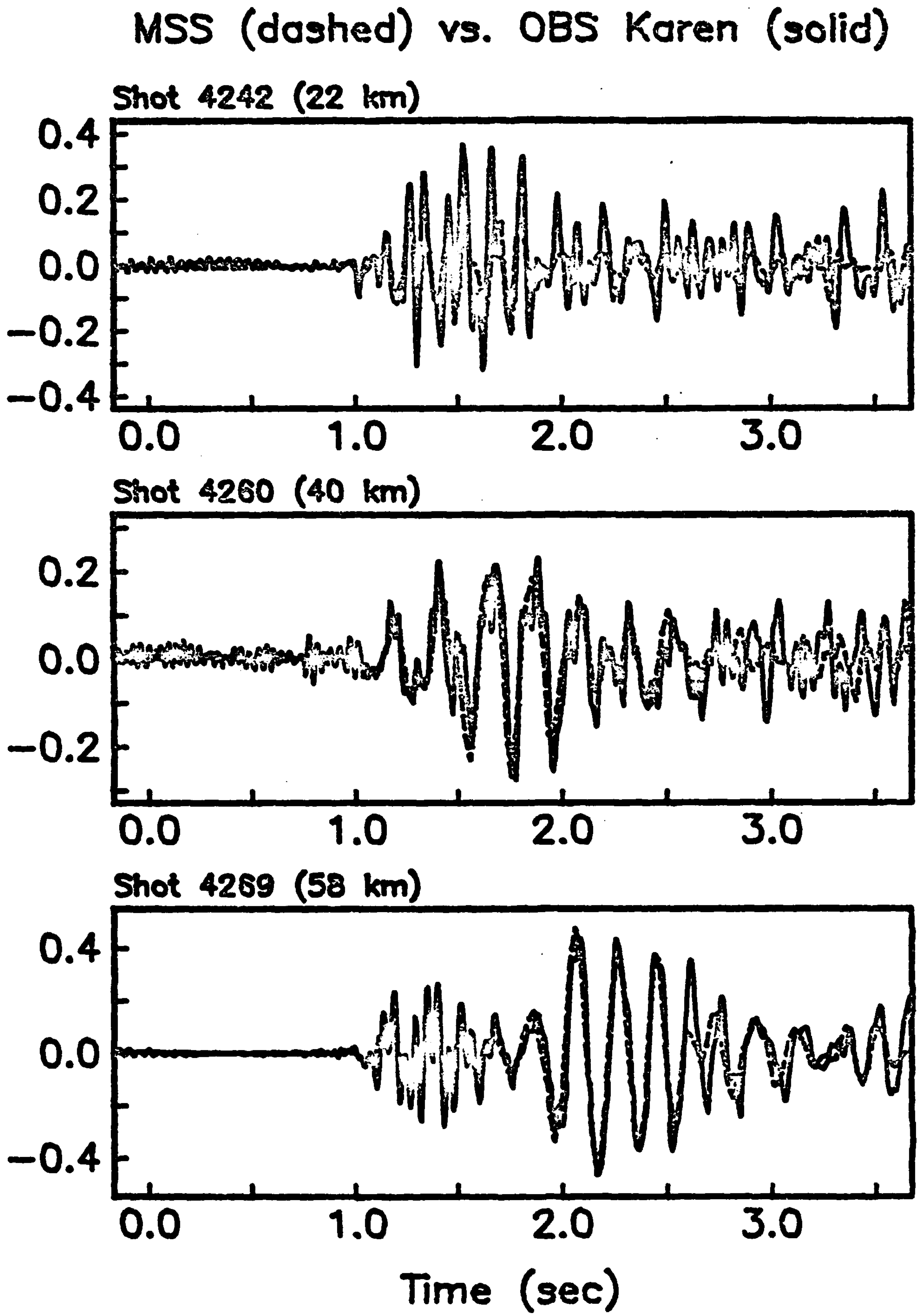

MSS (dashed) vs. OBS Karen (solid)
Shot 4242 (22 km)
Shot 4260 (40 km)
Shot 4269 (58 km)
0.4
0.2
0.0
−0.2
−0.4
1.0
2.0
3.0
Time (sec)

OBS Karen – Line 4b

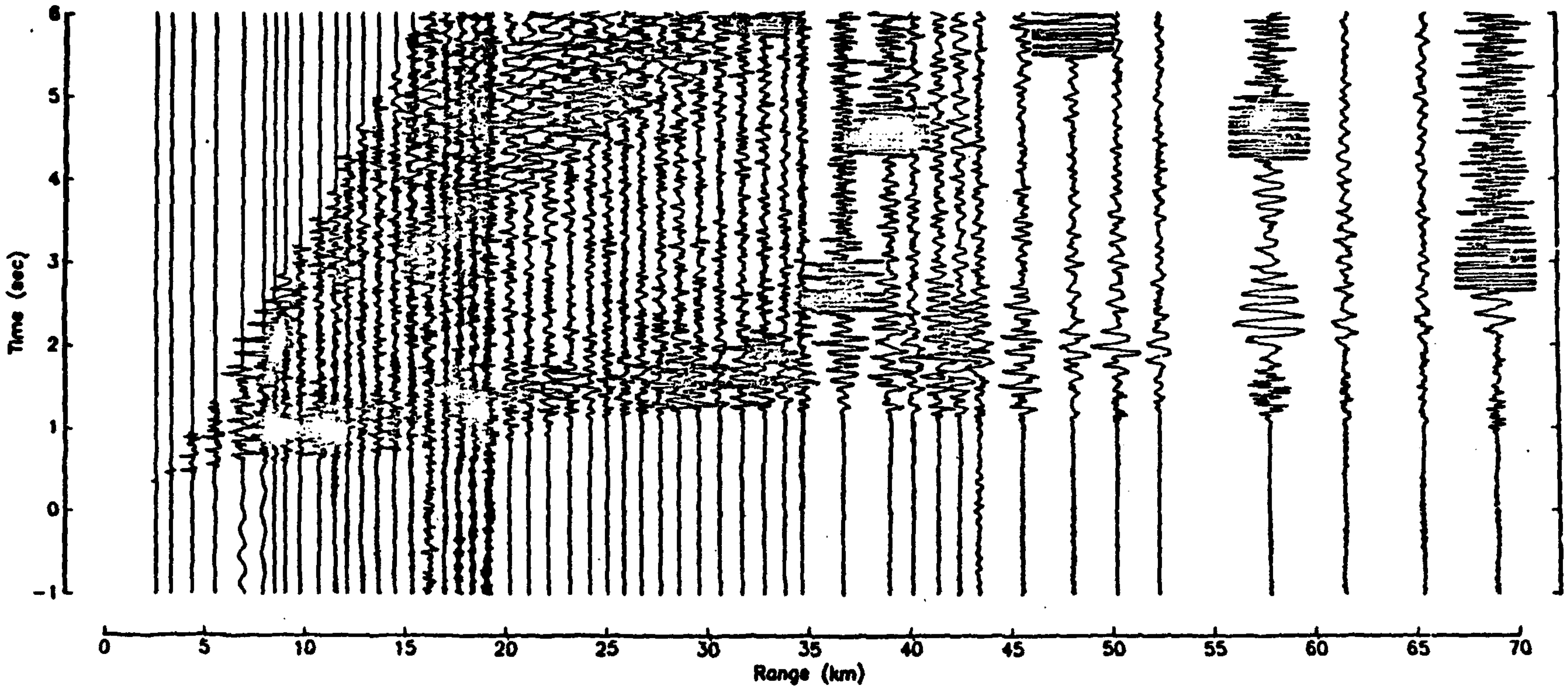

MSS – Line 4b

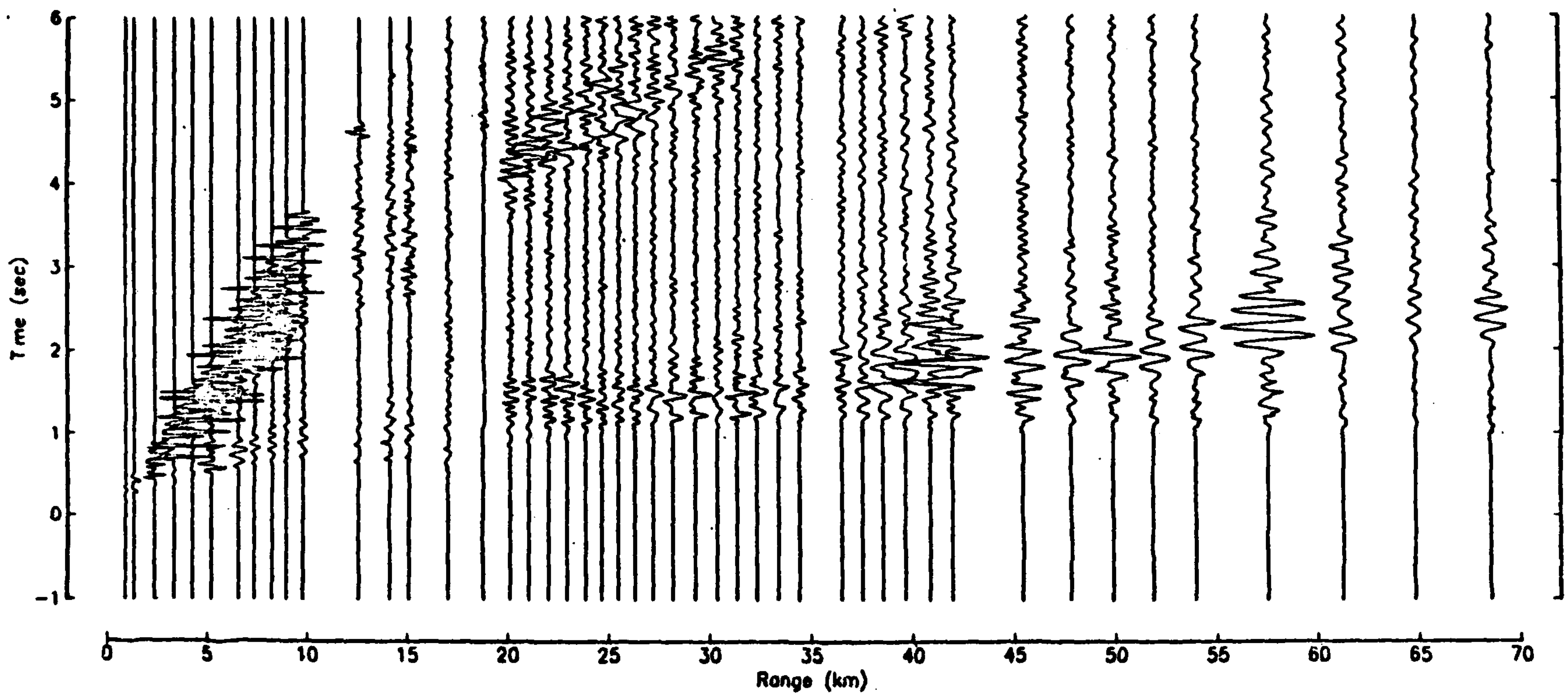

Time (sec)
6
5
4
3
2
1
0
-1
0
5
10
15
20
25
30
35
40
45
50
55
60
65
70
Range (km)

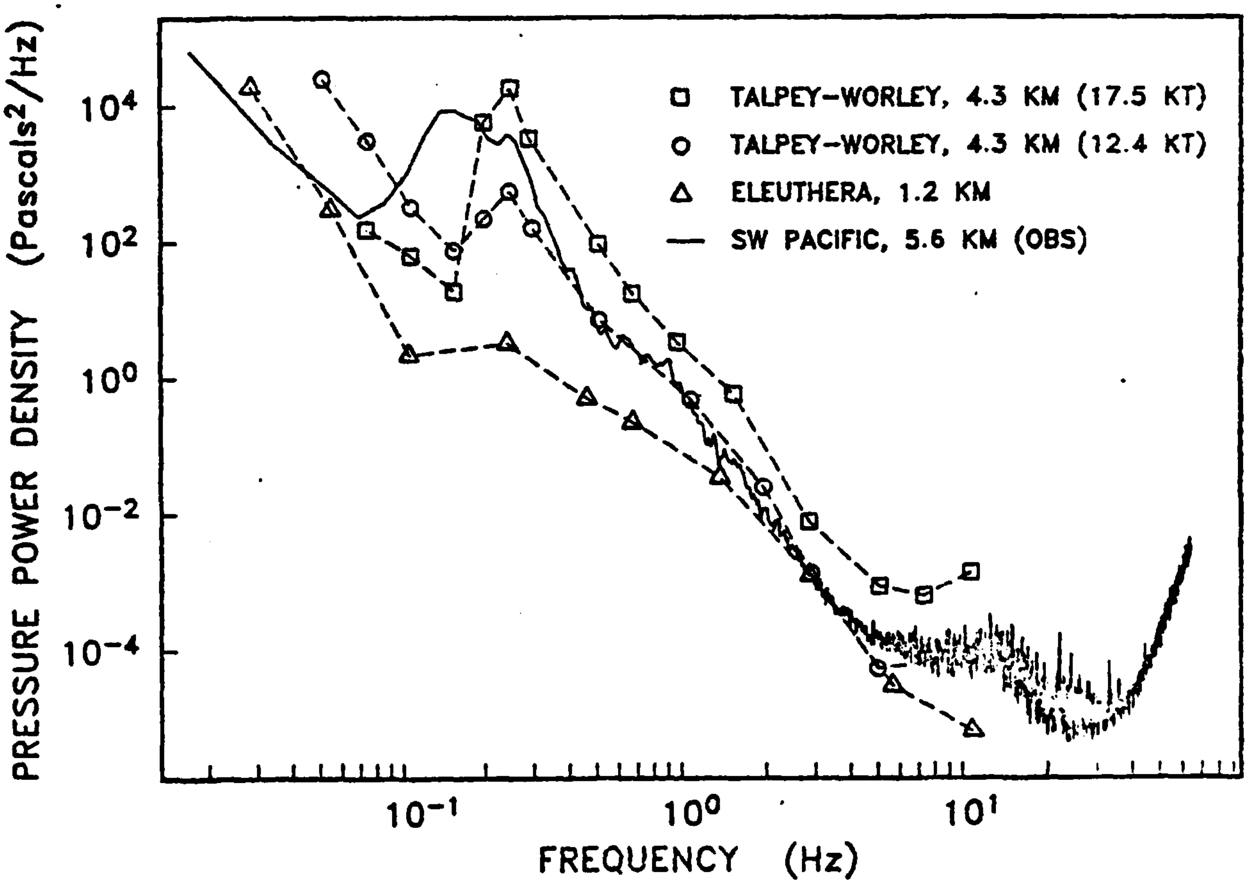

PRESSURE POWER DENSITY (Pascals²/Hz)
10^4
10^2
10^0
10^{-2}
10^{-4}
10^{-1}
10^0
10^1
FREQUENCY (Hz)
TALPEY-WORLEY, 4.3 KM (17.5 KT)
TALPEY-WORLEY, 4.3 KM (12.4 KT)
ELEUTHERA, 1.2 KM
SW PACIFIC, 5.6 KM (OBS)

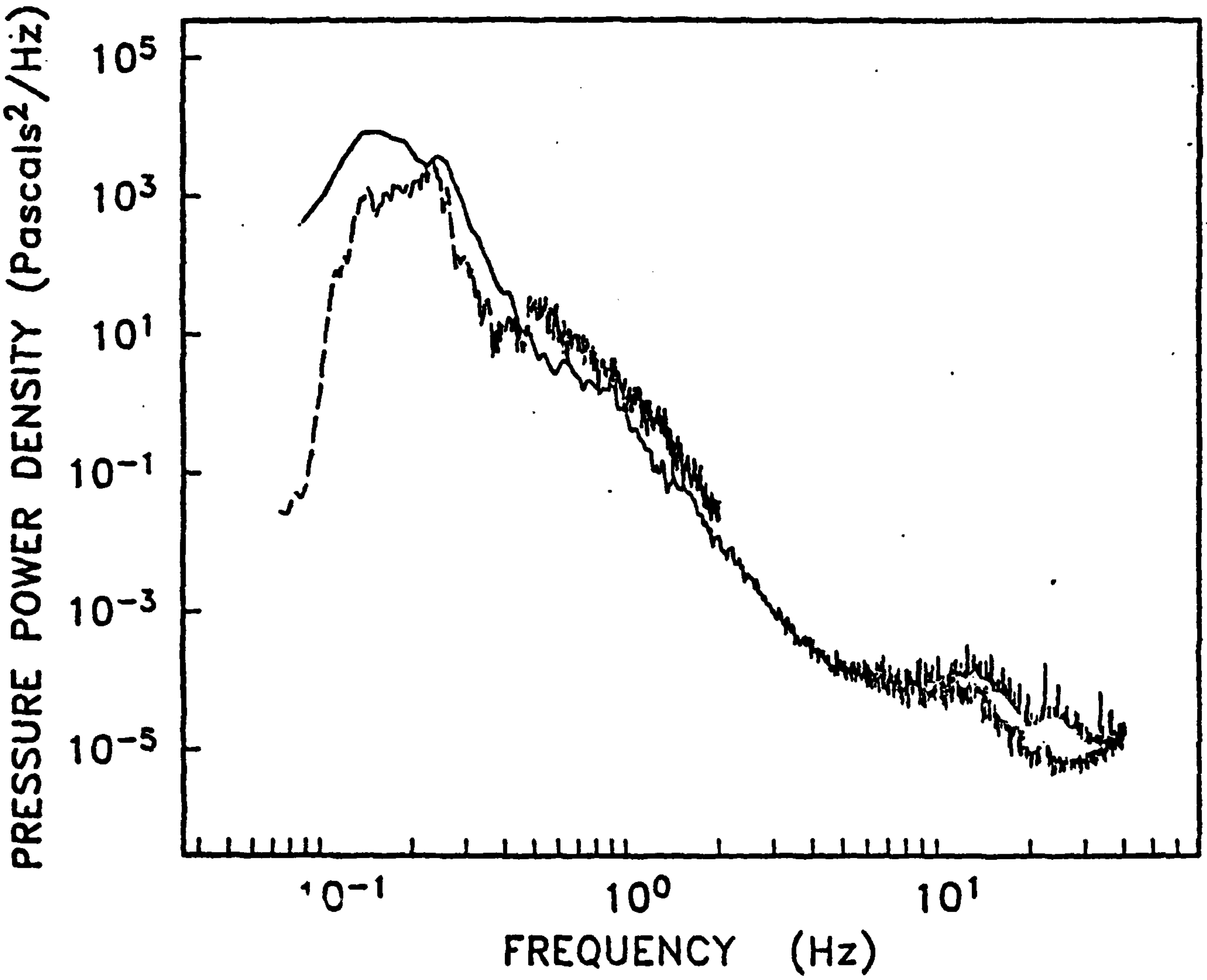

PRESSURE POWER DENSITY (Pascals²/Hz)
10⁵
10³
10¹
10⁻¹
10⁻³
10⁻⁵
10⁻¹
10⁰
10¹
FREQUENCY (Hz)

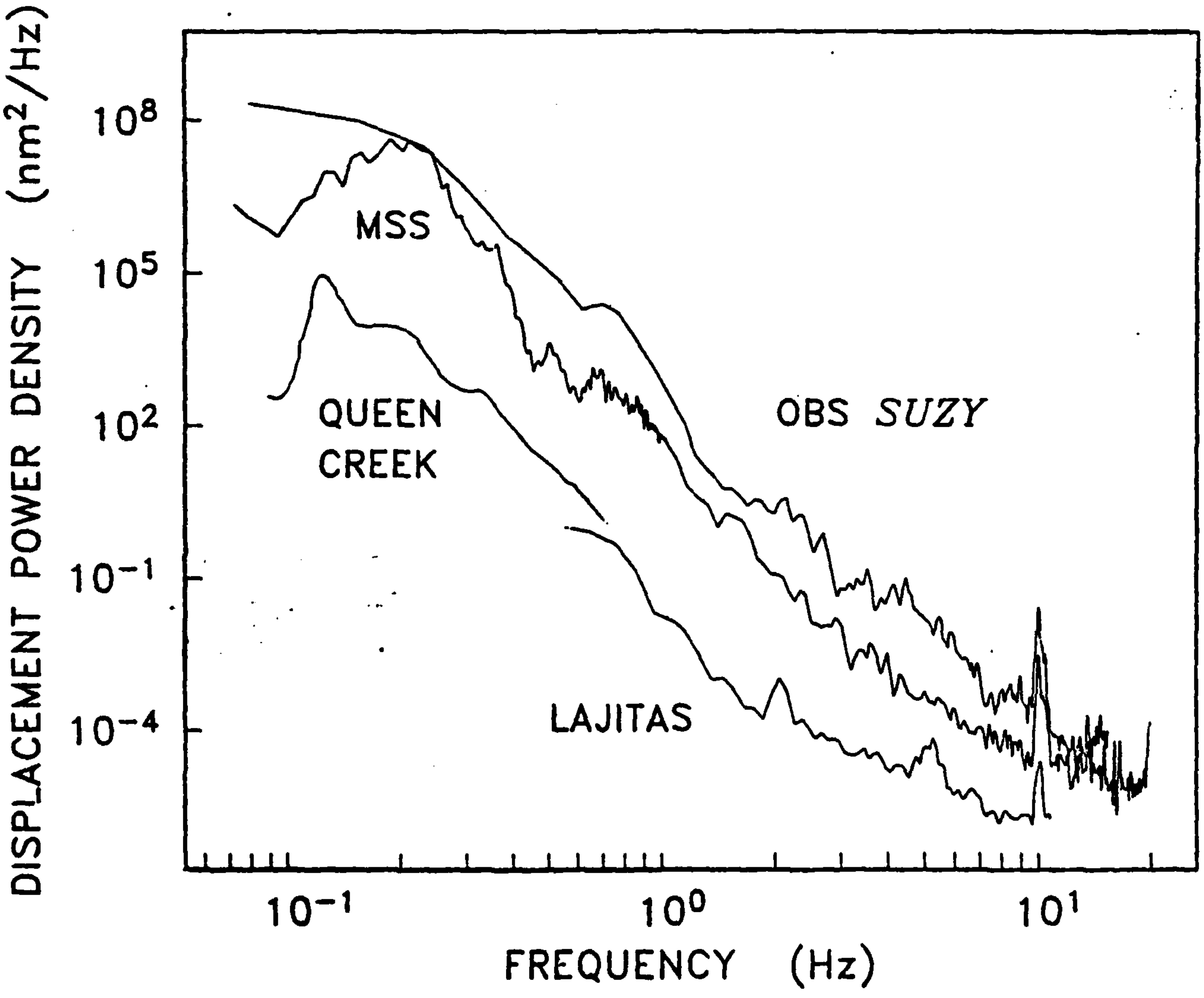
DISPLACEMENT POWER DENSITY (nm²/Hz)
10⁸
10⁵
10²
10⁻¹
10⁻⁴
MSS
QUEEN
CREEK
OBS SUZY
LAJITAS
10⁻¹
10⁰
10¹
FREQUENCY (Hz)

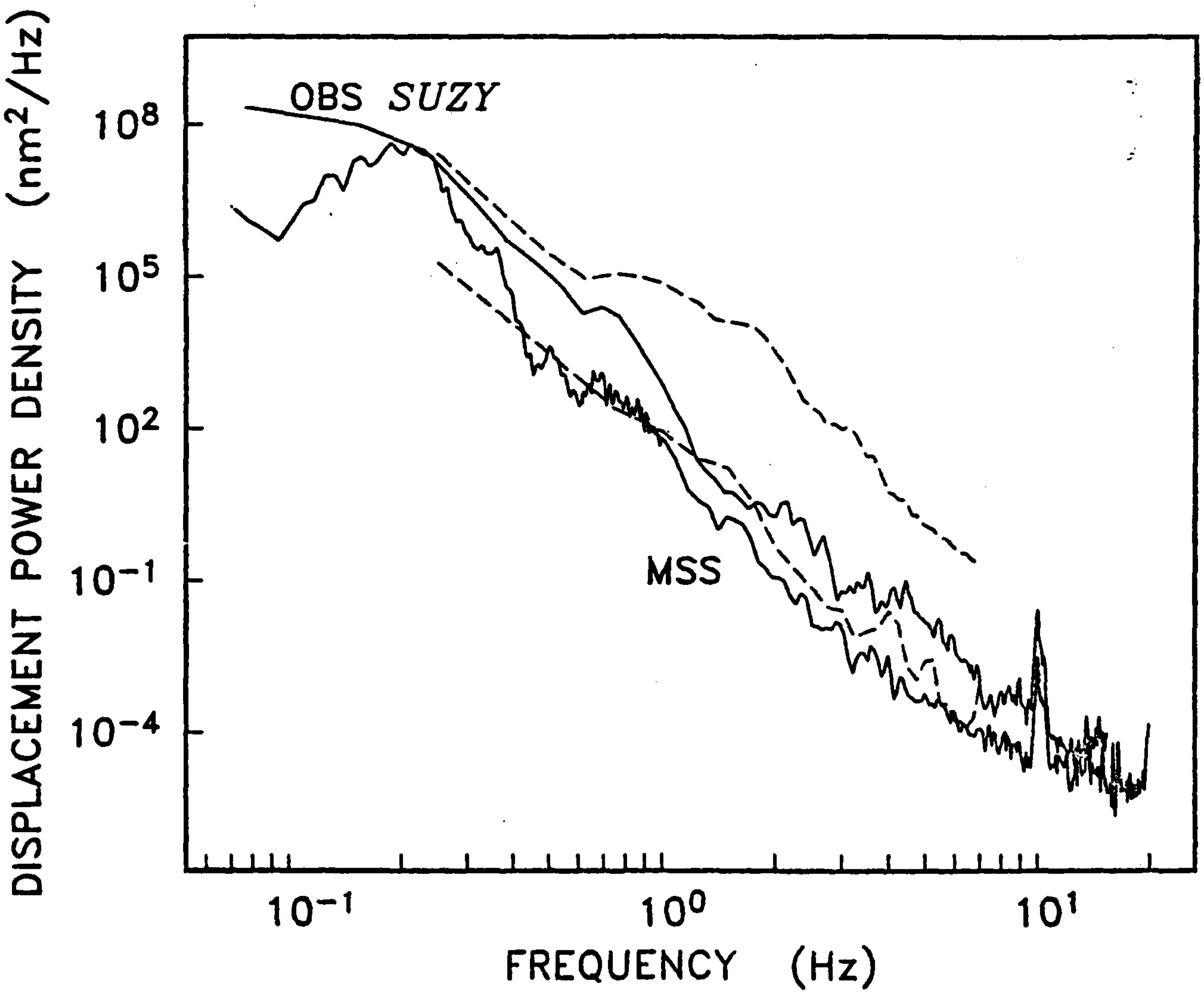

OBS SUZY
MSS
DISPLACEMENT POWER DENSITY (nm²/Hz)
10^8
10^5
10^2
10^{-1}
10^{-4}
10^{-1}
10^0
10^1
FREQUENCY (Hz)

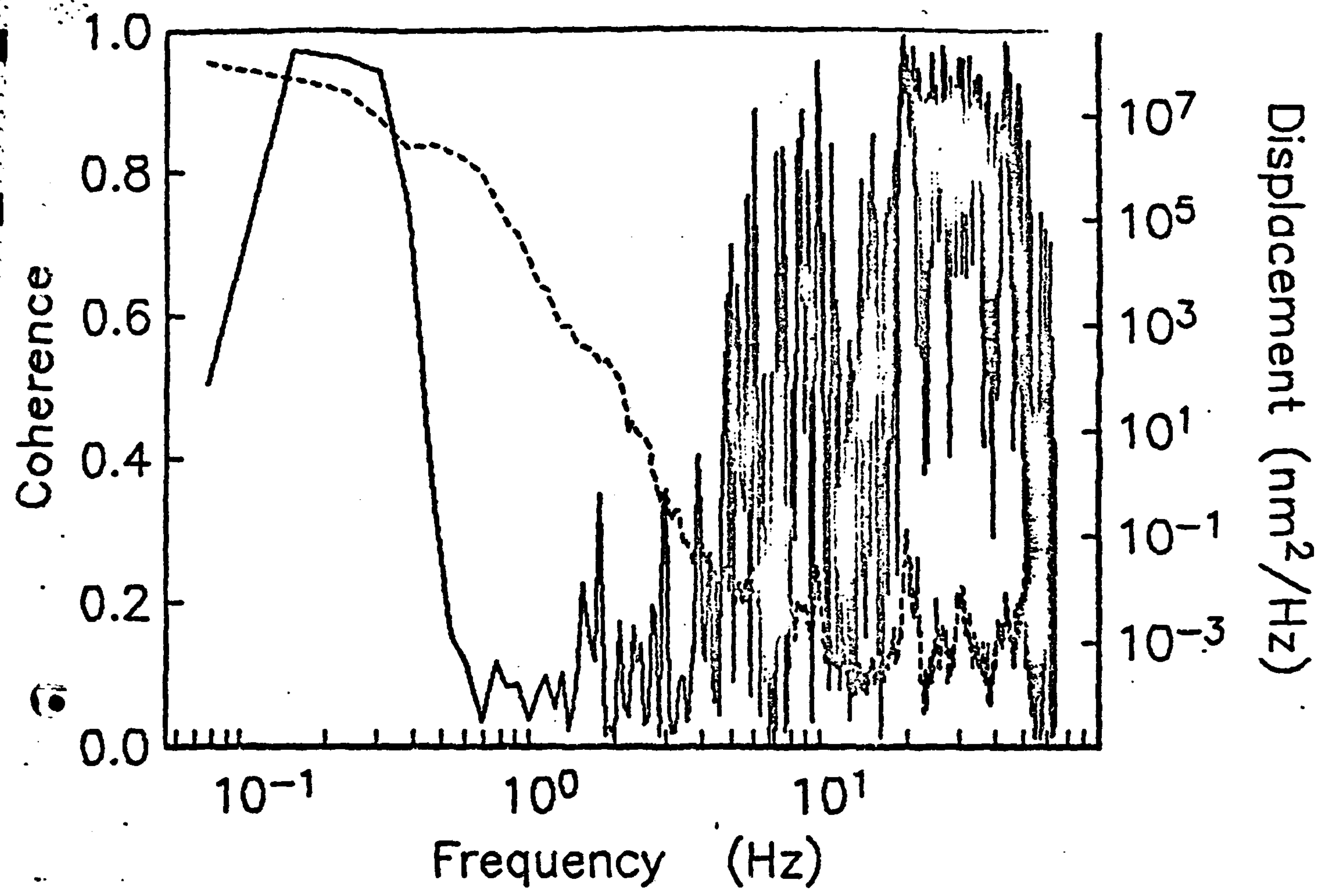

1.0
0.8
0.6
0.4
0.2
0.0
Coherence
10^{-1}
10^{0}
10^{1}
Frequency (Hz)
10^{7}
10^{5}
10^{3}
10^{1}
10^{-1}
10^{-3}
Displacement (nm^2/Hz)

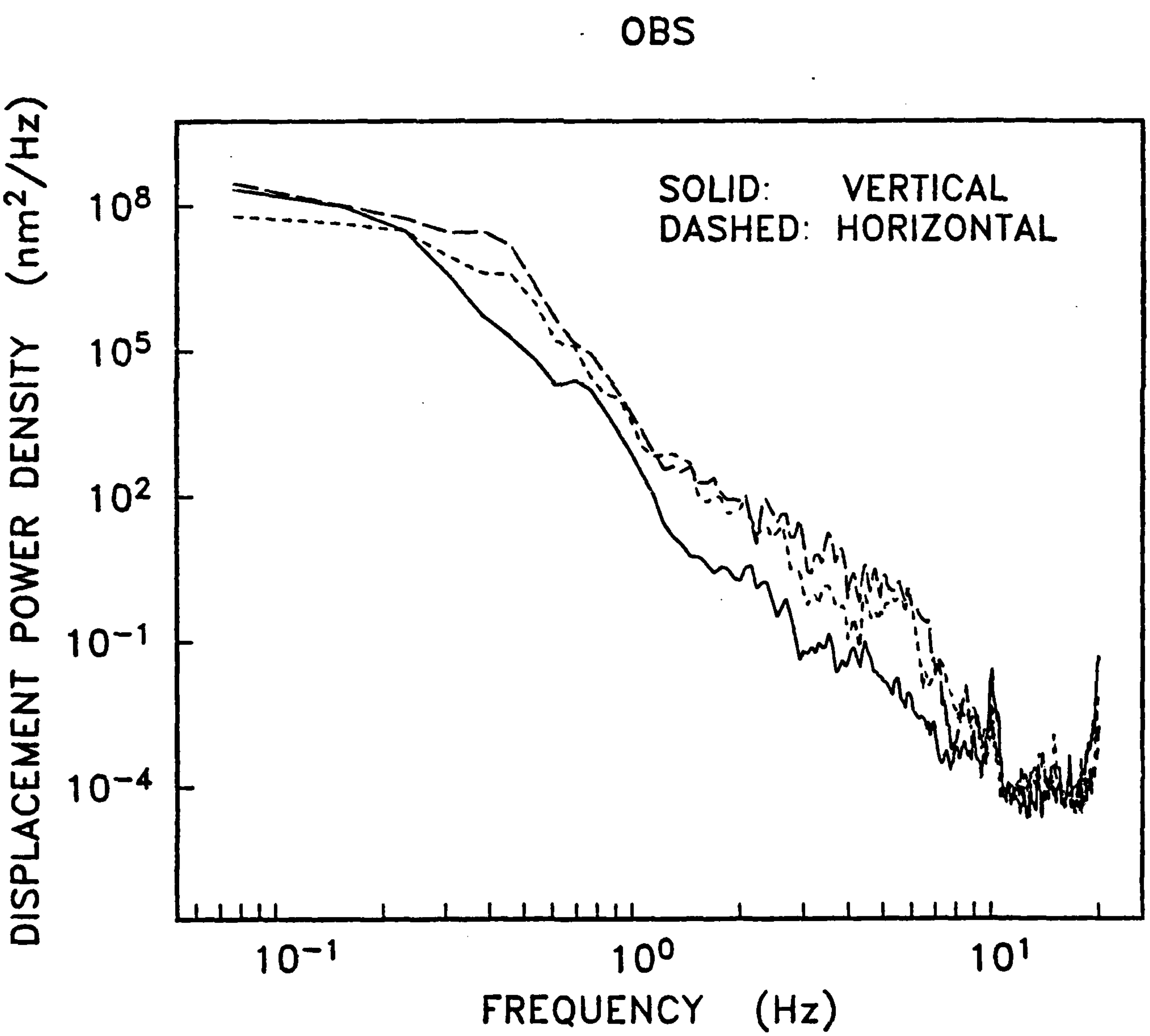
OBS
SOLID: VERTICAL
DASHED: HORIZONTAL
DISPLACEMENT POWER DENSITY (nm²/Hz)
10⁸
10⁵
10²
10⁻¹
10⁻⁴
10⁻¹
10⁰
10¹
FREQUENCY (Hz)

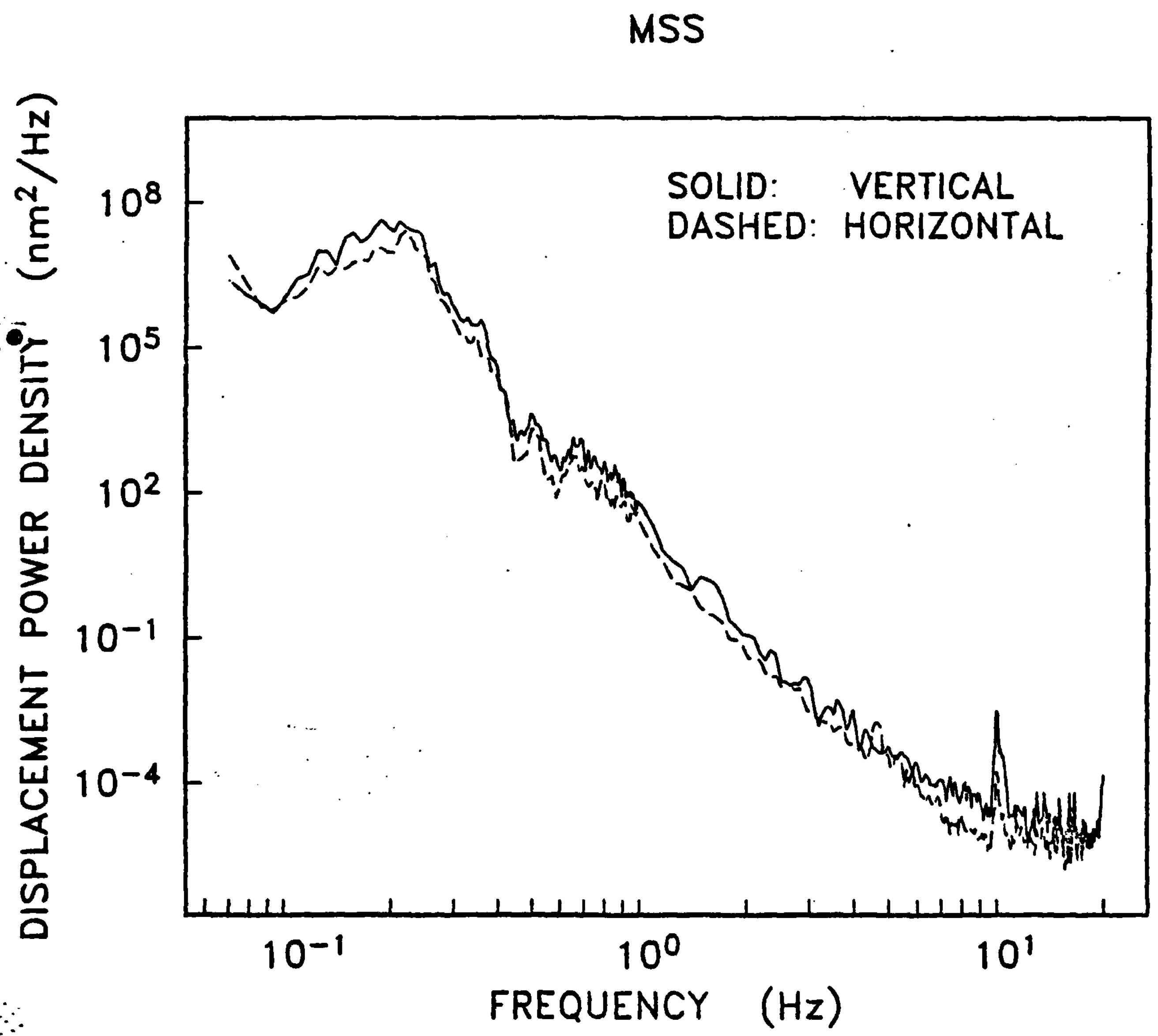

MSS
SOLID: VERTICAL
DASHED: HORIZONTAL
DISPLACEMENT POWER DENSITY (nm²/Hz)
10⁸
10⁵
10²
10⁻¹
10⁻⁴
10⁻¹
10⁰
10¹
FREQUENCY (Hz)

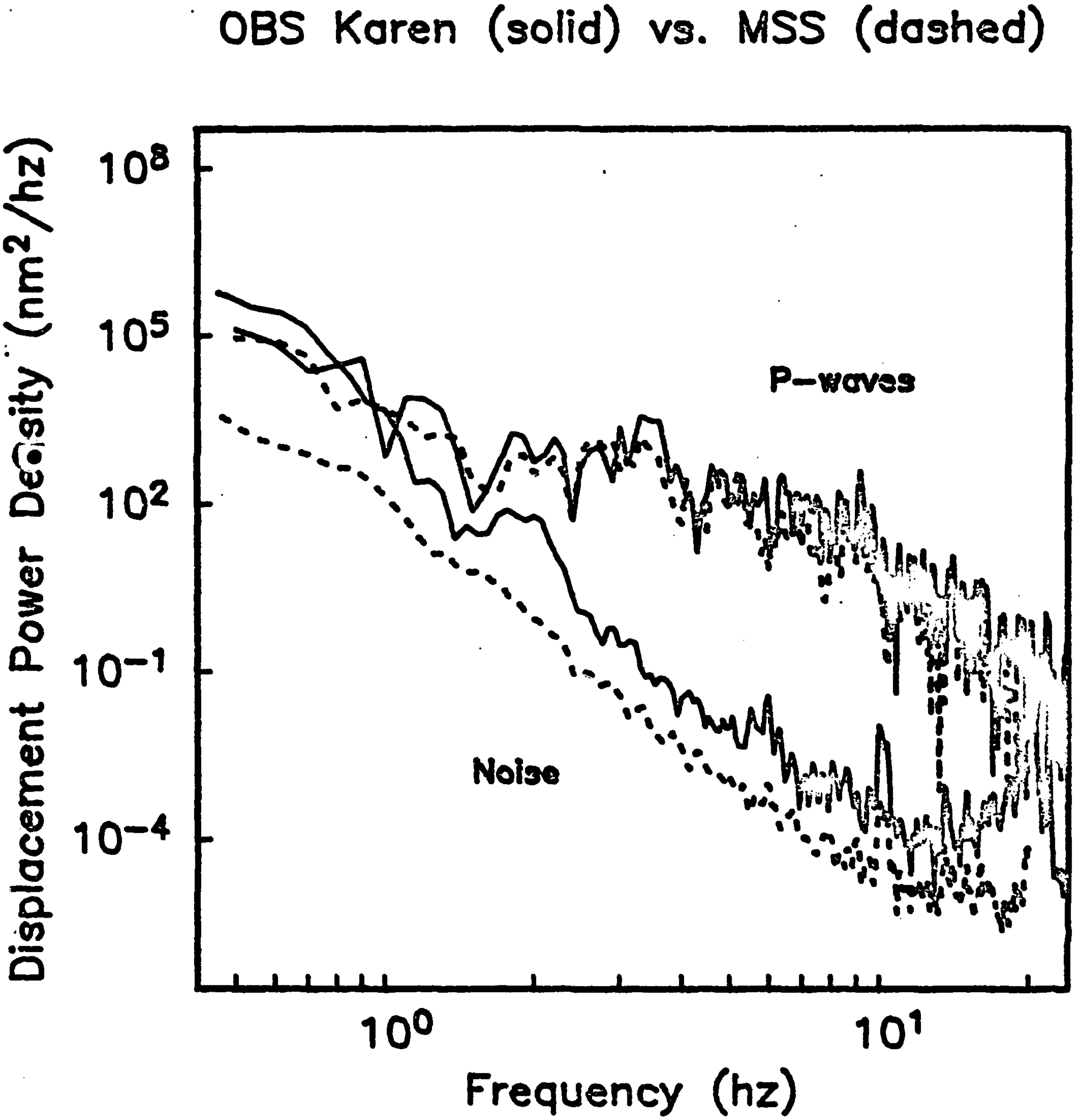

OBS Karen (solid) vs. MSS (dashed)
P-waves
Noise
10^8
10^5
10^2
10^-1
10^-4
10^0
10^1
Frequency (hz)
Displacement Power Density (nm^2/hz)

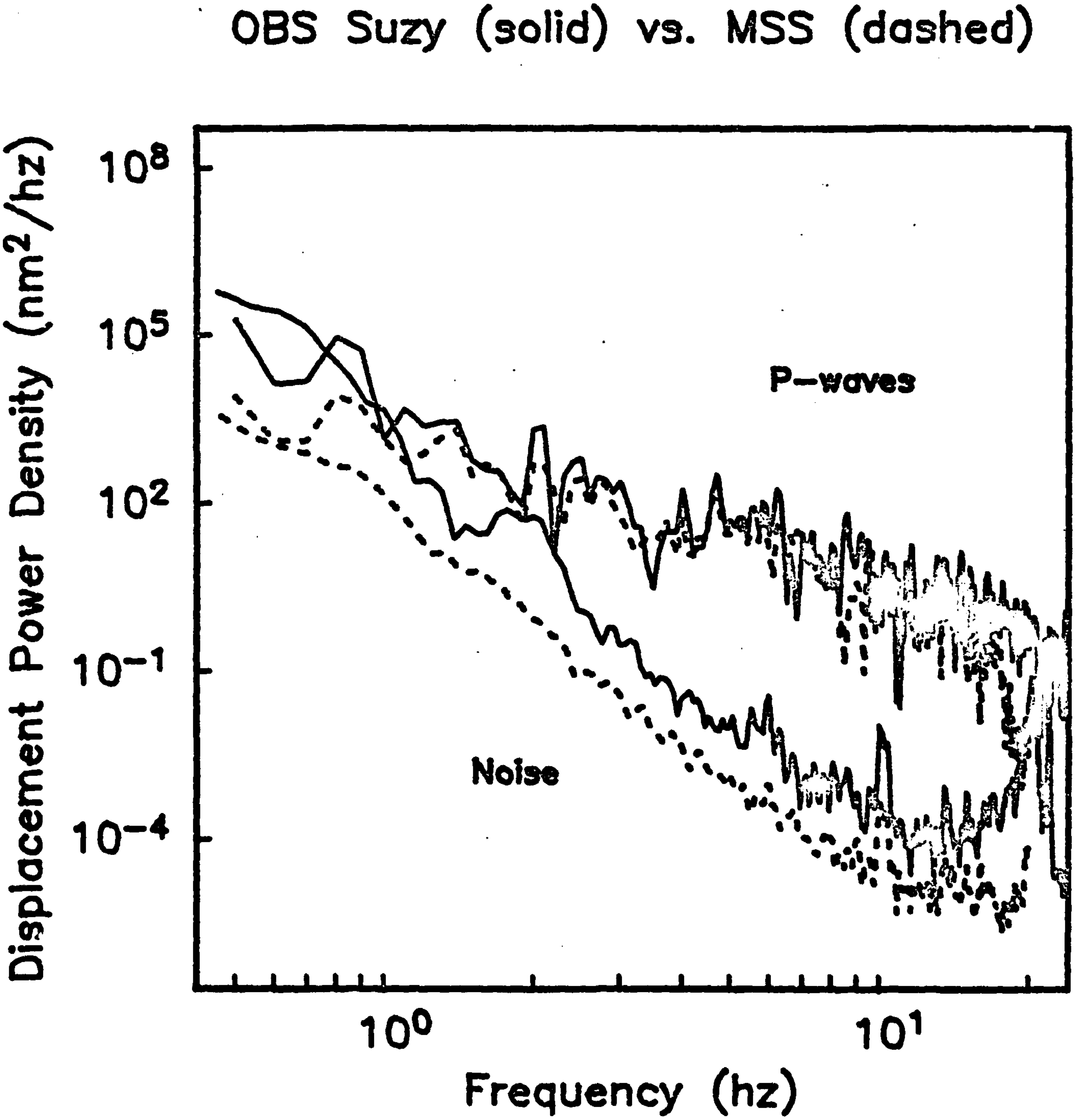
OBS Suzy (solid) vs. MSS (dashed)
Displacement Power Density (nm²/hz)
10⁸
10⁵
10²
10⁻¹
10⁻⁴
P-waves
Noise
10⁰
10¹
Frequency (hz)

Line 5b (OBS Suzy)

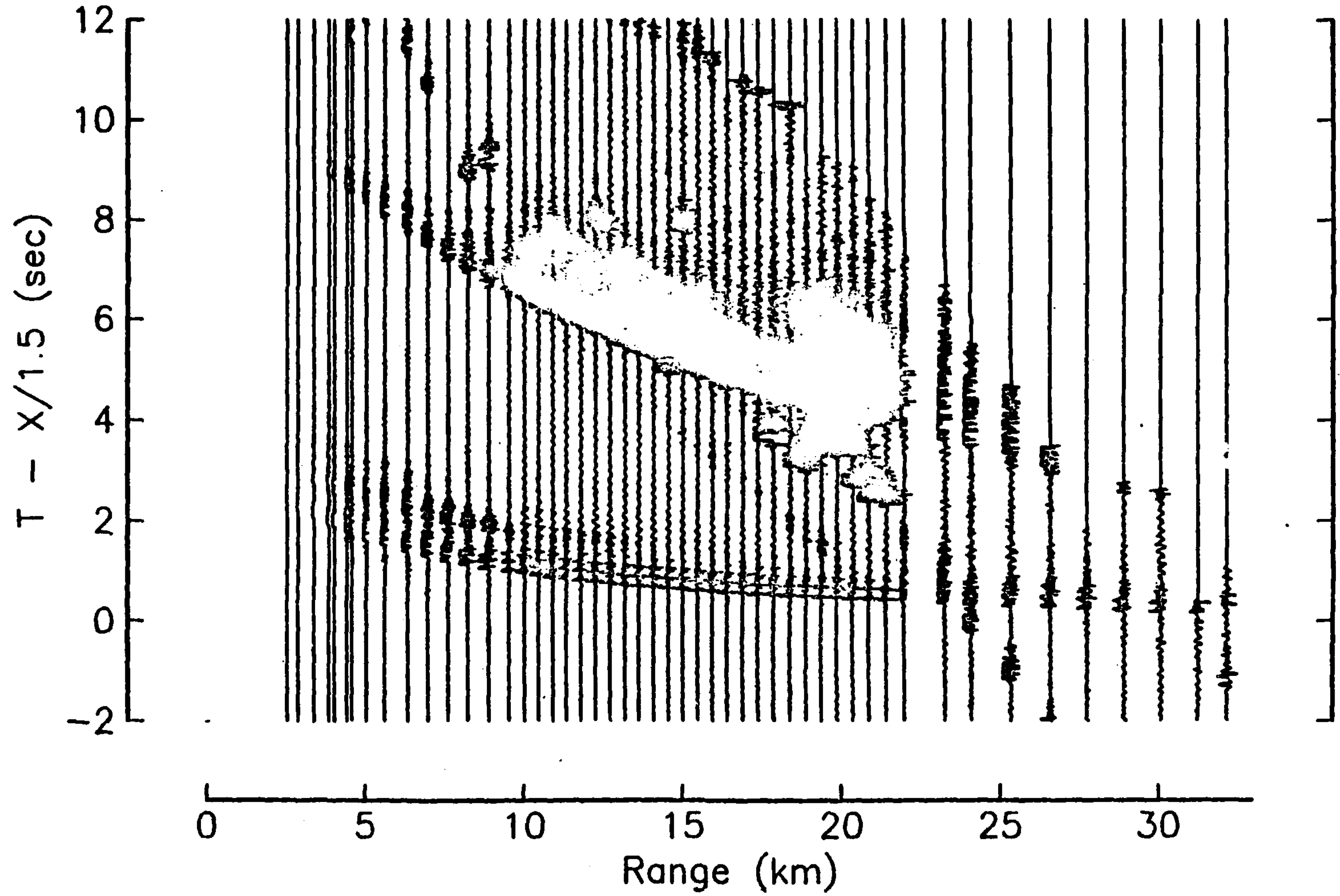

Line 5b (MSS)

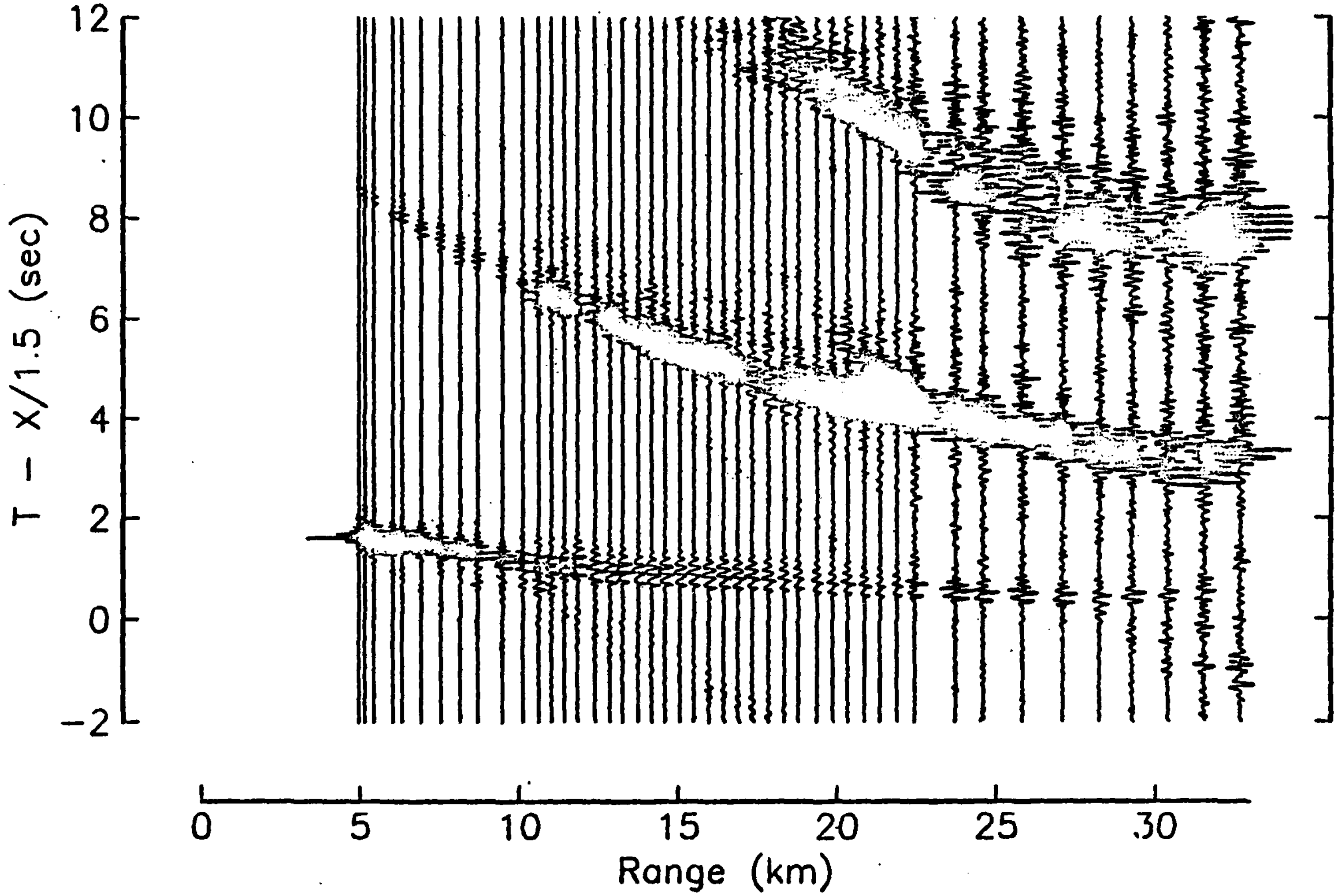

D

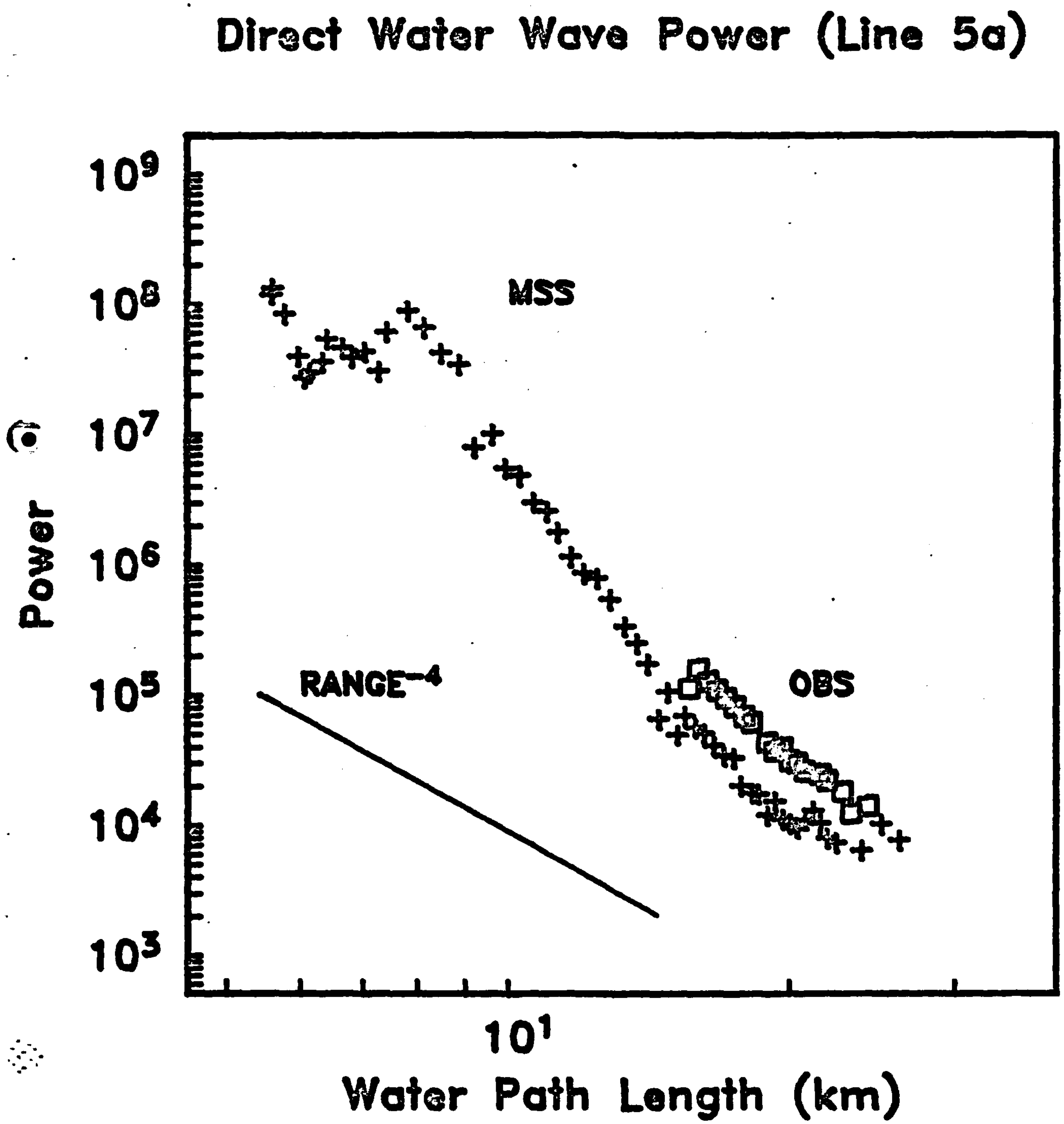
Direct Water Wave Power (Line 5a)
Power
10^9
10^8
10^7
10^6
10^5
10^4
10^3
MSS
RANGE^{-4}
OBS
10^1
Water Path Length (km)

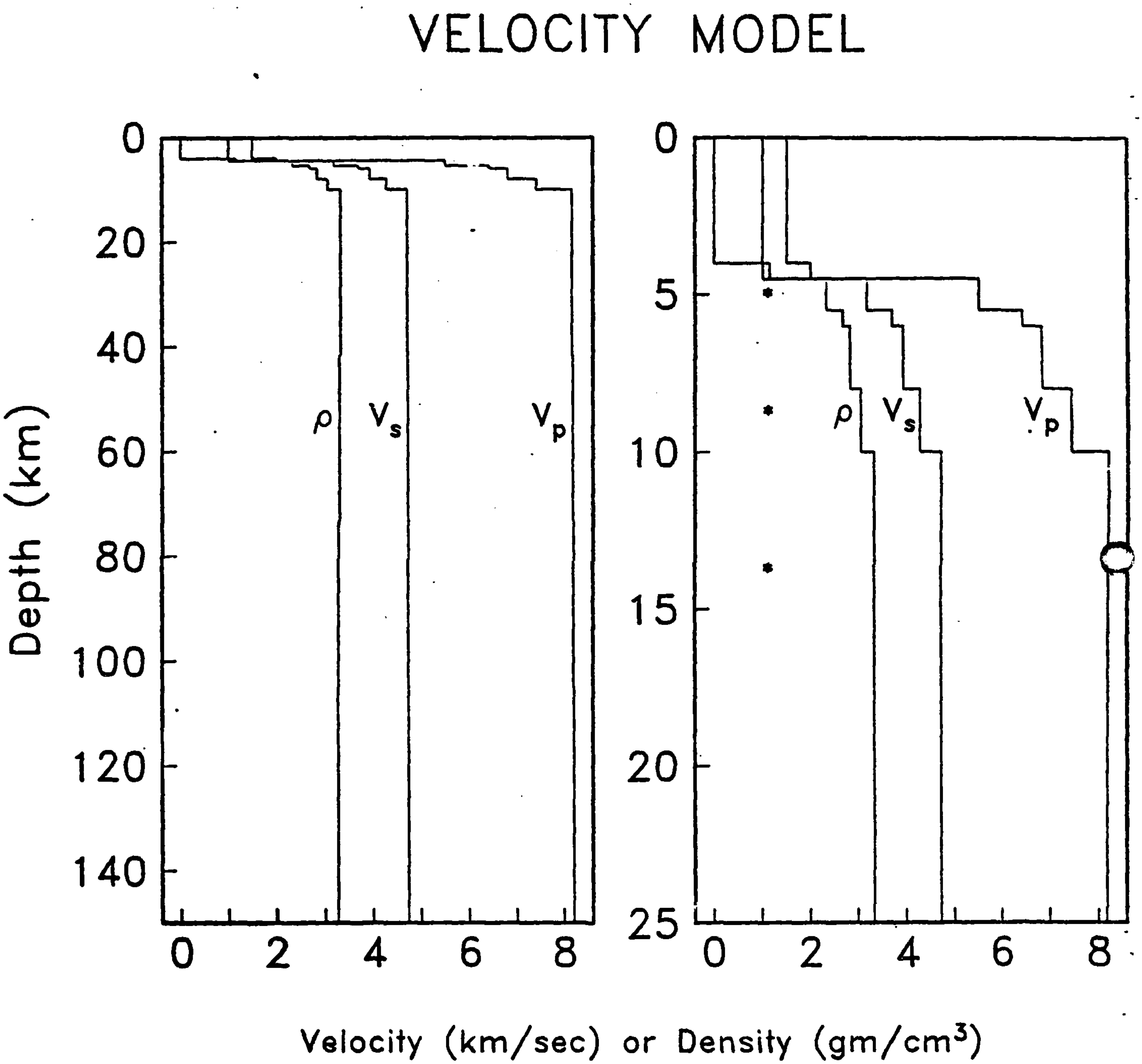

FIGURE 1. Velocity and density model. The left side shows the entire model while on the right the depth scale is expanded to show detail in the crust. Asterisks indicate source depths. The model is from Gettrust and Frazer (1981).

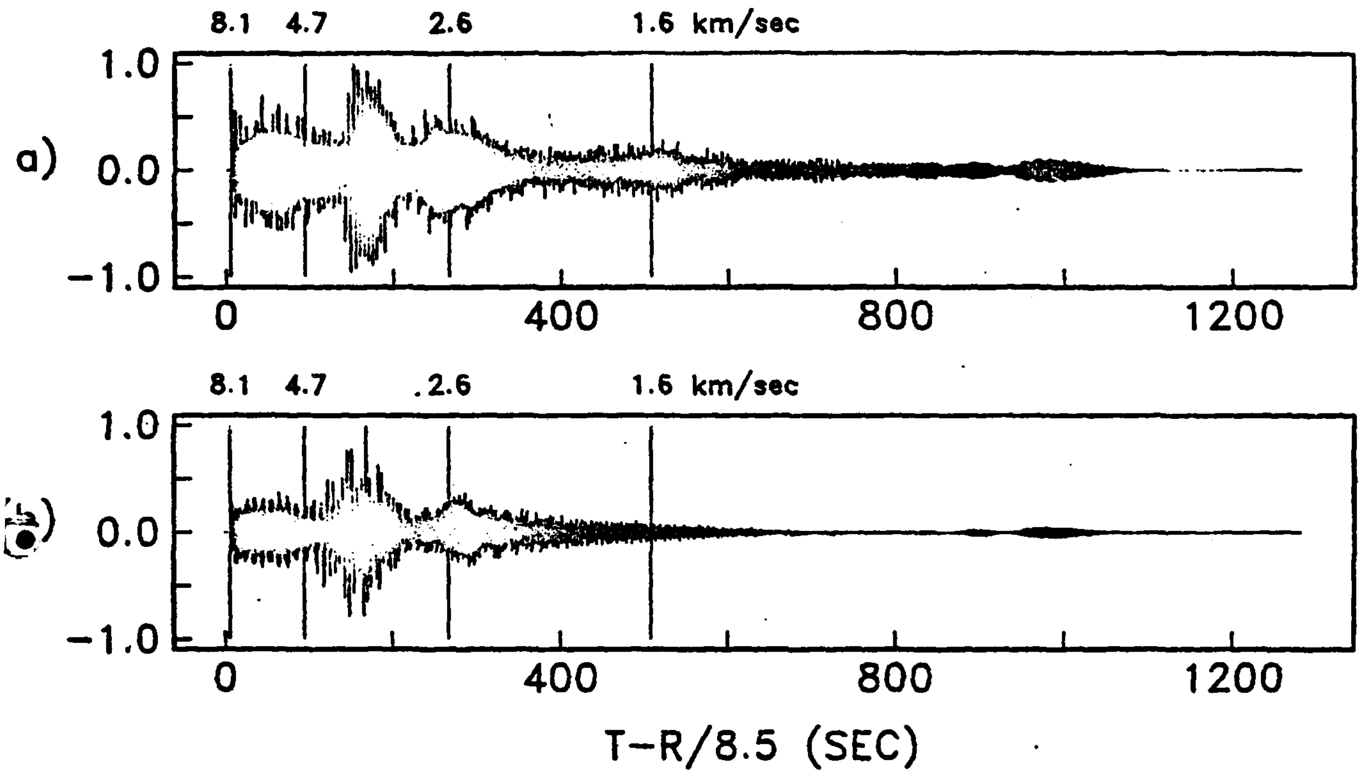

FIGURE 3. Complete synthectic seismograms for a thrust fault source at 14.0 km depth at an epicentral range of 1000 km. a) Vertical component, b) horizontal component rotated 25 degrees clockwise from the radial direction. Velocities of 8.1, 4.7, 2.6 and 1.6 km/sec are indicated.

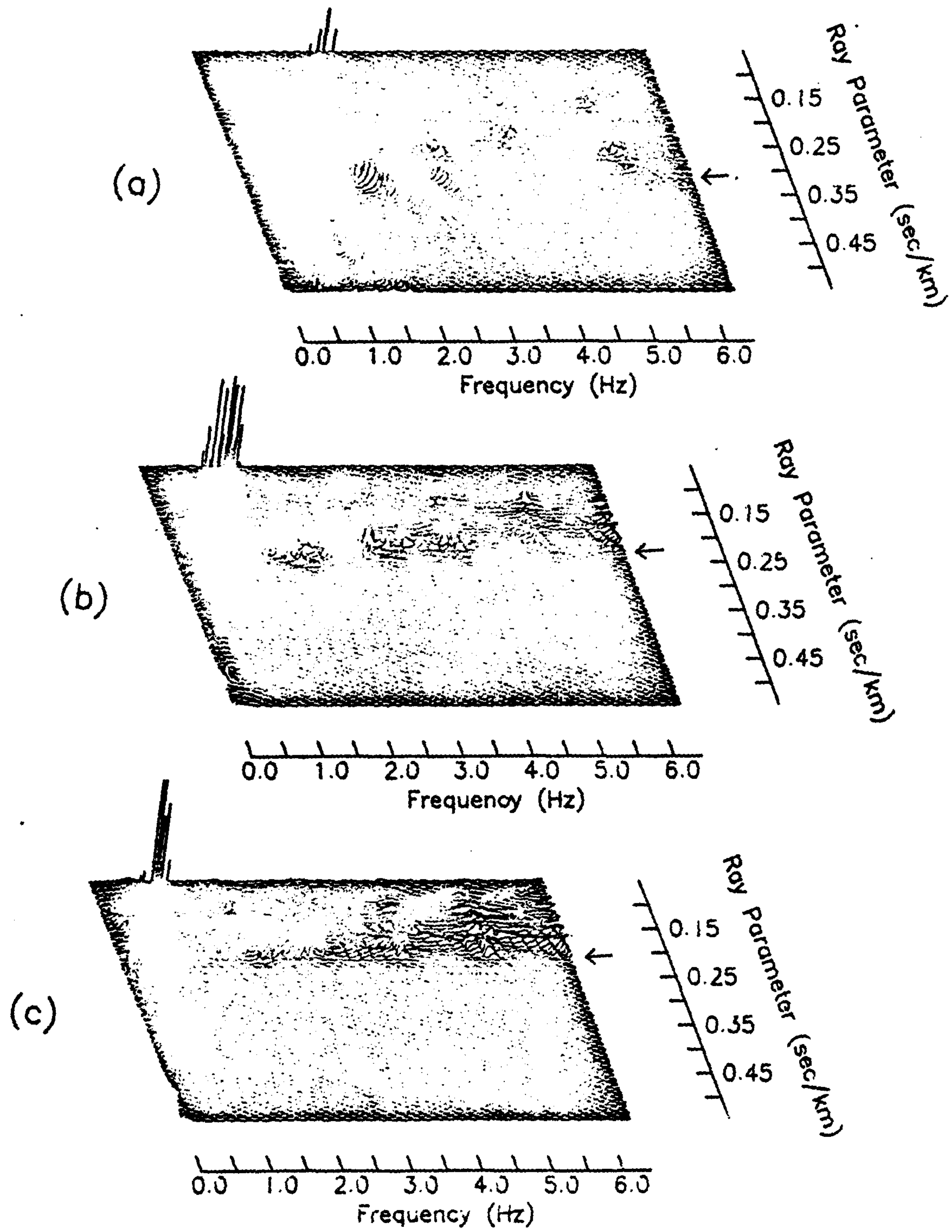

FIGURE 2. Modulus of the horizontal normal stress, $\sigma_{221}(\omega,k)$ at source depths of a) 5.25 km, b) 9.0 km and c) 14.0 km. Arrows indicate V_s^{-1} of the layer containing the source.

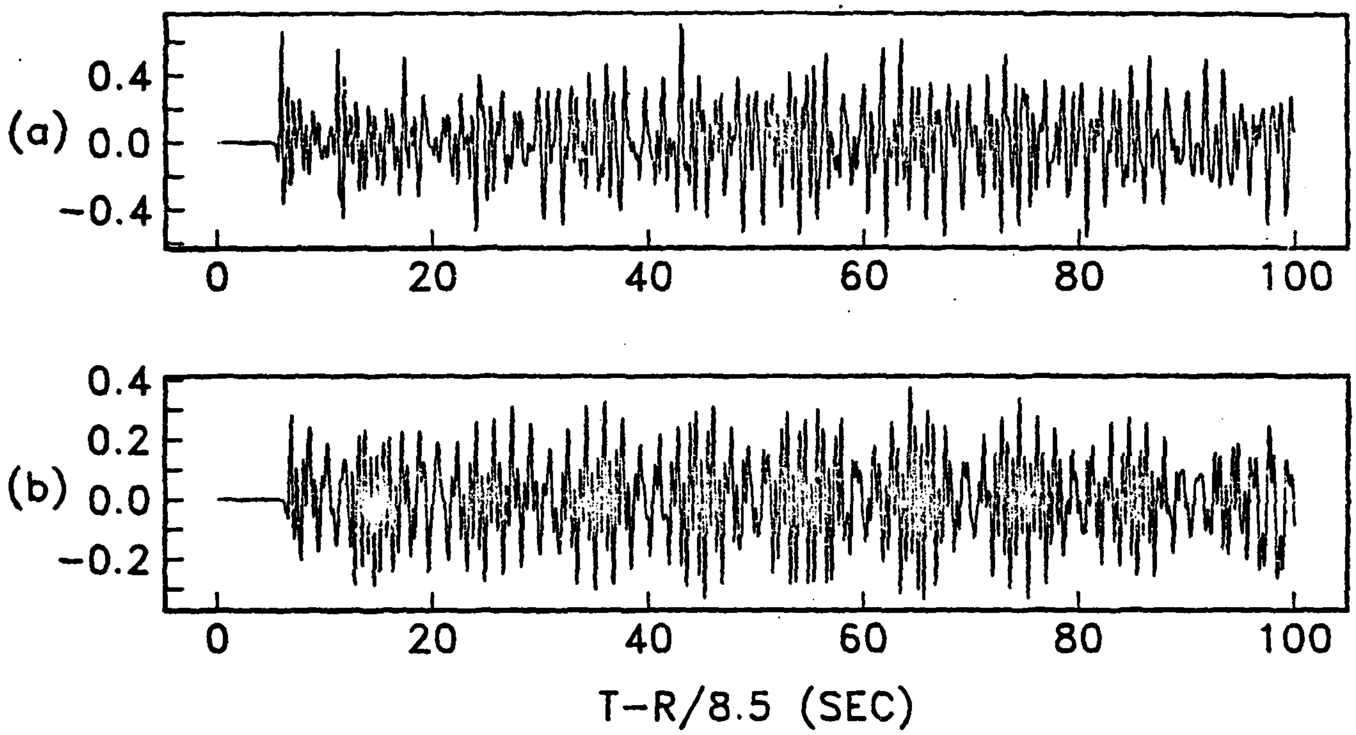

FIGURE 4. Synthetic P_n wavetrain. Contains the first 100 seconds of the records in figure 3. a) Vertical component and b) horizontal component.

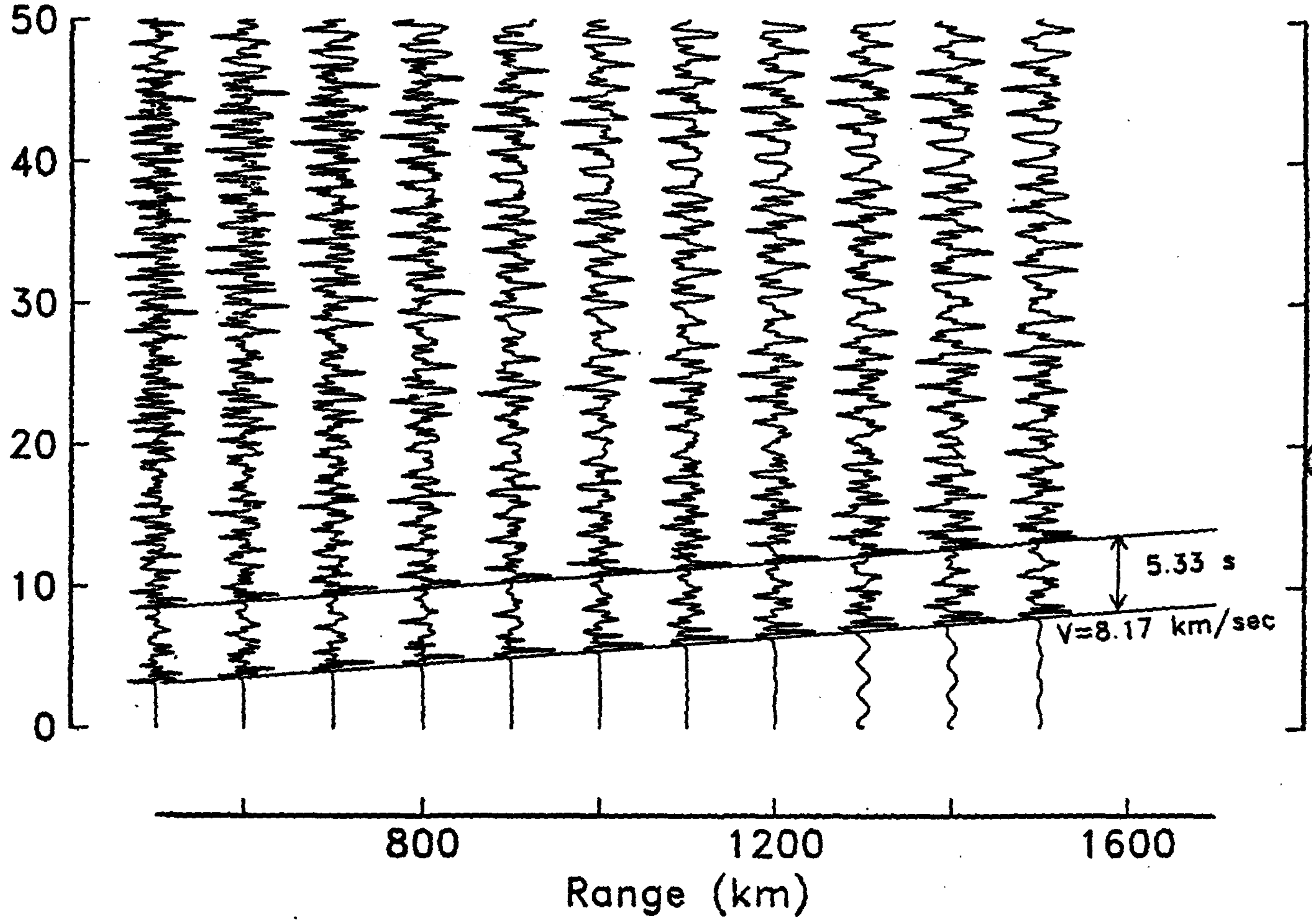

'IGURE 5. Record section of the vertical normal stress, σ_{zz0} at 14.0 km depth. Lines are drawn with an inverse slope of 8.17 km/sec separated by the two-way travel time in the water column, 5.33 sec.

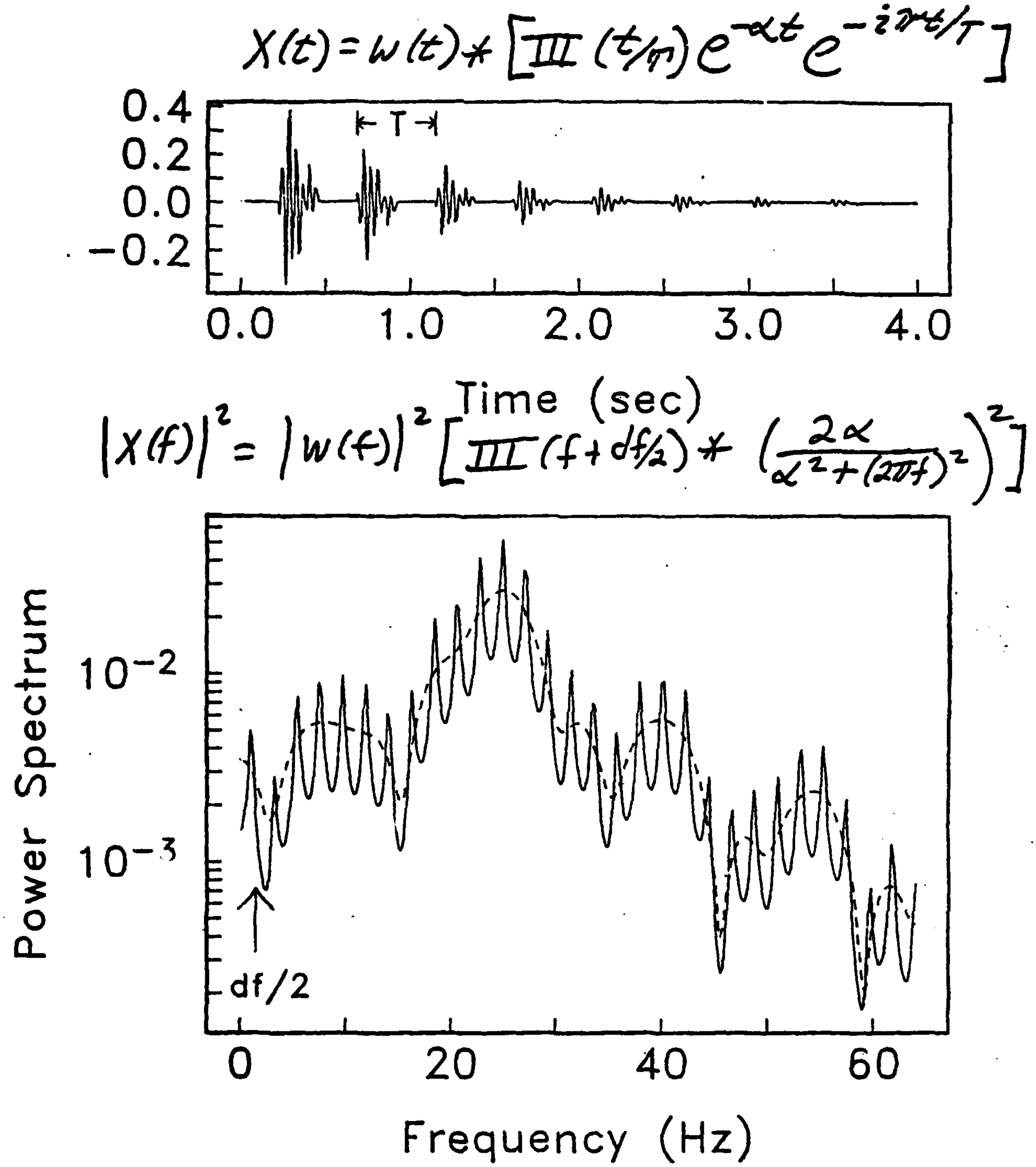

FIGURE 6. Power spectrum of a reverberating wavelet. a) Wavetrain comprised of a reverberating wavelet with a spacing between multiples of T=0.46 seconds and attenuation factor, α=1.0. b) Power spectrum of the wavetrain in (a) superimposed on the spectrum of a single wavelet (dashed). The peaks are equally spaced with df=1/T=2.17 hz and are offset by an amount df/2.

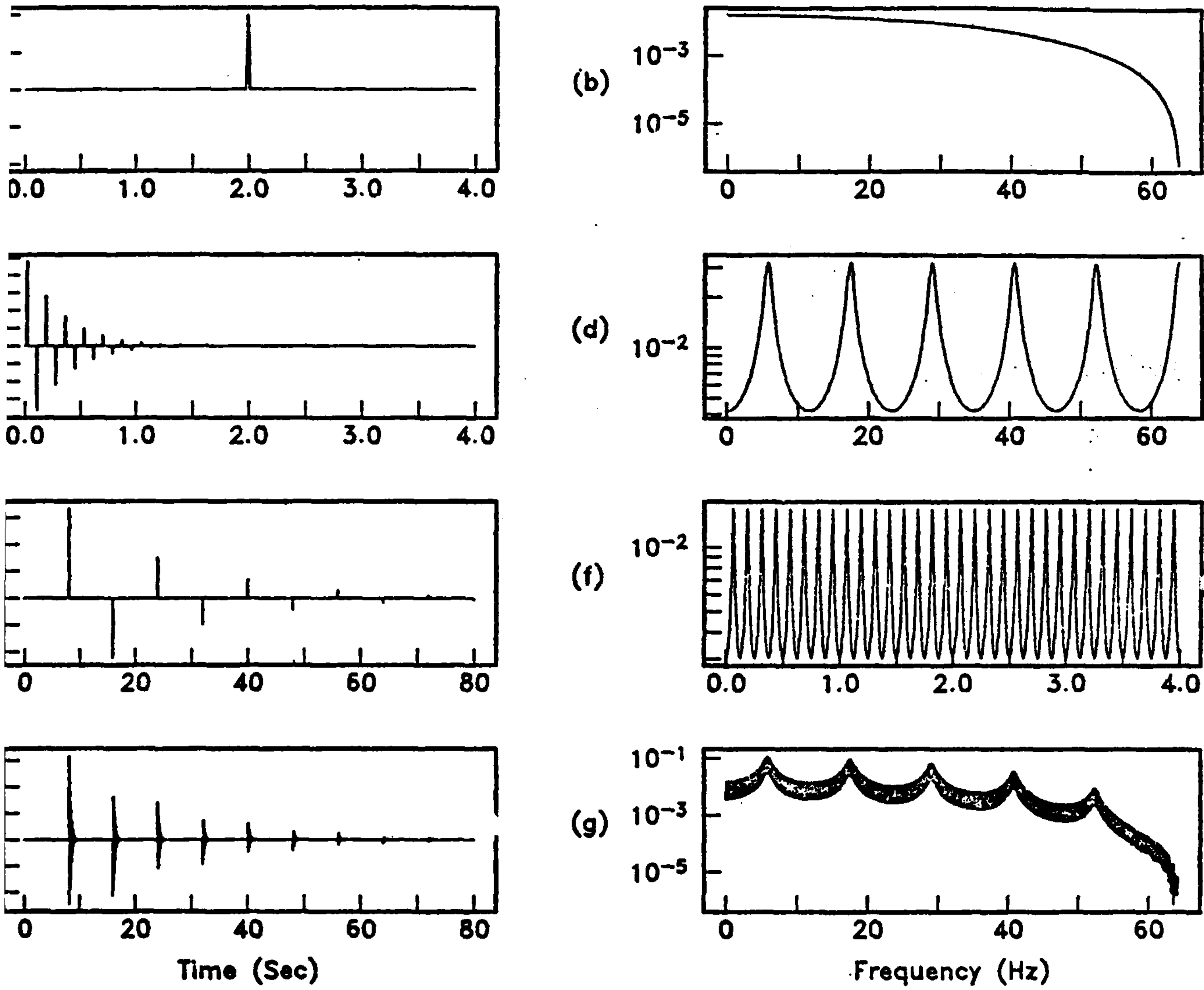

URE 9. Spectral characteristics of sediment and water everberations. a) Wavelet, w(t); b) wavelet spectrum, $|W(f)|^2$.) Sediment reverberation with $\alpha_s=3.0$ and $T_s=0.086$ sec;) sediment reverberation spectrum. e) Water reverberation ith $\alpha_w=0.05$ and $T_w=8.0$ sec; f) first 4.0 hz of the water everberation spectrum. g) Full wavetrain, x(t); h) wavetrain pectrum, $|X(f)|^2$.

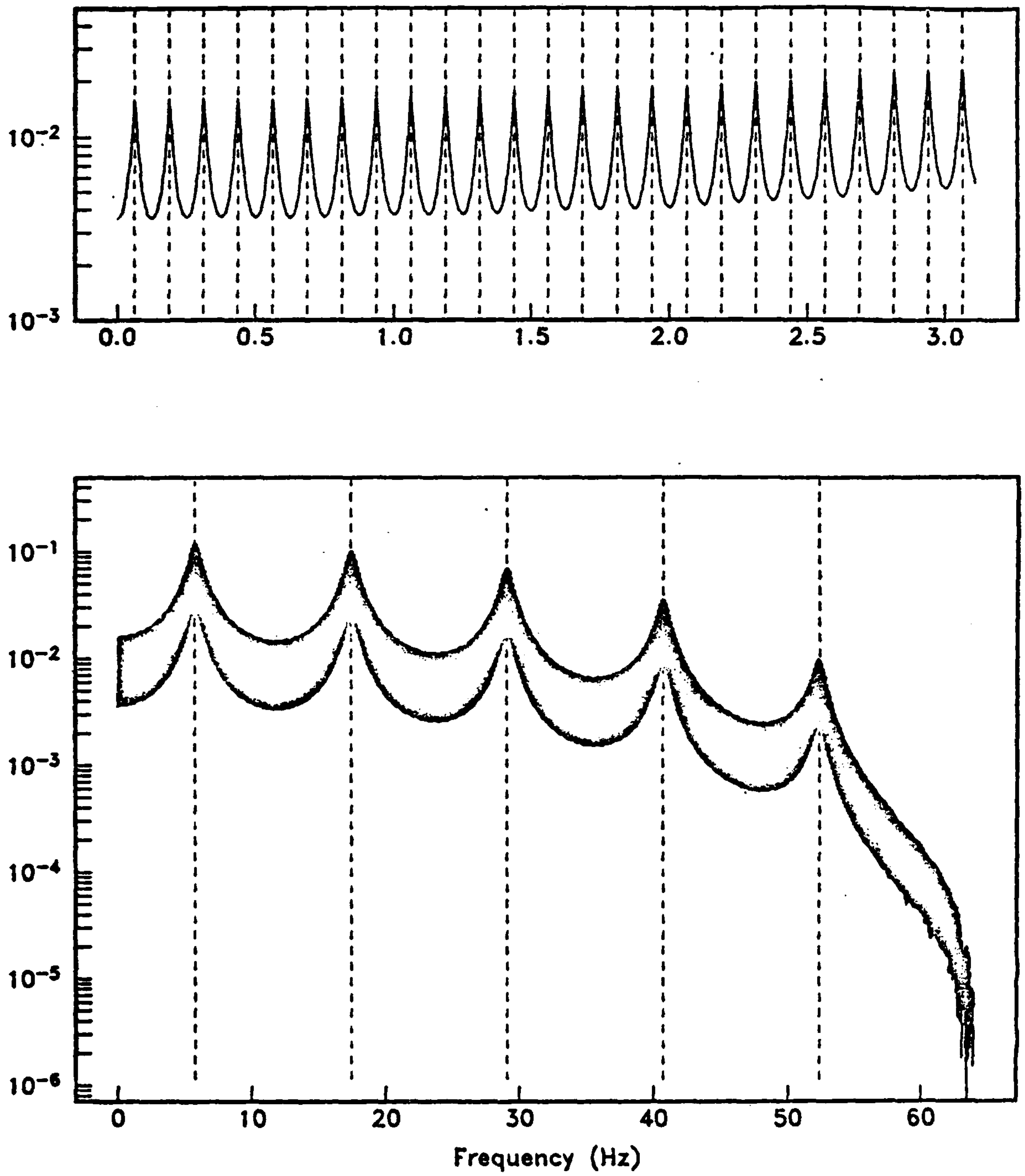

FIGURE 10. Full wavetrain spectrum, $|X(f)|^2$. a) First 3.0 hz of the spectrum with vertical lines at $f_n=(2n+1)df_w/2$, $(n=0,1,2,\ldots)$. b) Complete spectrum with vertical lines at $f_n=(2n+1)df_s/2$, $(n=0,1,2,\ldots)$.

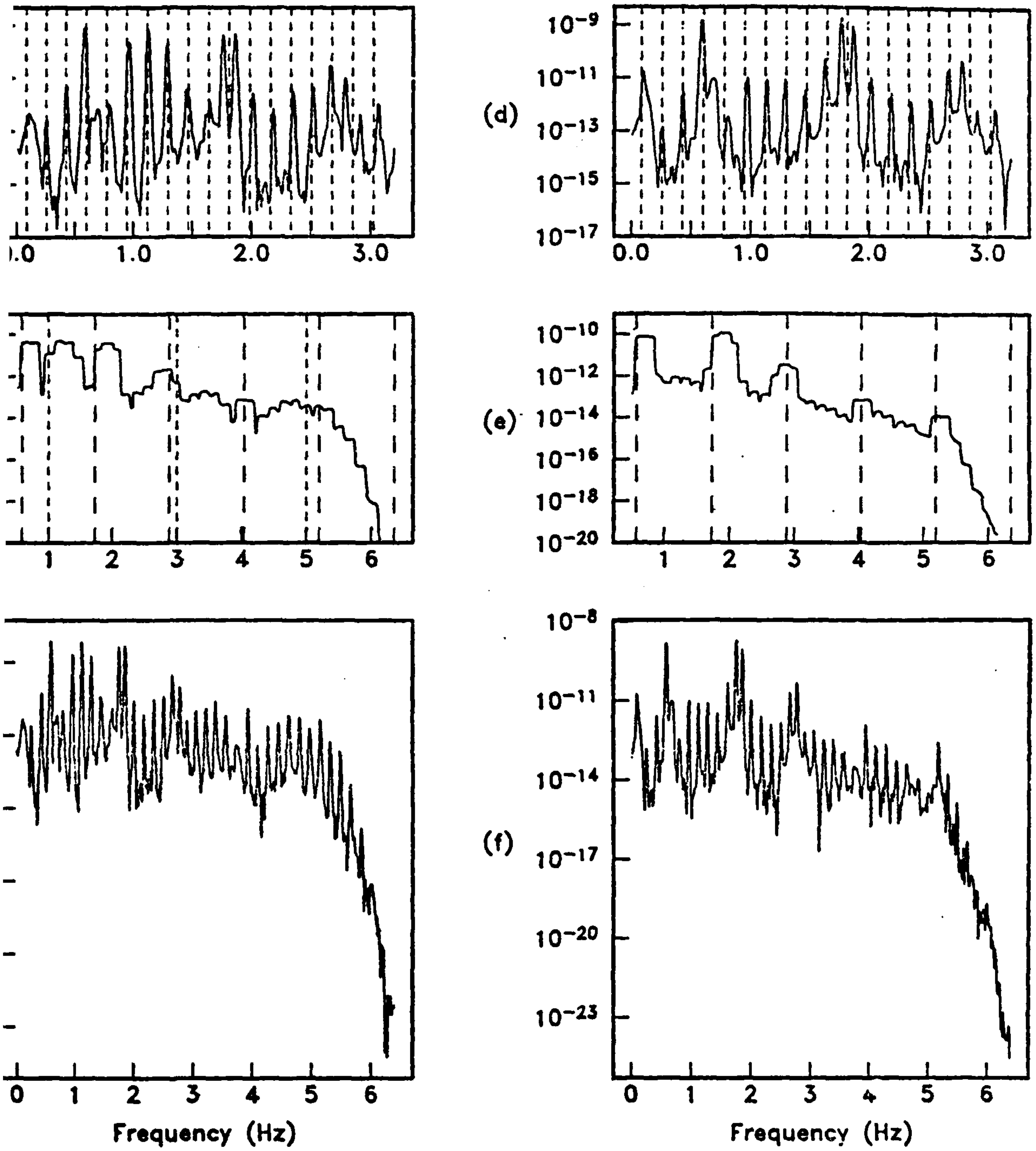

11. Power spectra of the synthetic P_n wavetrains in figure
e vertical component spectrum is shown in (a)–(c) and the
ntal component spectrum in (d)–(f). Figures (c) and (f)
e complete spectra. Figures (b) and (e) were obtained by
ation of a running mean filter to the complete spectra.
d lines indicate the predicted frequencies associated with
ent reverberation, long bars for S–waves and short bars for
ves. Figures (a) and (d) are the first 3.0 hz of the spectra
dashed lines at $f_n=(2n+1)df/2$ $(n=0,1,2,\ldots)$ where df is
d by equation (11).

AD-A154 652 VLF (VERY LOW FREQUENCY) WORKSHOP: HELD AT SAN DIEGO CALIFORNIA ON 24-25..(U) SCRIPPS INSTITUTION OF OCEANOGRAPHY LA JOLLA CA MARINE PHYSIC.. W S HODGKISS 2/3

UNCLASSIFIED 1985 MPL-U-11/85 N00014-80-C-0220 F/G 5/1 NL

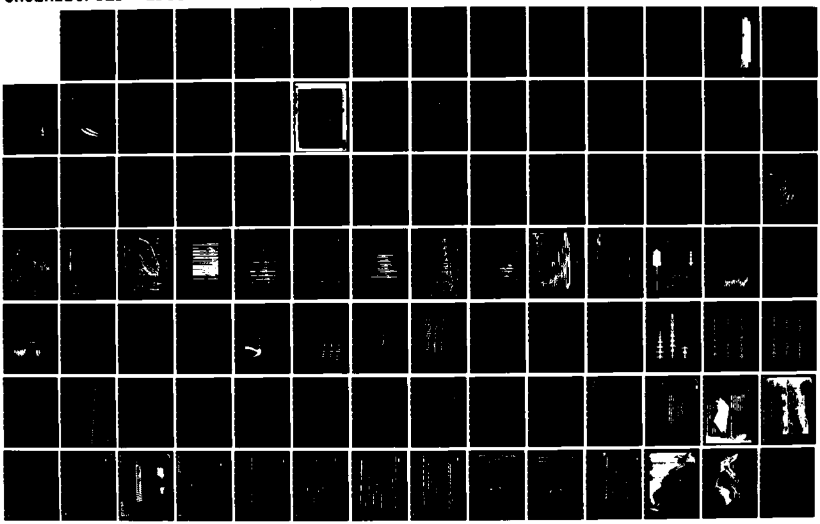

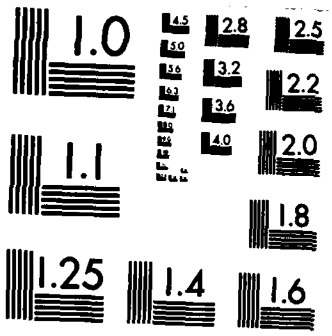

MICROCOPY RESOLUTION TEST CHART
NATIONAL BUREAU OF STANDARDS-1963-A

MSS Data

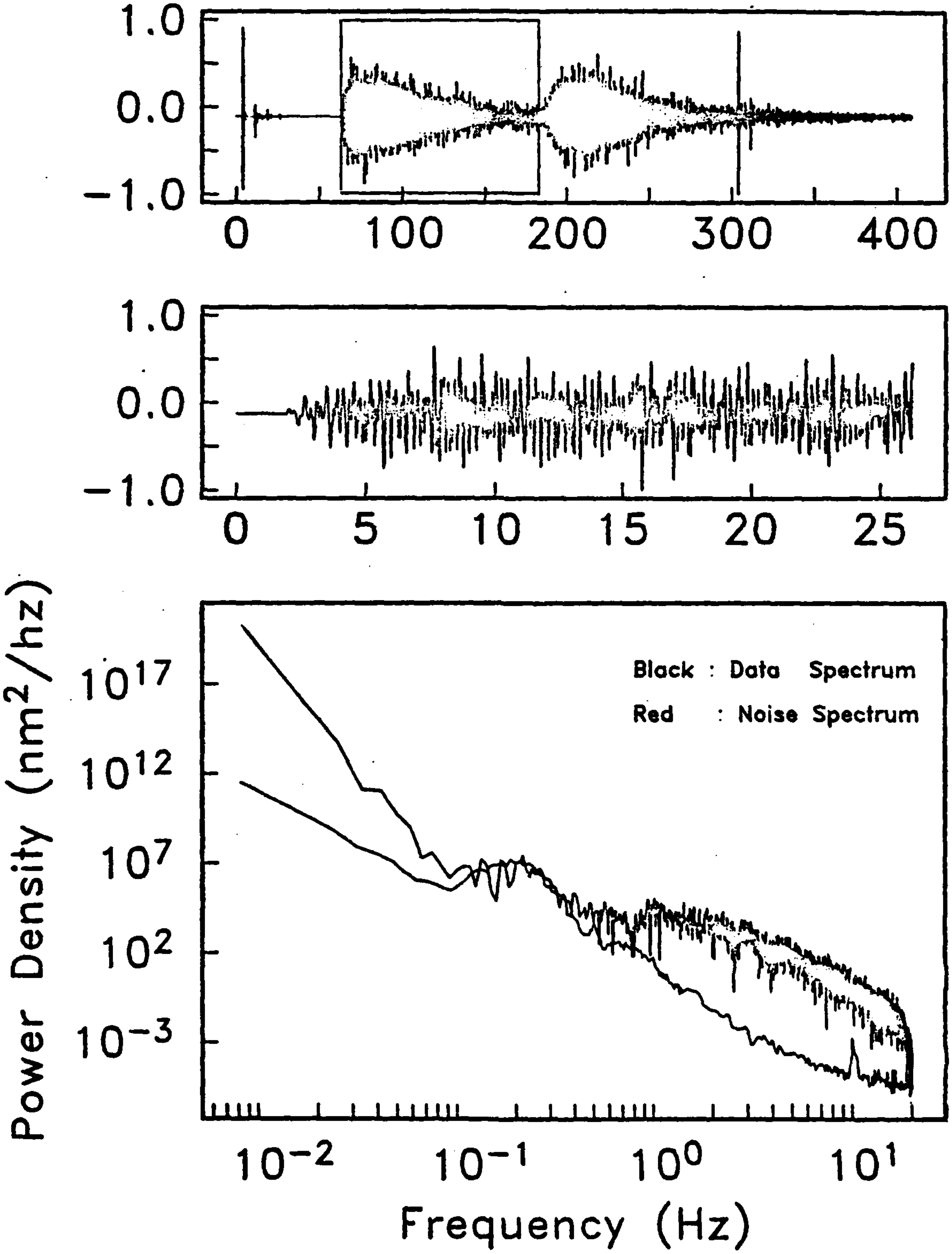
1.0
0.0
−1.0
0
100
200
300
400
1.0
0.0
−1.0
0
5
10
15
20
25
Power Density (nm^2/hz)
10^{17}
10^{12}
10^{7}
10^{2}
10^{-3}
Black : Data Spectrum
Red : Noise Spectrum
10^{-2}
10^{-1}
10^{0}
10^{1}
Frequency (Hz)

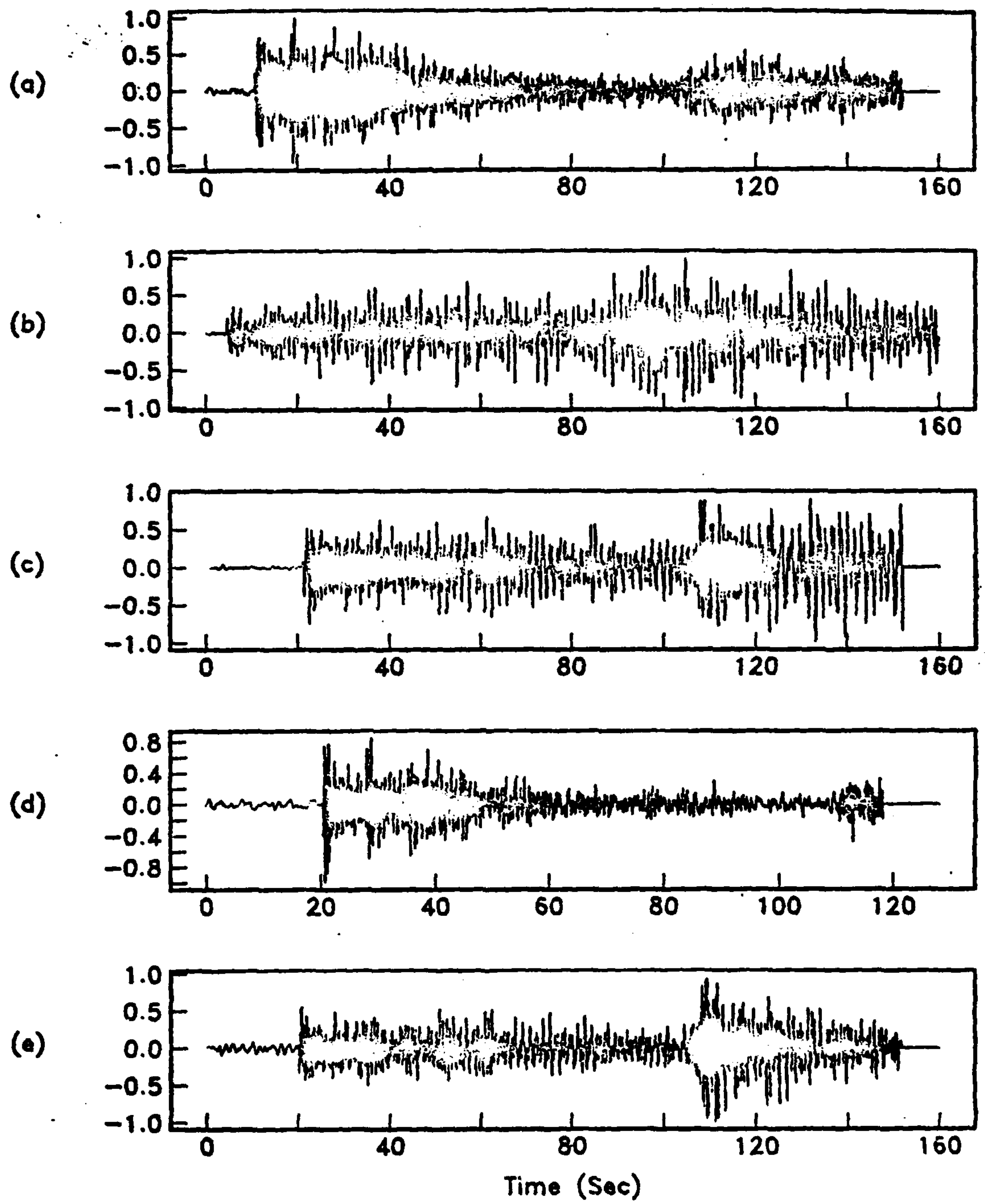

FIGURE 15. OBS data, vertical component. a) OBS Juan, event 14, b) OBS Karen, event 24, c) OBS Suzy, event 25, d) OBS Suzy, event 100 and e) OBS Suzy, event 130.

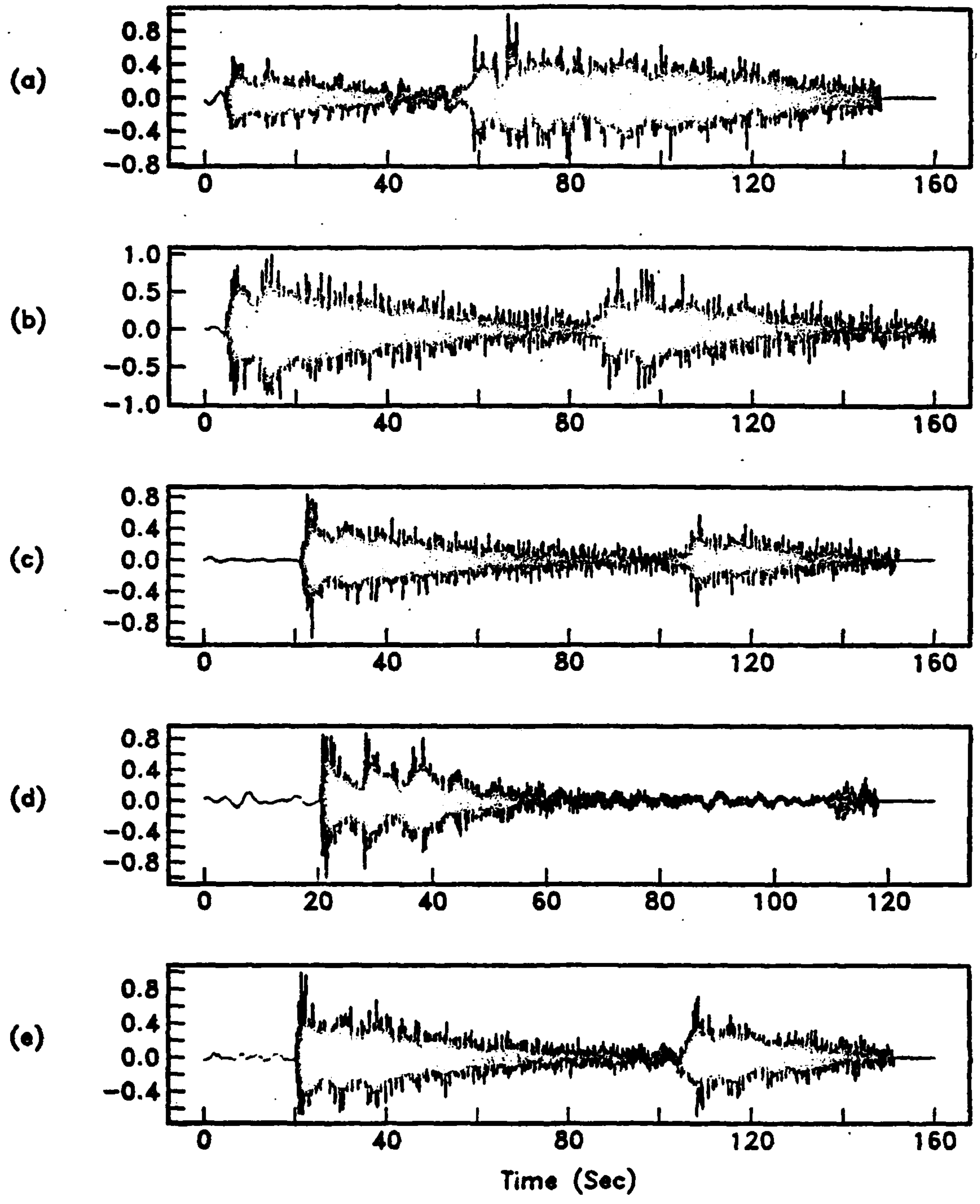

FIGURE 16. OBS data, hydrophone. a) OBS Suzy, event 35, b) OBS Karen, event 24, c) OBS Suzy, event 25, d) OBS Suzy, event 100 and e) OBS Suzy, event 130.

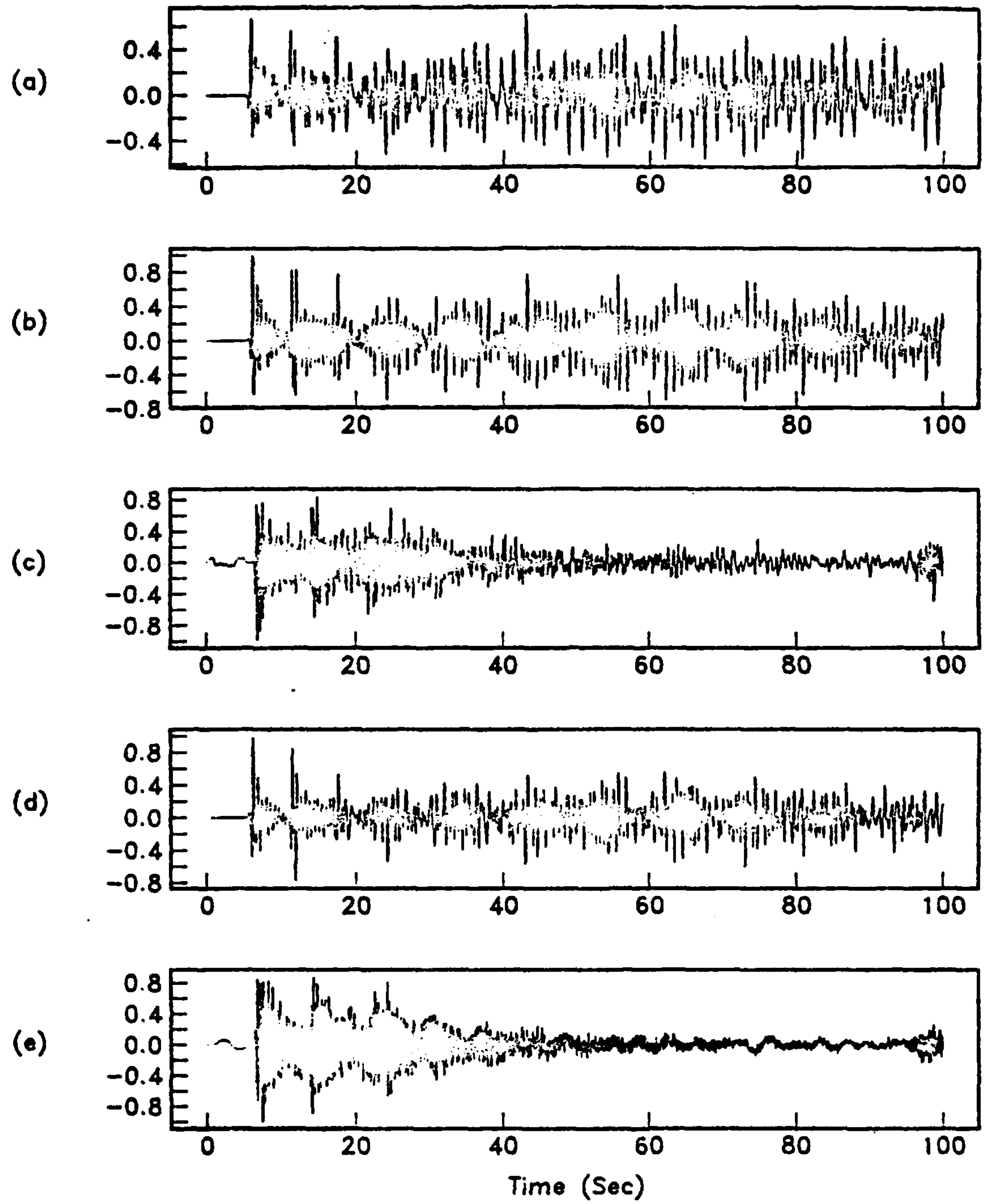

FIGURE 17. The effect of the instrument on the synthetic P_n wavetrain. (a) Synthetic P_n wavetrain of figure 4a with no instrument and (b) with the vertical component OBS response included. (c) OBS Suzy, event 100: vertical component, (d) synthetic P_n wavetrain with hydrophone response included and (e) OBS Suzy, event 100; hydrophone.

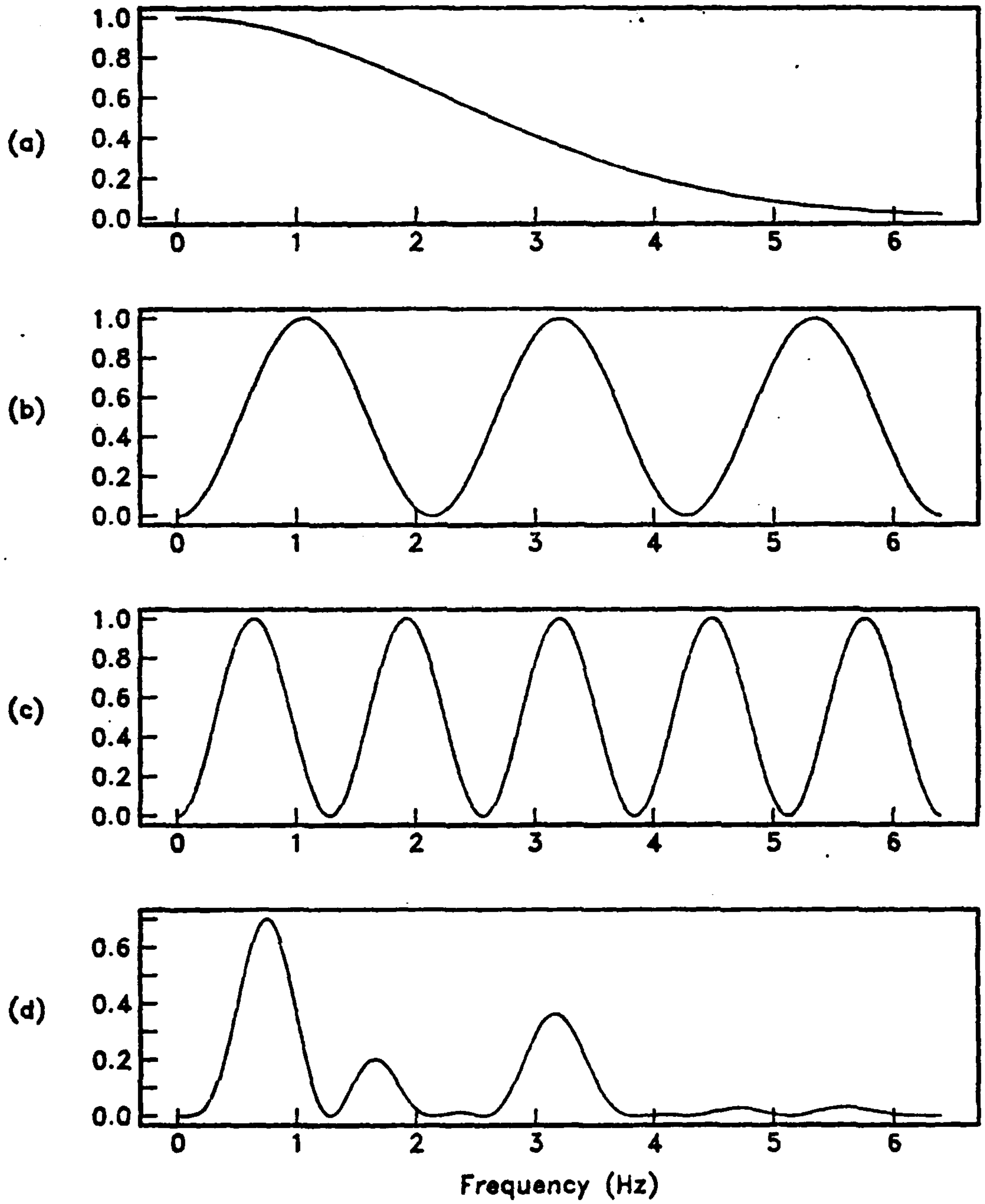

FIGURE 14. Schematic representation of the isolation of a low frequency spectral peak through the constructive interference of different layer reverberations. The figures represent idealized spectra. a) Wavelet spectrum, b) P-wave sediment reverberation spectrum, c) S-wave sediment reverberation spectrum and d) wavetrain spectrum.

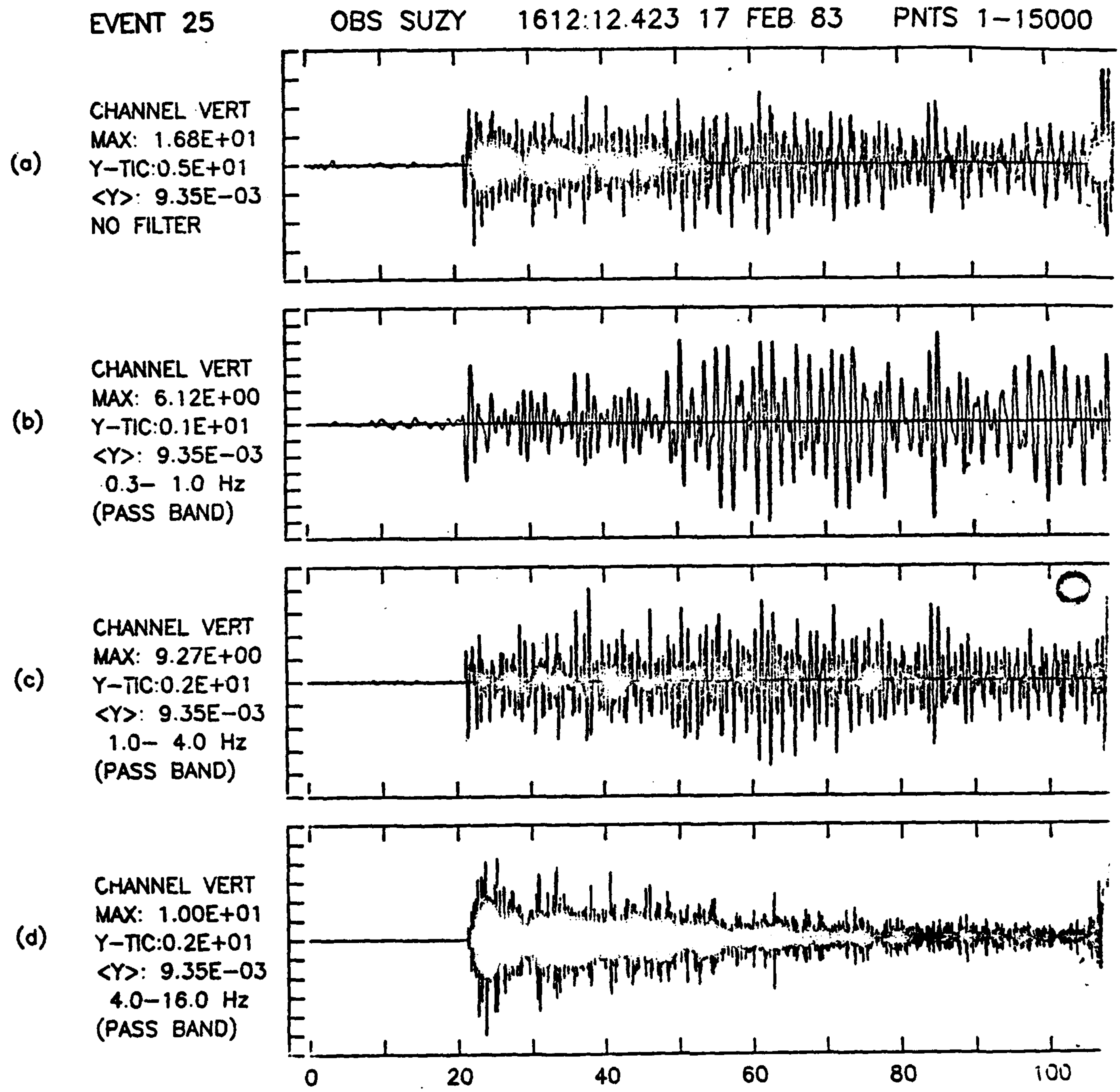

FIGURE 19. Bandpassed versions of the seismog 15(c). The seismogram in (a) is unfilterea and t bands in (b)-(d) are 0.25 to 1.0 hz, 1.0 to 4.C 4.0 to 16.0 hz respectively.

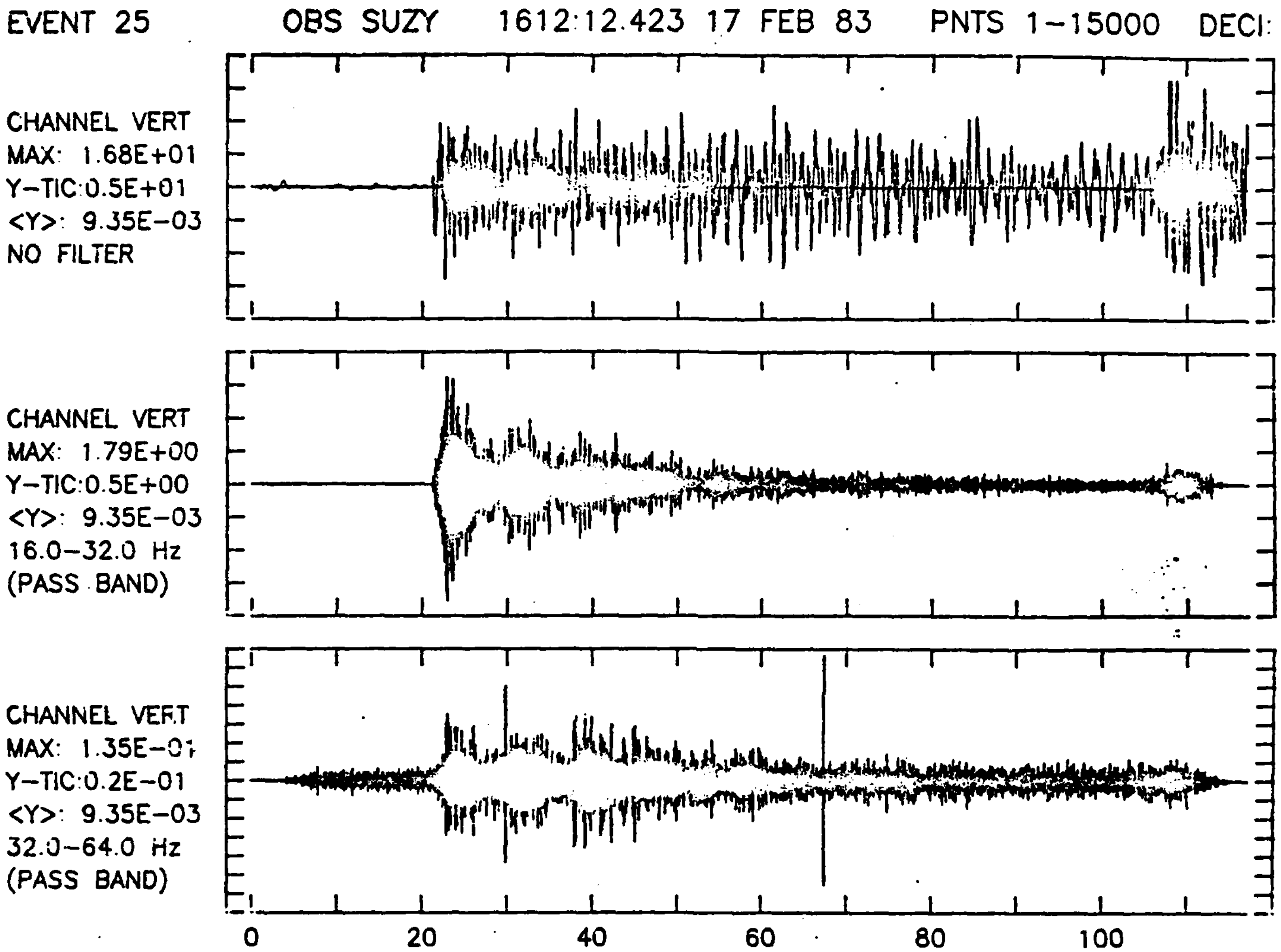
EVENT 25
OBS SUZY
1612:12.423 17 FEB 83
PNTS 1-15000
DECI: 1
CHANNEL VERT
MAX: 1.68E+01
Y-TIC:0.5E+01
<Y>: 9.35E-03
NO FILTER
CHANNEL VERT
MAX: 1.79E+00
Y-TIC:0.5E+00
<Y>: 9.35E-03
16.0-32.0 Hz
(PASS BAND)
CHANNEL VERT
MAX: 1.35E-01
Y-TIC:0.2E-01
<Y>: 9.35E-03
32.0-64.0 Hz
(PASS BAND)
0
20
40
60
80
100

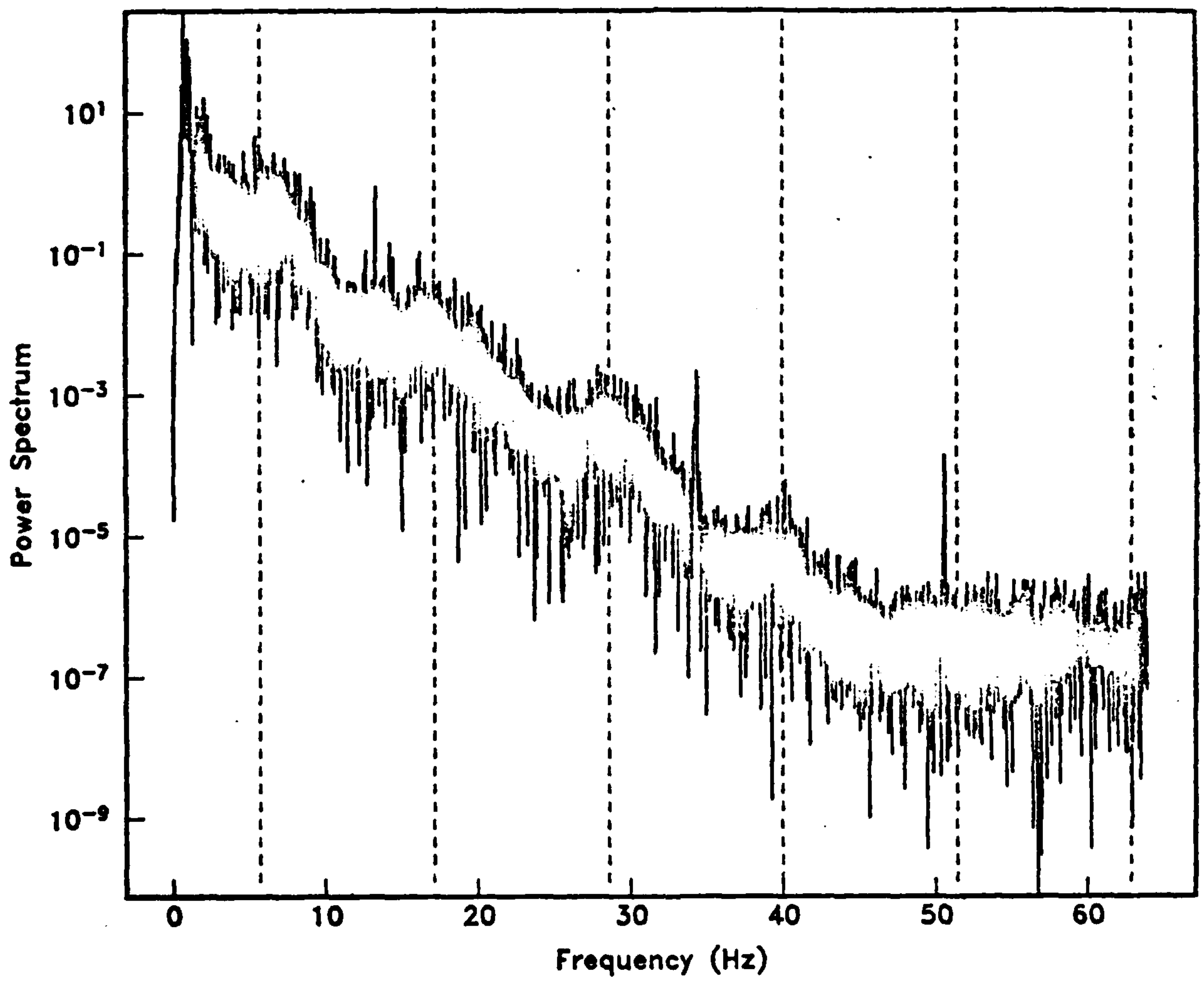

FIGURE 20. Power spectrum of the seismogram in figure 15(b). Dashed lines indicate predicted positions of the spectral peaks associated with P-wave reverberations in the sediments.

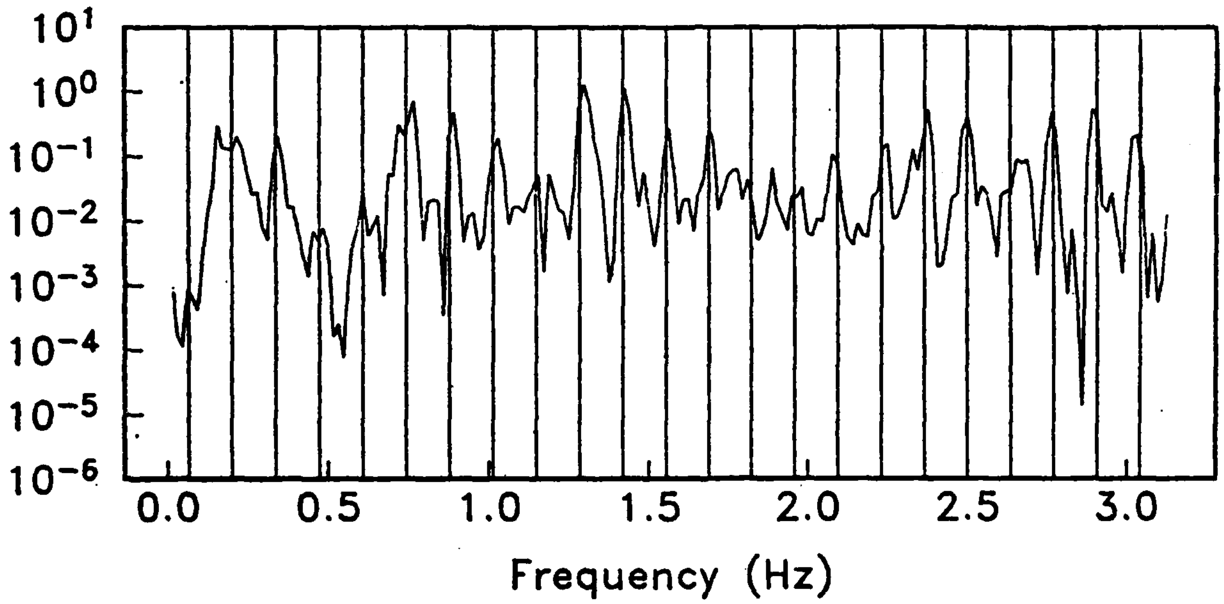

FIGURE 21. First 3.0 hz of the power spectrum of the seismogram in figure 16(e). Vertical lines indicate the predicted positions of the spectral peaks corresponding to water reverberations.

OBSERVATIONS OF STONELEY WAVES USING SEA FLOOR SHOTS AND RECEIVERS

LeRoy M. Dorman
Allan W. Sauter
Anthony E. Schreiner

The spatial and temporal correlation properties of background noise are primarily controlled by two things: 1) the excitation and 2) the waveguides in which the noise travels. We focus our attention here on the waveguide at the sea floor. We have excited and recorded Stoneley waves along the sea floor in order to extract the physical properties of the top few meters of the sea floor. Our location was the site of DSDP hole #469, in 3800 m of water at the base of the Patton escarpment west of San Diego. We used 2.5 kg charges of TNT fired by electronic timers. Five of the eight shots attempted performed satisfactorily. Three records, at ranges between 500 and 1500 m showed Stoneley waves, while shots at greater ranges did not. Fitting the observed group velocities (or slownesses) to a simple model by trial and error yielded a model with a linear shear velocity gradient of $3.5 s^{-1}$ and shear velocity at the sea floor of about $50 ms^{-1}$.

We also measured the response of the sea floor to excitation by the instrument and find that data consistent with a damped system with a resonant frequency of 18 Hz and a Q of 5.

Both the physical property work and the resonance measurement bear on the problem of equalization of OBS responses so that they may be used productively in arrays.

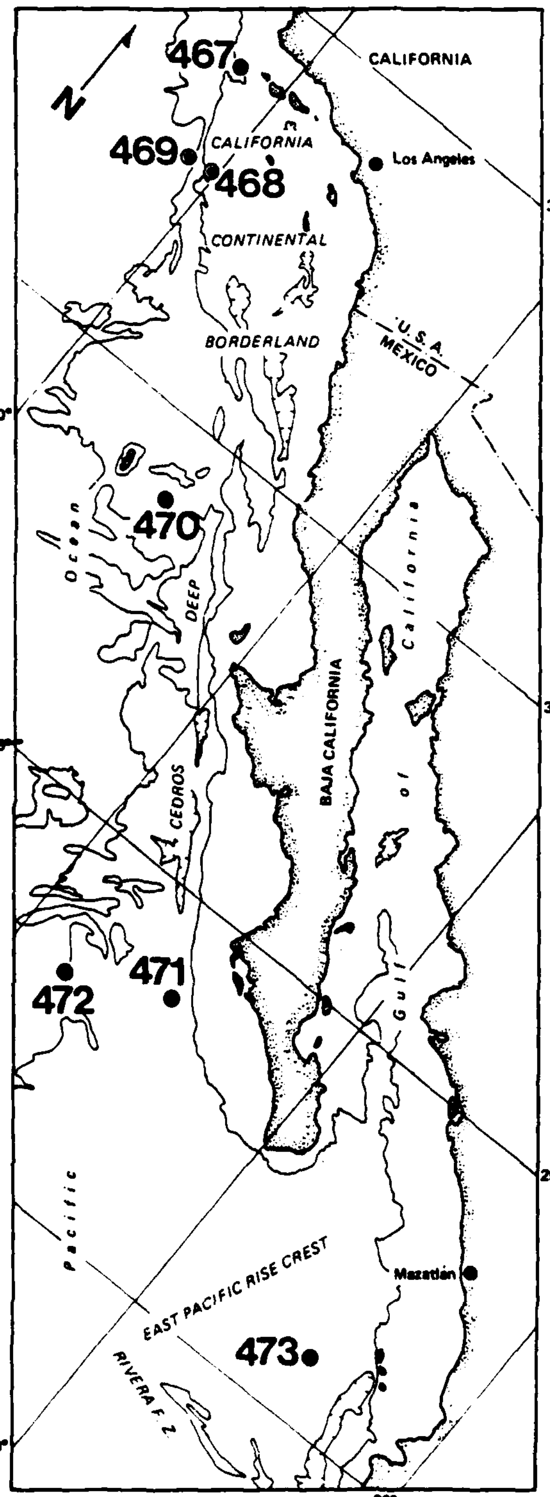

Figure 2. Location of Leg 63 sites.

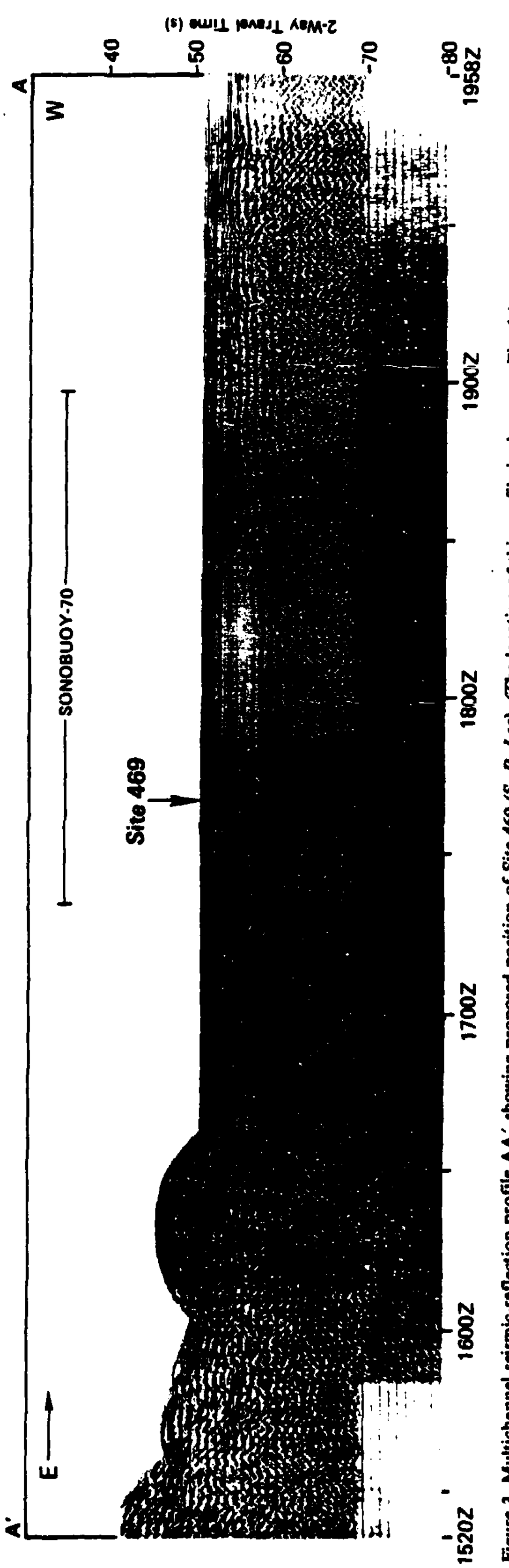

Figure 3. Multichannel seismic-reflection profile AA' showing proposed position of Site 469 (*S. P. Lee*). (The location of this profile is shown on Fig. 1.)

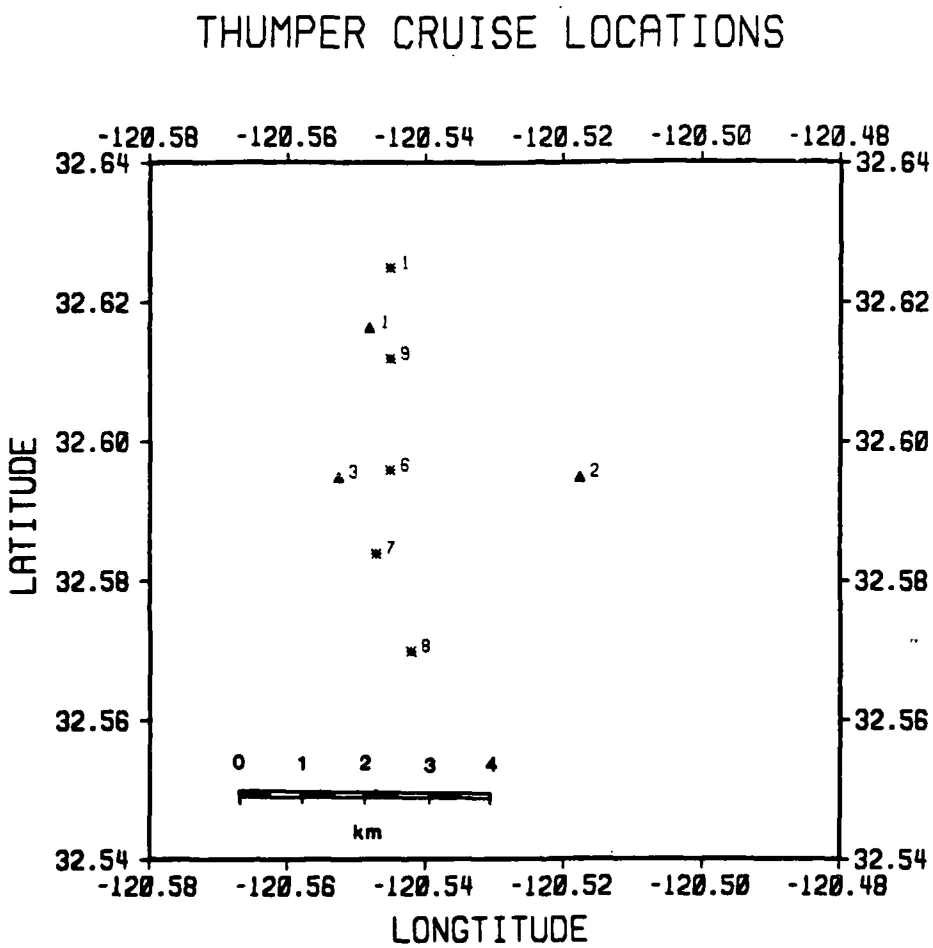

'he least squares solution for the shot and OBS locations. triangles are OBSs while the stars represent shots.

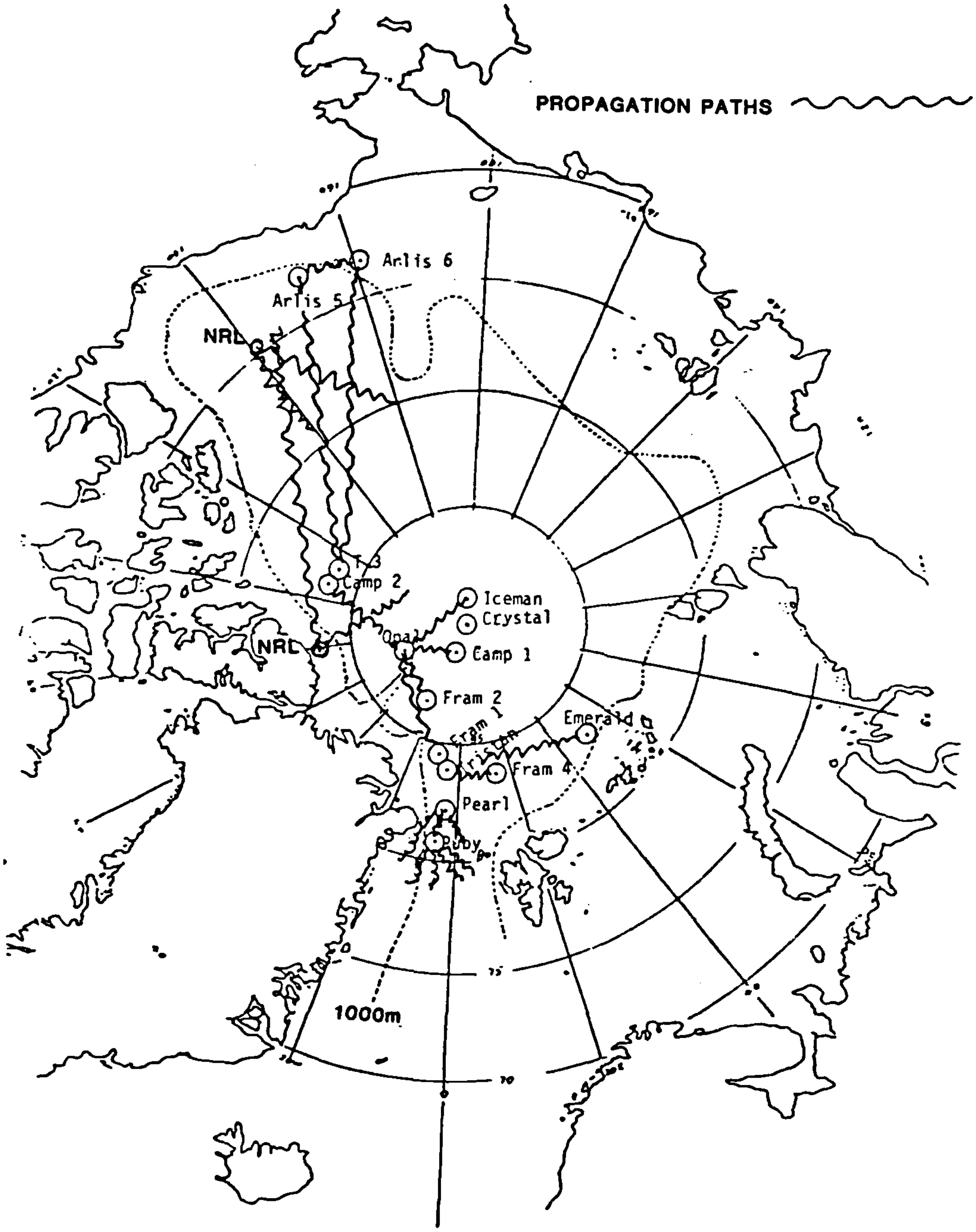

PROPAGATION PATHS
Arlis 6
Arlis 5
NRL
T-3
Camp 2
Iceman
Crystal
Opal
NRL
Camp 1
Fram 2
Fram 1
Emerald
Fram 4
Pearl
1000m

$$TL = TL_o(f,R) + 10\log R + \Delta TL(z_s, z_r, f) + \alpha(f,\sigma)$$

$$TL_o(f) = \min \begin{array}{c} \text{Short Range Spreading} \\ \begin{bmatrix} 57.50+.10(f-10)+\alpha_o(f)R & 10\text{Hz}\leq f\leq 20\text{Hz} \\ 58.50+.50(f-20)^{.5}+\alpha_o(f)R & 20\text{Hz}\leq f\leq 200\text{Hz} \\ 65.20+.01(f-200)+\alpha_o(f)R & 200\text{Hz}\leq f\leq 800\text{Hz} \end{bmatrix} \\ \text{Long Range Spreading} \\ \begin{bmatrix} 62.00+.30(f-10) & 10\text{Hz}\leq f\leq 20\text{Hz} \\ 65.00+.65(f-20)^{.6} & 20\text{Hz}\leq f\leq 200\text{Hz} \\ 79.65+.01(f-200) & 200\text{Hz}\leq f\leq 300\text{hz} \end{bmatrix} \end{array}$$

$$\Delta TL_r = \Delta TL_s = -10 \log \sin^2(2\pi \sin\theta zf/c)$$

$$\Delta TL = \begin{bmatrix} .5zf/c-.72 & 10\text{Hz}\leq f\leq 50\text{Hz} \\ (.9-.008f)zf/c-(1.296-.01152f) & 50\text{Hz}\leq f\leq 100\text{ Hz} \\ (.1zf/c-.144)\left(\frac{100}{f}\right)^2 & 100\text{Hz}\leq f\leq 800\text{ Hz} \end{bmatrix}$$

$$\alpha(f,\sigma) = C_o(f)\sigma^{n(f)}$$

$$n(f) = \frac{2f^2+550}{f^2+50}$$

$$C_o(f) = \begin{array}{ll} 2.35\text{x}10^{-9}\ f^{4.32} & 10\text{Hz}\leq f\leq 20\text{Hz} \\ 2.40\text{x}10^{-6}\ f^{2.00} & 20\text{Hz}\leq f\leq 100\text{Hz} \\ 2.40\text{x}10^{-3}\ f^{0.500} & 100\text{Hz}\leq f\leq 200\text{Hz} \\ 3.40\text{x}10^{-2} & 200\text{Hz}\leq f\leq 300\text{Hz} \end{array}$$

quantitative difference in the values of these functions are found, because the assumptions about the nature of ice scattering is very different in different models. The Buck/Wilson ice scattering function derived in this paper is divided into two parts for ~~shot~~ short and long ranges and given a physical interpretation.

The development of the TL model and analysis of the data uncovered a possible "megaphone" or slope enhanced propagation effect on the eastern slopes of the Northwind Ridge. It is emphasized that the megaphone effect is very site dependent and no implications are made for the existance of the megaphone effect over other sloping areas.

ABSTRACT

A semi-empirical Arctic transmission Loss (TL) model is developed based on TL data collected between ice camps and/or aircraft in the deep Arctic basins since 1970. The model is limited to frequencies between 10Hz and 800Hz, to source and receiver depths above 800 ft., and to minimum water depths between source and receiver of 1000m ~~100m~~ or greater. The model estimates average TL and no attempt is made to account for spread in TL at fixed ranges.

The Buck/Wilson Arctic TL Model consists of four components: the source/receiver depth dependence of TL; cyclindrical spreading; spherical spreading plus low ($<10^{\circ}$) angle and bottom interaction loss; and long range, ice scattering attenuation. Since measured TL data connot be uniquely divided into these four areas, care is taken to use basic TL properties known to be true in the open ocean. The depth dependence of TL is modeled using standard surface/image interference functions and the data show that the pressure release surface is the sea/ice interface and not the air/ice interface. The parabolic equation (PE) and the ASEPS Transmission Loss (ASTRAL) model estimates of spreading loss are used as a guide in deriving spreading loss functions. The "residual" TL, defined as the measured TL minus the model TL depth and spreading functions, is used to derive the attenuation due to ice scattering loss as a function of frequency and ice roughness (standard deviation). The comparison of the drived ice scattering attenuation with other model ice scattering attenuation or reflection functions will be adressed in a future paper. A large

Jim Wilson

Buck/Wilson Deep Water Arctic Transmission Loss Model

General Specifications

SCRIPPS INSTITUTION OF OCEANOGRAPHY OCEAN BOTTOM SEISMOGRAPHS

RECORDER:	10" reel-to reel 1/4" tape
TAPE:	7200 feet.
TAPE FORMAT:	4 tracks digital serial biphase. System status and time distributed with the data. 3 seismometer channels. 1 hydrophone.
CAPACITY:	24 hours recording.
MEMORY:	5.2 minutes for 4 components at 128 samples per second per channel.
DYNAMIC RANGE:	102 DB (12 bit ADC with 64 x high speed gain ranging).
MODES:	Programmed and/or triggered
SCHEDULE PROGRAMMING:	Flexible
STATUS:	Message containing noise level, tape usage, battery voltages transmitted to surface on acoustic command.
INTERNAL TIMING:	TCXO to 60 days
POSITIONING:	Acoustic transponder
POWER:	About 400 MW
DIMENSIONS:	About 1 m^2 footprint. 22 "i.d. sphere with 6" center ring.
WEIGHT:	About 550 pounds in air, with ballast tripod.
REFERENCE:	Moore, R.D., L.M. Dorman, C-Y Huan, and D.L. Berliner. An Ocean bottom, microprocessor based seismometer, Marine Geophysical Researches, 4, 451-477, 1981.

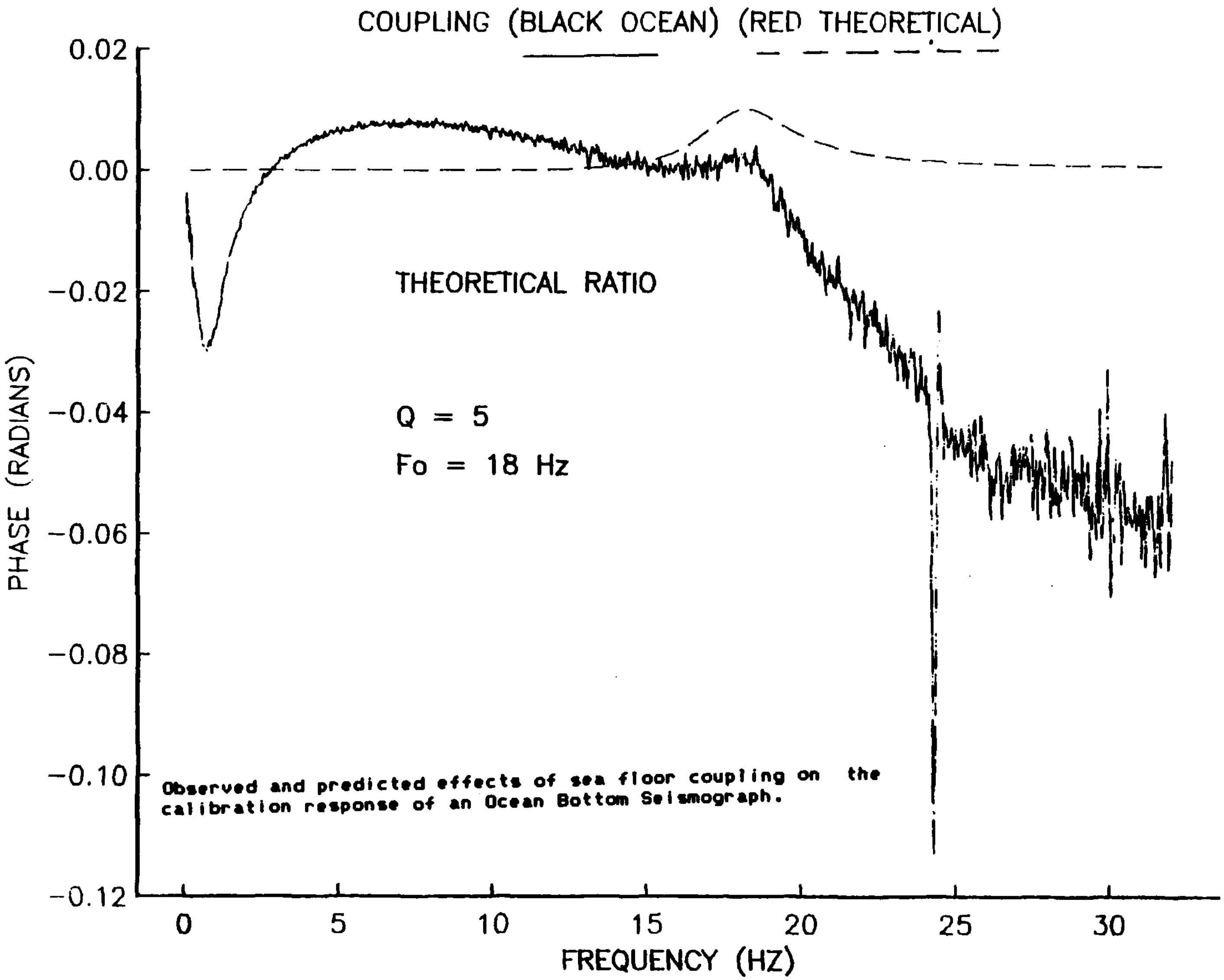

Observed and predicted effects of sea floor coupling on the calibration response of an Ocean Bottom Seismograph.

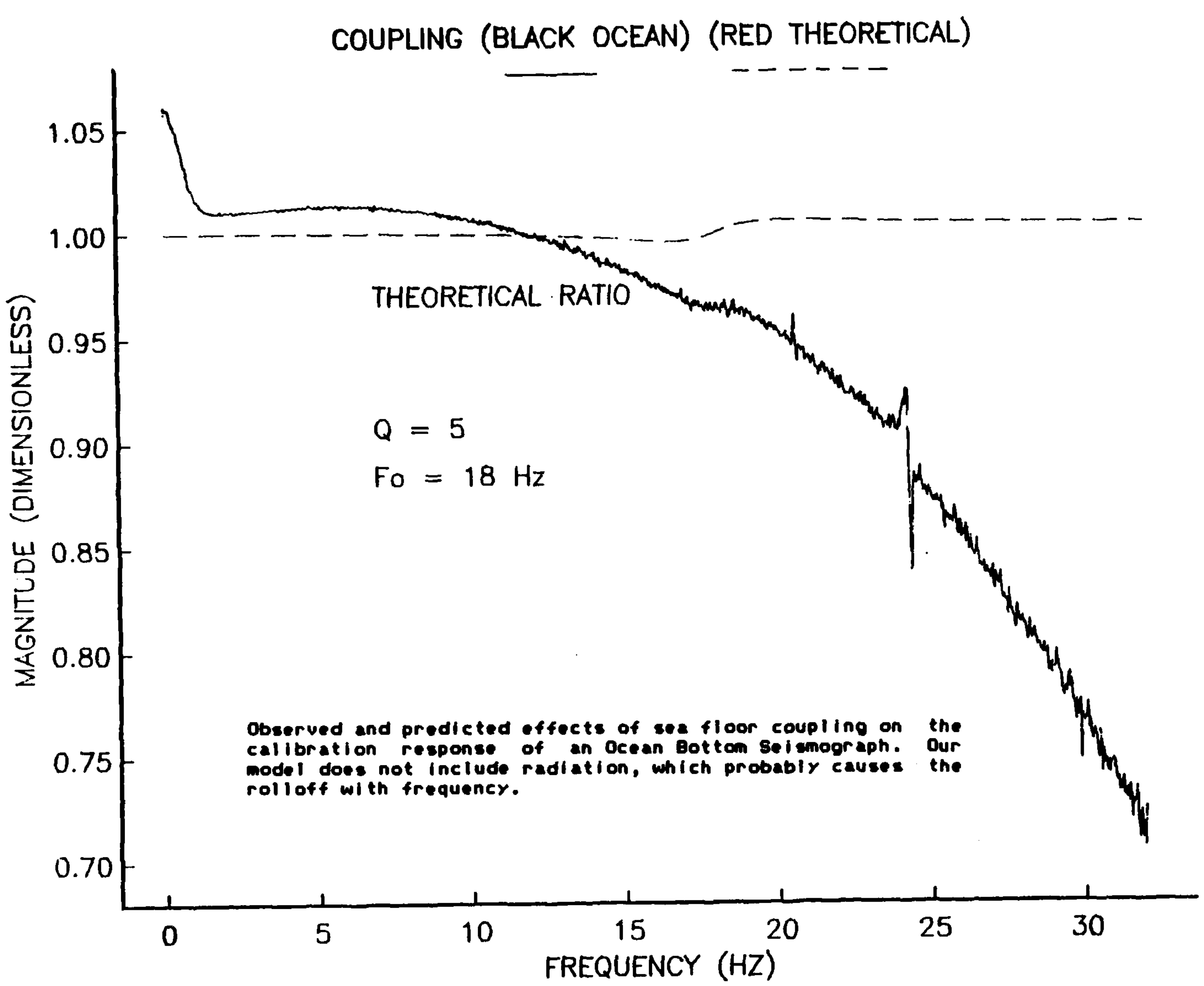

Observed and predicted effects of sea floor coupling on the calibration response of an Ocean Bottom Seismograph. Our model does not include radiation, which probably causes the rolloff with frequency.

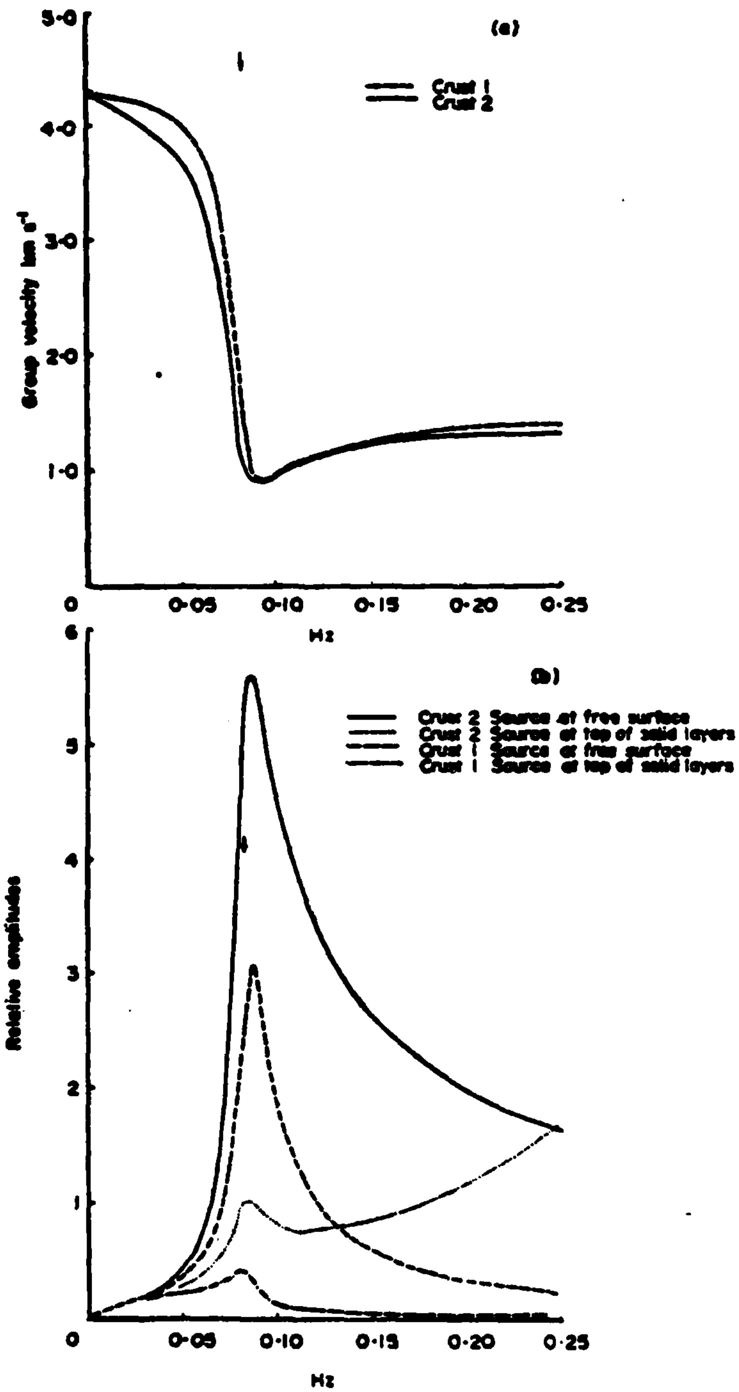

The relationship between group velocity of a mode and amplitude resulting from a point force excitation. It shows that the largest spectral amplitude occurs at the minimum of the group velocity of the mode.

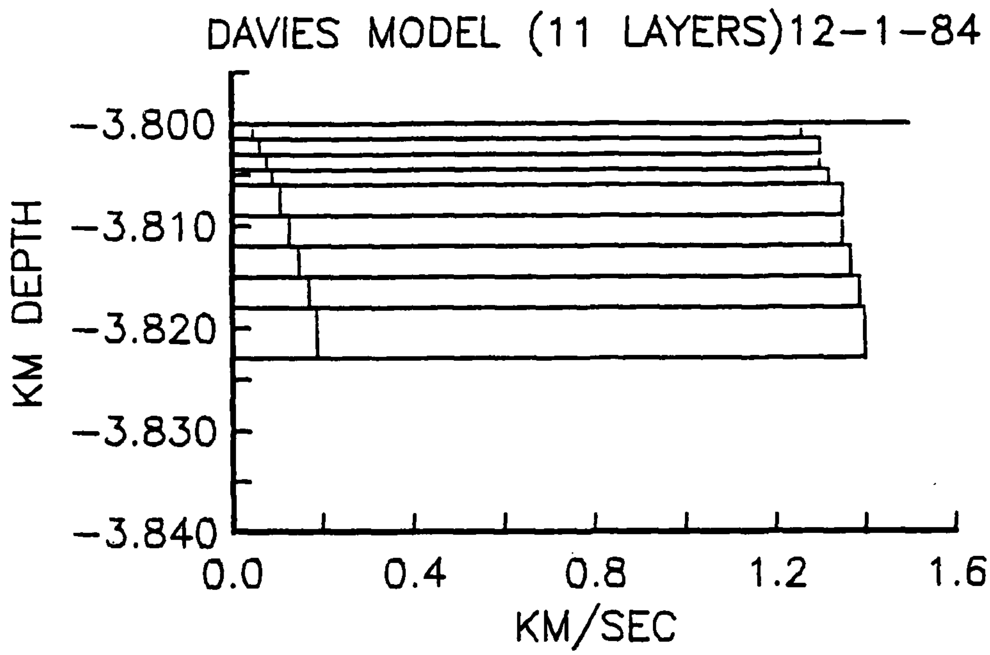

A model obtained by D. Davies using data from the northwest Indian Ocean.

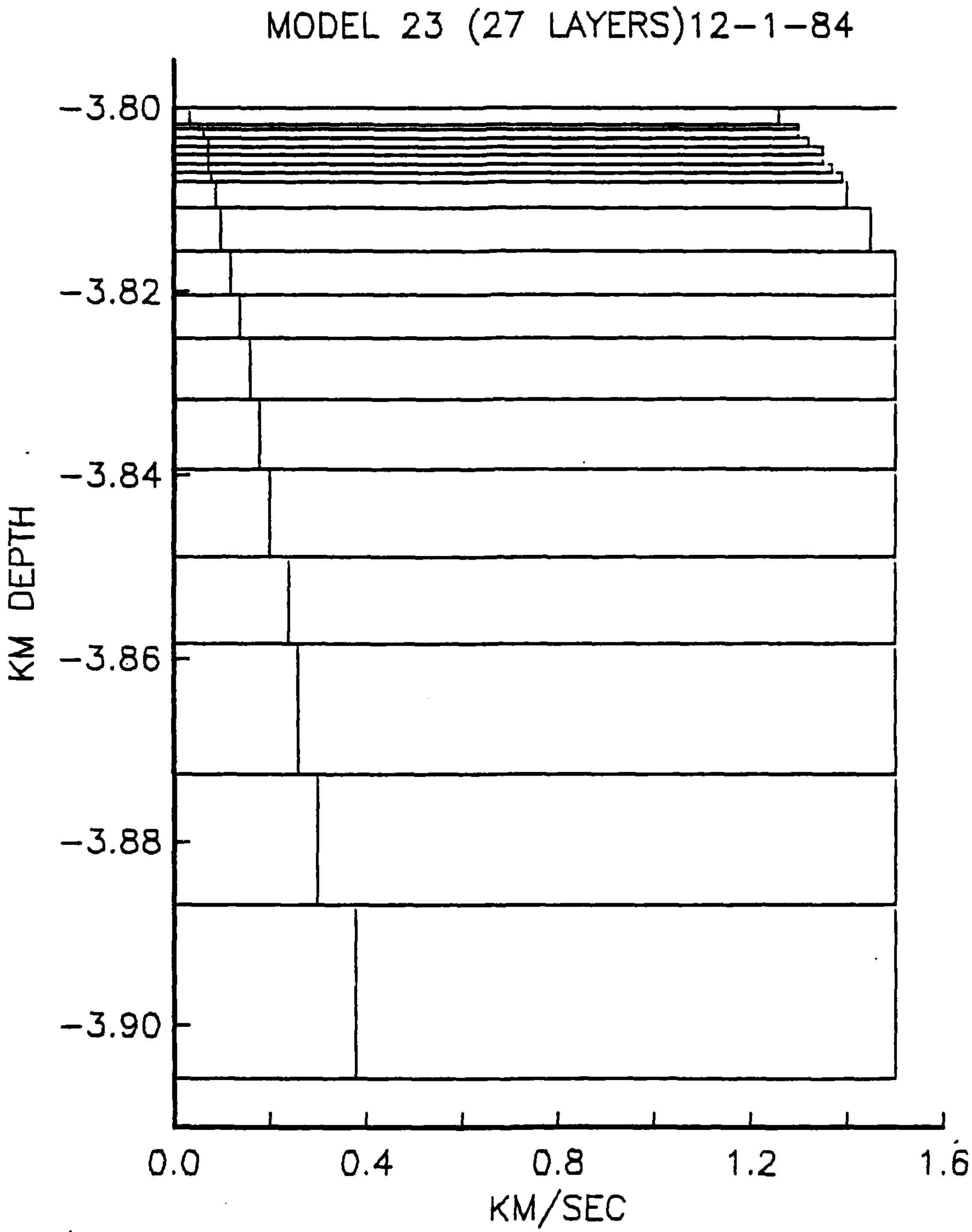

A model whose group velocities are consistent with our data.

GROUP DISPERSION FOR MODEL 23

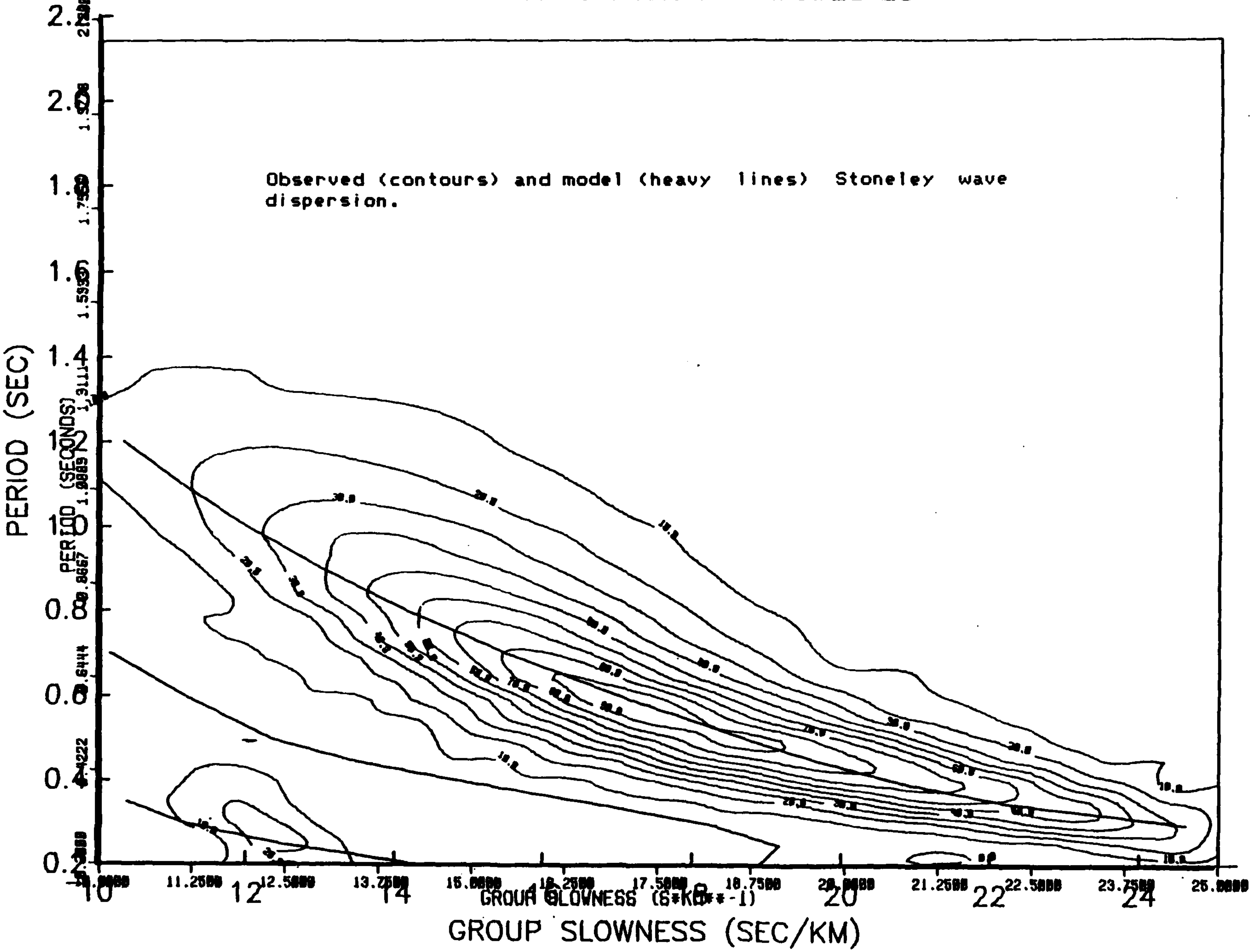

INSTRUMENT 1 EVENT 1009
RANGE 0.578 KM

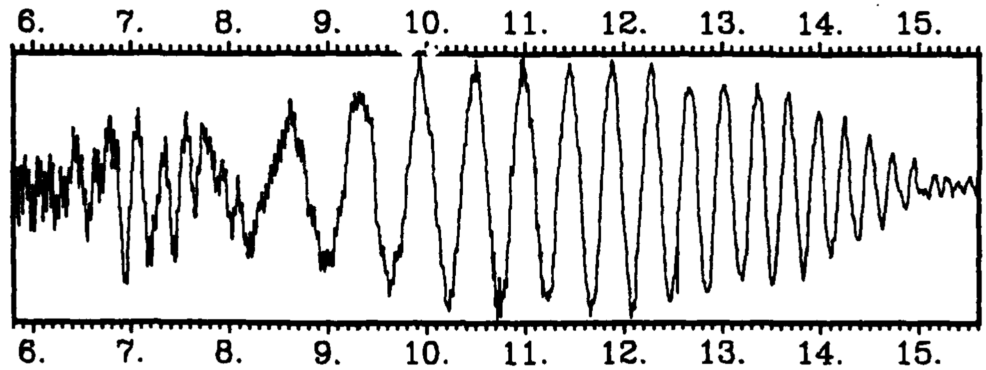

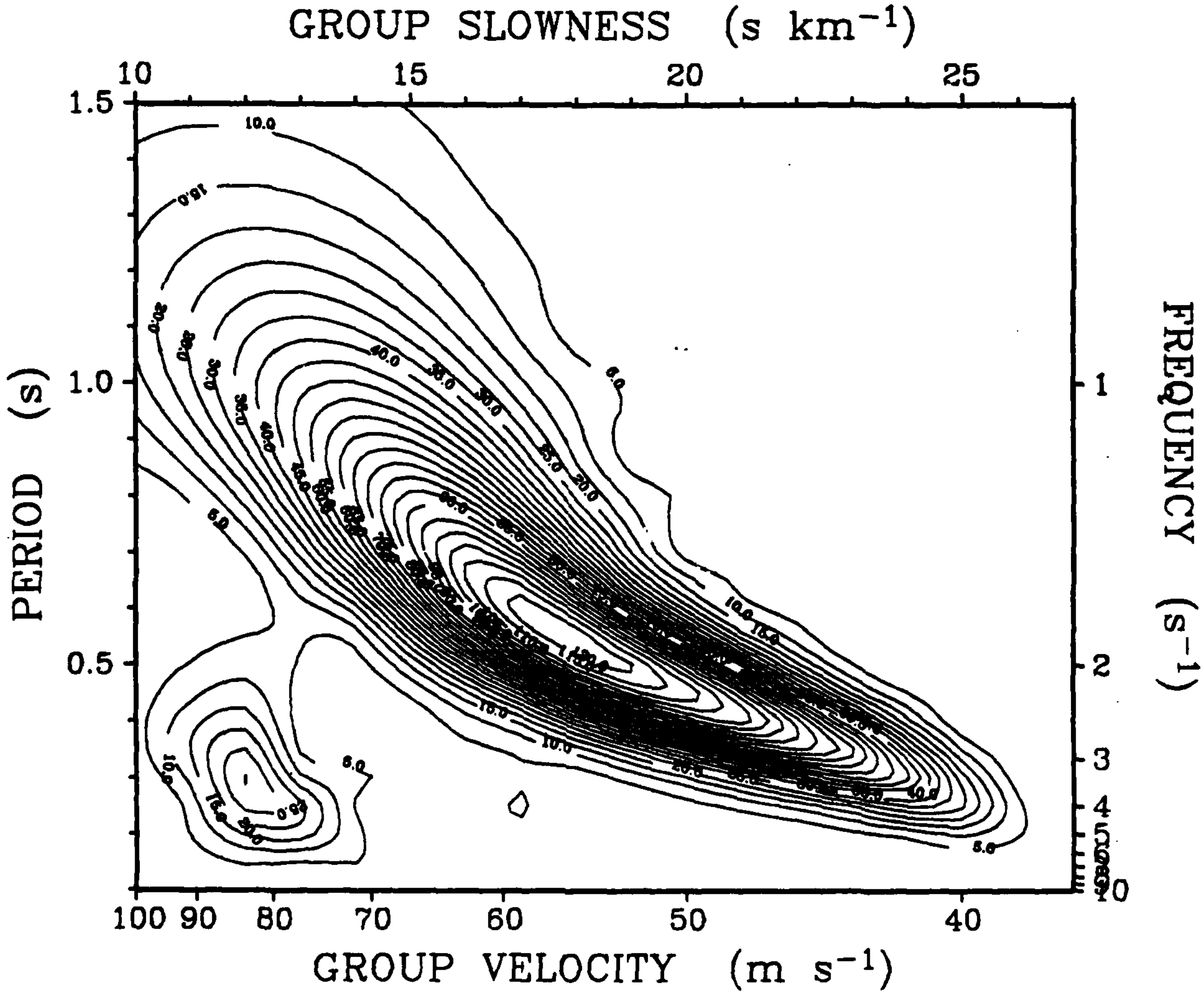

A Stoneley wave filtered in time and period by the multiple filtering scheme of Dziewonski et. al. (1969). The plot is of the amplitude of the analytic signal envelope as a function of time and period. This presentation is what would be seen if a sonogram were contoured.

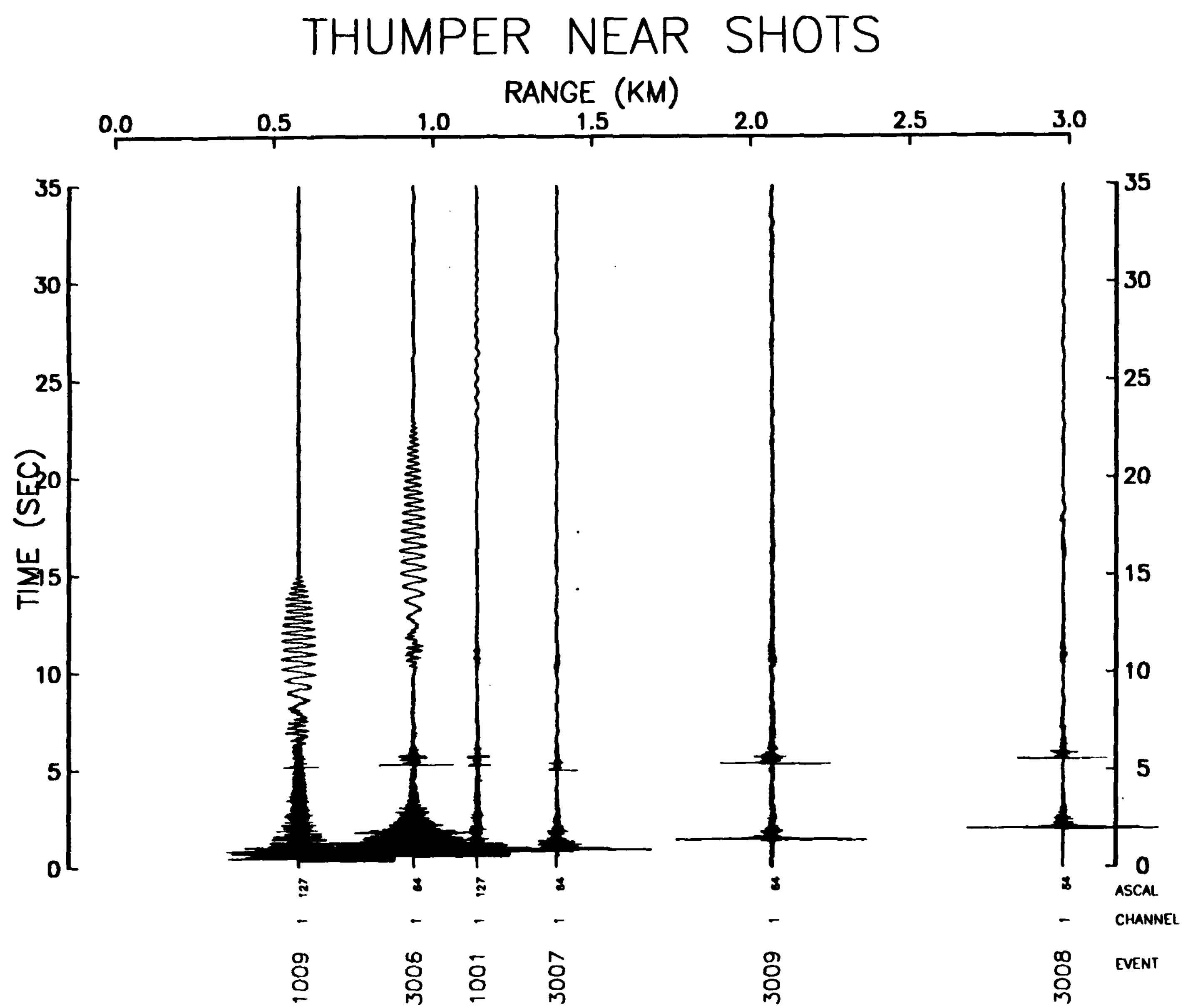

A record section showing data from the near shots.

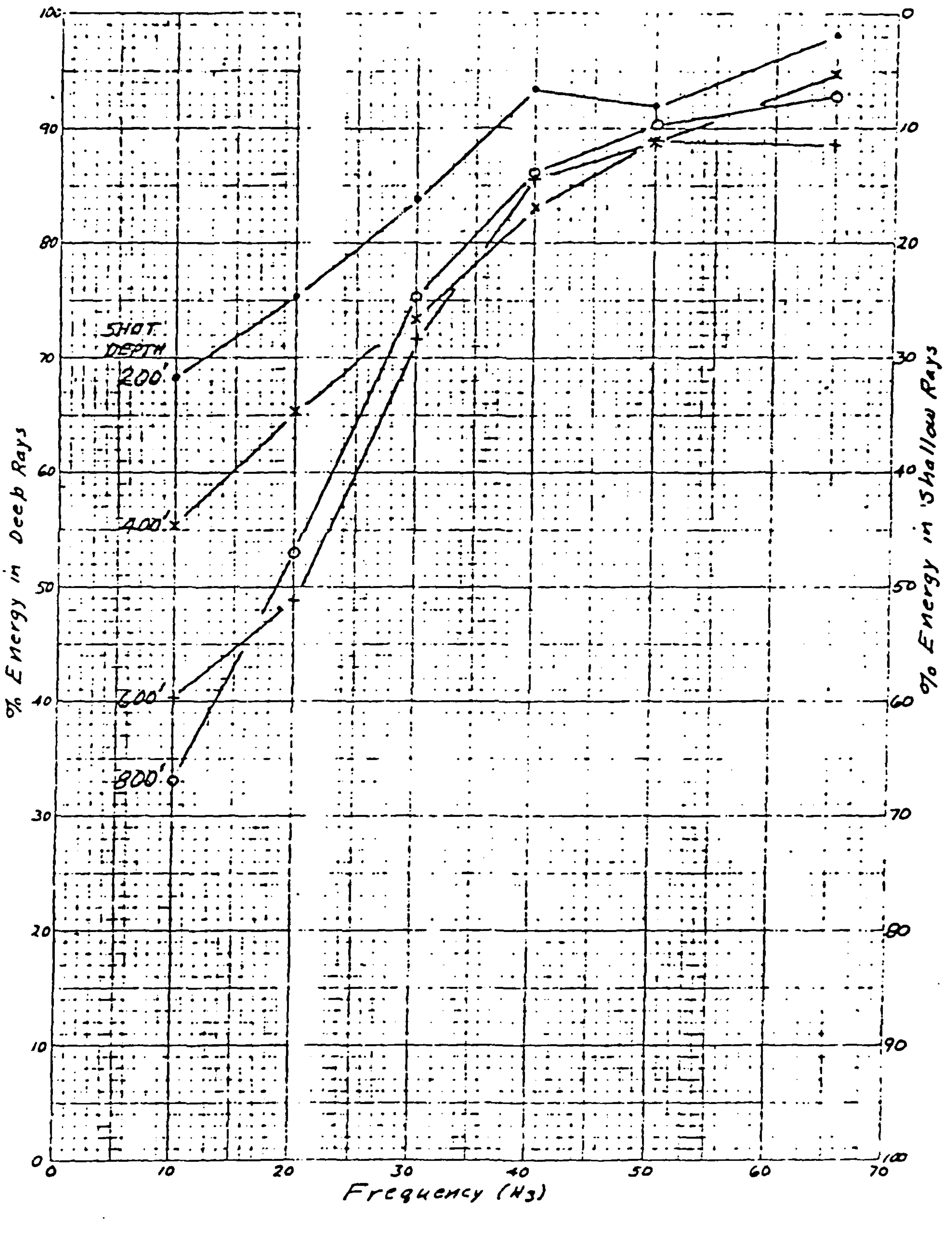

Figure 63 Relative Energy of Deep and Shallow RSR Rays for 4 Source Depths (Average for all 4 Bottom Categories)

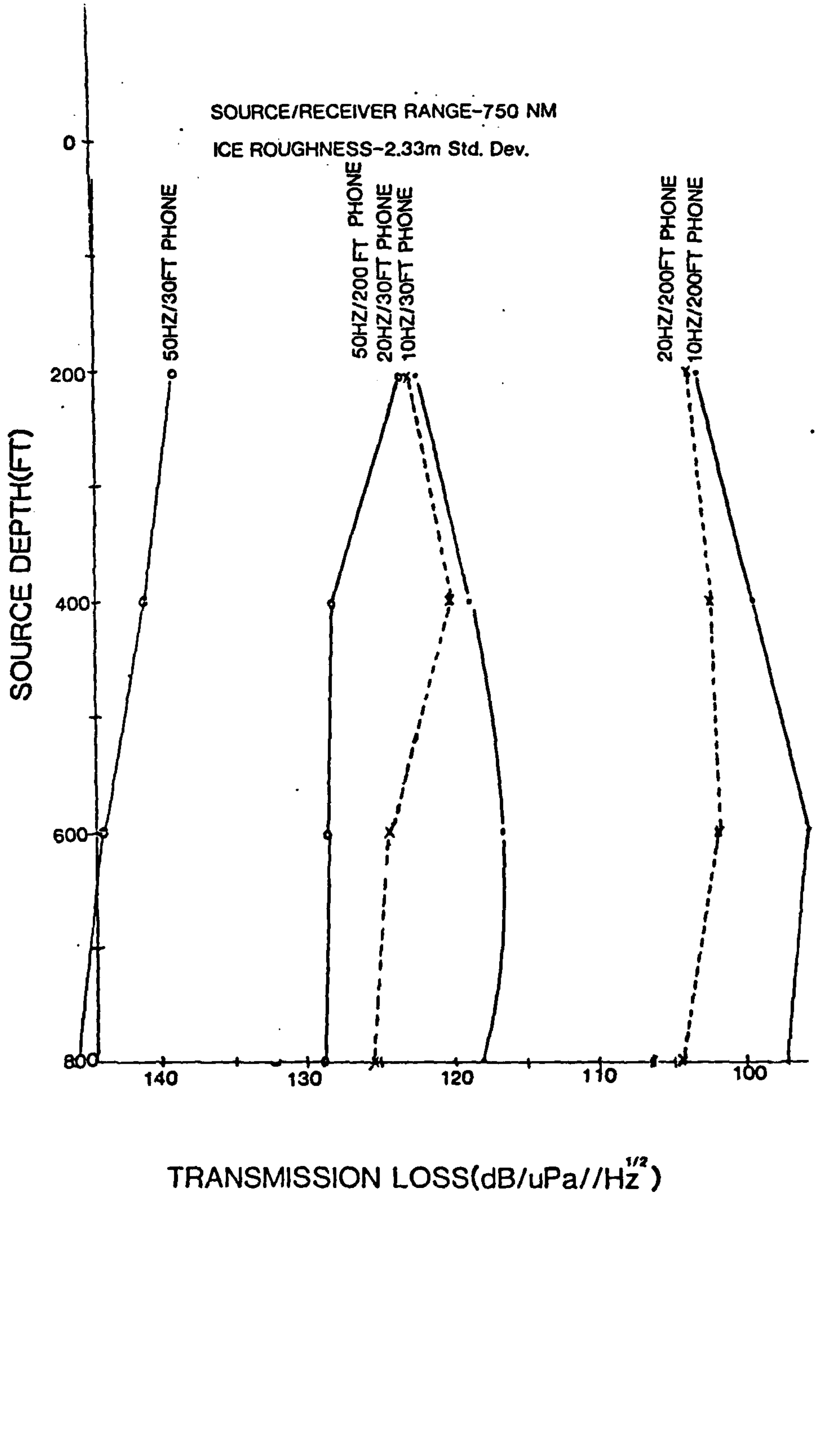
SOURCE/RECEIVER RANGE-750 NM
ICE ROUGHNESS-2.33m Std. Dev.
50HZ/30FT PHONE
50HZ/200 FT PHONE
20HZ/30FT PHONE
10HZ/30FT PHONE
20HZ/200FT PHONE
10HZ/200FT PHONE
SOURCE DEPTH(FT)
0
200
400
600
800
140
130
120
110
100
TRANSMISSION LOSS(dB/uPa//Hz^1/2)

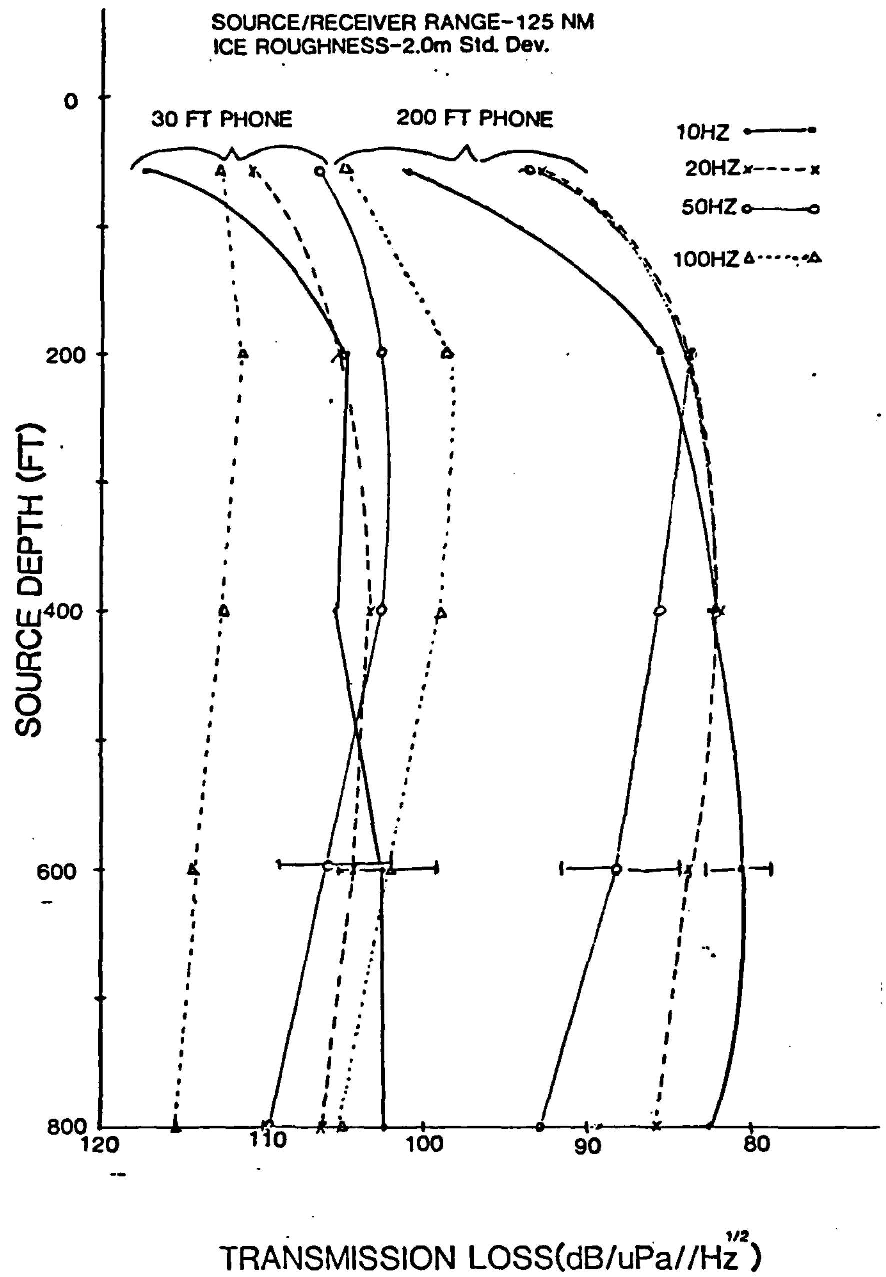
SOURCE/RECEIVER RANGE-125 NM
ICE ROUGHNESS-2.0m Std. Dev.
30 FT PHONE
200 FT PHONE
10HZ
20HZ
50HZ
100HZ
SOURCE DEPTH (FT)
0
200
400
600
800
120
110
100
90
80
TRANSMISSION LOSS(dB/uPa//Hz^1/2)

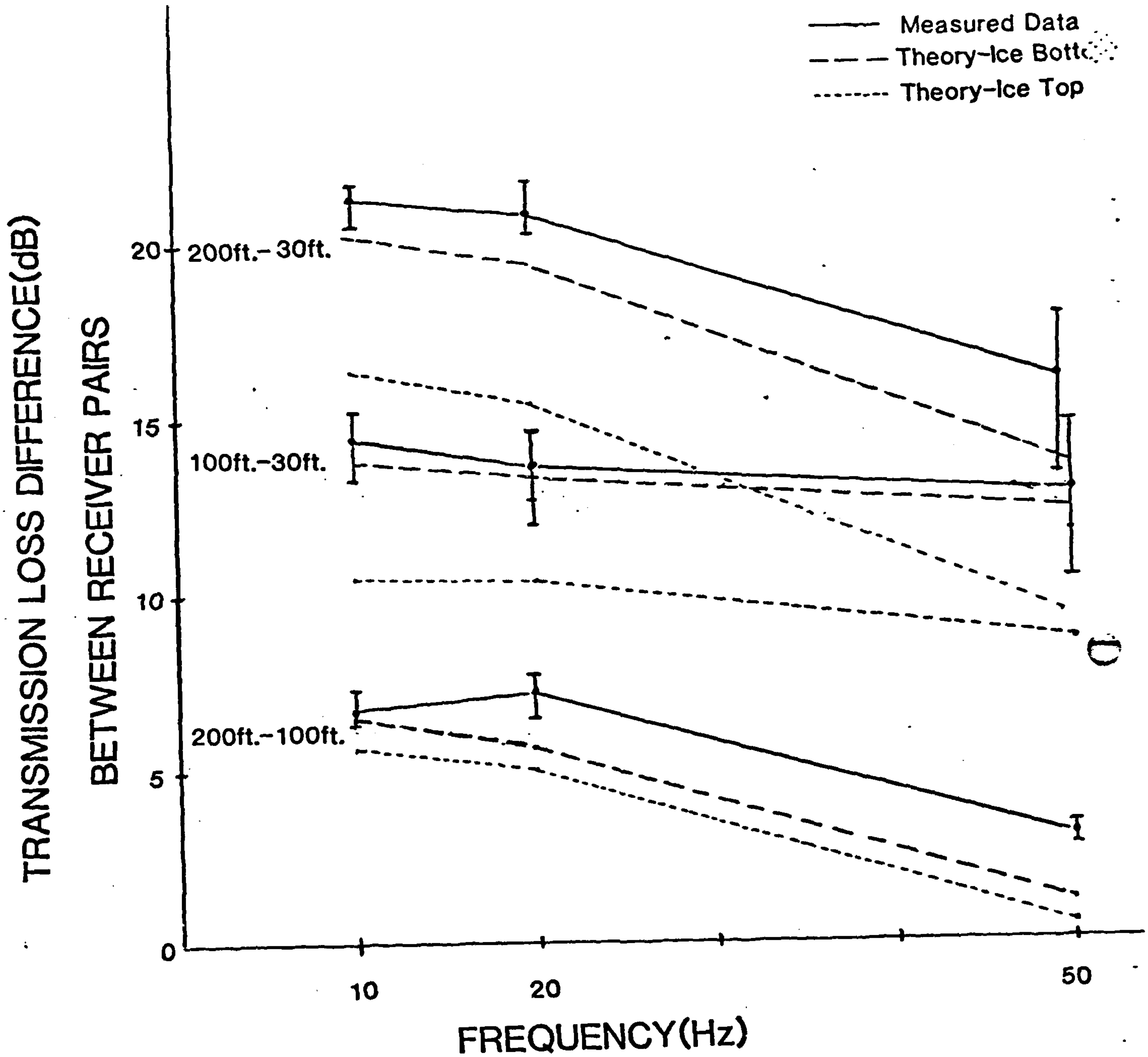
Measured Data
Theory-Ice Bott
Theory-Ice Top
TRANSMISSION LOSS DIFFERENCE(dB)
BETWEEN RECEIVER PAIRS
200ft.-30ft.
100ft.-30ft.
200ft.-100ft.
20
15
10
5
0
10
20
50
FREQUENCY(Hz)

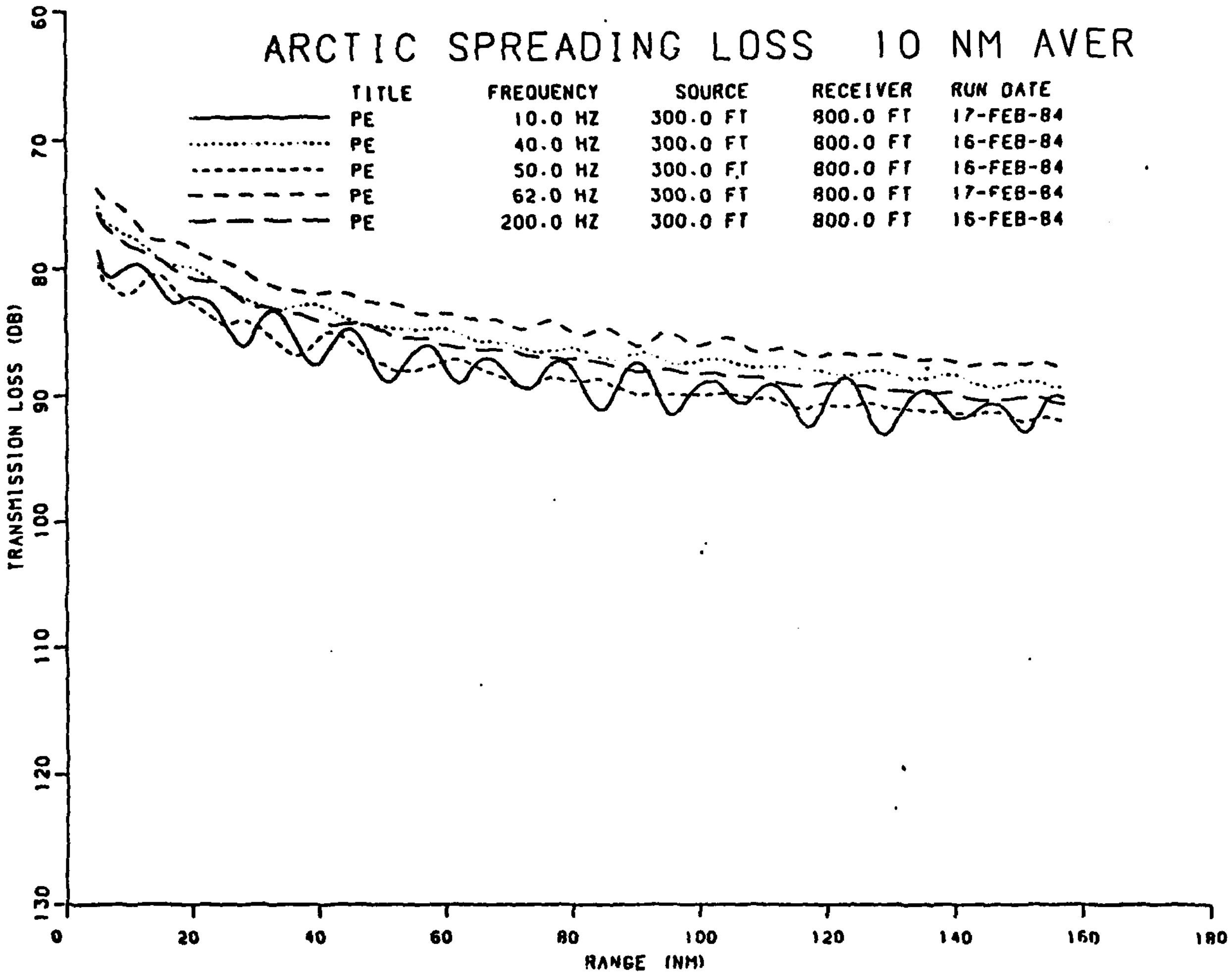

ARCTIC SPREADING LOSS 10 NM AVER
TITLE FREQUENCY SOURCE RECEIVER RUN DATE
PE 10.0 HZ 300.0 FT 800.0 FT 17-FEB-84
PE 40.0 HZ 300.0 FT 800.0 FT 16-FEB-84
PE 50.0 HZ 300.0 FT 800.0 FT 16-FEB-84
PE 62.0 HZ 300.0 FT 800.0 FT 17-FEB-84
PE 200.0 HZ 300.0 FT 800.0 FT 16-FEB-84
TRANSMISSION LOSS (DB)
60
70
80
90
100
110
120
130
0
20
40
60
80
100
120
140
160
180
RANGE (NM)

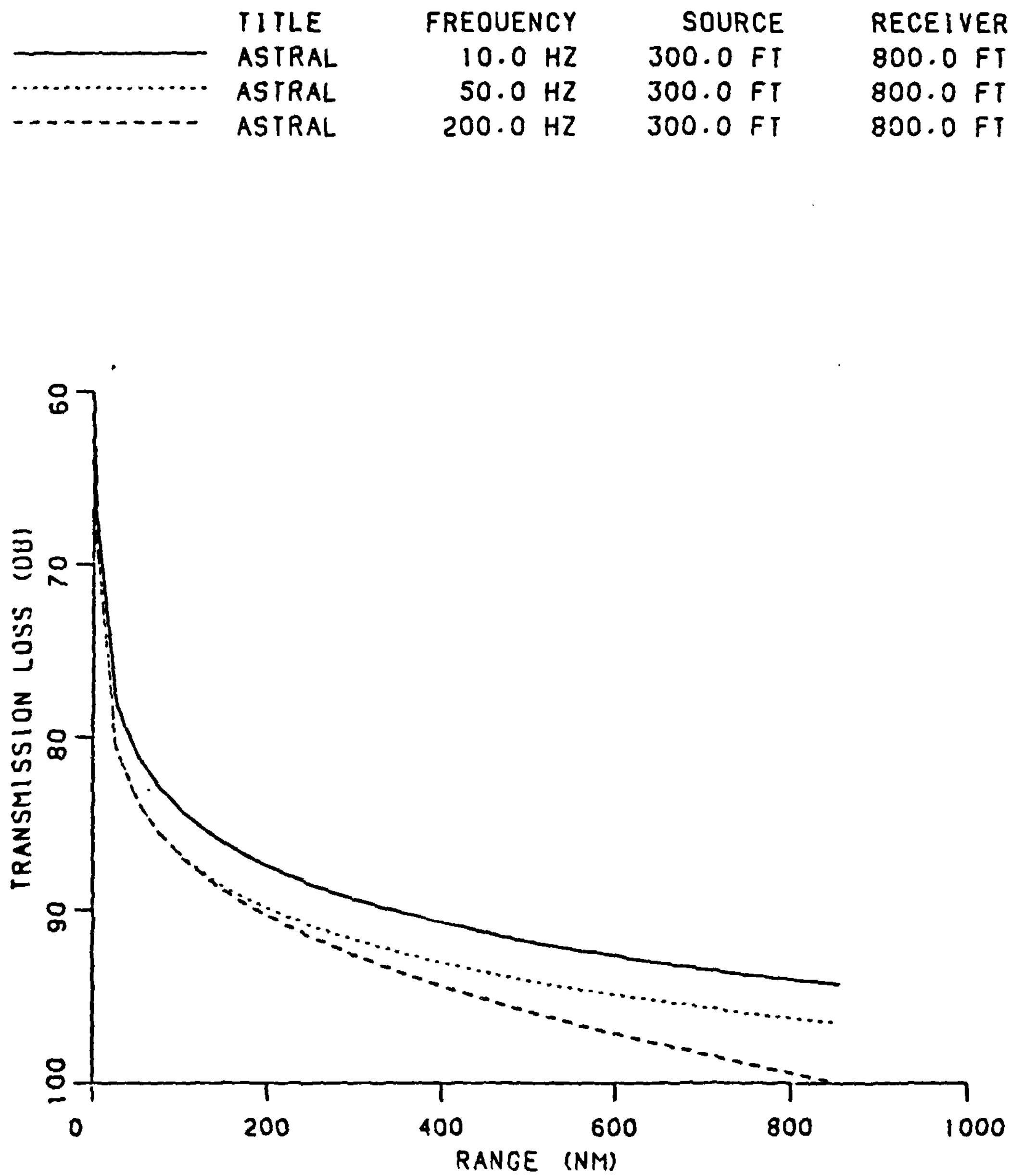
TITLE FREQUENCY SOURCE RECEIVER
ASTRAL 10.0 HZ 300.0 FT 800.0 FT
ASTRAL 50.0 HZ 300.0 FT 800.0 FT
ASTRAL 200.0 HZ 300.0 FT 800.0 FT
TRANSMISSION LOSS (DB)
60
70
80
90
100
0
200
400
600
800
1000
RANGE (NM)

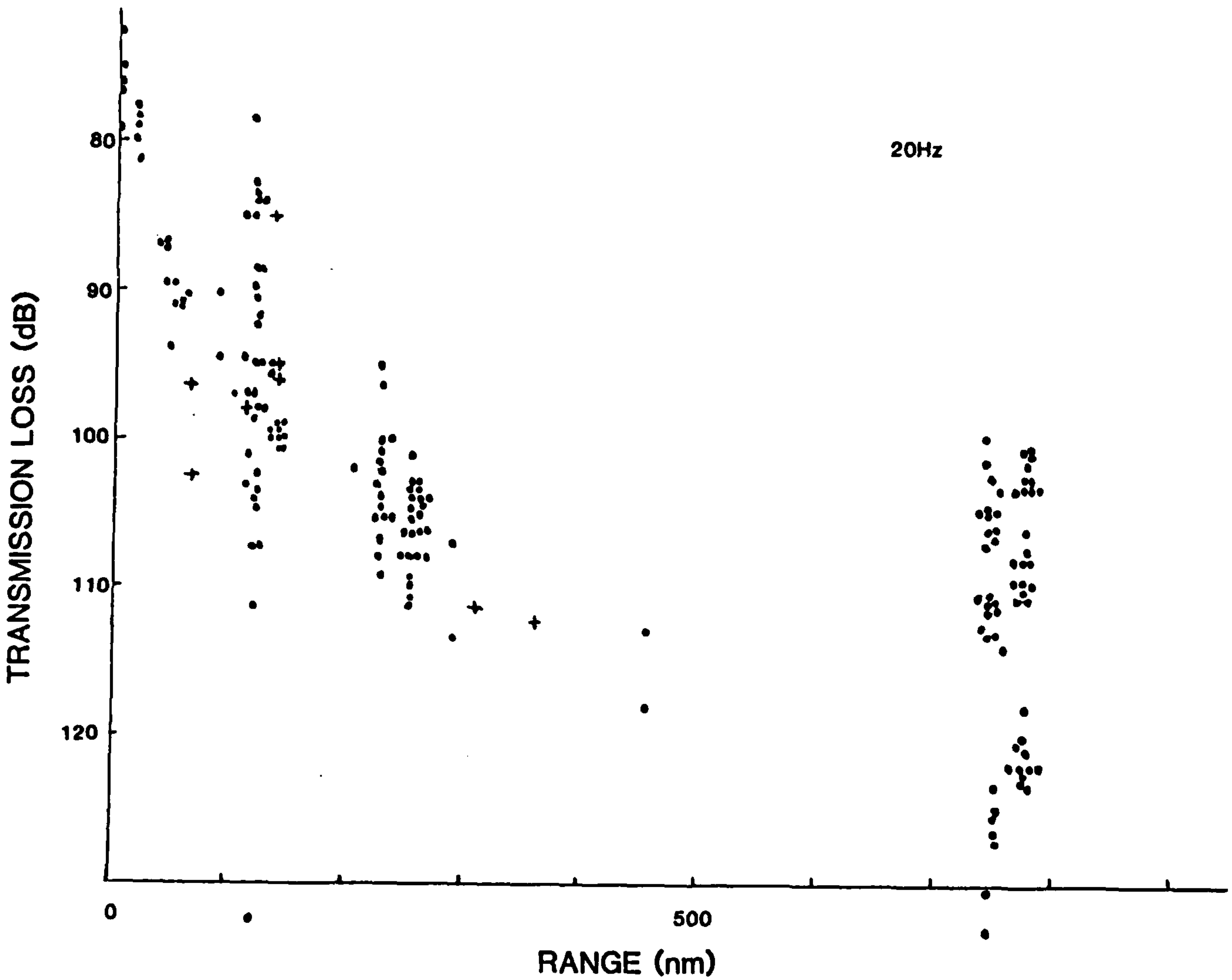

20Hz
TRANSMISSION LOSS (dB)
80
90
100
110
120
0
500
RANGE (nm)

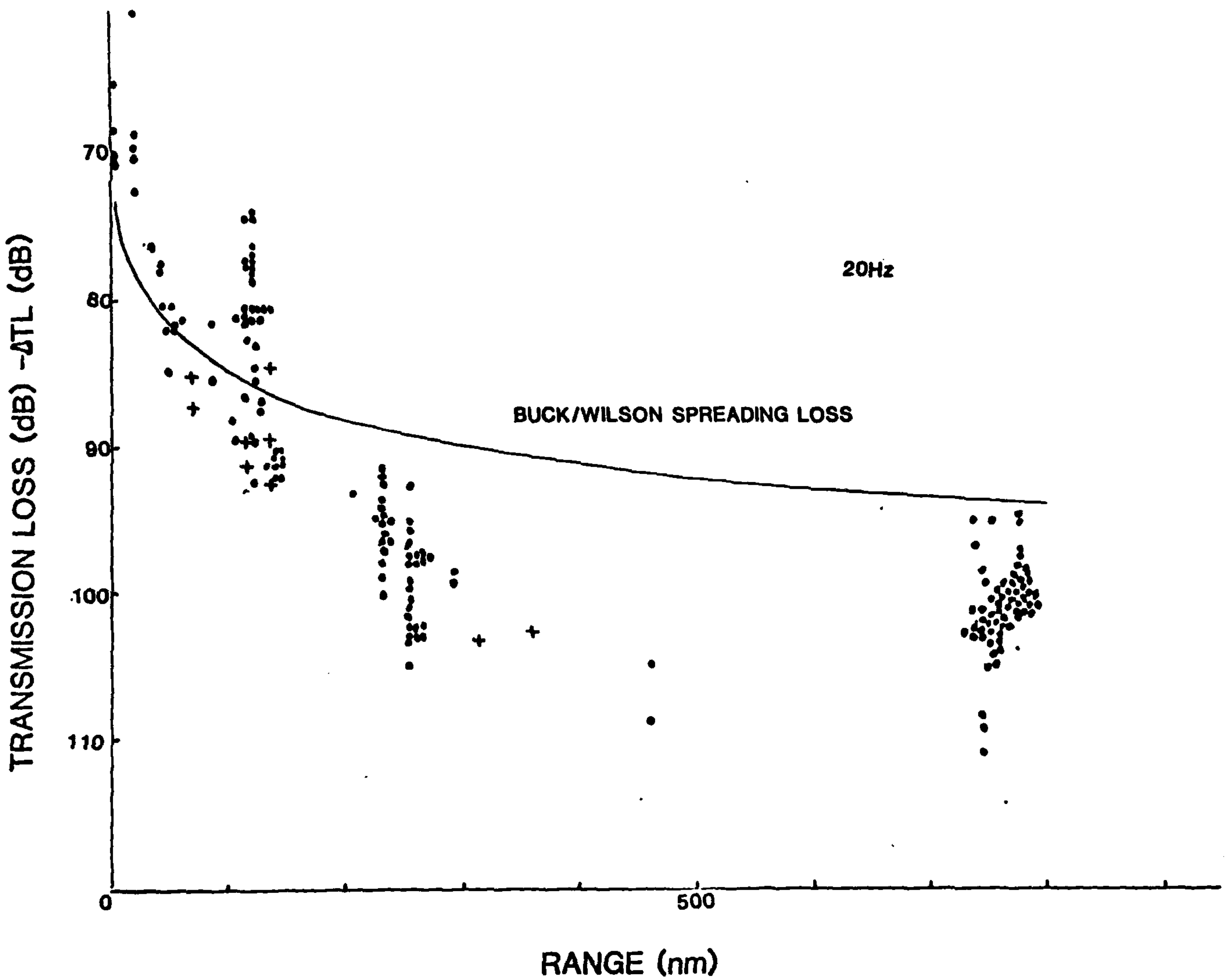

20Hz
BUCK/WILSON SPREADING LOSS
TRANSMISSION LOSS (dB) -ΔTL (dB)
70
80
90
100
110
0
500
RANGE (nm)

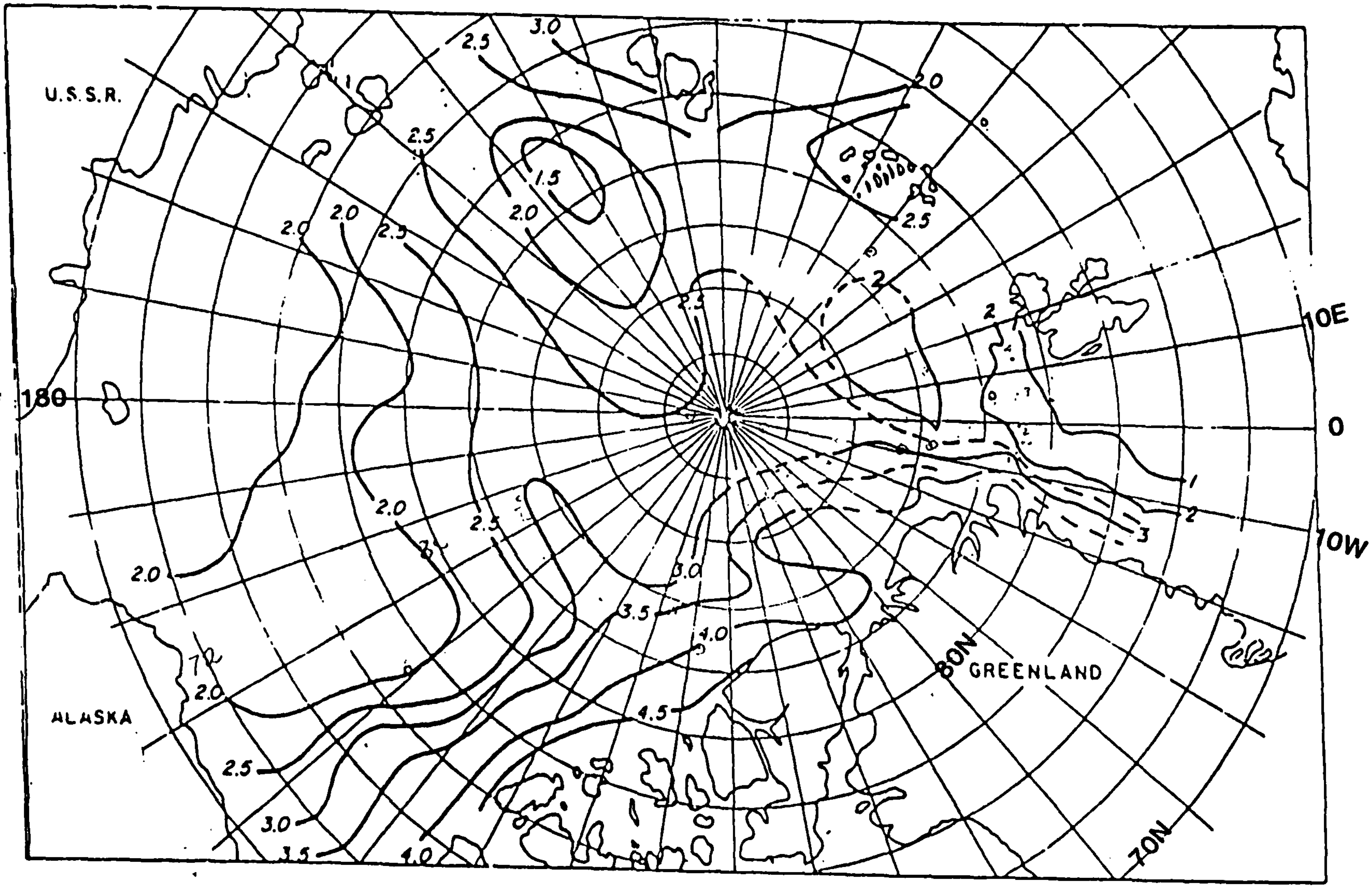

U.S.S.R.
ALASKA
GREENLAND
180
0
10E
10W
80N
70N
1.5
2.0
2.5
3.0
3.5
4.0
4.5

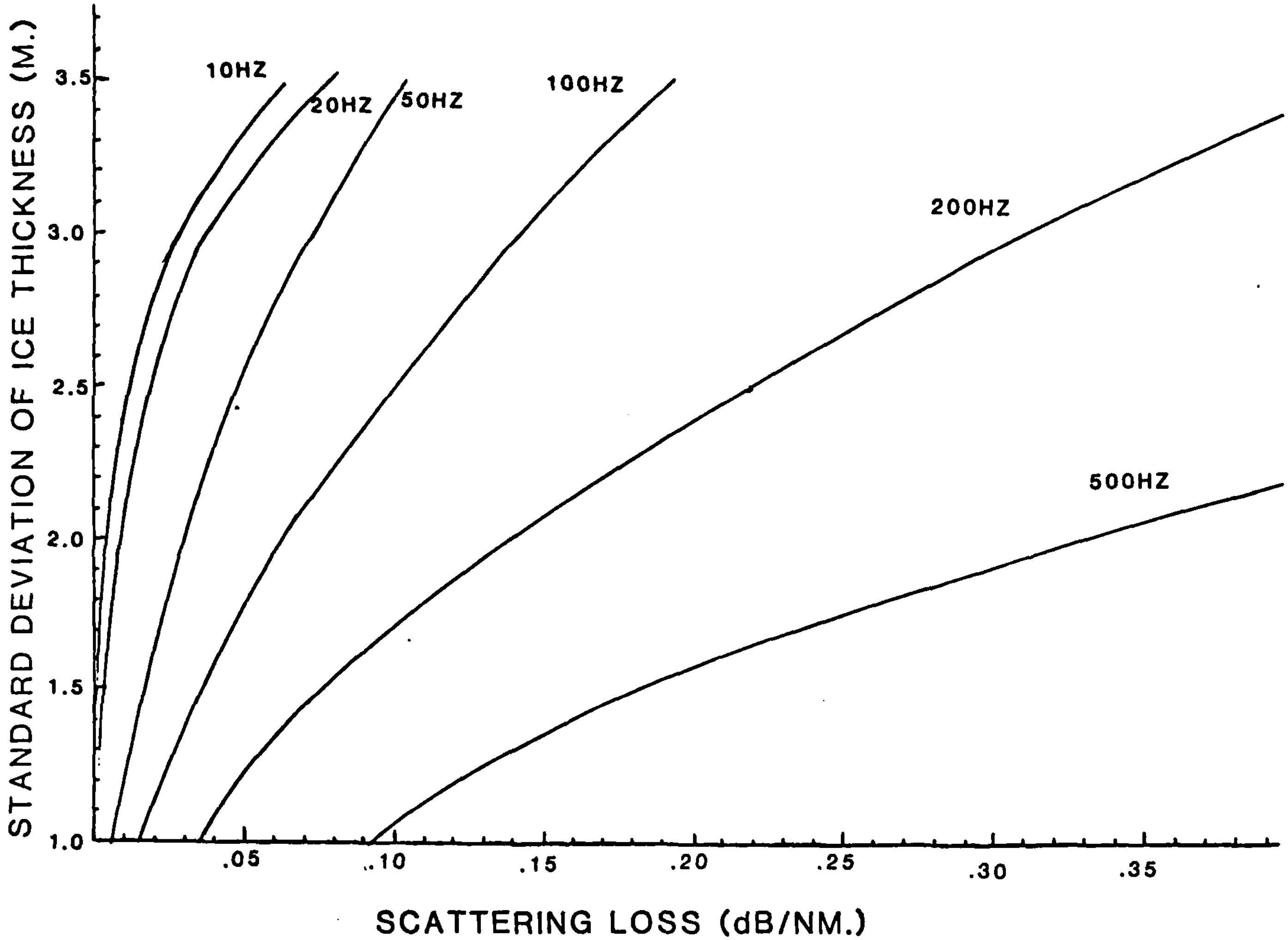

STANDARD DEVIATION OF ICE THICKNESS (M.)
3.5
3.0
2.5
2.0
1.5
1.0
10HZ
20HZ
50HZ
100HZ
200HZ
500HZ
.05
.10
.15
.20
.25
.30
.35
SCATTERING LOSS (dB/NM.)

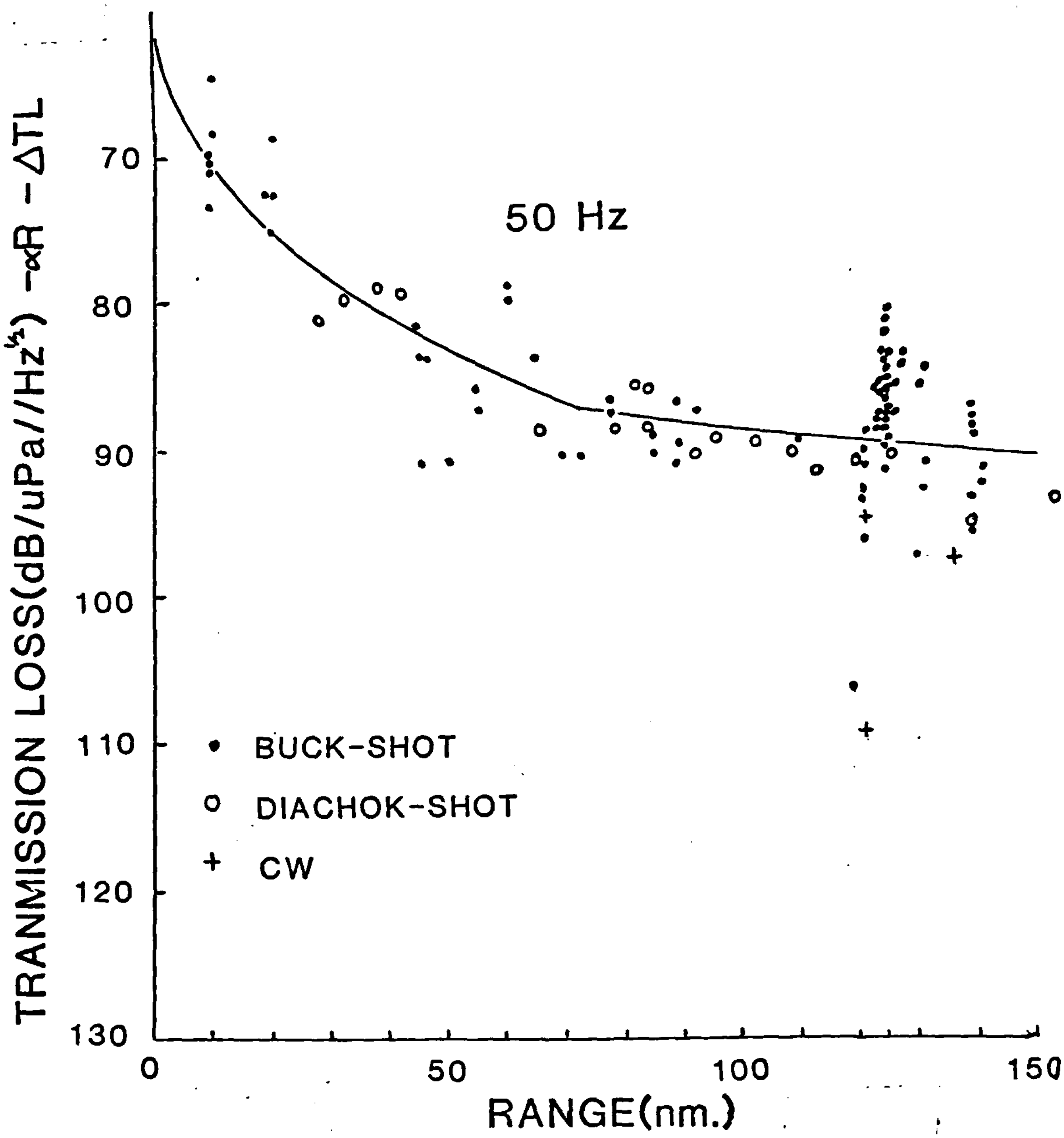

TRANMISSION LOSS(dB/uPa//Hz½) -αR -ΔTL
70
80
90
100
110
120
130
0
50
100
150
RANGE(nm.)
50 Hz
BUCK-SHOT
DIACHOK-SHOT
CW

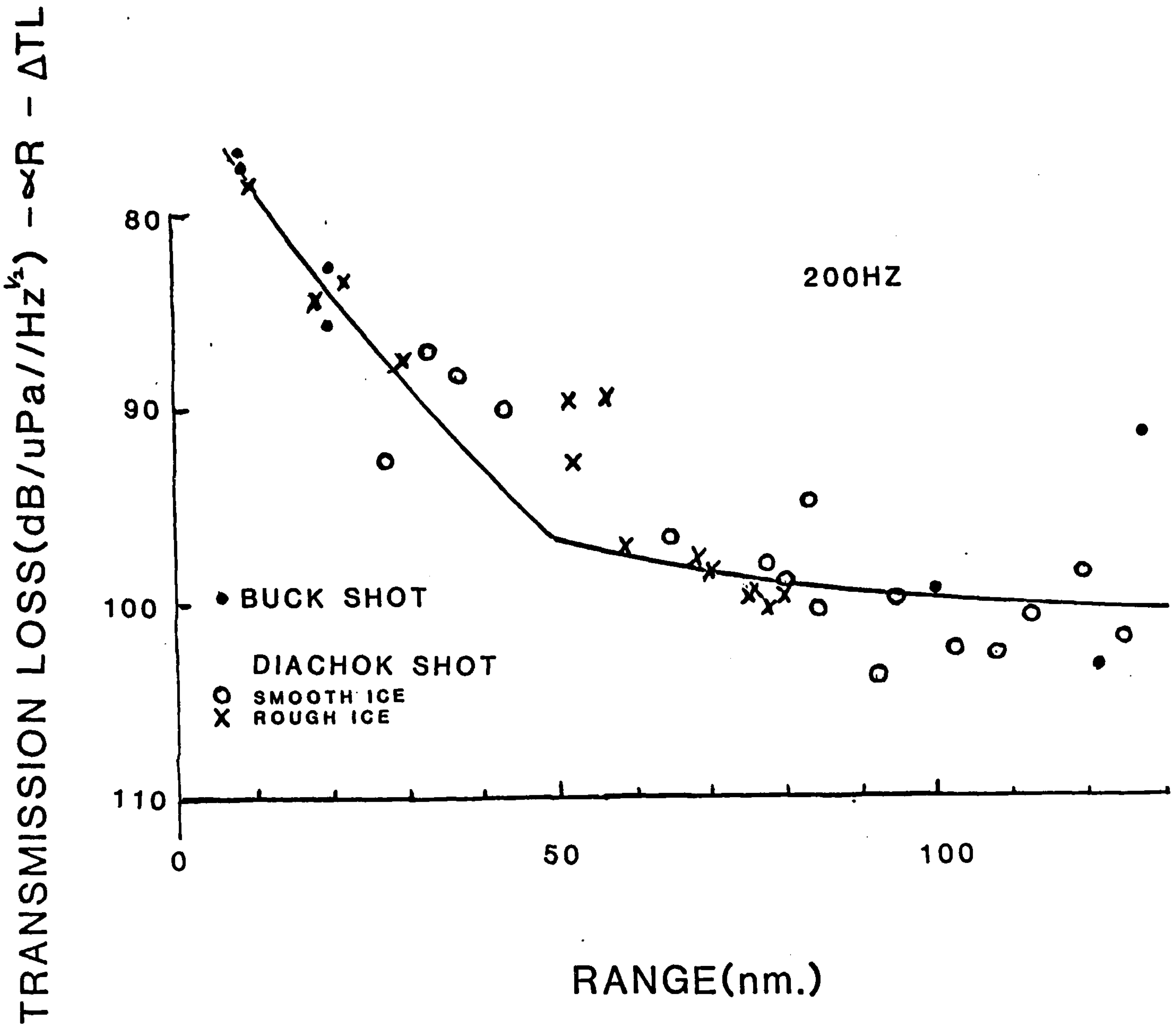

TRANSMISSION LOSS(dB/uPa//Hz^½) −∝R − ΔTL
200HZ
80
90
100
110
0
50
100
RANGE(nm.)
• BUCK SHOT
DIACHOK SHOT
O SMOOTH ICE
X ROUGH ICE

Art Baggeroer

VLF PROPAGATION #1

ENERGY PARTITIONING FOR LONG RANGE, LOW FREQUENCY PROPAGATION IN THE ARCTIC OCEAN

The partitioning of energy from explosive signals propagating in the Arctic Ocean for ranges up to 350 km was determined as a function of frequency using a 1 km x 1 km array during the FRAM ice station experiments. The energy was resolved into three classes: i) dispersive, low order modes (1-3) trapped in the upward refracting Arctic sound channel; ii) multiple RSR paths; and iii) and extensive set of bottom refracted signals on a reversed branch of the travel time curve. Estimating the energy of each component as a function of travel time and ray parameter indicates that below 20 Hz, the bottom interacting components contain well over half the total observed energy when the bathymetry between the source and receiver is smooth.

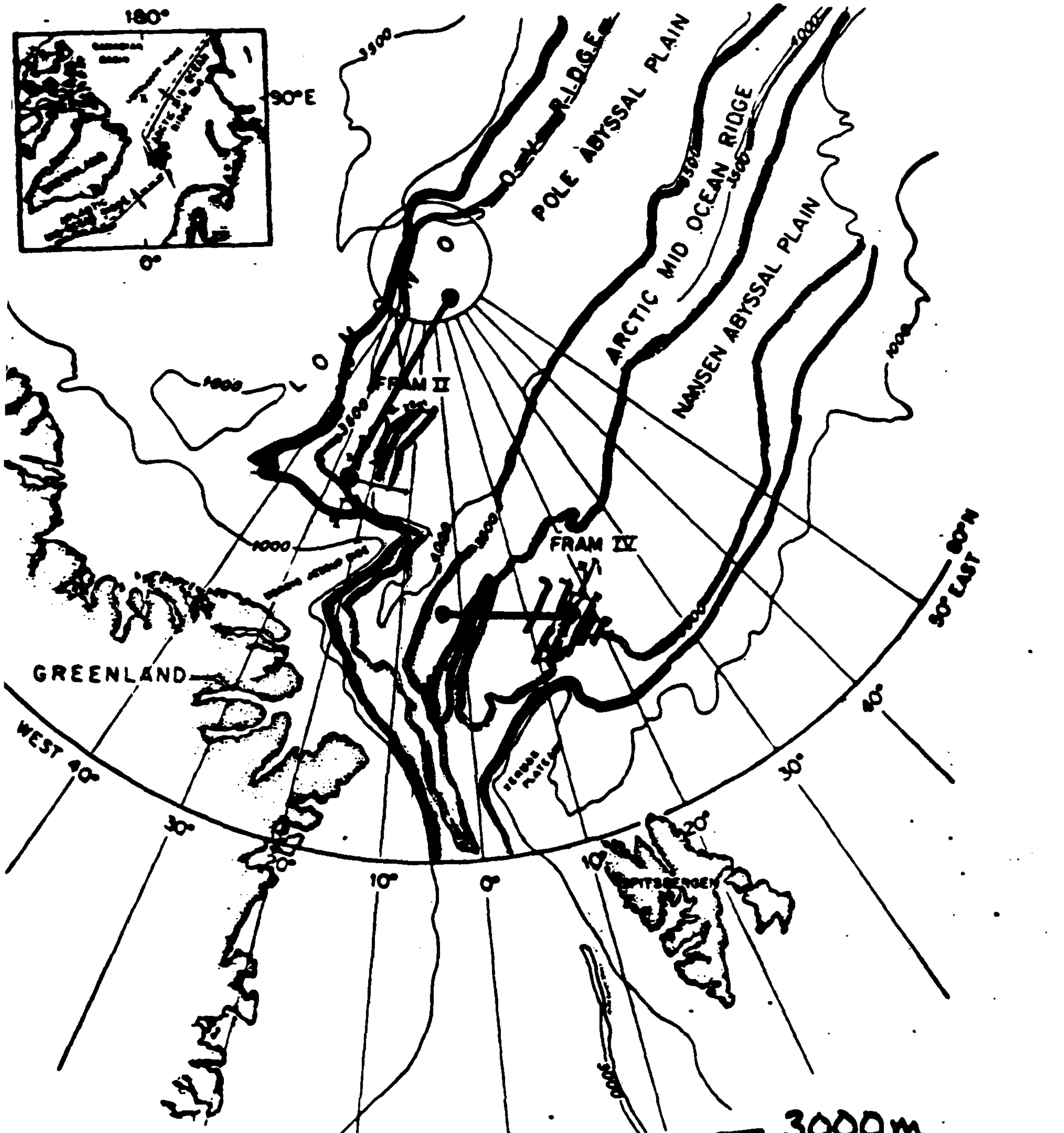

180°
90°E
0°
POLE ABYSSAL PLAIN
ARCTIC MID OCEAN RIDGE
NANSEN ABYSSAL PLAIN
FRAM II
FRAM IV
GREENLAND
SPITSBERGEN
WEST 40°
30°
10°
0°
10°
20°
30°
40°
80°N
50° EAST
1000
3500
3000
= 3000m
= 3500m

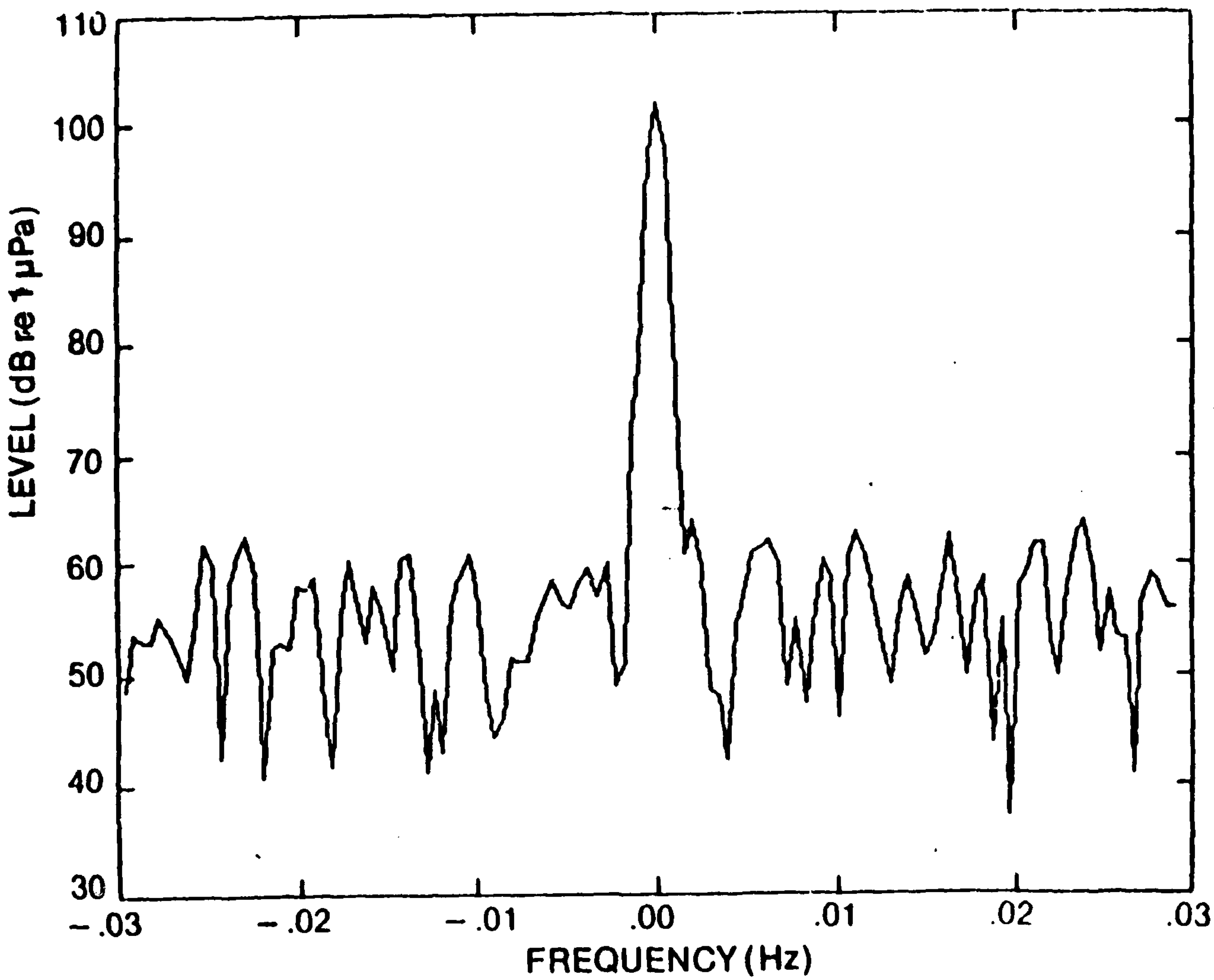
LEVEL (dB re 1 μPa)
110
100
90
80
70
60
50
40
30
−.03
−.02
−.01
.00
.01
.02
.03
FREQUENCY (Hz)

AMPLITUDE AND PHASE FOR 15 Hz CW SIGNAL AT 300 km RANGE

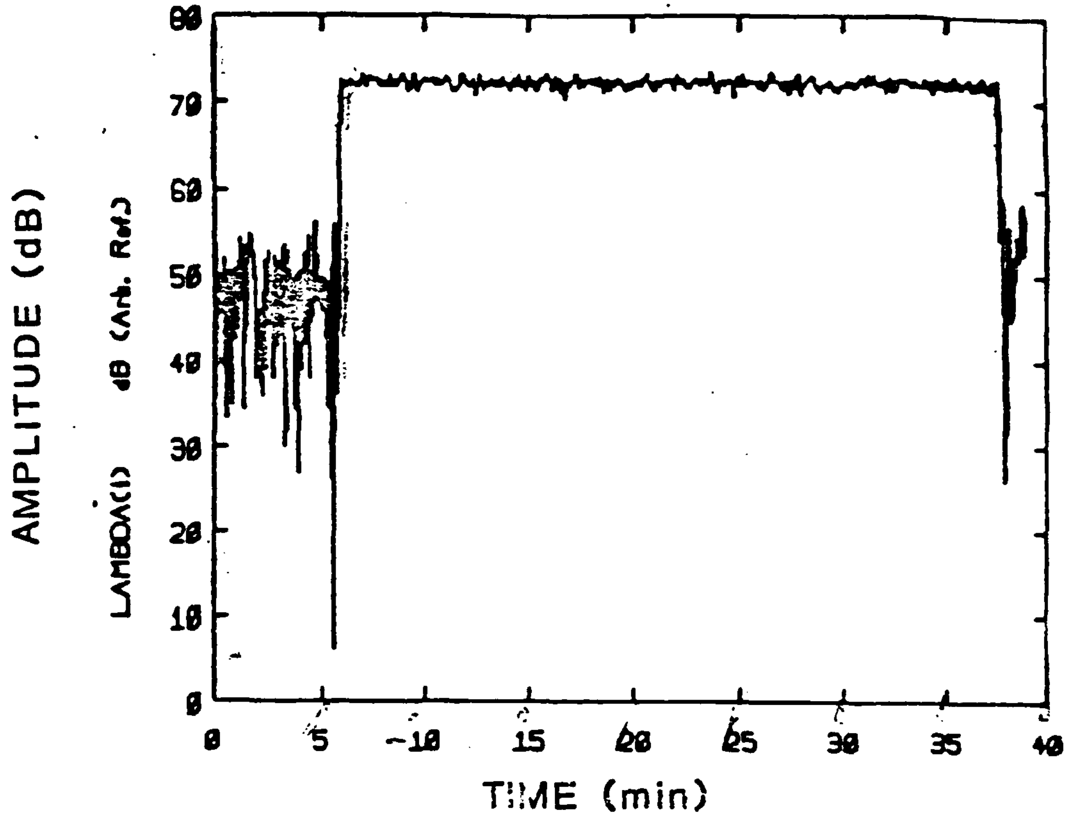

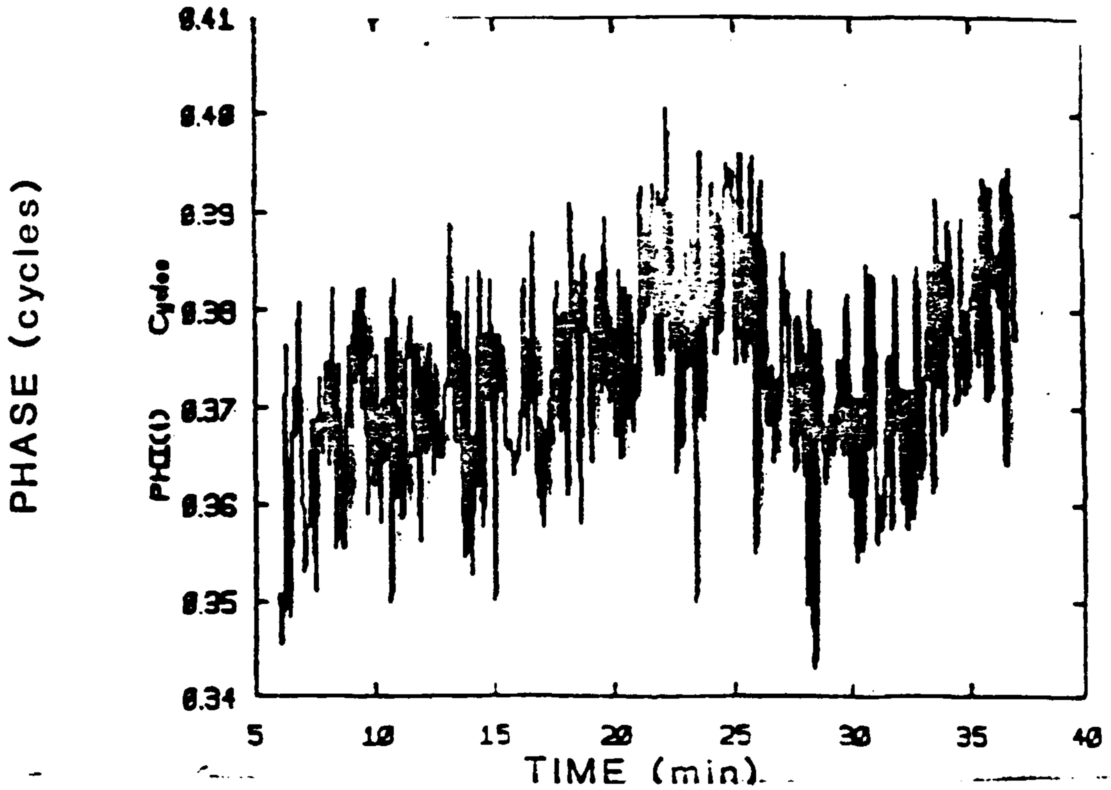

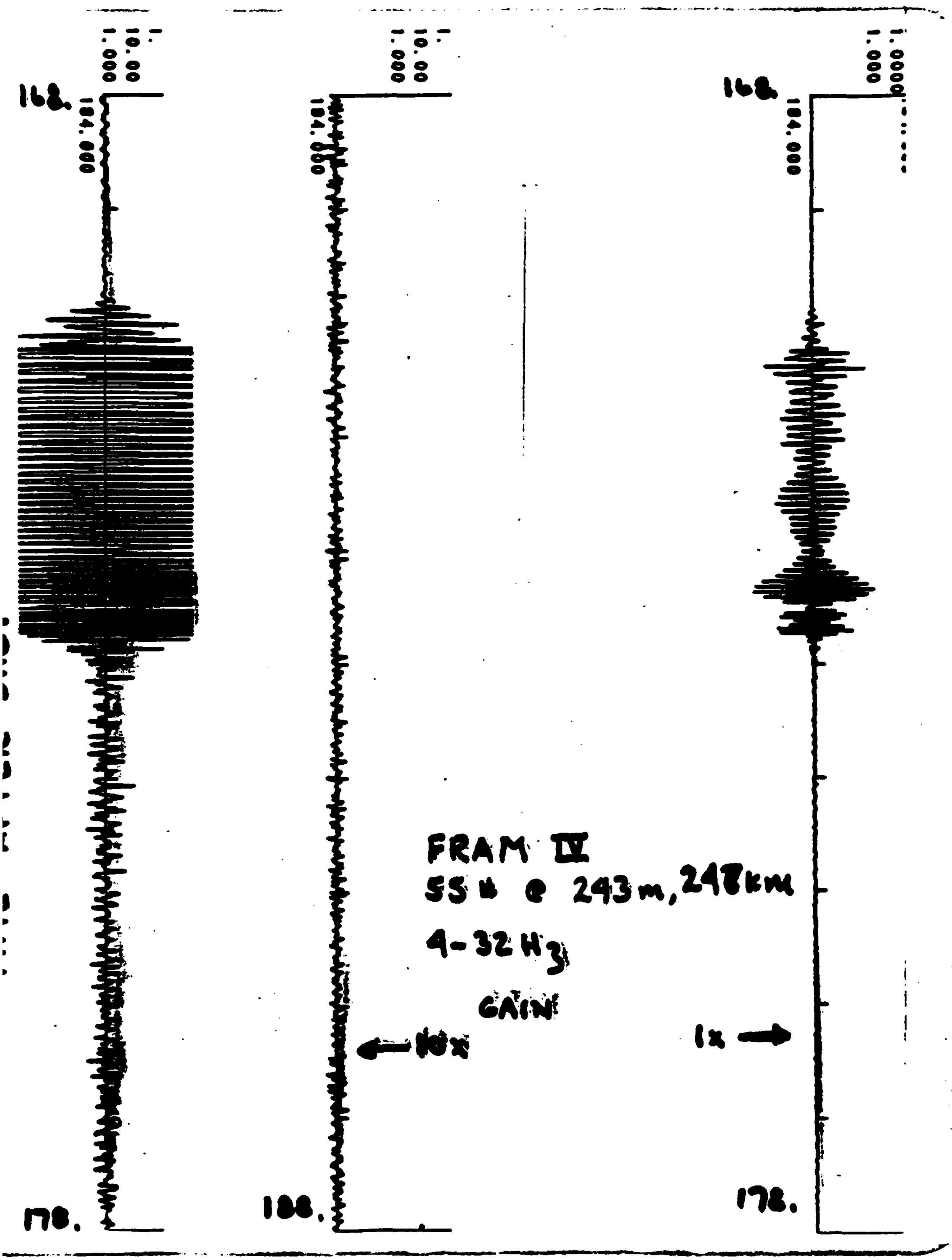
168.
178.
188.
168.
178.
FRAM IV
55 lb @ 243 m, 248 km
4-32 Hz
GAIN
10x
1x

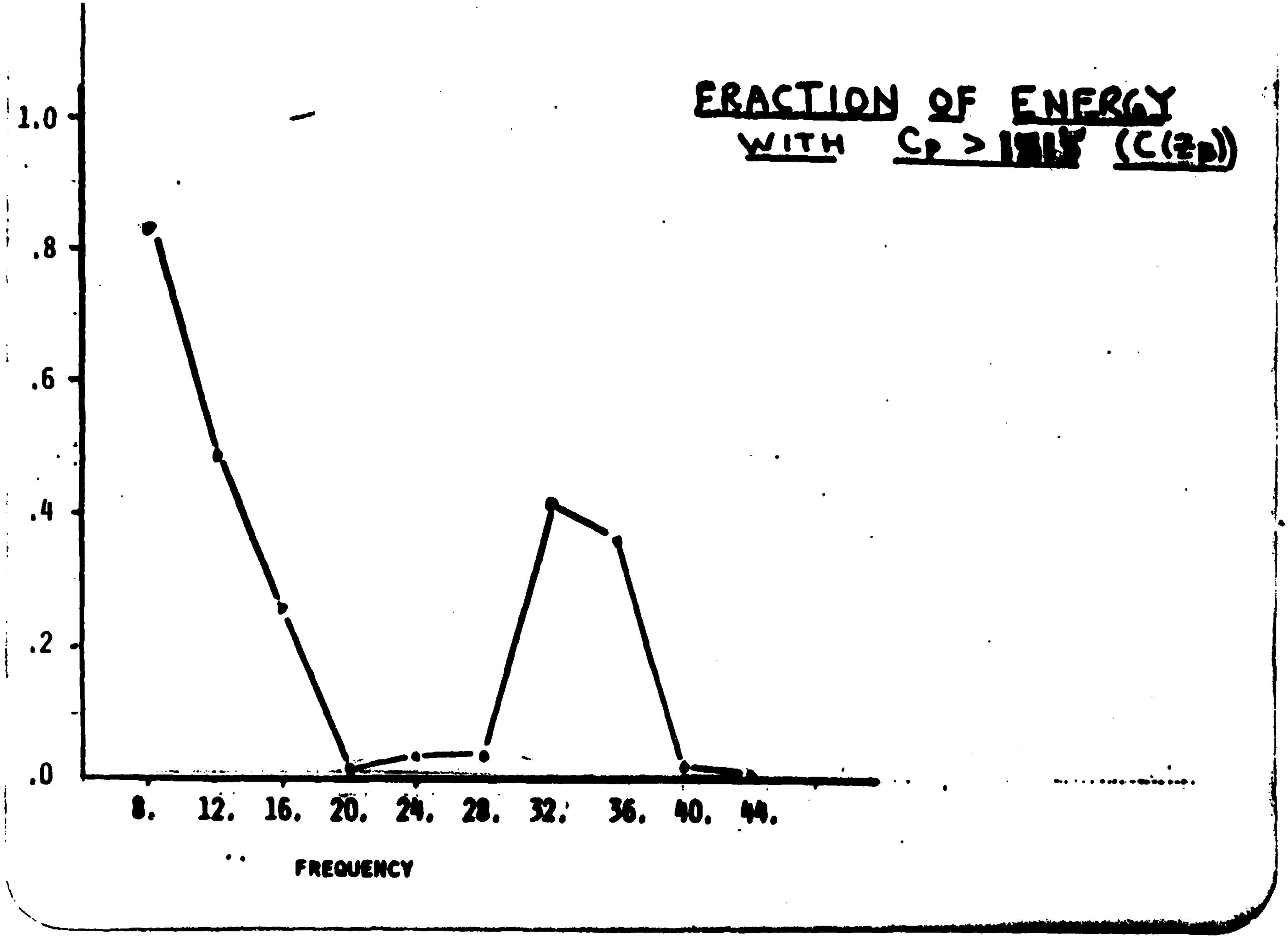
FRACTION OF ENERGY
WITH $C_p >$ [redacted] $(C(z_p))$
1.0
.8
.6
.4
.2
.0
8.
12.
16.
20.
24.
28.
32.
36.
40.
44.
FREQUENCY

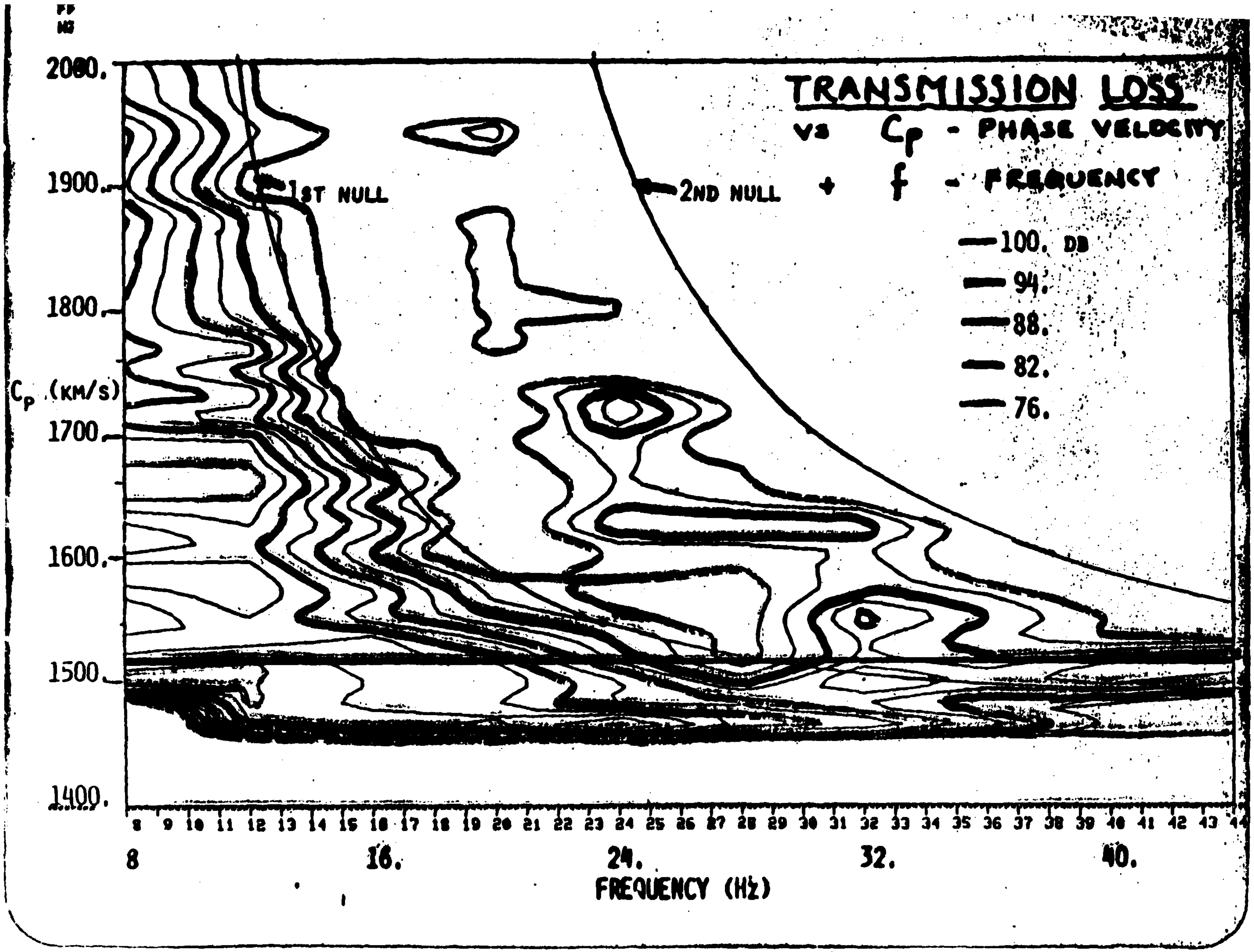
TRANSMISSION LOSS
vs C_p - PHASE VELOCITY
+ f - FREQUENCY
100. DB
94.
88.
82.
76.
1ST NULL
2ND NULL
2000.
1900.
1800.
1700.
1600.
1500.
1400.
C_p (KM/S)
8 9 10 11 12 13 14 15 16 17 18 19 20 21 22 23 24 25 26 27 28 29 30 31 32 33 34 35 36 37 38 39 40 41 42 43 44
8
16.
24.
32.
40.
FREQUENCY (Hz)

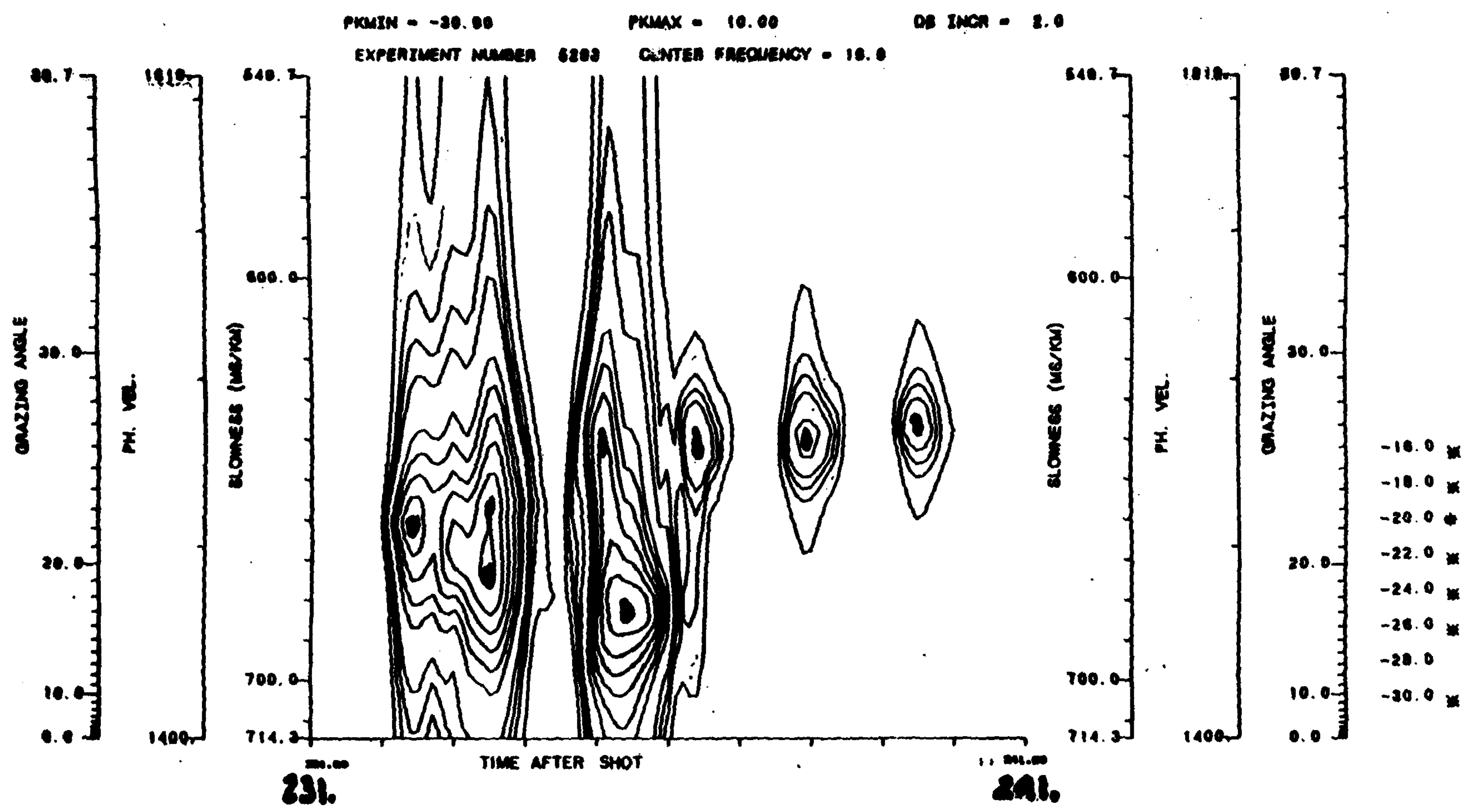

PKMIN = -30.00
PKMAX = 10.00
DB INCR = 2.0
EXPERIMENT NUMBER 5283
CENTER FREQUENCY = 16.0
GRAZING ANGLE
PH. VEL.
SLOWNESS (MS/KM)
TIME AFTER SHOT
231.
241.
-16.0
-18.0
-20.0
-22.0
-24.0
-26.0
-28.0
-30.0

LONG RANGE PROPAGATION DATA: VELOCITY SPECTRUM AND NORMAL MODE AND WKBJ PREDICTIONS

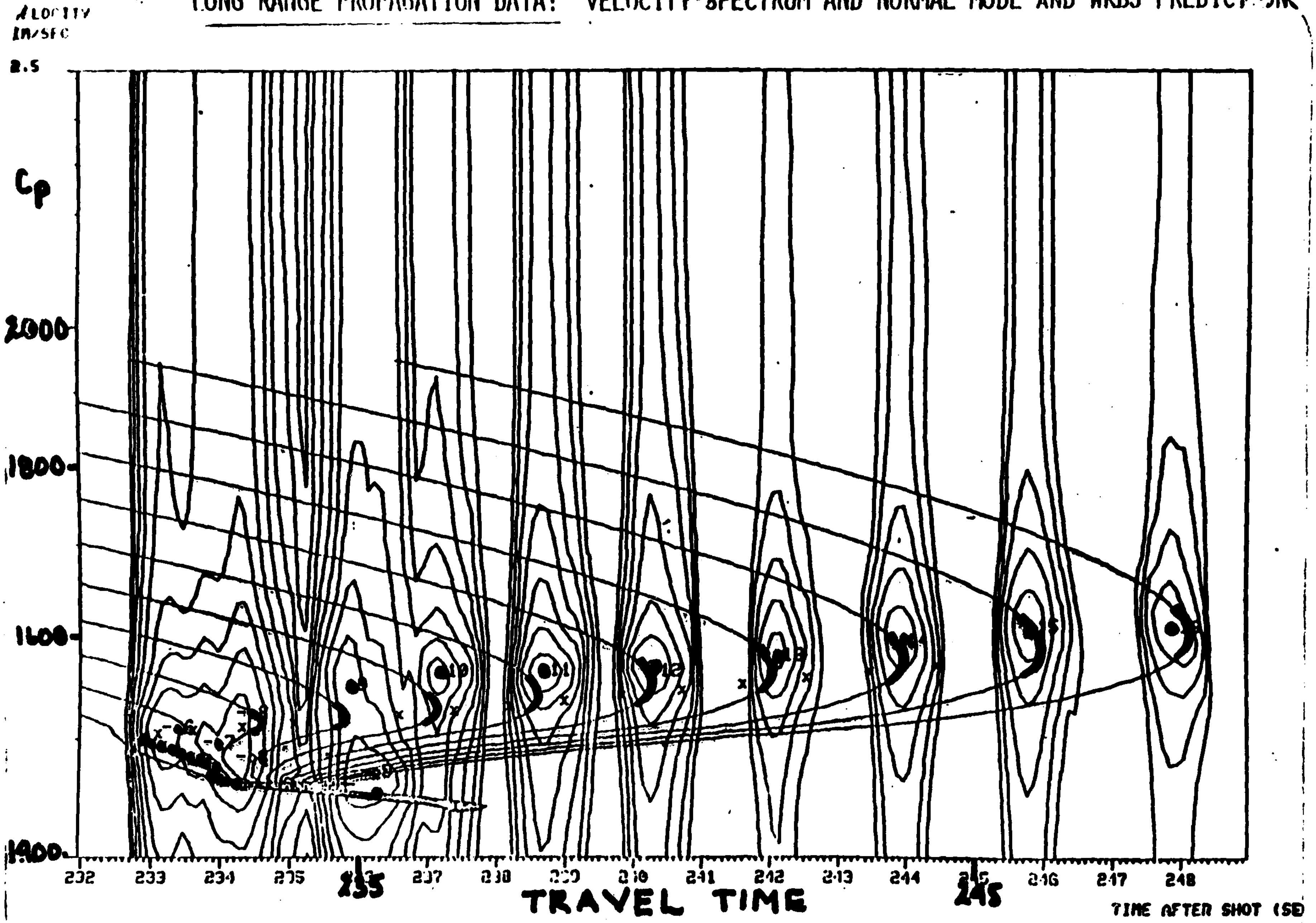

Velocity Spectrum of multichannel data. (Contour interval = 5 dB.)

Legend: ●# denotes multiplicity of turning points.

● denotes mode dispersion curve

solid curves denote travel time vs. phase vel fcn. for corrected

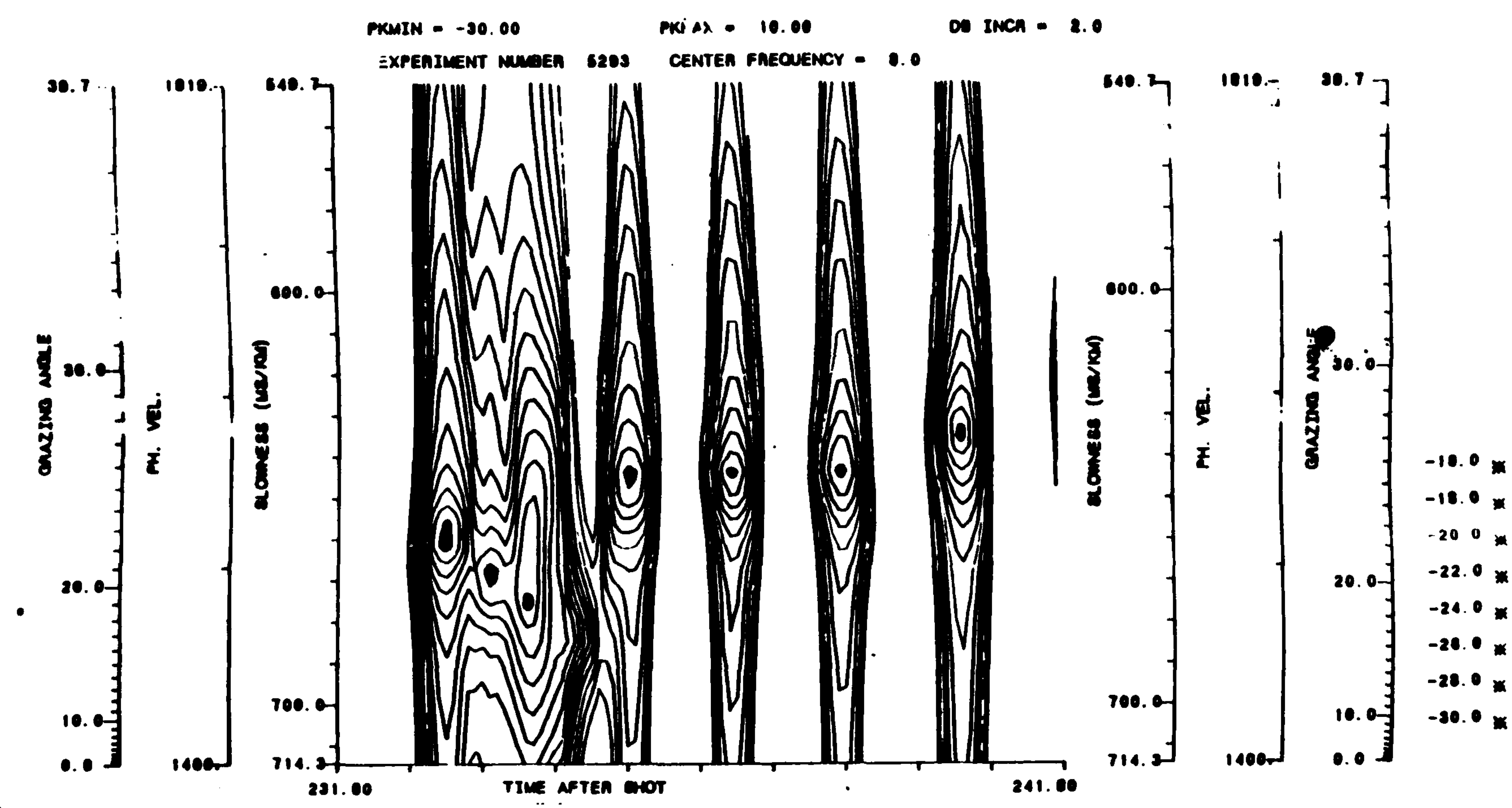
PKMIN = -30.00
PKMAX = 10.00
DB INCR = 2.0
EXPERIMENT NUMBER 5293
CENTER FREQUENCY = 8.0
GRAZING ANGLE
PH. VEL.
SLOWNESS (MS/KM)
TIME AFTER SHOT
231.00
241.00
38.7
30.0
20.0
10.0
0.0
1819.
1400.
549.7
600.0
700.0
714.3
-16.0
-18.0
-20.0
-22.0
-24.0
-26.0
-28.0
-30.0

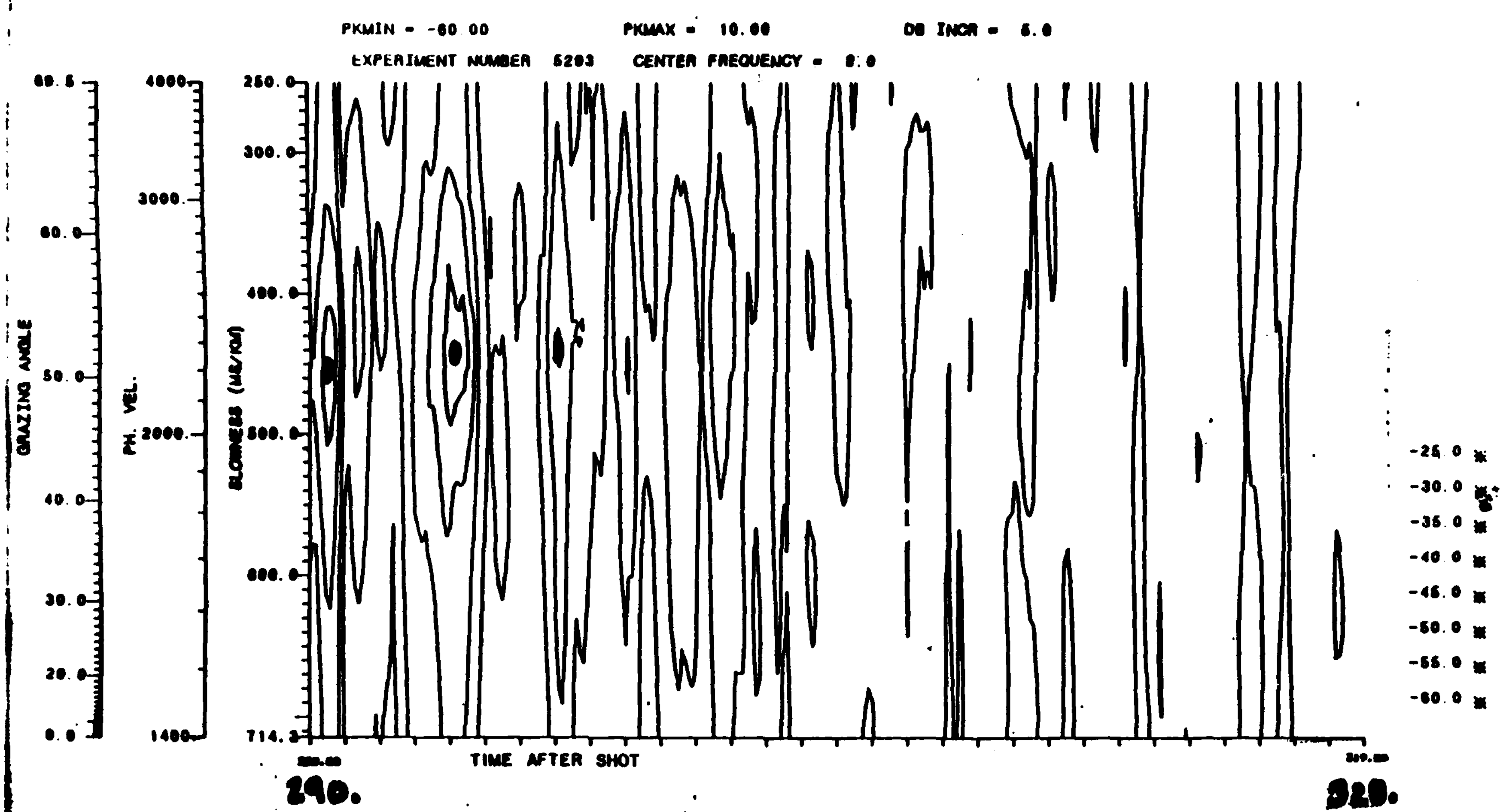

PKMIN = -60.00
PKMAX = 10.00
DB INCR = 5.0
EXPERIMENT NUMBER 5203
CENTER FREQUENCY = 8.0
GRAZING ANGLE
PH. VEL.
SLOWNESS (MS/KM)
TIME AFTER SHOT
290.
320.
-25.0
-30.0
-35.0
-40.0
-45.0
-50.0
-55.0
-60.0

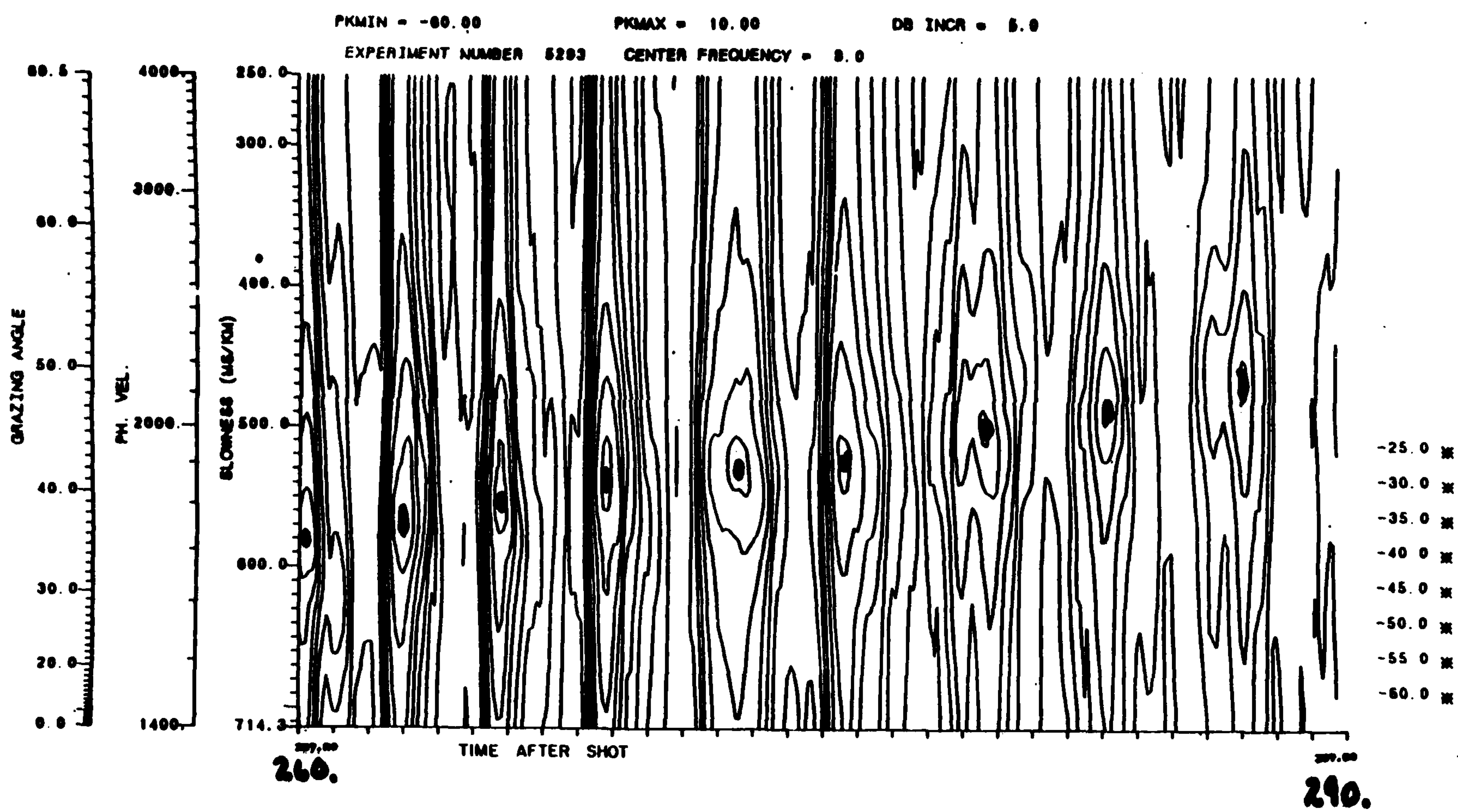
PKMIN = -60.00
PKMAX = 10.00
DB INCR = 5.0
EXPERIMENT NUMBER 5293
CENTER FREQUENCY = 8.0
GRAZING ANGLE
PH. VEL.
SLOWNESS (MS/KM)
TIME AFTER SHOT
260.
290.
-25.0
-30.0
-35.0
-40.0
-45.0
-50.0
-55.0
-60.0

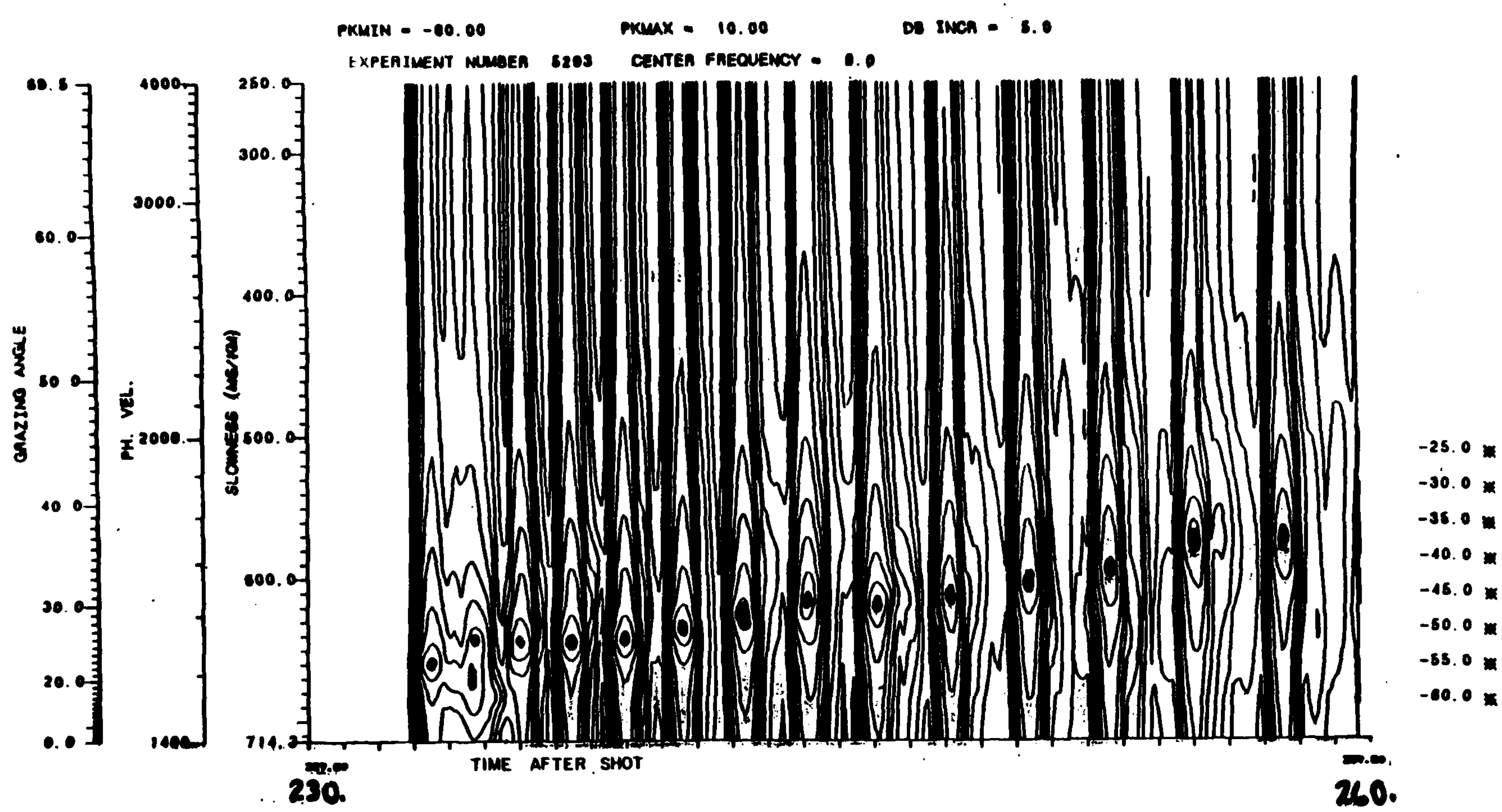
PKMIN = -80.00
PKMAX = 10.00
DB INCR = 5.0
EXPERIMENT NUMBER 5203
CENTER FREQUENCY = 8.0
GRAZING ANGLE
PH. VEL.
SLOWNESS (MS/KM)
TIME AFTER SHOT
230.
260.
-25.0
-30.0
-35.0
-40.0
-45.0
-50.0
-55.0
-60.0

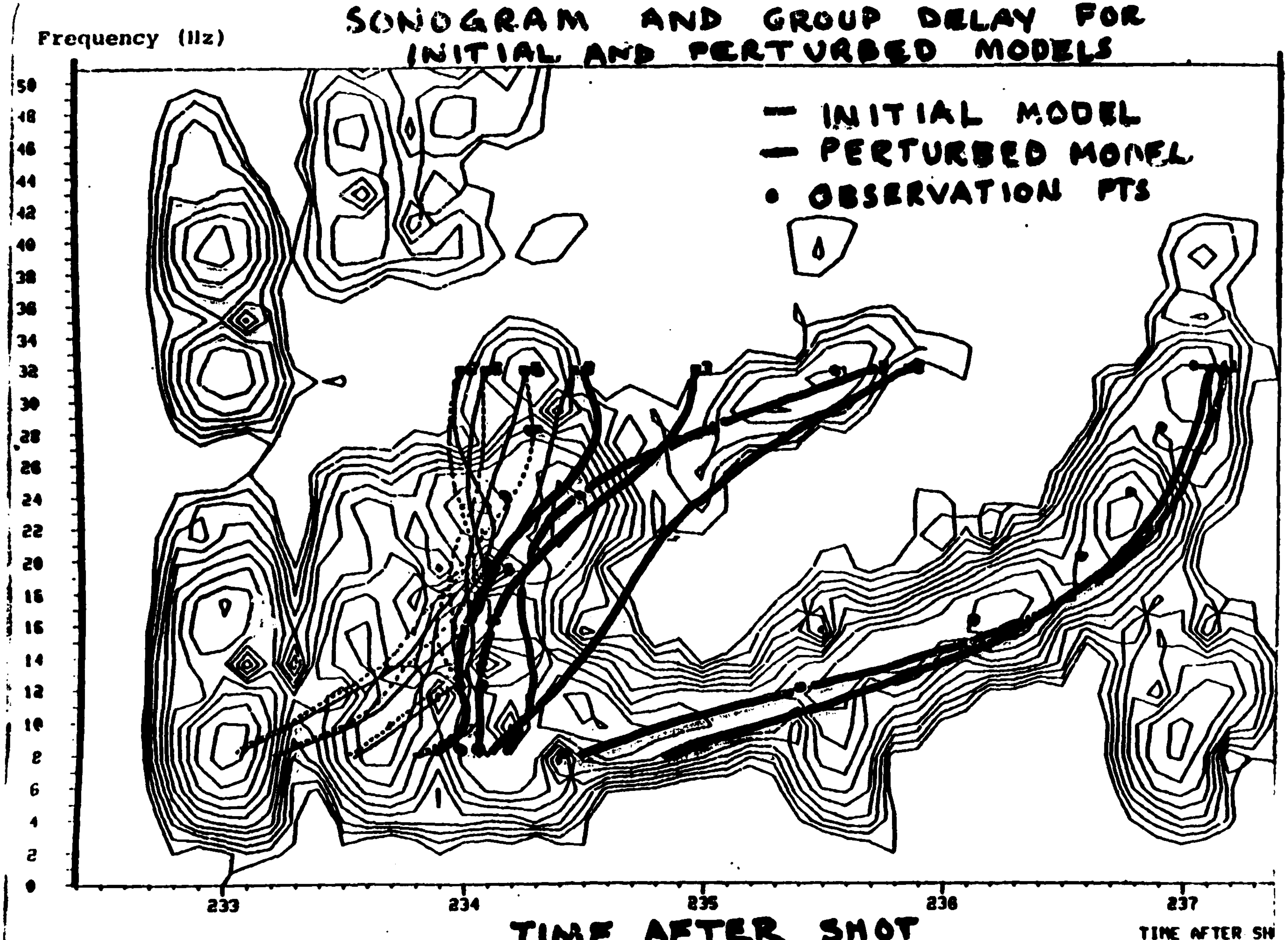

Figure 2. Sonogram analysis of channel 1. Contour interval = 3 dB.
Solid curve = initial model; Dotted curve = corrected model.

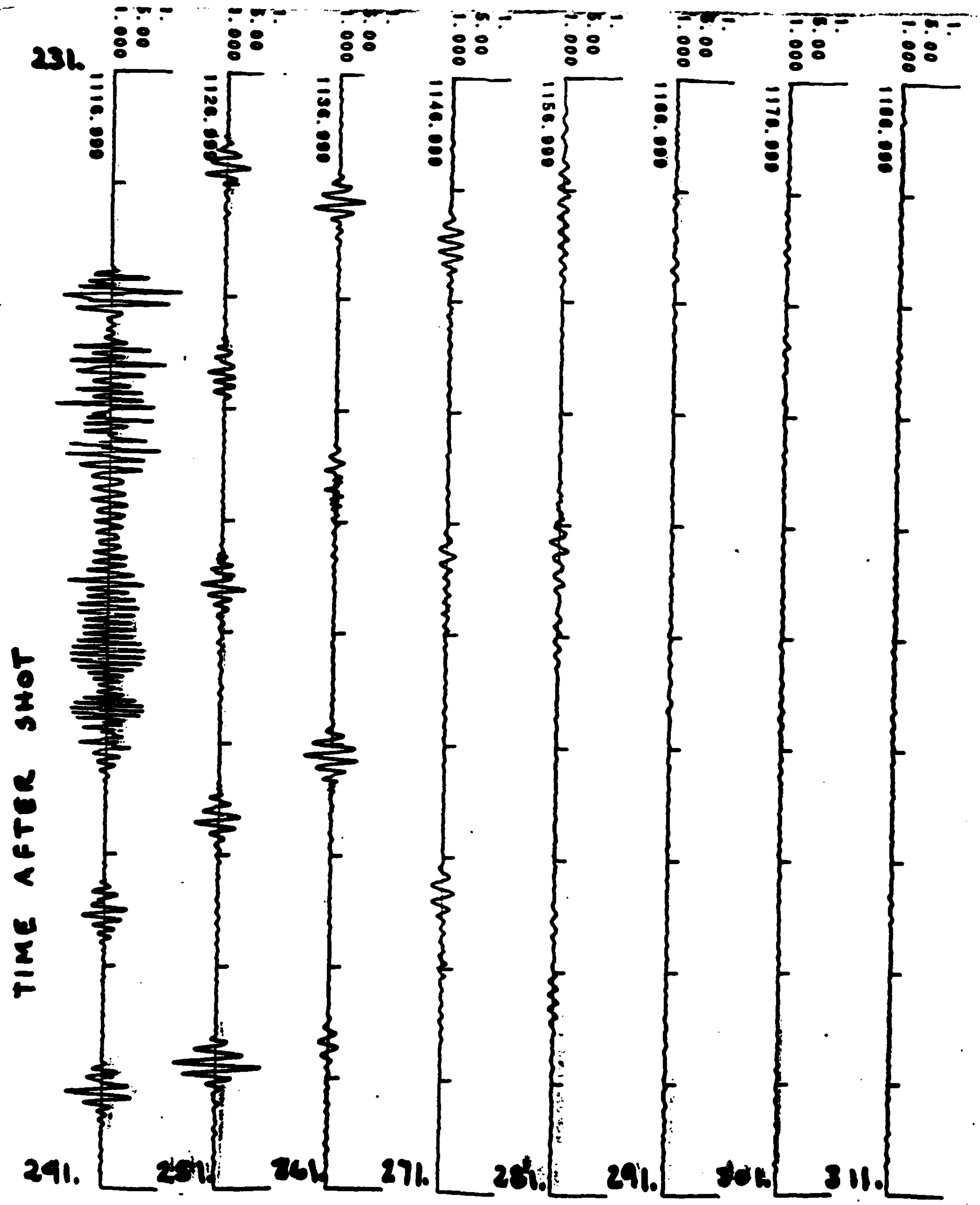

FRAM II - 55 # SHOT @ 93 m, 391 km
2-32 Hz, 5X

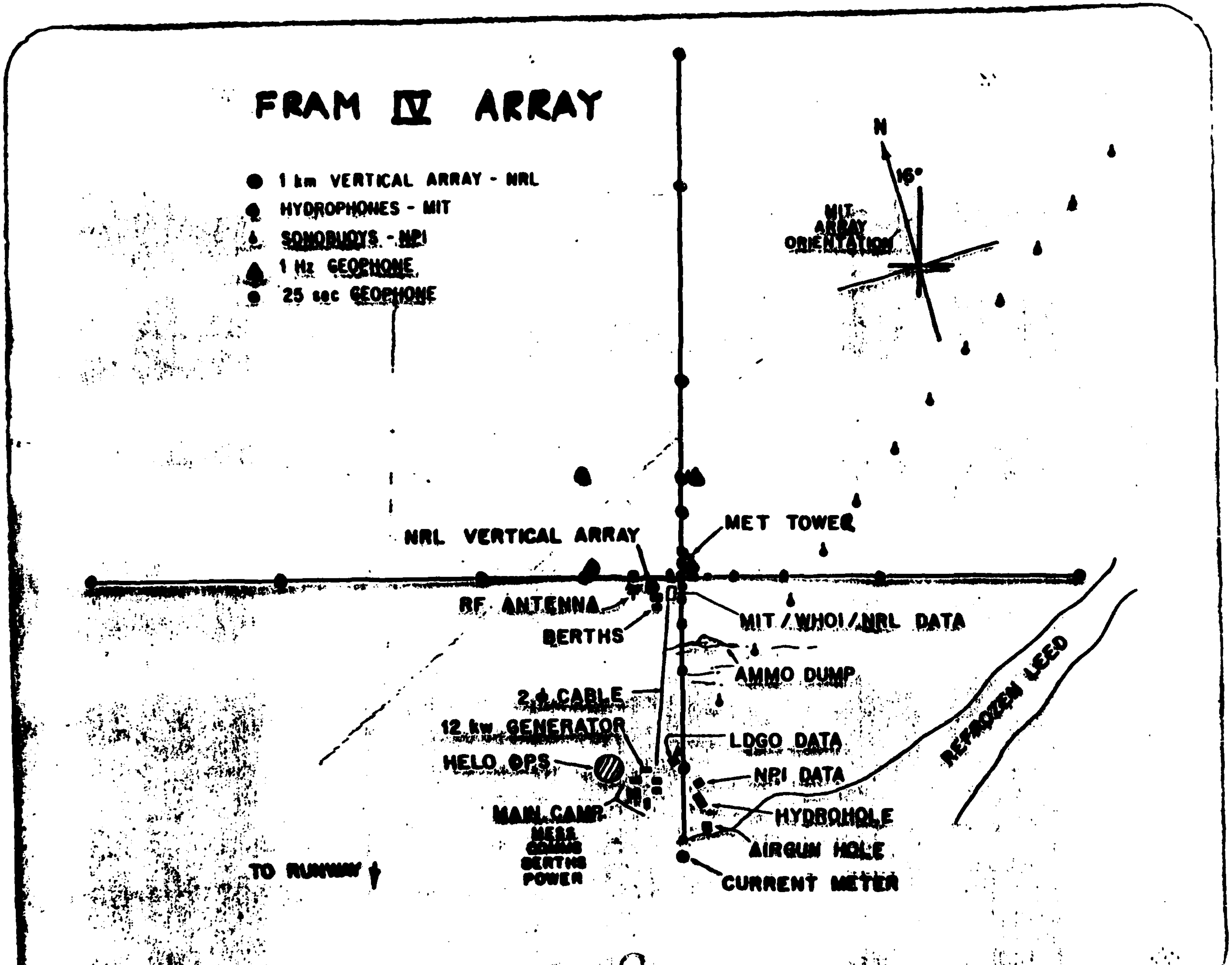
FRAM IV ARRAY
1 km VERTICAL ARRAY - NRL
HYDROPHONES - MIT
SONOBUOYS - NPI
1 Hz GEOPHONE
25 sec GEOPHONE
N
16°
MIT ARRAY ORIENTATION
MET TOWER
NRL VERTICAL ARRAY
RF ANTENNA
BERTHS
MIT / WHOI / NRL DATA
AMMO DUMP
2 ϕ CABLE
12 kw GENERATOR
LDGO DATA
HELO OPS
NPI DATA
MAIN CAMP
MESS
COMMS
BERTHS
POWER
HYDROHOLE
AIRGUN HOLE
CURRENT METER
TO RUNWAY
REFROZEN LEED

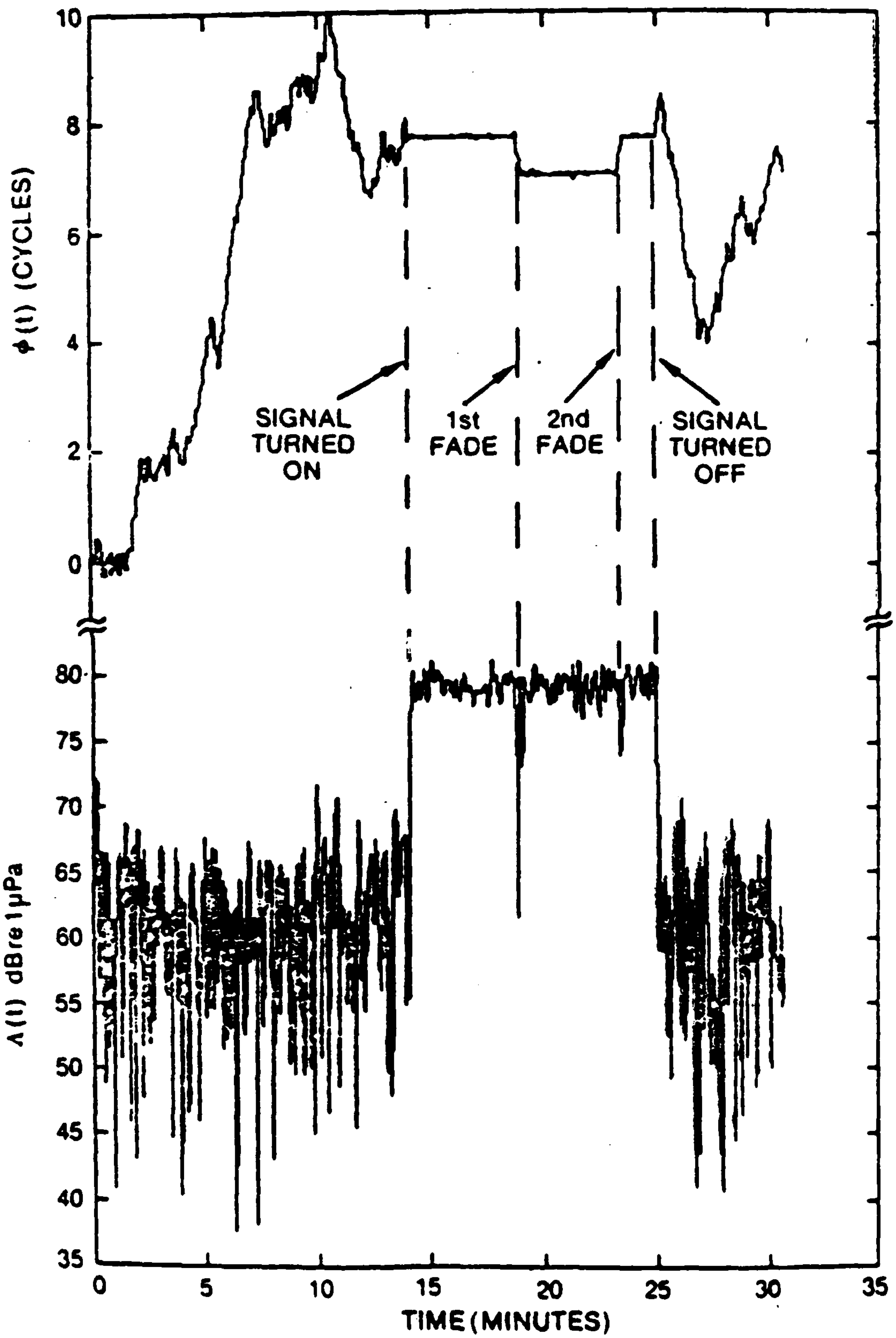

CM CATALOG NO. 15 - 1006

John Ewing

VLF Propagation in the Oceanic Crust and Upper Mantle

Abstract

Studies of the characteristics of VLF (1-5 Hz) propagation at ranges greater than 30 km show considerable coherency both in primary, intracrustal, and water column multiple refraction energy. The data utilized were generated by large explosive charges and recorded by Ocean Bottom Hydrophones on the East Pacific Rise during the ROSE project, along with some comparable data obtained from the Mid Atlantic Ridge. The water-crust-upper-mantle wave guide behaves in an orderly and predictable fashion that accounts for the distribution of energy among the primary and multiple paths. Preliminary tests using corsscorrelation between nearby seismograms suggests that for a number of range windows, in which multipath influence does not seriously degrade the data, coherency is sufficiently high to permit signal summation of array elements distributed over an area with dimensions as large as 10 km.

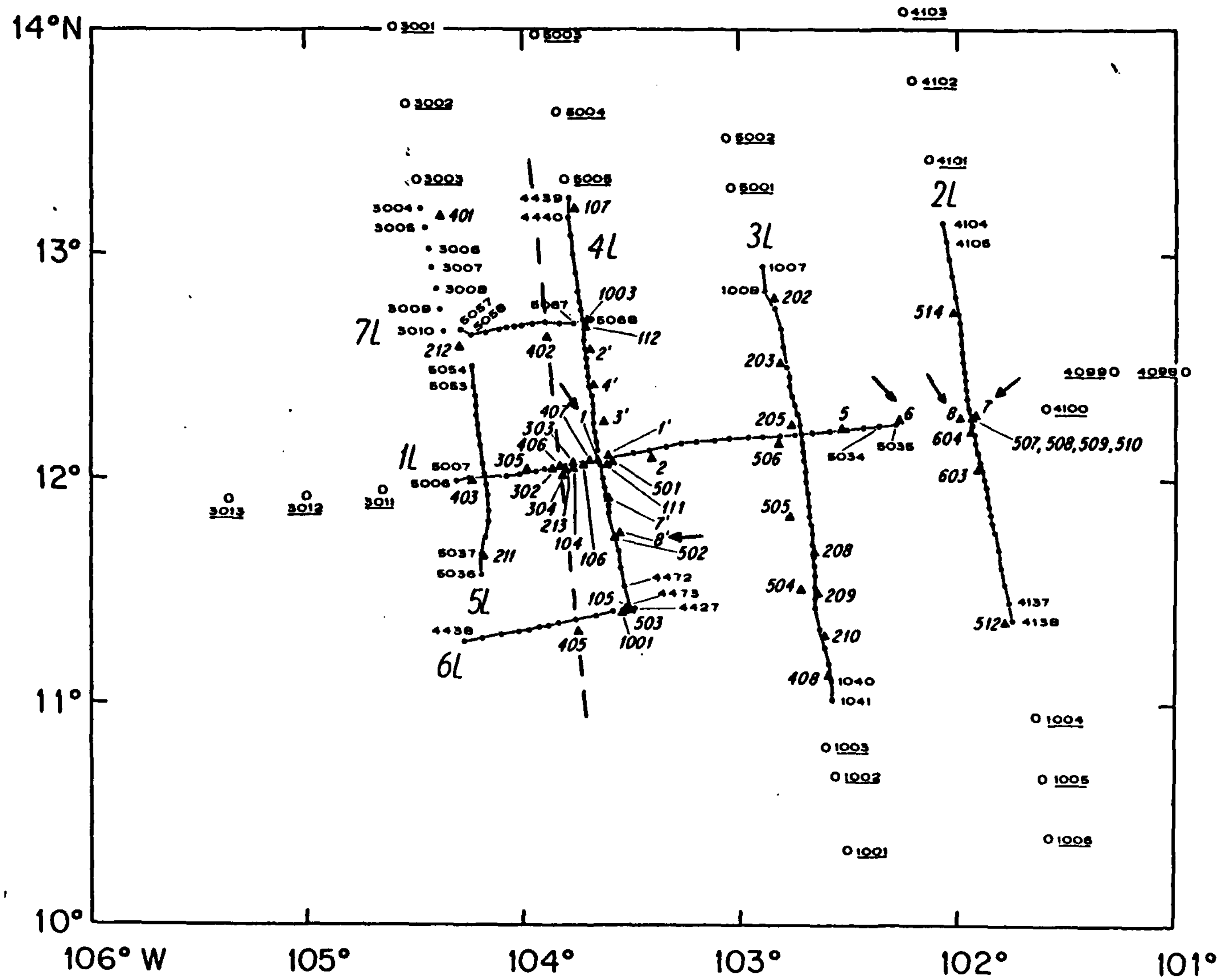

Figure 1: Locations of receivers and large shots for ROSE data study. OBH seismogram sections recorded at 1, 6, 7, 8, and 8', indicated by arrows are shown in figures. Dashed line shows location of the East Pacific Rise axis.

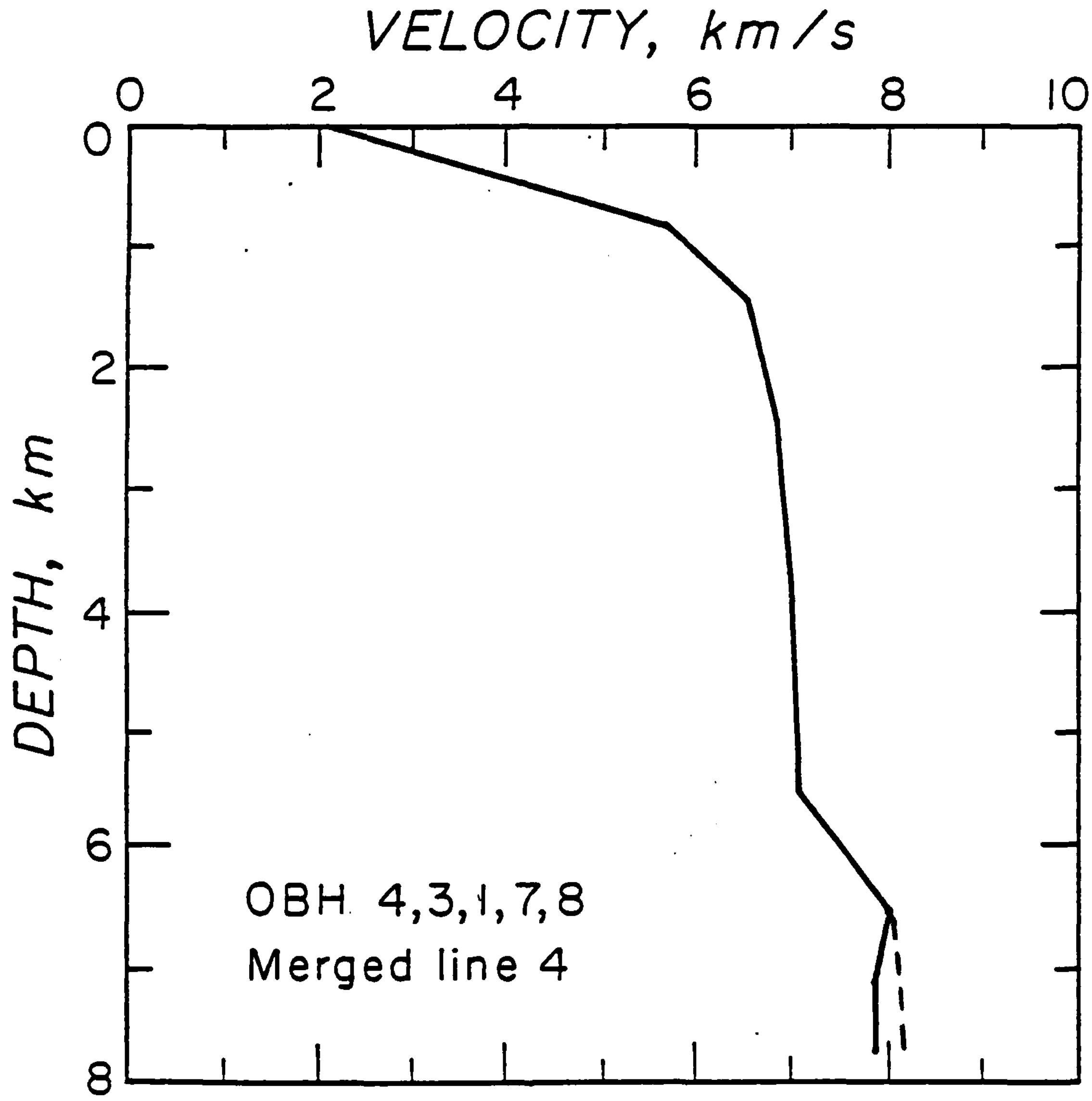

Fig 2. **Velocity-depth model determined from shots and instruments along Line 4, from Bratt and Purdy, in press. Dashed line below 6.7 km indicates velocity structure appropriate for upper mantle for propagation perpendicular to ridge axis.**

Ray diagram for typical velocity-depth relationship demonstrating Moho convergence zone

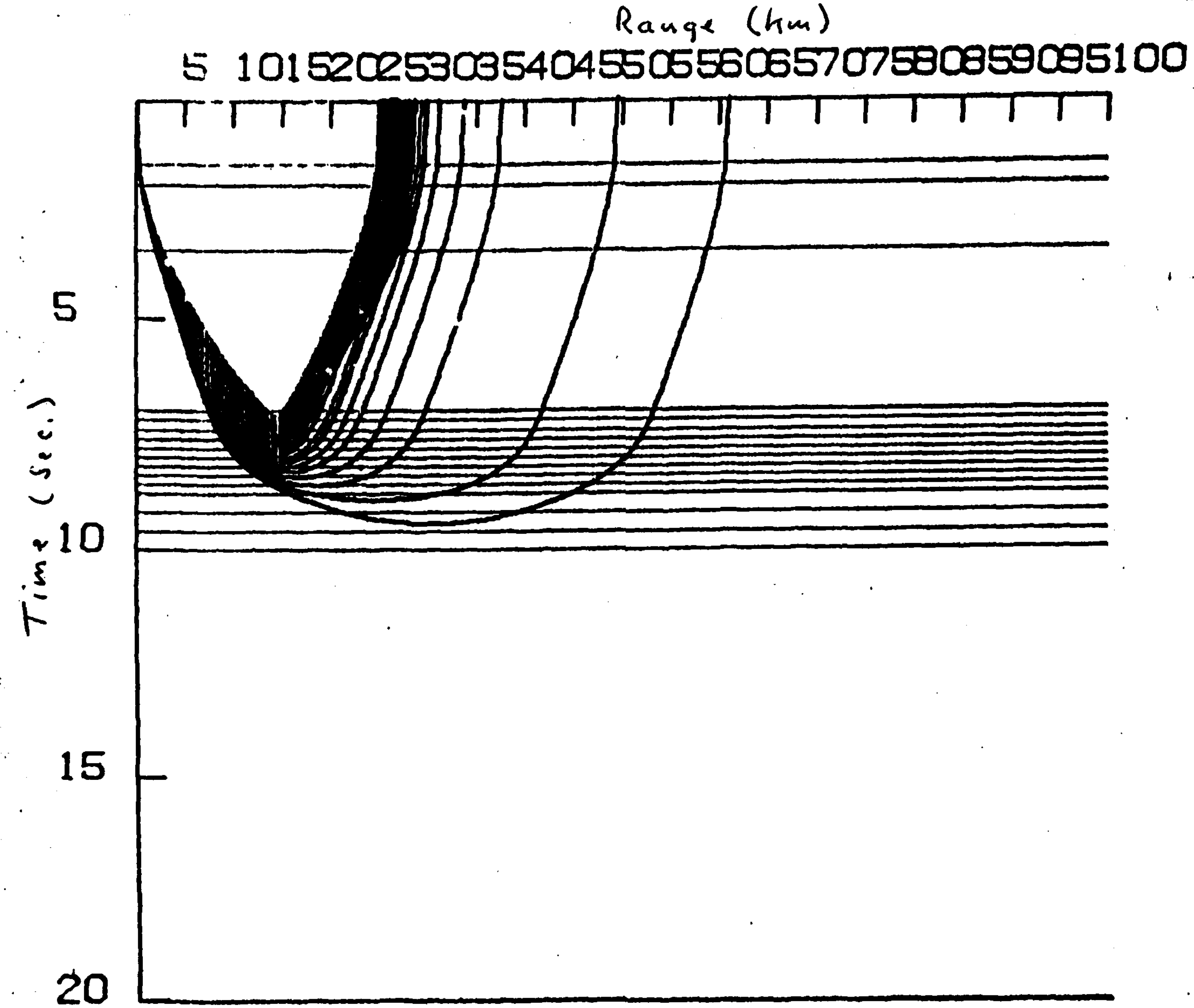

Fig. 5

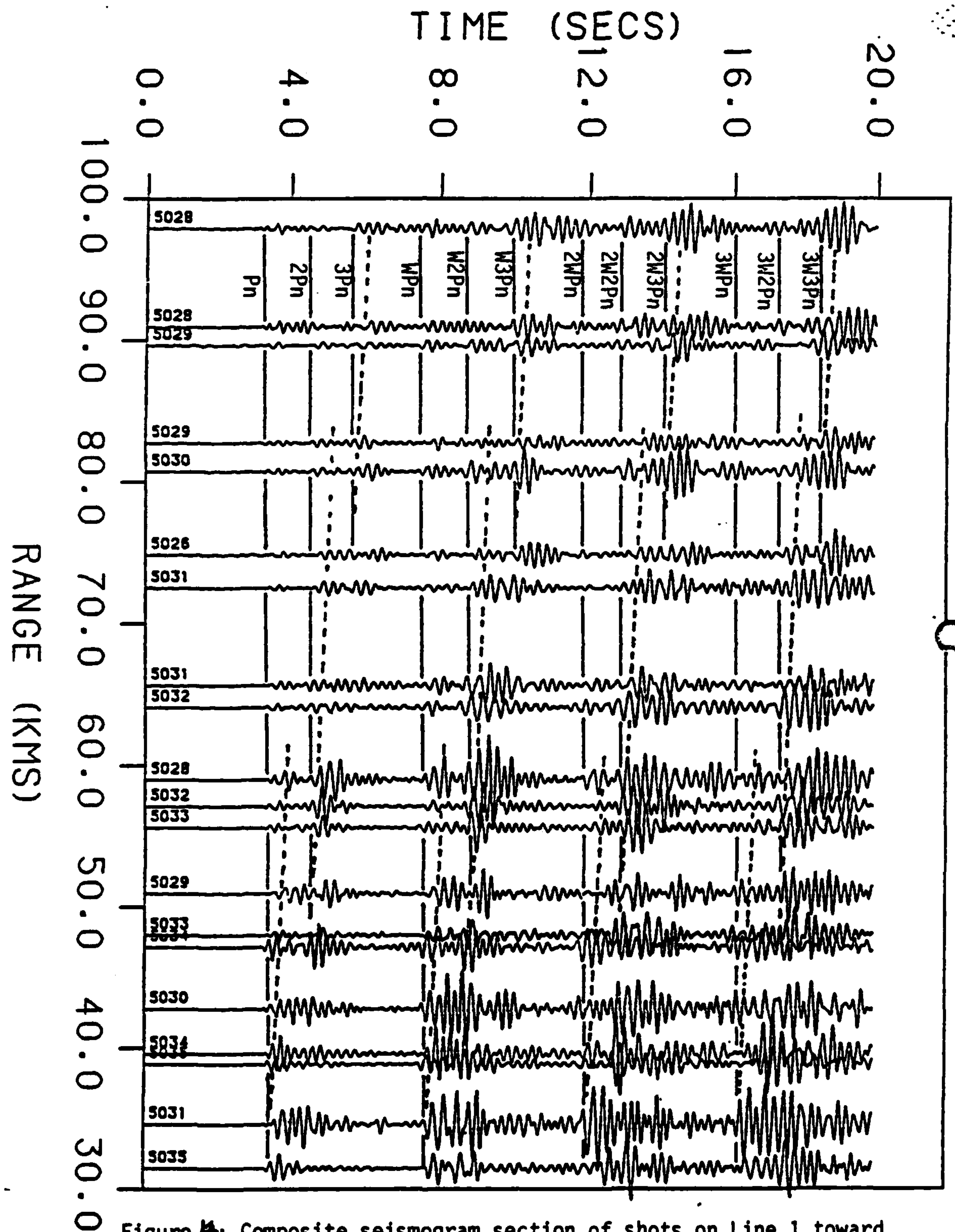

Figure 4: Composite seismogram section of shots on Line 1 toward the west from instruments 6, 7, and 8. Solid lines are drawn through primary Pn and multiple path Pn arrival times; dashed lines connect the primary PmP and multiple path PmP arrivals. Examples of propagation paths are shown for Pn, WPn, 2WPn, and W2Pn arrivals in Figure 3. Note the shift of peak energy to higher-order multiples at ranges of 50 and 75 km.

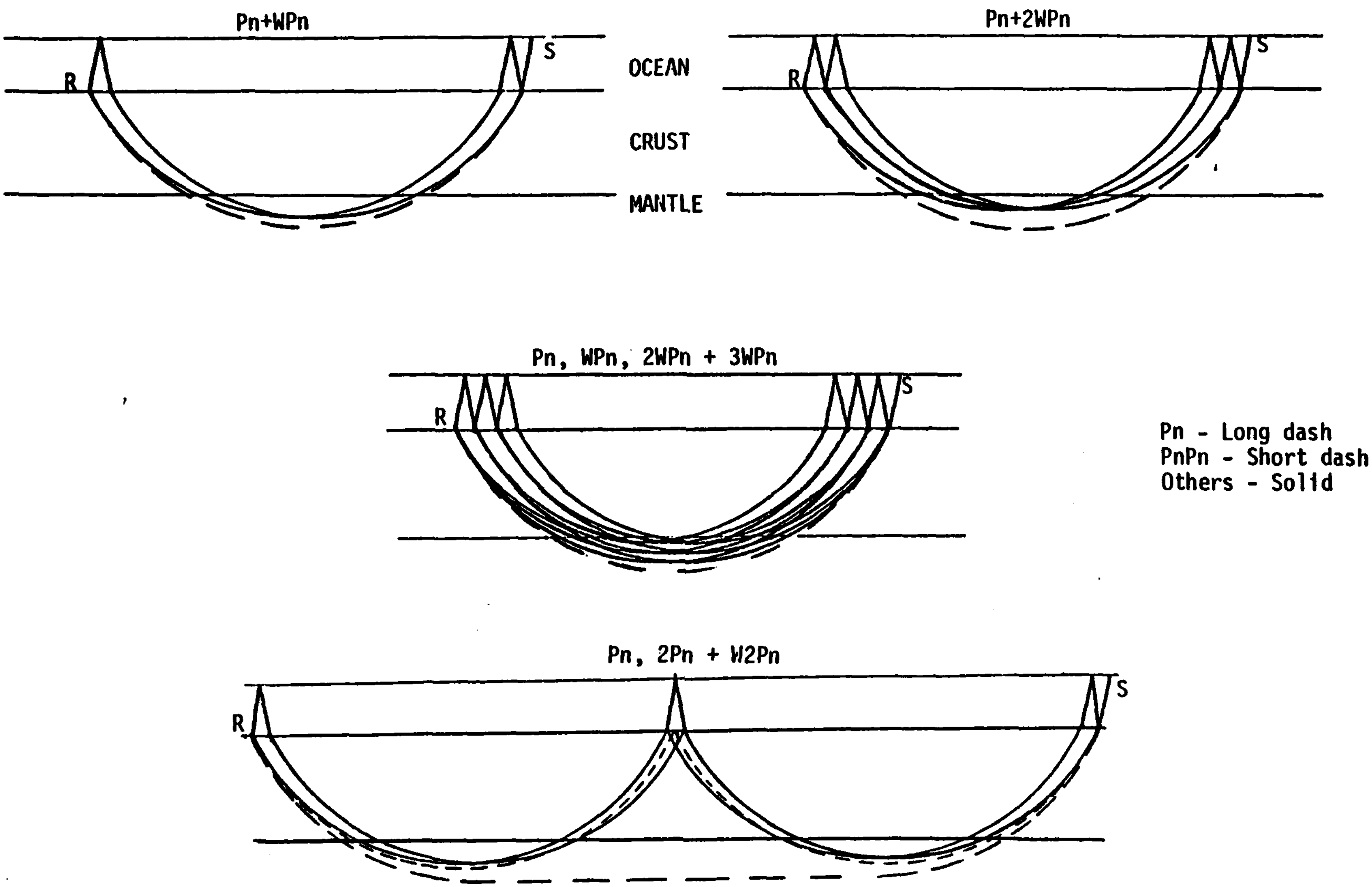

Figure 5: Propagation paths for several primary and multiple phases observed in the data. Phase designations are the same as those in Figure 2.

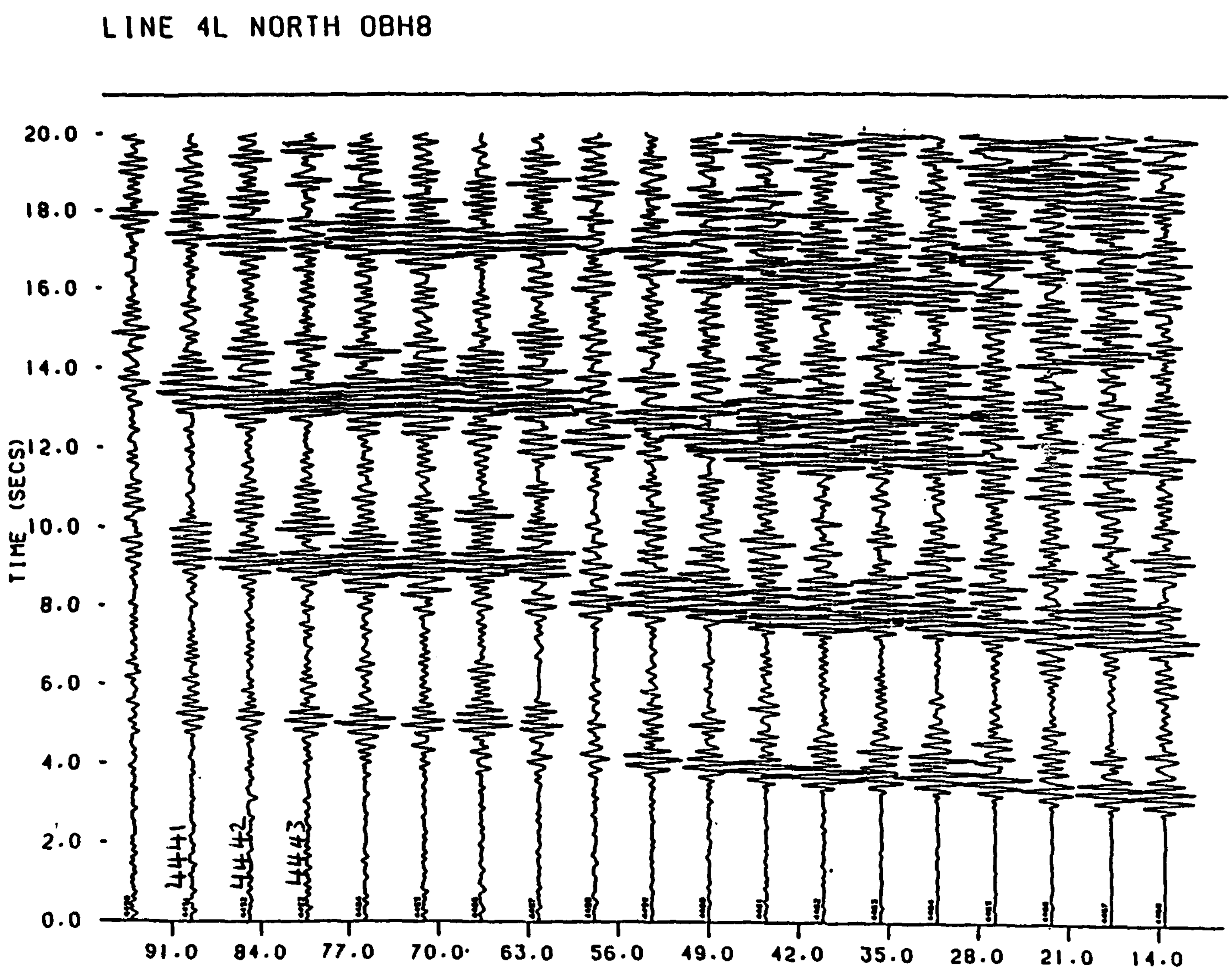

Fig 6. *Seismogram section* recorded at OBH 8' on Line 4. Shots are north of the instrument. Note the absence of Pn energy and the dominance of primary PmP and multiple PmP phases.

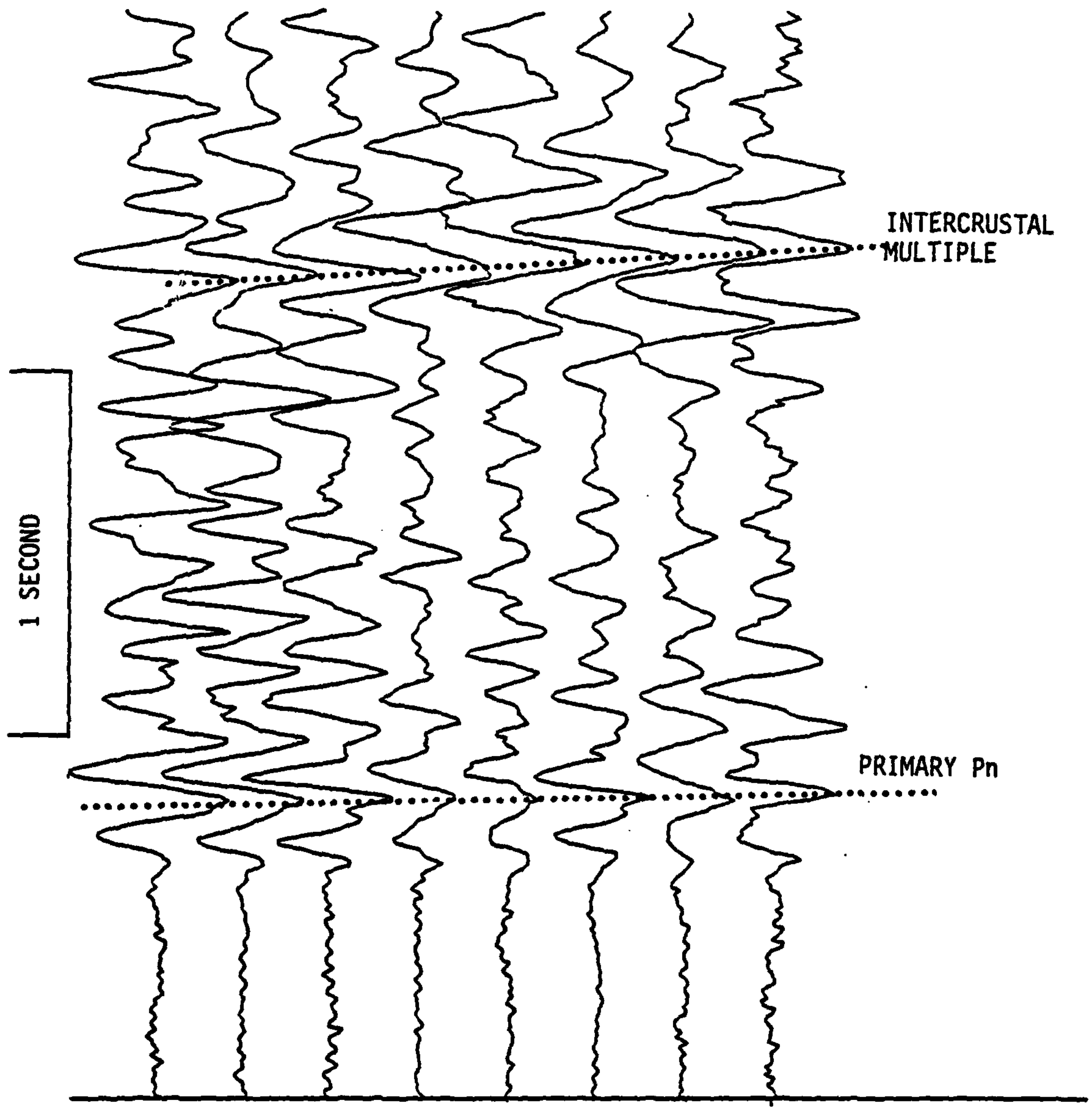

Fig. 9 Coherent refractions and intercrustal multiples from 32 lb charges recorded by an OBH in the median valley of the MAR in the range window 28km to 42km.

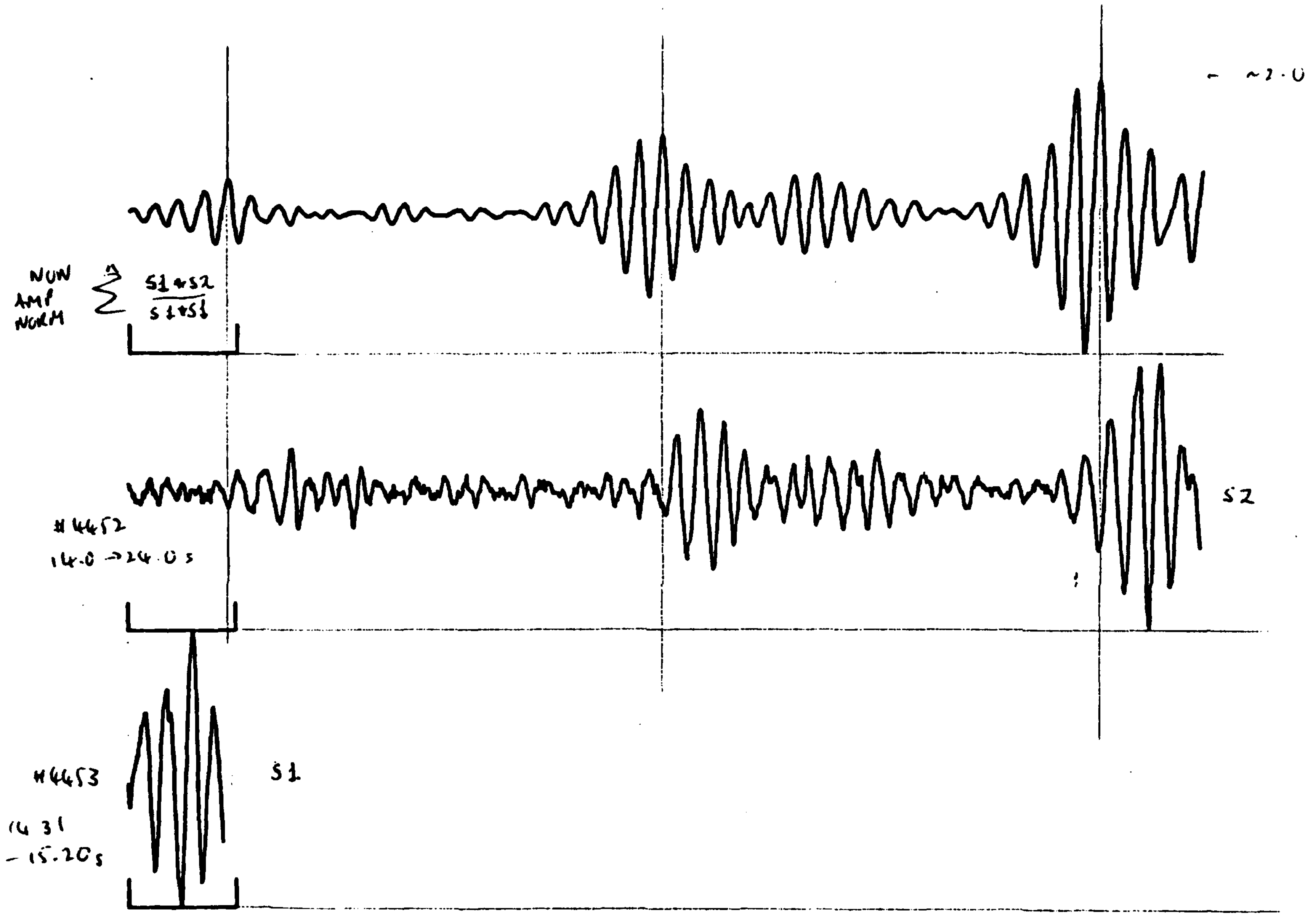

CB11#8

Fig. 8

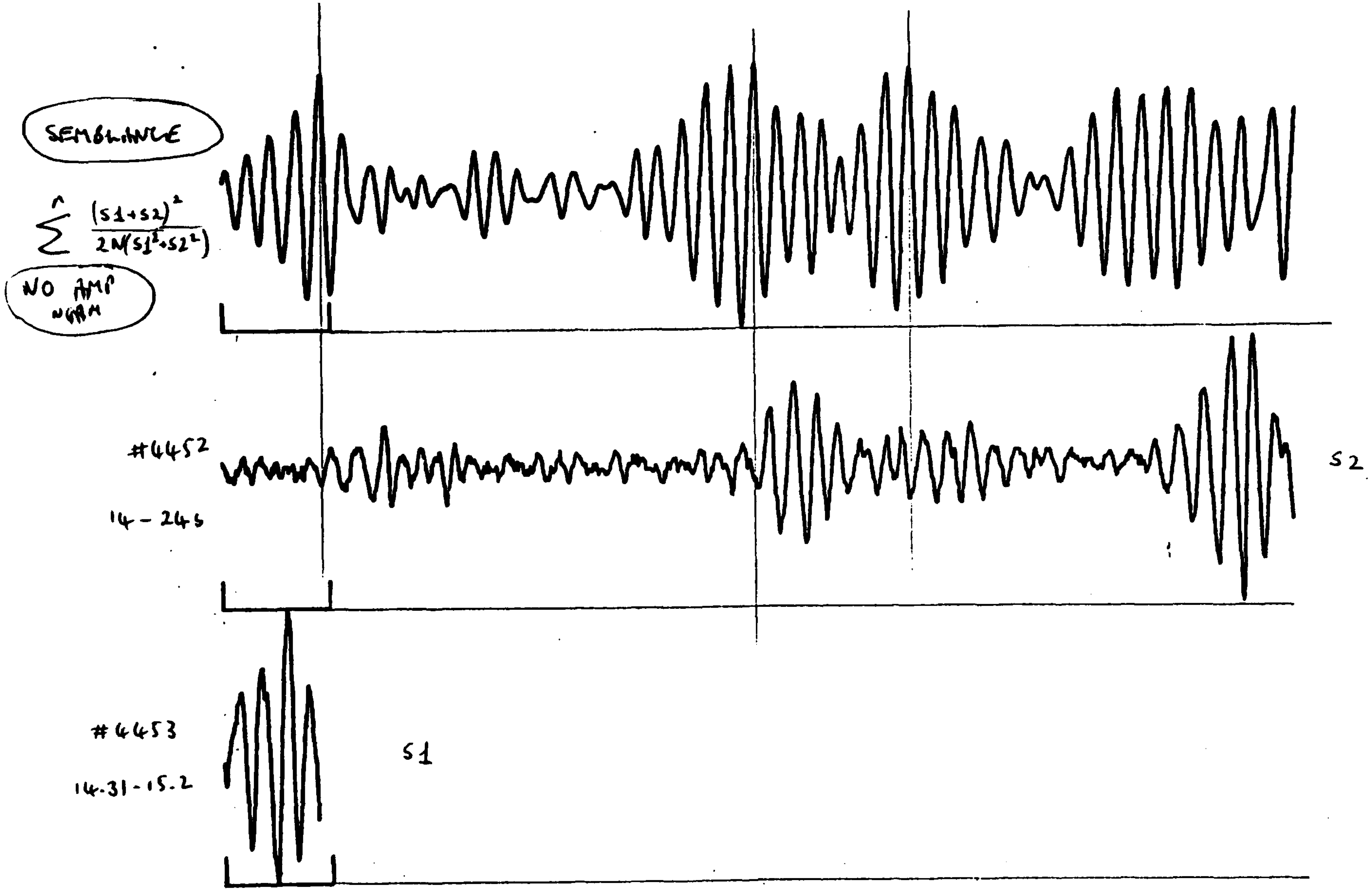
SEMBLANCE
$\sum^{n} \frac{(S1+S2)^2}{2N(S1^2+S2^2)}$
NO AMP NORM
#4452
14 - 24 s
S2
#4453
14.31 - 15.2
S1

Fig. 9

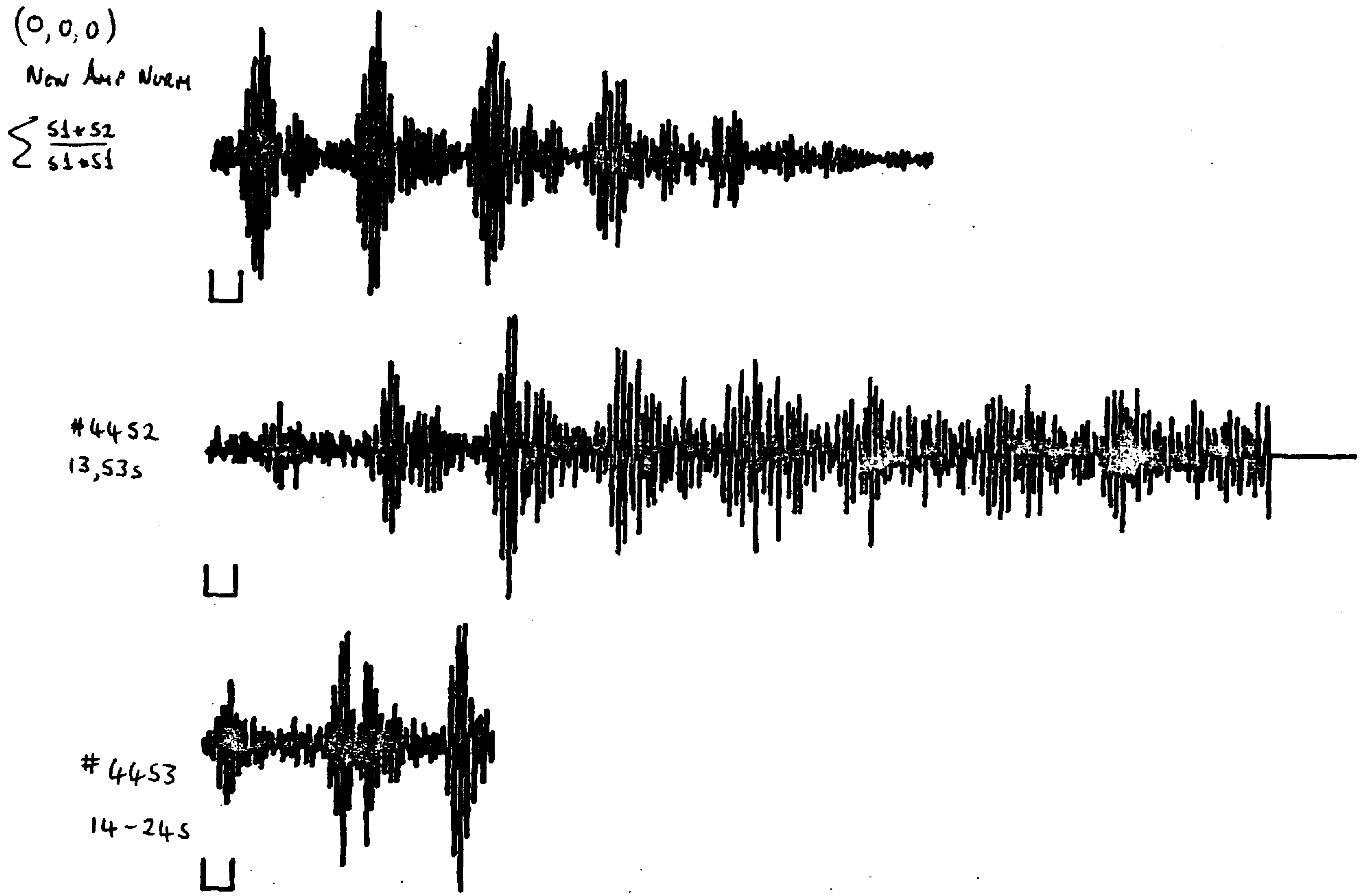

ROSE. 02 GBH 8

LINE 4

Fig 10

COR5352.DAT

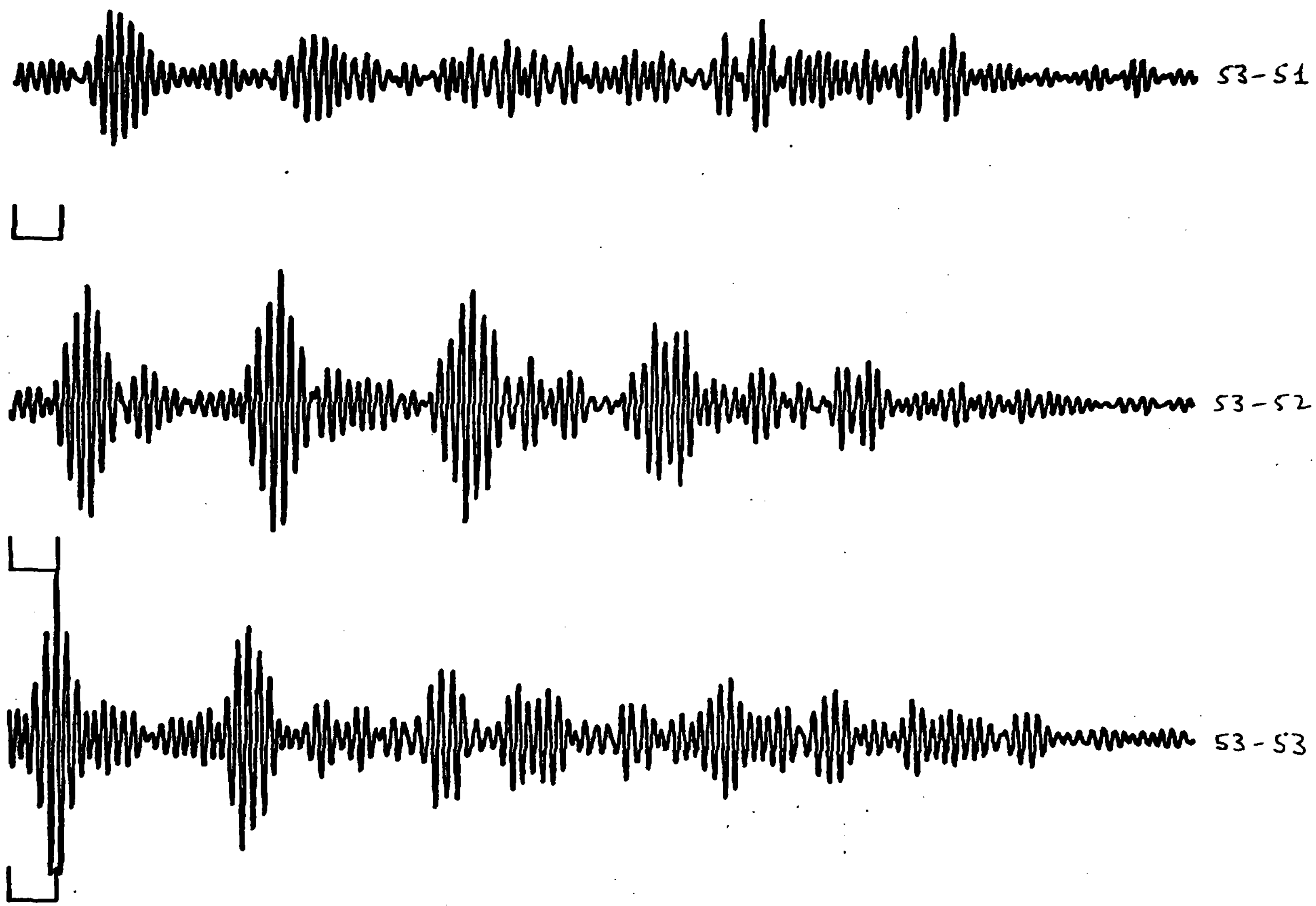

Fig. 11

COR5353.DAT
COR 5352.DAT
COR 5351.DAT

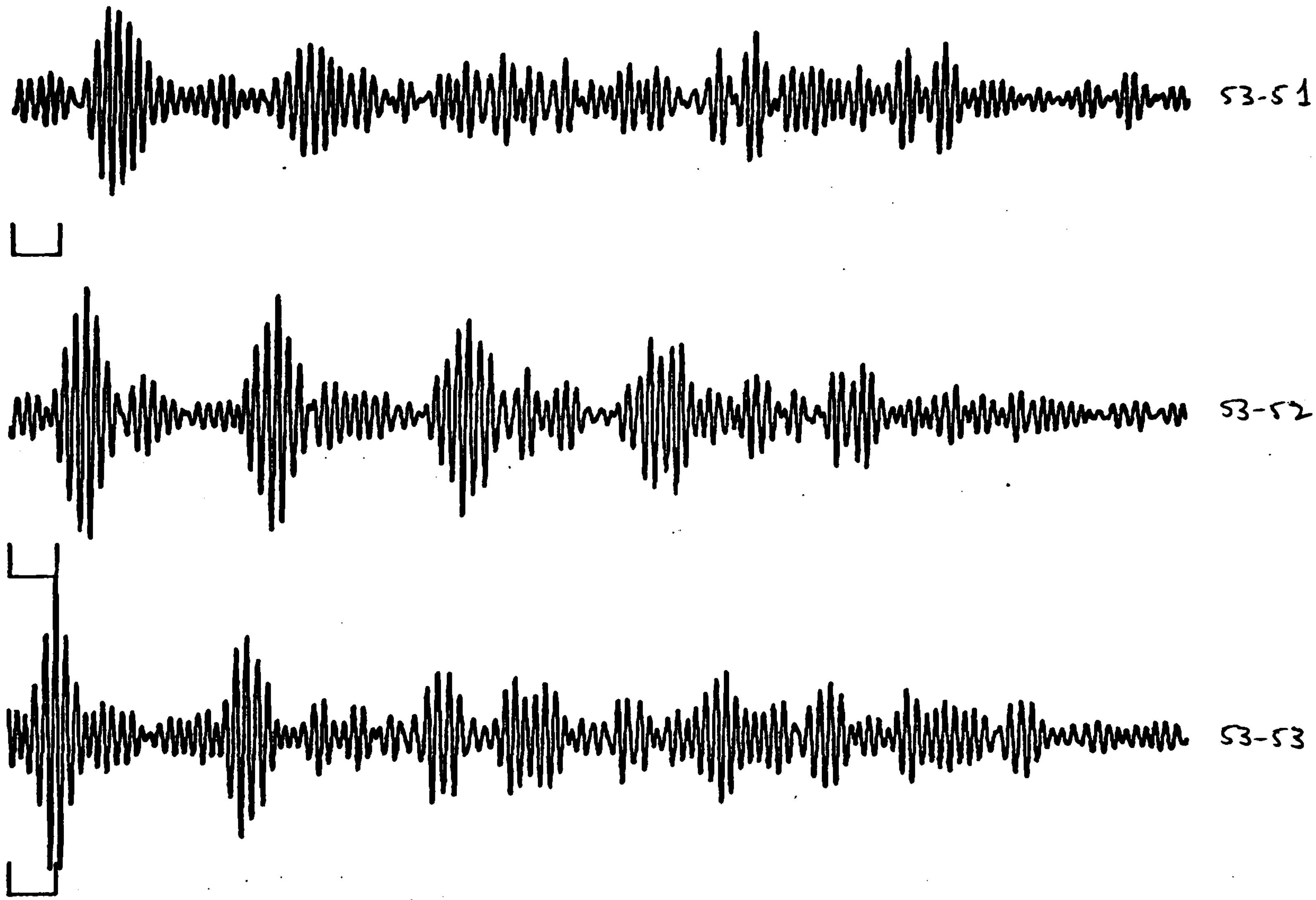

Fig. 12

SEMBLANCE

COR 5353S.DAT
COR 5352S.DAT
COR 5351S.DAT

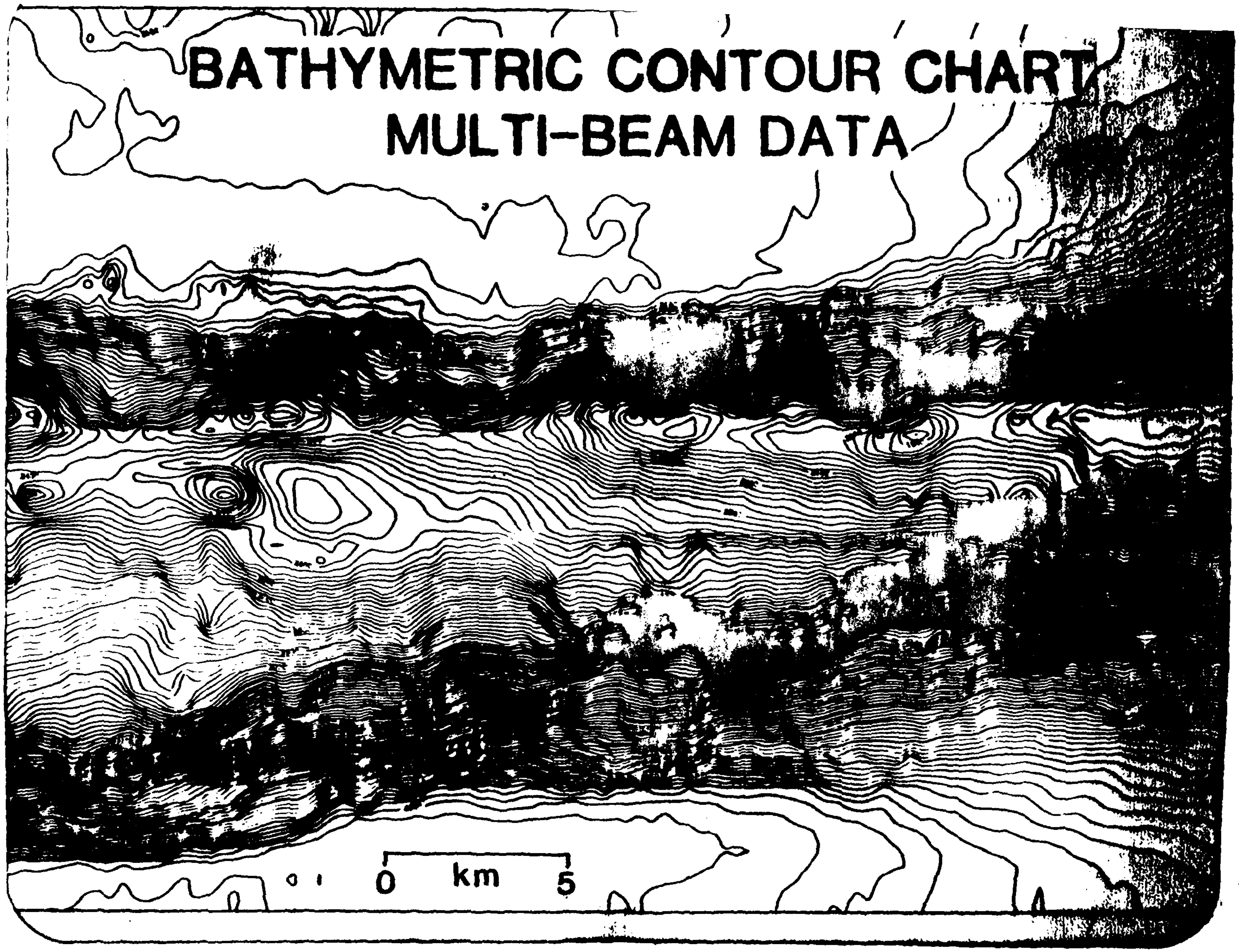
BATHYMETRIC CONTOUR CHART
MULTI-BEAM DATA
0 km 5

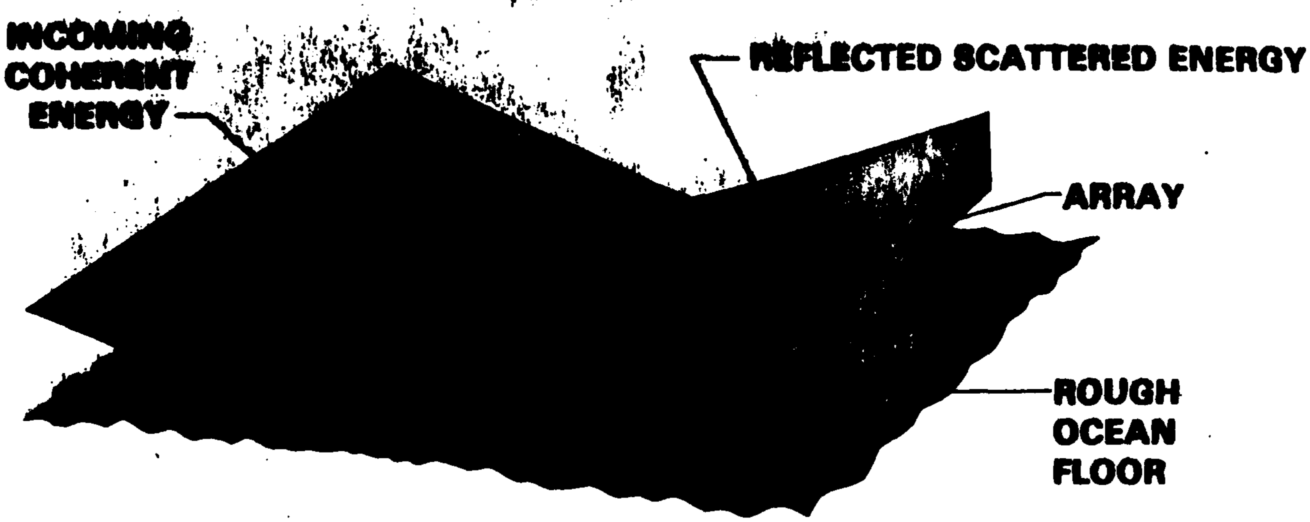

ANGULAR DISTRIBUTION OF ENERGY

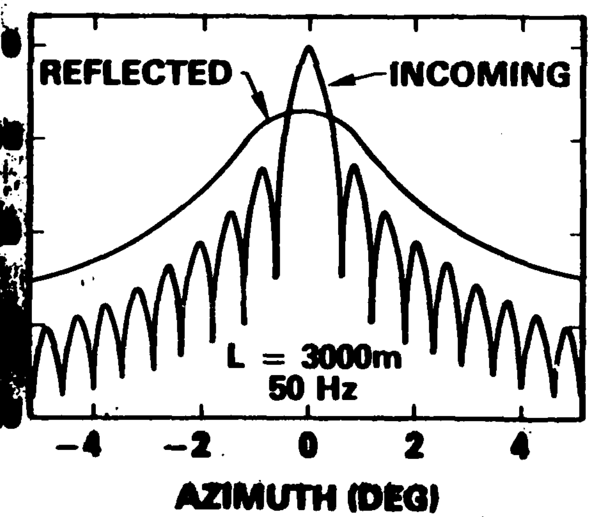

PROGRAM COMPONENTS

- THEORETICAL AND COMPUTATIONAL FORMULATION PREDICTING THE ANGULAR DISTRIBUTION OF ENERGY INFLUENCED BY STATISTICALLY DESCRIBED BATHYMETRY
- STATISTICAL CHARACTERIZATION OF THE SPECTRUM OF OCEAN BOTTOM ROUGHNESS

A THREE-DIMENSIONAL MODEL FOR BATHYMETRIC SCATTERING WITH VLF APPLICATIONS

R.N. BAER, J.S. PERKINS, E.B. WRIGHT, and B.B. ADAMS

CODE 5160
U.S. NAVAL RESEARCH LABORATORY
WASHINGTON, DC 20375

DEPARTMENT OF THE NAVY
NAVAL RESEARCH LABORATORY
WASHINGTON, D.C. 20375

IN REPLY REFER TO:

23 January 1985

A Three-Dimensional Model for Bathymetric Scattering with VLF Applications

R.N. Baer, J.S. Perkins, E.B. Wright, and B.B. Adams

We have developed a computer model to simulate the performance of acoustic arrays receiving energy scattered from rough ocean bathymetry. The model has been applied using a 30 Hz source in the vicinity of a seamount where bathymetric statistics are available. Predictions have been obtained for a long horizontal array and a short vertical array. We discuss the degrading effects of the rough bathymetry (including the high sidelobe levels) and the possibility of discriminating against the scattered component of the energy. The model is stochastic, producing a statistical result based on the statistics of the bathymetry. It is also three-dimensional as it incorporates scattering out of a vertical plane. The acoustic field is propagated from the source to the vicinity of the boundary interaction using a split-step parabolic-equation calculation where the coherence function is formed. The coherence function is determined at the array by propagating along characteristic curves. A modified Kirchhoff formulation is used in weighting the scattering directions at the points of bottom interaction. We have developed a fast and accurate way to estimate the large number of scattering integrals which must be evaluated.

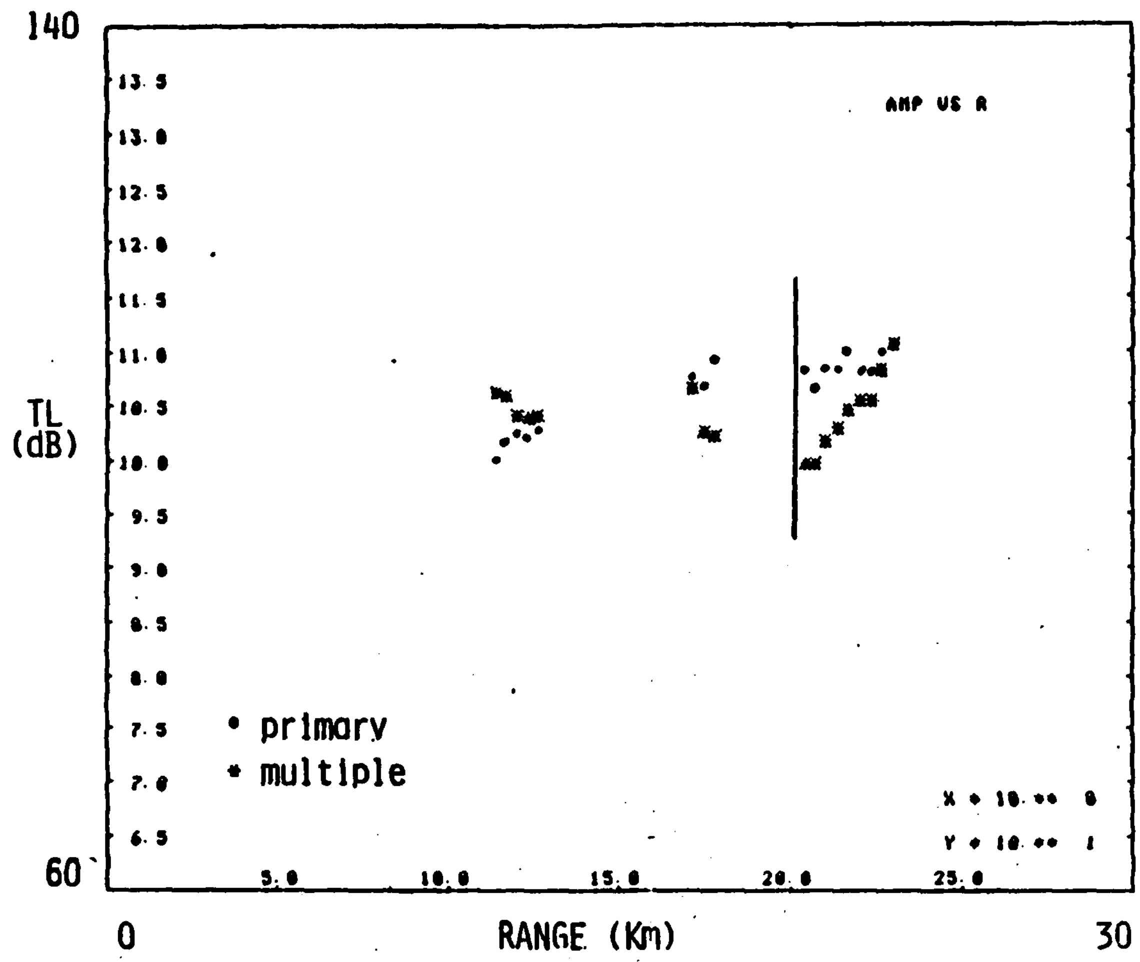
140
TL (dB)
60
AMP VS R
• primary
* multiple
X * 10 ** 0
Y * 10 ** 1
0
RANGE (Km)
30

PHASE VELOCITY VS RANGE

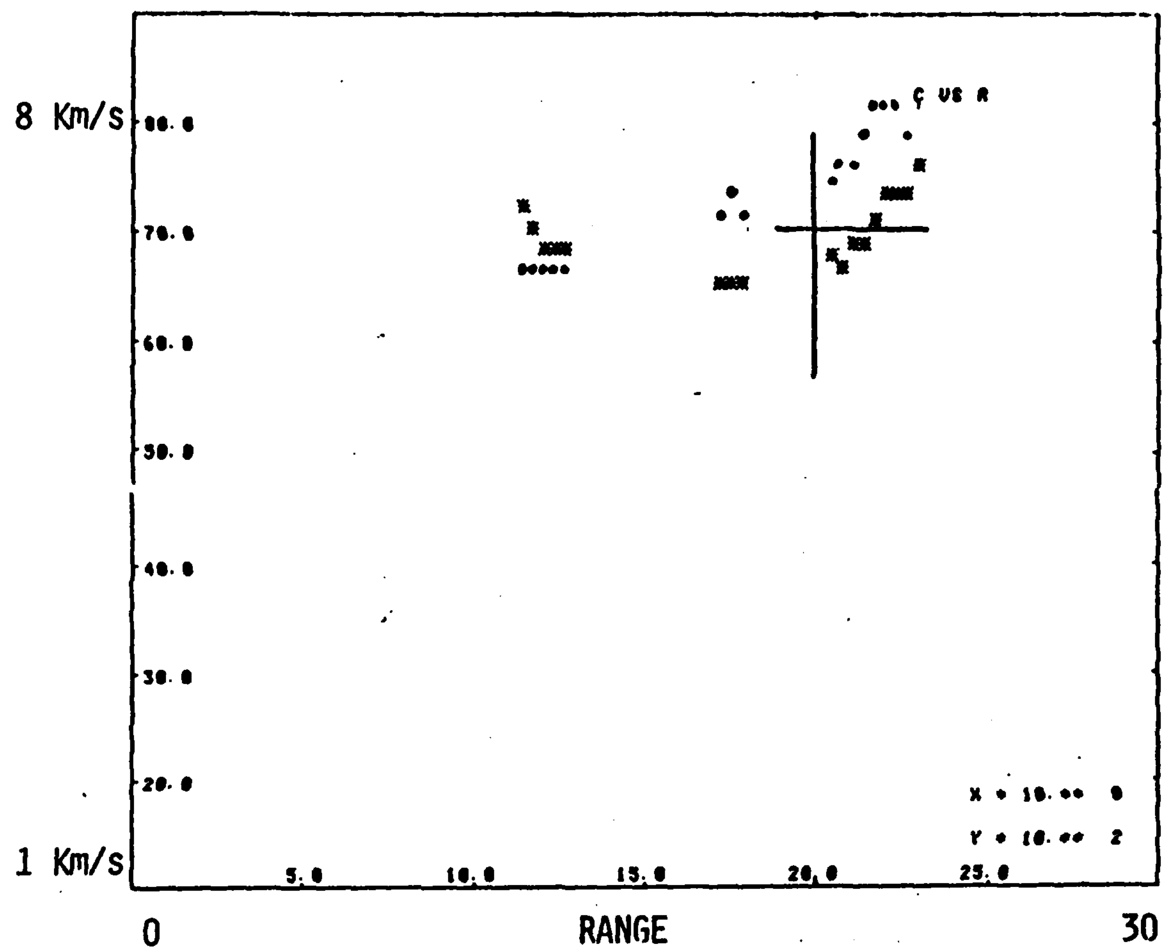

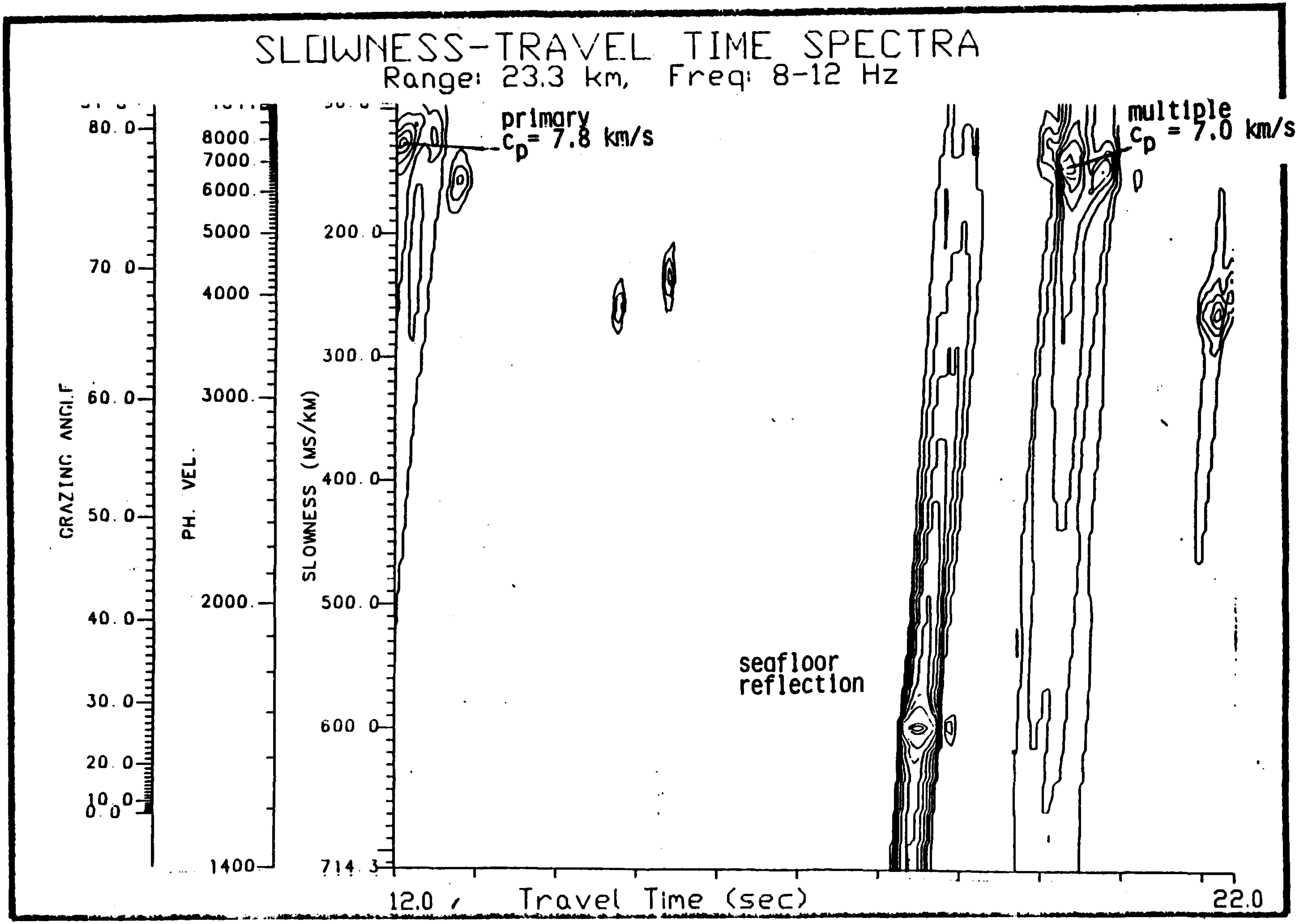
SLOWNESS-TRAVEL TIME SPECTRA
Range: 23.3 km, Freq: 8-12 Hz
primary
c_p = 7.8 km/s
multiple
c_p = 7.0 km/s
seafloor
reflection
GRAZING ANGLE
80.0
70.0
60.0
50.0
40.0
30.0
20.0
10.0
0.0
PH. VEL.
8000
7000
6000
5000
4000
3000
2000
1400
SLOWNESS (MS/KM)
200.0
300.0
400.0
500.0
600.0
714.3
12.0
Travel Time (sec)
22.0

Velocity vs Depth
ESP Data

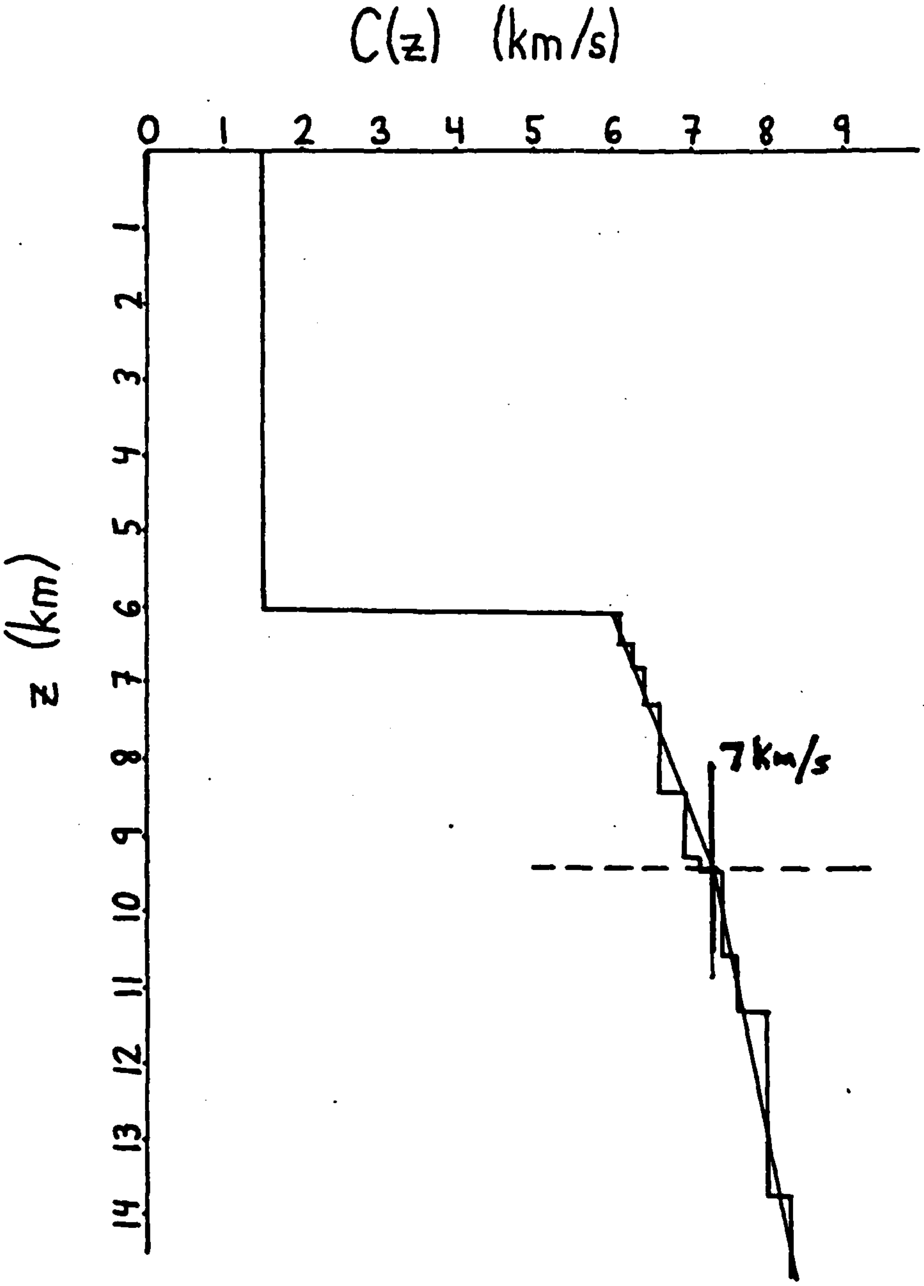

TRANSMISSION LOSS (dB)

for

3 GRADIENT MODELS

for the

BASEMENT

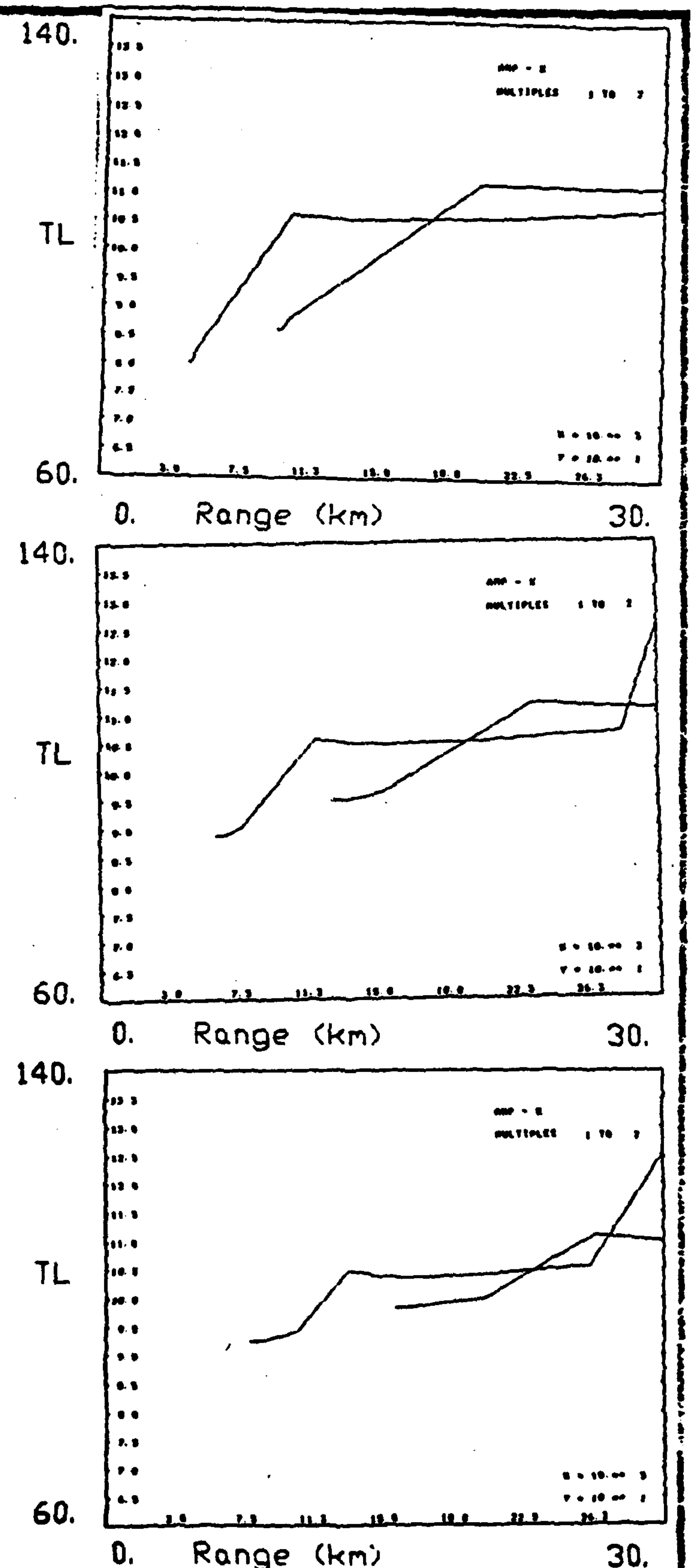

Velocity vs Depth
Synthetic Data

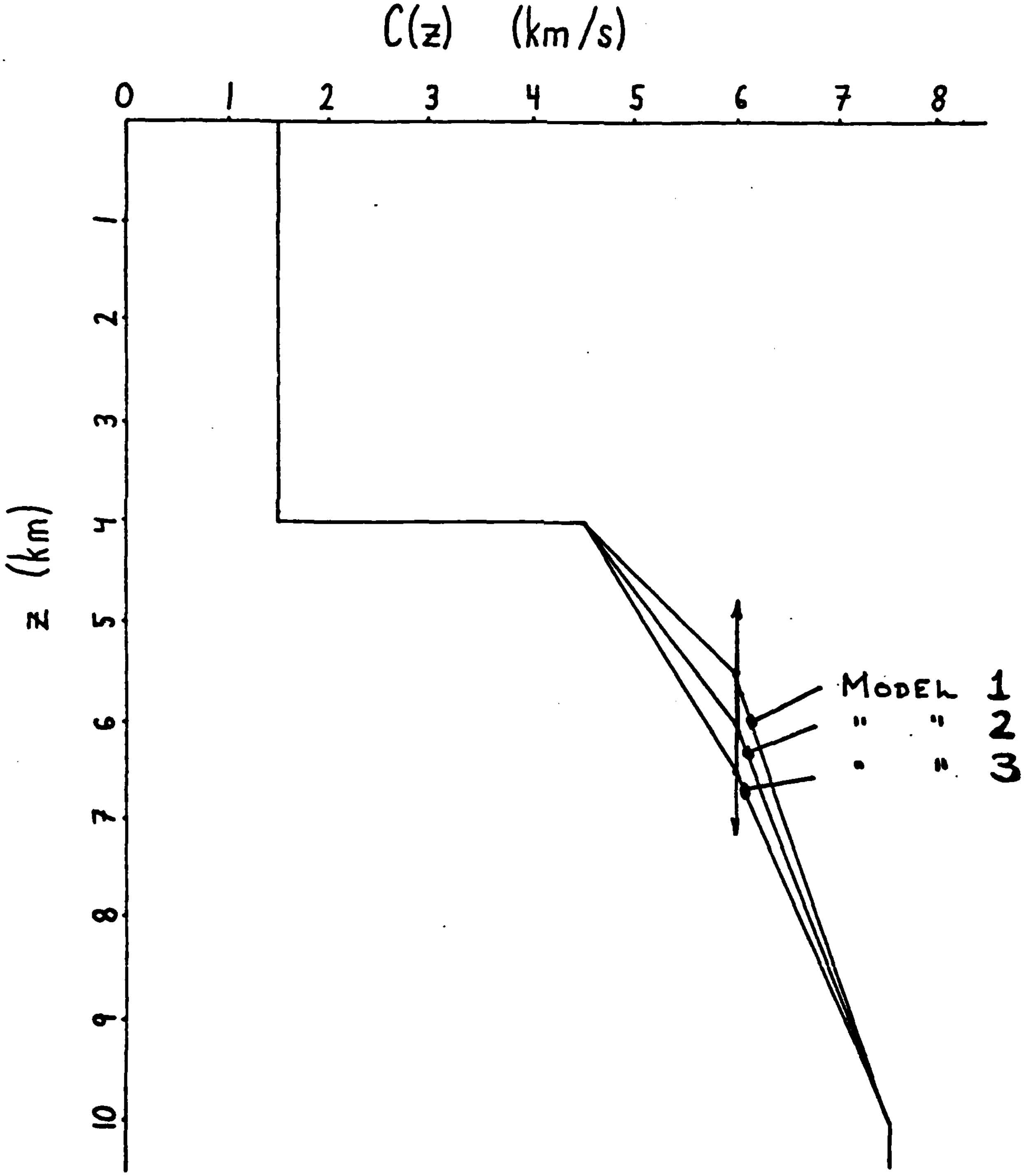

TRANSMISSION LOSS @ OFFSET X(p)

$$TL(p) = -10 \log_{10}\left(\left[\frac{p}{X(p)\,\frac{dX(p)}{dp}}\right]\cdot\left[\frac{1-(pc_\circ)^2}{c_\circ^{\,2}}\right]\right)$$

p: ray parameter

X(p): offset function

LINEAR GRADIENTS in C(z)

$$\frac{dX(p)}{dp} = -\frac{2}{p^2}\sum_{\text{layers}}\frac{1}{b_k^{\,2}}\left|\frac{1}{\cos(\theta_{i,k})} - \frac{1}{\cos(\theta_{b,k})}\right|$$

$$-\frac{2}{p^2}\,\frac{1}{b_t^{\,2}}\,\frac{1}{\cos(\theta_{i,t})}$$

b_k: gradient in layer k

b_t: gradient in turning point

$\theta_{i,k}$: angle at top of layer k

$\theta_{b,k}$: angle at bottom of layer k

$\theta_{i,t}$: angle at top of turning laver

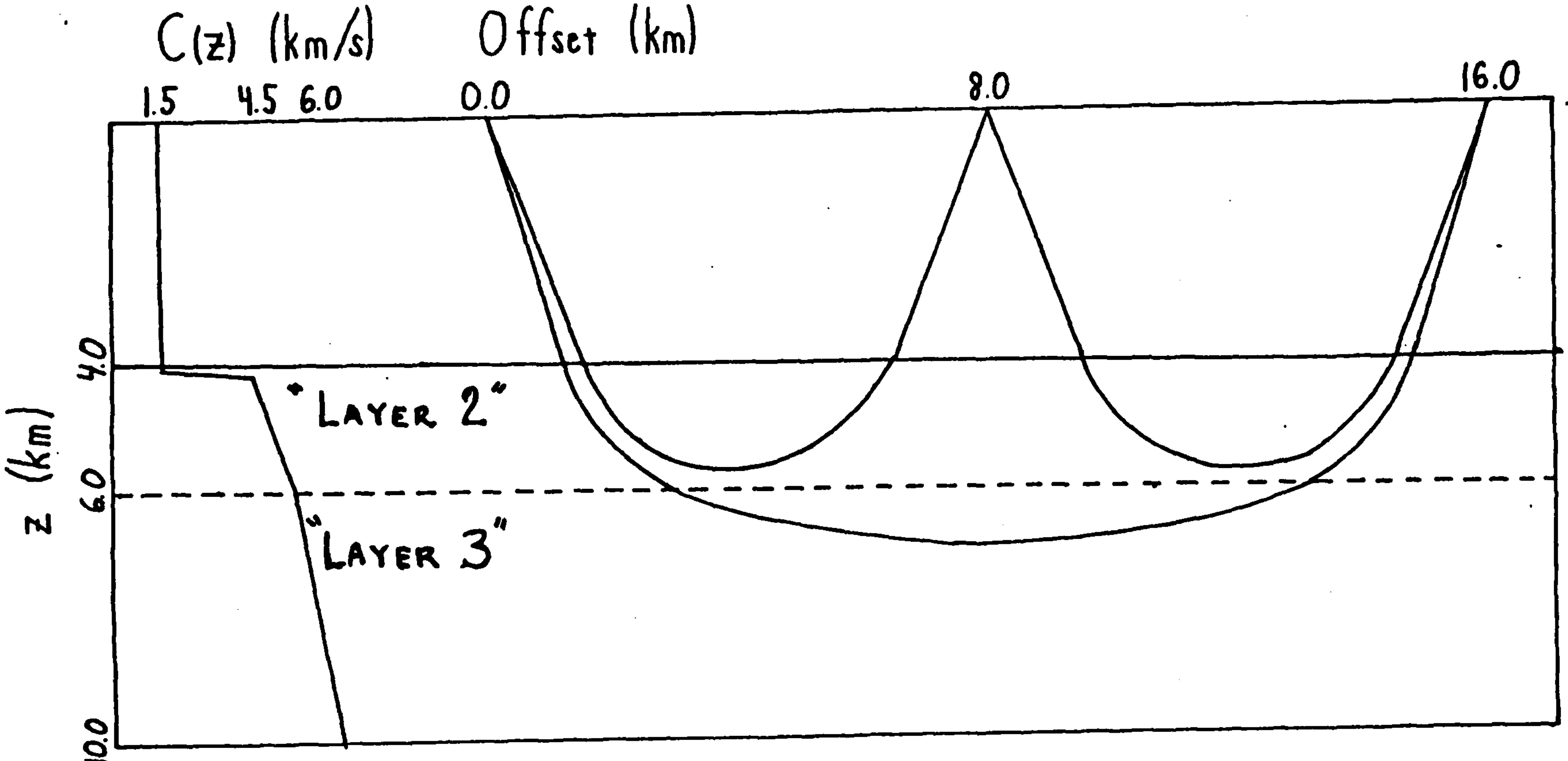
C(z) (km/s)
Offset (km)
1.5
4.5
6.0
0.0
8.0
16.0
"LAYER 2"
"LAYER 3"
z (km)
4.0
6.0
10.0

MULTICHANNEL TRACES

Range: 23.3 km, Length: 2.4 km

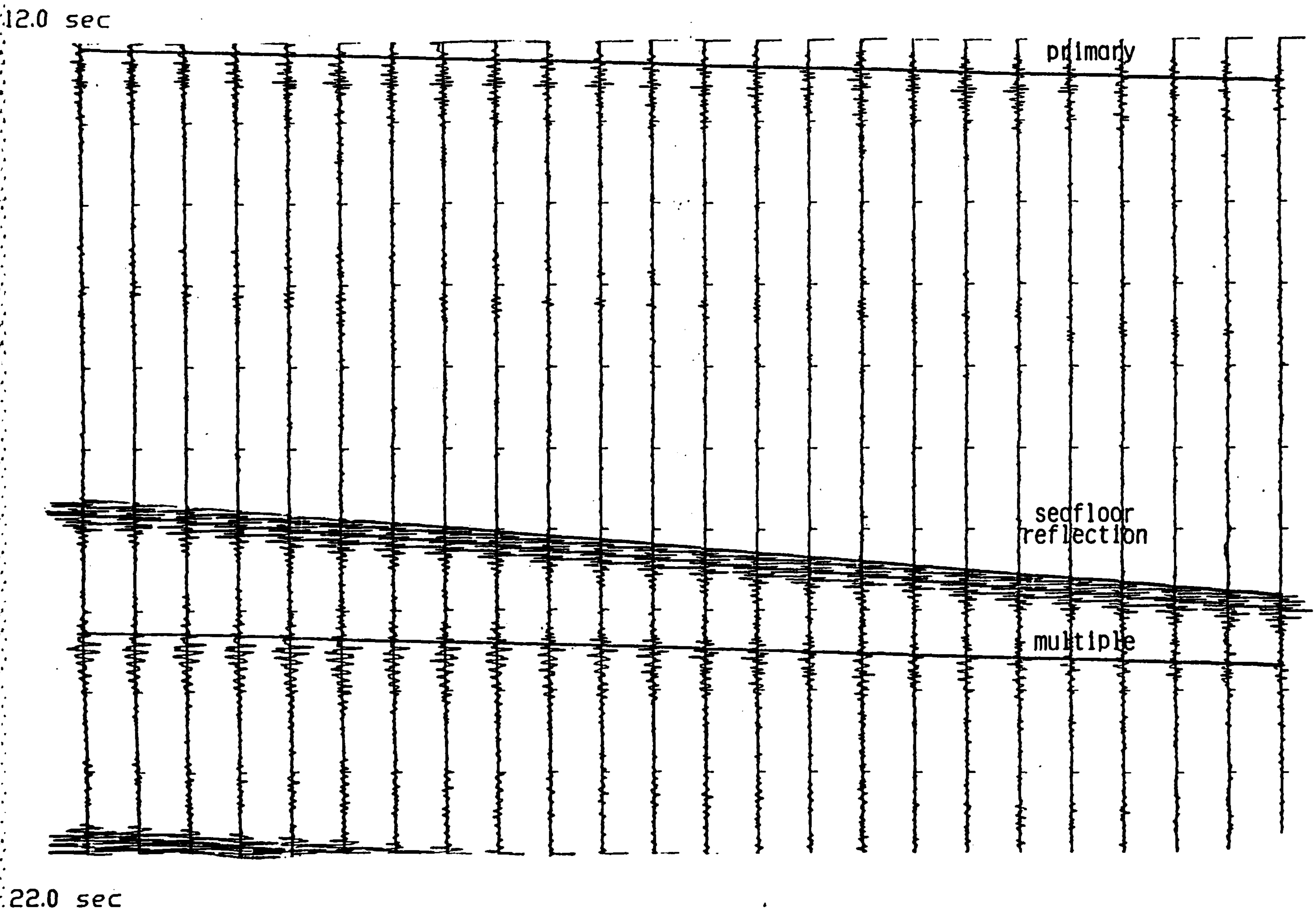

Art Baggeroer

VLF PROPAGATION #2

ON THE RELATIVE AMPLITUDES BETWEEN PRIMARY AND MULTIPLE SIGNALS FROM SEISMIC REFRACTIONS IN OCEANIC CRUST

In deep ocean seismic refraction experiments the energy in the primary signal is often less than that in the multiple arriving at approximately twice the travel time. This has perplexed interpreters since the multiple has a path length greater than the primary and its amplitude presumably should be less. High resolution slowness/travel-time analysis of an expanding spread data set suggests an explanation in terms of differences in the sound speed gradients in the oceanic crust. The gradient in the upper part of the crust is typically much greater than that of the deeper crust; therefore, energy refracting in the upper crust is focused more and has a decreased geometrical offset. The multiple then should have a lower phase velocity and a higher amplitude over a range window when it is refracting in the higher gradient part of the crust. Synthetic modeling using the WKBJ seismogram method and the amplitude and velocity analysis of the ESP data set support this hypothesis.

5

OCEAN REFRACTION AND BATHYMETRIC SCATTERING MODEL (ORBS)

FEATURES

THREE-DIMENSIONAL

BATHYMETRIC SPECTRUM AND OCEAN SOUND-SPEED STRUCTURE USED AS ENVIRONMENTAL INPUT

ALLOWS FOR ANISOTROPIC STATISTICS

SCATTERING USES COMBINED SMALL PERTURBATION - KIRCHHOFF FORMULATION

PROPAGATION BY COMBINATION OF SPLIT-STEP PARABOLIC EQUATION METHOD AND COHERENCE FUNCTION ALONG CHARACTERISTICS.

MODULAR

ONR NRL

6

ORBS FEATURES (CONTINUED)

ARBITRARILY POSITIONED ARRAY:

- DEPTH
- RANGE
- TILT
- YAW

COMPUTES TOTAL FIELD (SCATTERED, REFLECTED, DIRECT)

ARRAY PERFORMANCE PREDICTIONS:

- ANGULAR DISTRIBUTION OF RECEIVED ENERGY
- ARRAY SIGNAL GAIN
- 3-dB WIDTH

BOTTOM SCATTERING PROPAGATION MODEL

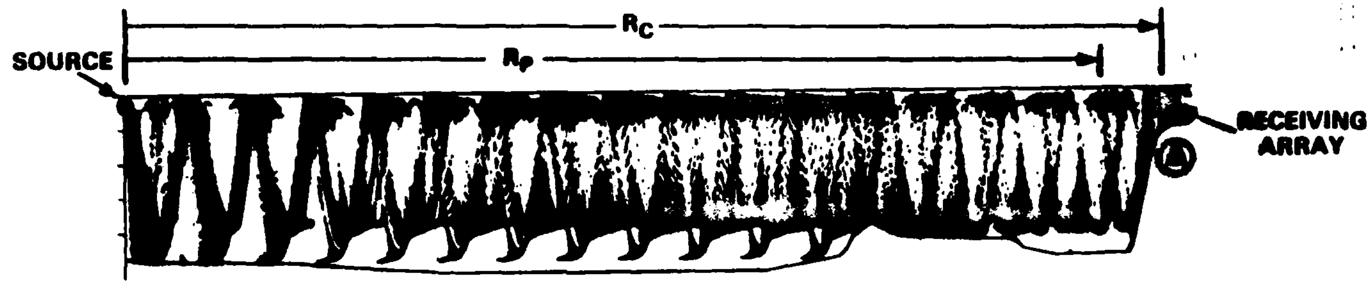

PROPAGATE THE P.E. SOLUTION TO $R = R_p$

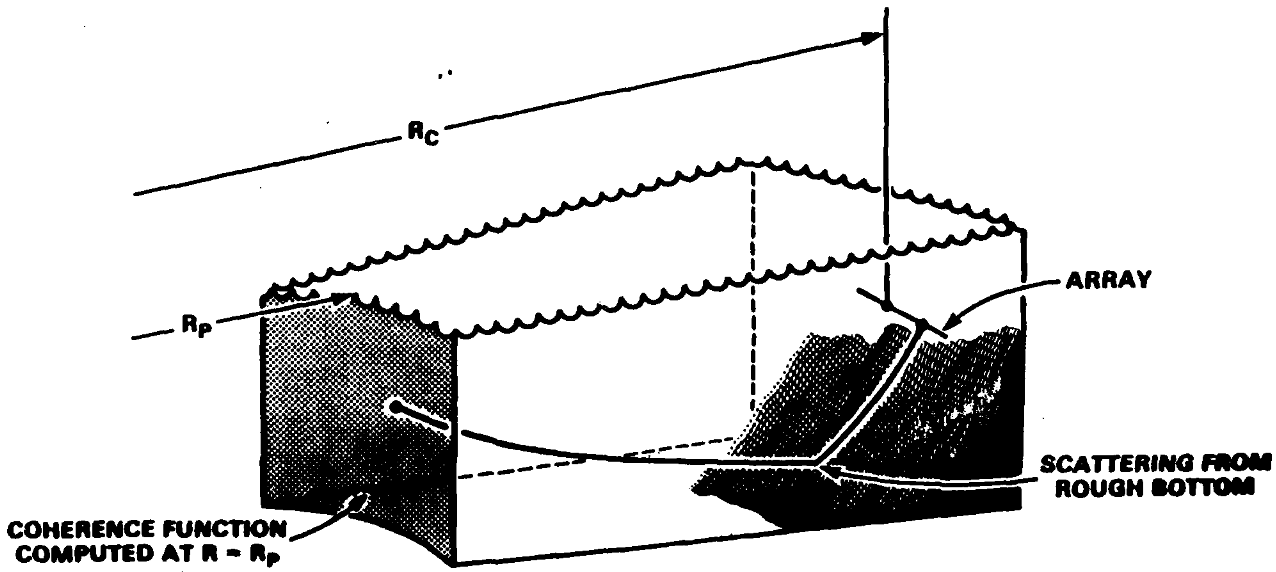

PROPAGATION ALGORITHM IN REGION Ⓐ

BOTTOM SCATTERING PROPAGATION MODEL

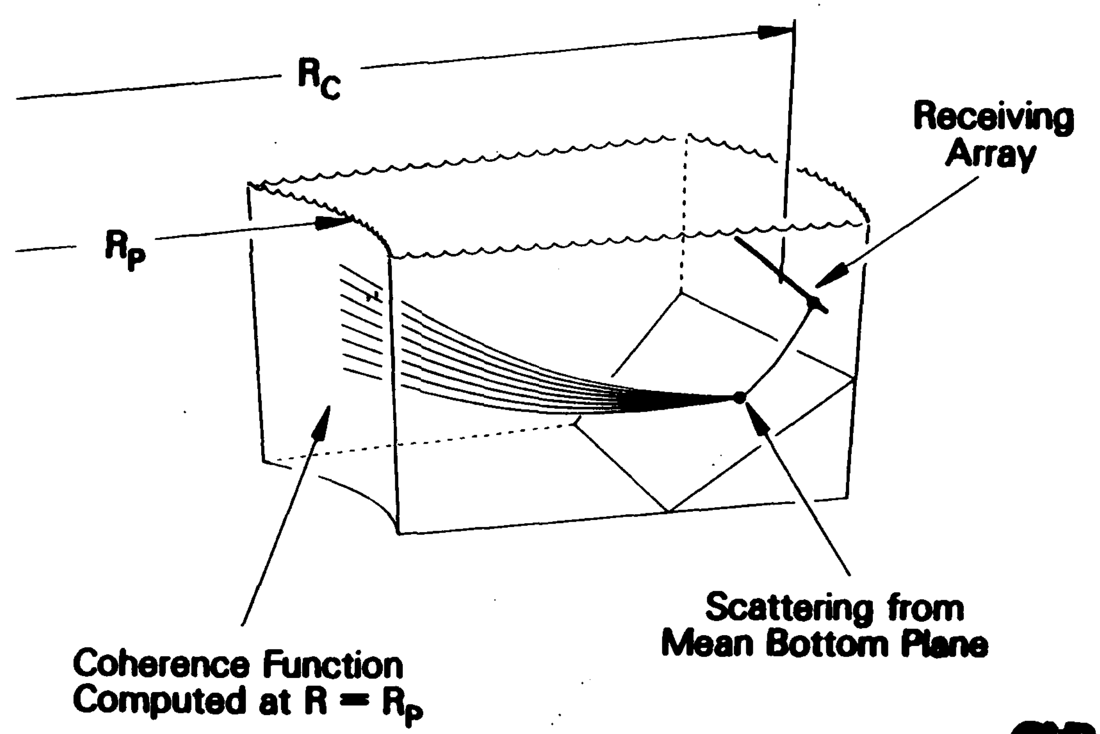

7

INCOHERENT PART OF SCATTERING CROSS-SECTION

$$\Sigma_{incoh}(\underset{\sim}{q} \rightarrow \underset{\sim}{k}) = \frac{\delta(|\underset{\sim}{k}| - |\underset{\sim}{q}|)}{16\pi^2 q_z |\underset{\sim}{q}|} [b_1^2 I_{1,1} + b_1 b_{-1} I_{1,-1} + b_{-1}^2 I_{-1,-1}]$$

where

$$I_{m,n} = \iint \exp[i(\underset{\sim}{q}_{\parallel} - \underset{\sim}{k}_{\parallel}) \cdot \underset{\sim}{\rho}_{\parallel}] \, [\exp[\lambda_m \lambda_n \sigma^2 W(\underset{\sim}{\rho}_{\parallel})] - 1] / (\lambda_m \lambda_n) \, d\underset{\sim}{\rho}_{\parallel}$$

$$\lambda_m = q_z + mk_z, \quad m = \pm 1$$

$$b_m = [(q_z + mk_z)^2 + |\underset{\sim}{q}_{\parallel} - \underset{\sim}{k}_{\parallel}|^2] \exp(-\lambda_m^2 \sigma^2 / 2)$$

GR

EXPONENTIAL SUBSTITUTION

FOR EVERY PATH AN INTEGRAL MUST BE EVALUATED TO CALCULATE THE CONTRIBUTION OF SCATTERING.

TENS OF THOUSANDS OF PATHS NEED TO BE CALCULATED RESULTING IN LONG CALCULATION TIME.

EXPONENTIAL SUBSTITUTION REDUCES EXECUTION TIME BETWEEN ONE AND TWO ORDERS OF MAGNITUDE WITHOUT SIGNIFICANT LOSS OF ACCURACY.

EXPONENTIAL SUBSTITUTION APPROXIMATION

CONSIDER

$$I(\underline{Q}) = \iint \exp(i\underline{Q}\cdot\underline{s})\,[\exp[H\,W(\underline{s})] - 1\,]\,d^2\underline{s}$$

APPROXIMATE THIS BY

$$J(\underline{Q}) = \iint \exp(i\underline{Q}\cdot\underline{s})\,\Lambda W(\underline{s}/s_o)\,d^2\underline{s}$$

CHANGING VARIABLES

$$J(\underline{Q}) = s_o^2\Lambda \iint \exp(i s_o \underline{Q}\cdot\underline{x})\,W(\underline{x})\,d^2\underline{x}$$

THUS,

$$J(\underline{Q}) = s_o^2\Lambda S(\underline{Q}s_o)\ ,$$

WHERE S IS THE SPECTRUM OF THE BATHYMETRIC CORRELATION FUNCTION

EXPONENTIAL SUBSTITUTION APPROXIMATION (CONT'D)

CHOOSE Λ SO THAT THE INTEGRANDS OF I AND J ARE EQUAL FOR $\underline{s} = \underline{0}$

$$\Lambda = \mathrm{EXP}(H) - 1$$

CHOOSE s_o SO THAT $J(\underline{Q} = \underline{0}) = I(\underline{Q} = \underline{0})$

$$s_o = \left\{ \frac{\iint \{\exp[HW(\underline{s})] - 1\}\, d^2\underline{s}}{S(\underline{0})[\exp(H) - 1]} \right\}^{1/2}$$

THIS IS A SMOOTH FUNCTION OF H WHICH CAN BE TABULATED. ITS EVALUATION IS THUS SIMPLY A MATTER OF TABLE LOOKUPS AND INTERPOLATION.

GR

DIFFERENTIAL CROSS SECTION

KIRCHHOFF

λ = 50.0 m σ = 20 m

φ_{in} = 20 deg L = 400 m

W = (R/L)K_1(R/L) HARD SURFACE

Σ (20.0, 0.0) = 28.48

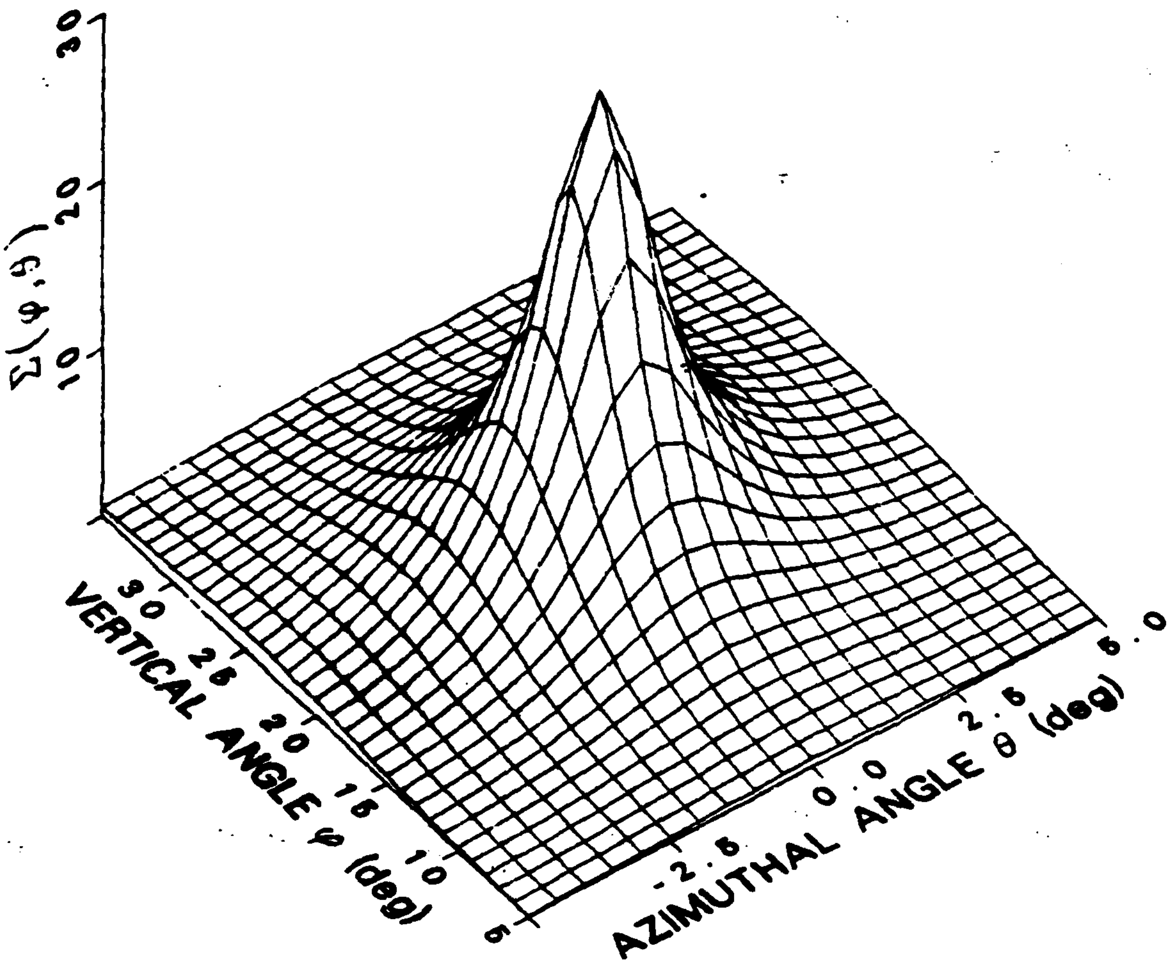

DIFFERENTIAL CROSS SECTION

KIRCHHOFF WITH EXPONENTIAL SUBSTITUTION

λ = 50.0 m σ = 20 m

φ_{in} = 20 deg   L = 400 m

W = (R/L)K_1(R/L)   HARD SURFACE

Σ (20.0, 0.0) = 28.95

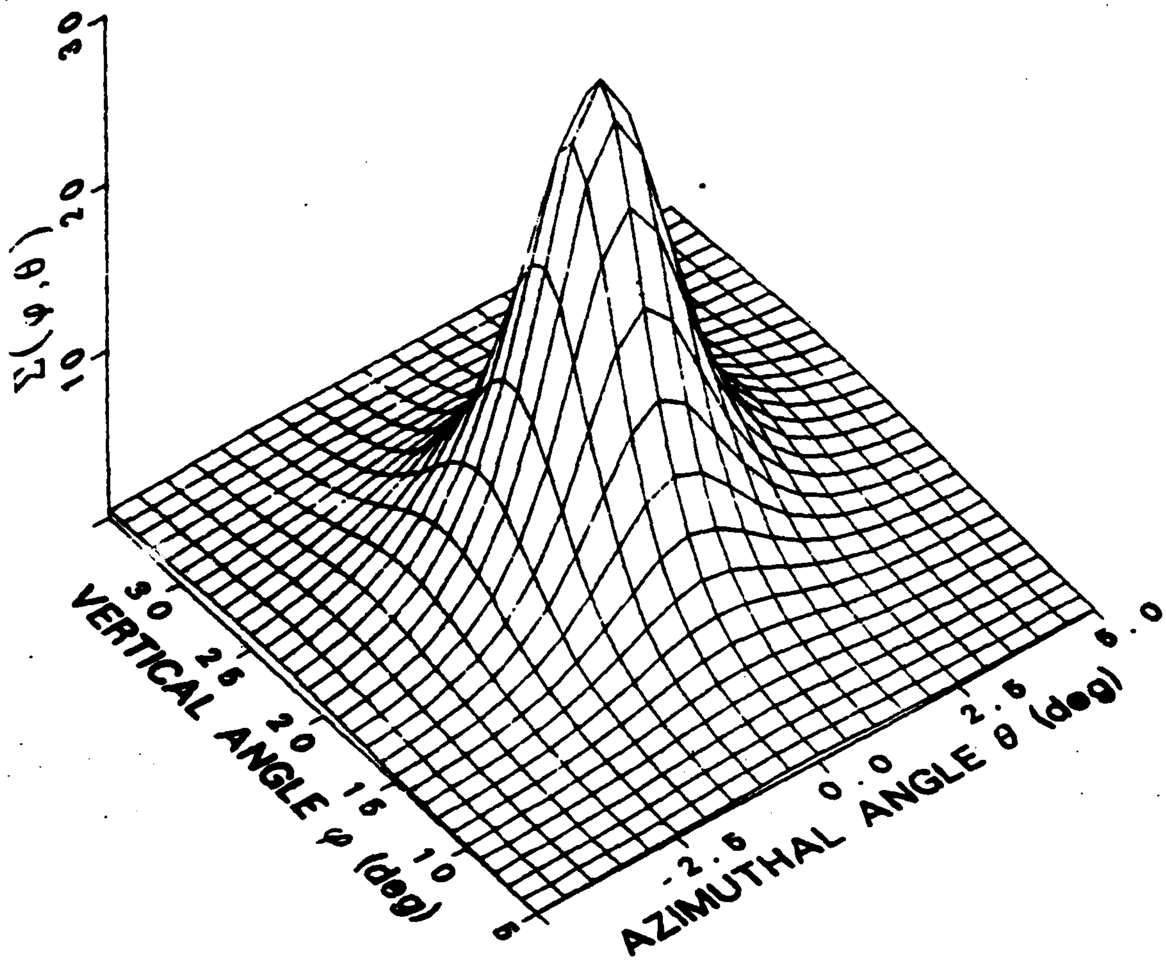

BOTTOM SLOPE MOUNTED ARRAY ENVIRONMENT

TYPICAL NEW ENGLAND SEAMOUNT -- ATLANTIS II

SOUTH FACE, 15 DEGREE SLOPE, SIGMA = 20 METERS*

BASIN FLOOR FLAT AT 4,800 METERS OF DEPTH*

VELOCITY STRUCTURE: RANGE INDEPENDENT*

*(ISOTROPIC, FLAT FLOOR, CONSTANT PROFILE
FOR SIMPLIFIED EXAMPLE ONLY.)


200m
1
2
3
4
5

VIEW FROM THE SOUTH

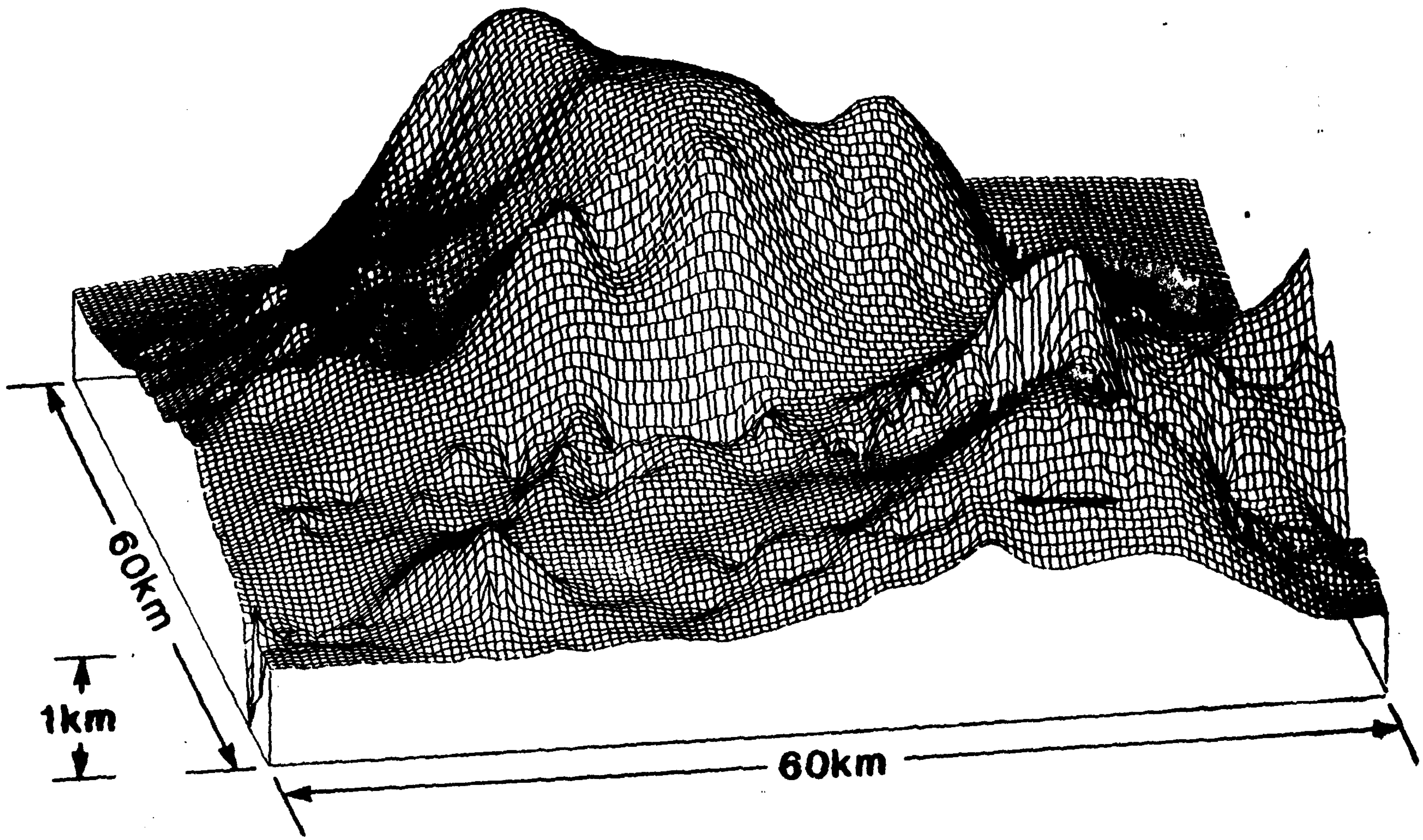

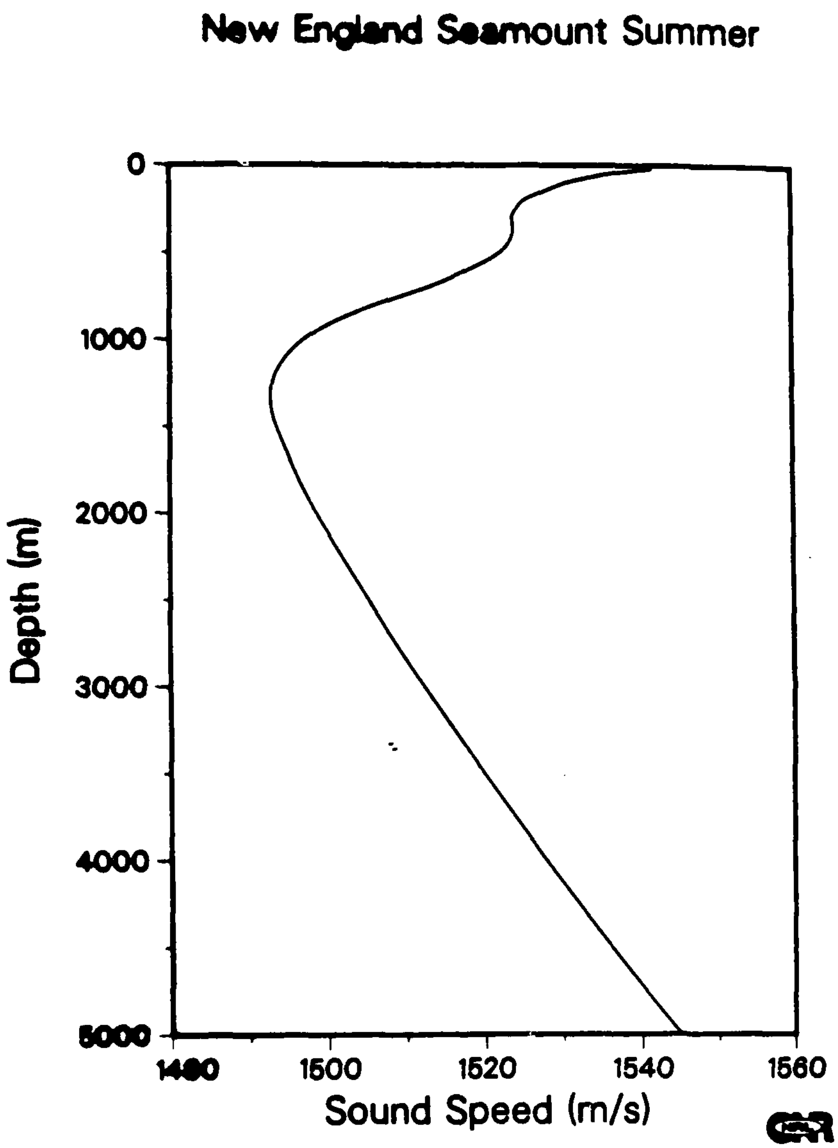
New England Seamount Summer
Depth (m)
0
1000
2000
3000
4000
5000
1480
1500
1520
1540
1560
Sound Speed (m/s)

AD-A154 652 VLF (VERY LOW FREQUENCY) WORKSHOP: HELD AT SAN DIEGO CALIFORNIA ON 24-25..(U) SCRIPPS INSTITUTION OF OCEANOGRAPHY LA JOLLA CA MARINE PHYSIC.. W S HODGKISS 3/3

UNCLASSIFIED 1985 MPL-U-11/85 N00014-80-C-0220 F/G 5/1 NL

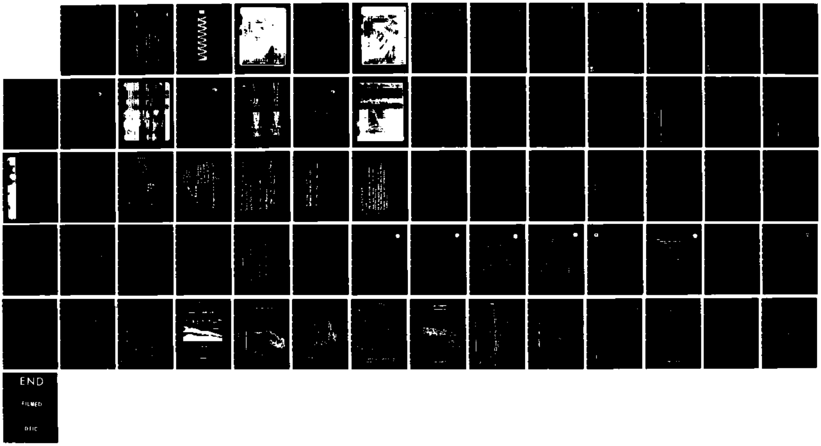

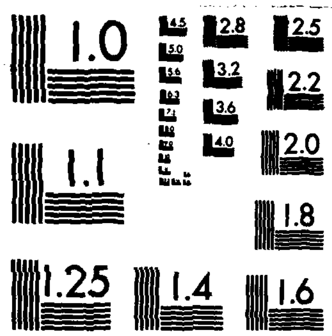

MICROCOPY RESOLUTION TEST CHART
NATIONAL BUREAU OF STANDARDS-1963-A

BOTTOM SLOPE MOUNTED ARRAY SPECIFICATIONS

FREQUENCY 30 HZ

SOURCE DEPTH 3 WAVELENGTHS (150 M)

HORIZONTAL ARRAY SIZE 100 WAVELENGTHS (5 KM)

VERTICAL ARRAY SIZE 3 WAVELENGTHS (150 M)

ARRAY CENTERS 5 WAVELENGTHS ABOVE SLOPE

OMNI-DIRECTIONAL HYDROPHONES

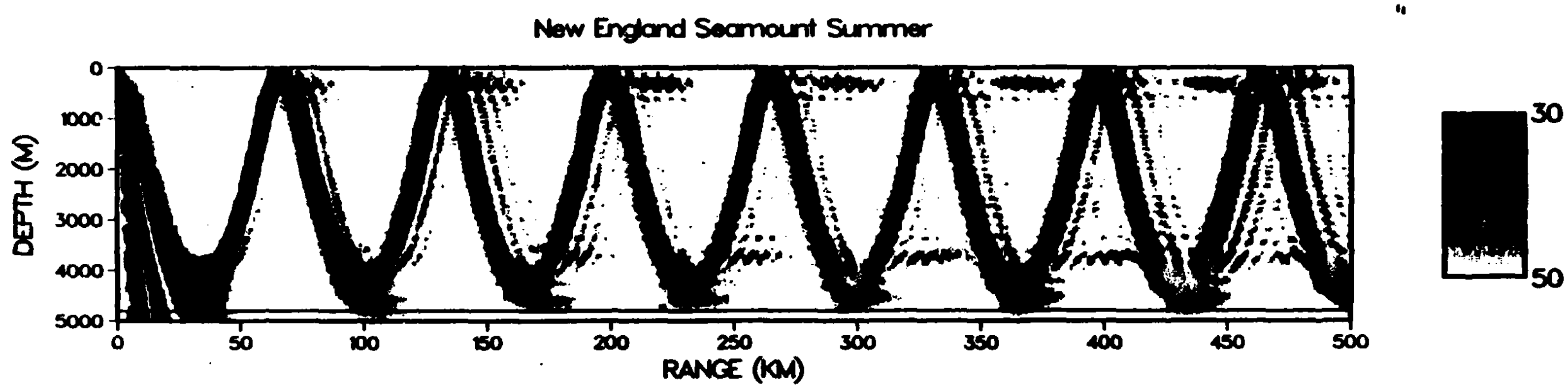
New England Seamount Summer
DEPTH (M)
0
1000
2000
3000
4000
5000
0
50
100
150
200
250
300
350
400
450
500
RANGE (KM)
30
50


4000
4500

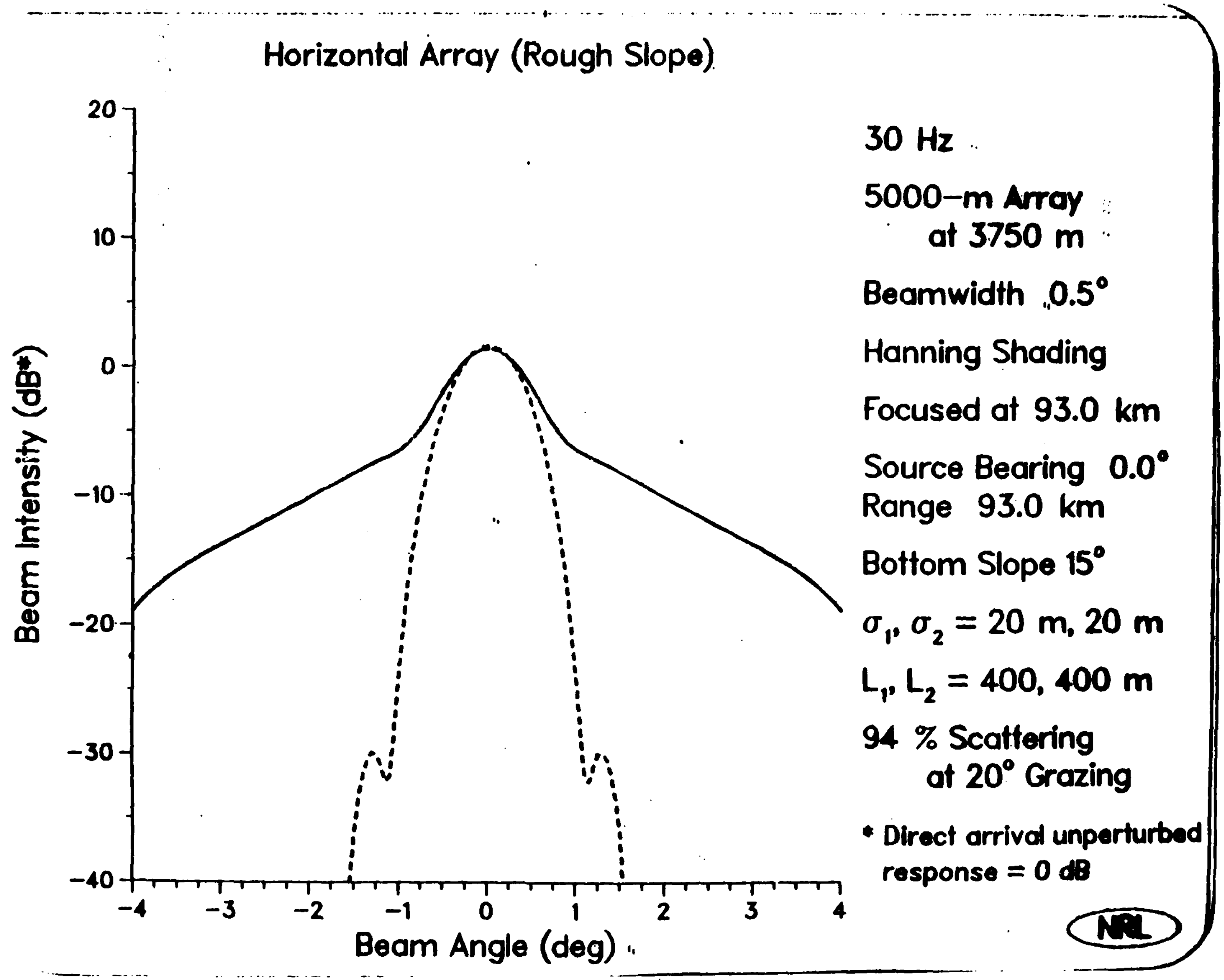

Horizontal Array (Rough Slope)
Beam Intensity (dB*)
20
10
0
−10
−20
−30
−40
−4
−3
−2
−1
0
1
2
3
4
Beam Angle (deg)
30 Hz
5000−m Array
at 3750 m
Beamwidth 0.5°
Hanning Shading
Focused at 93.0 km
Source Bearing 0.0°
Range 93.0 km
Bottom Slope 15°
σ1, σ2 = 20 m, 20 m
L1, L2 = 400, 400 m
94 % Scattering
at 20° Grazing
* Direct arrival unperturbed
response = 0 dB
NRL

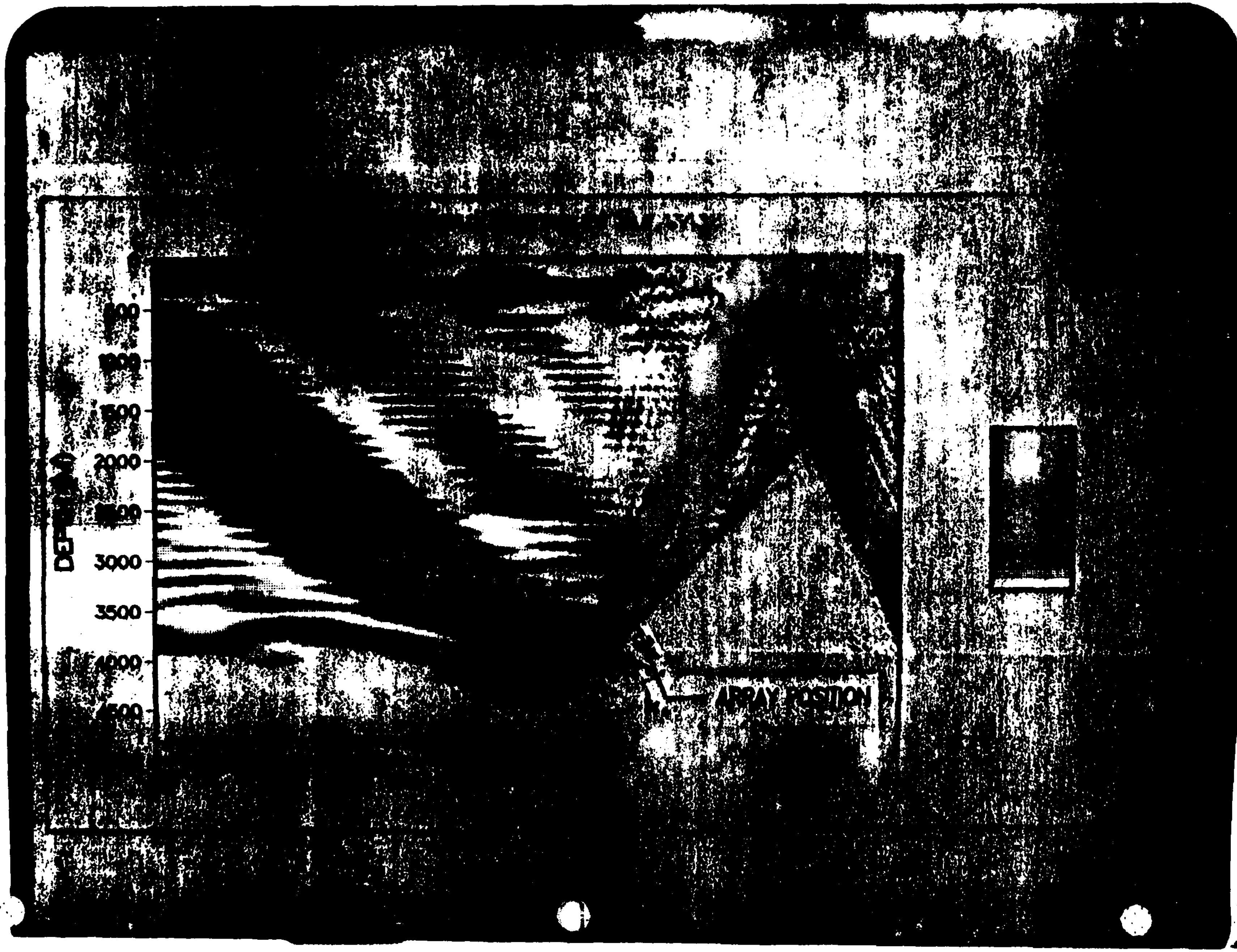

500
1000
1500
2000
2500
3000
3500
4000
4500
ARRAY POSITION

Horizontal Array (Rough Slope)
Long Range

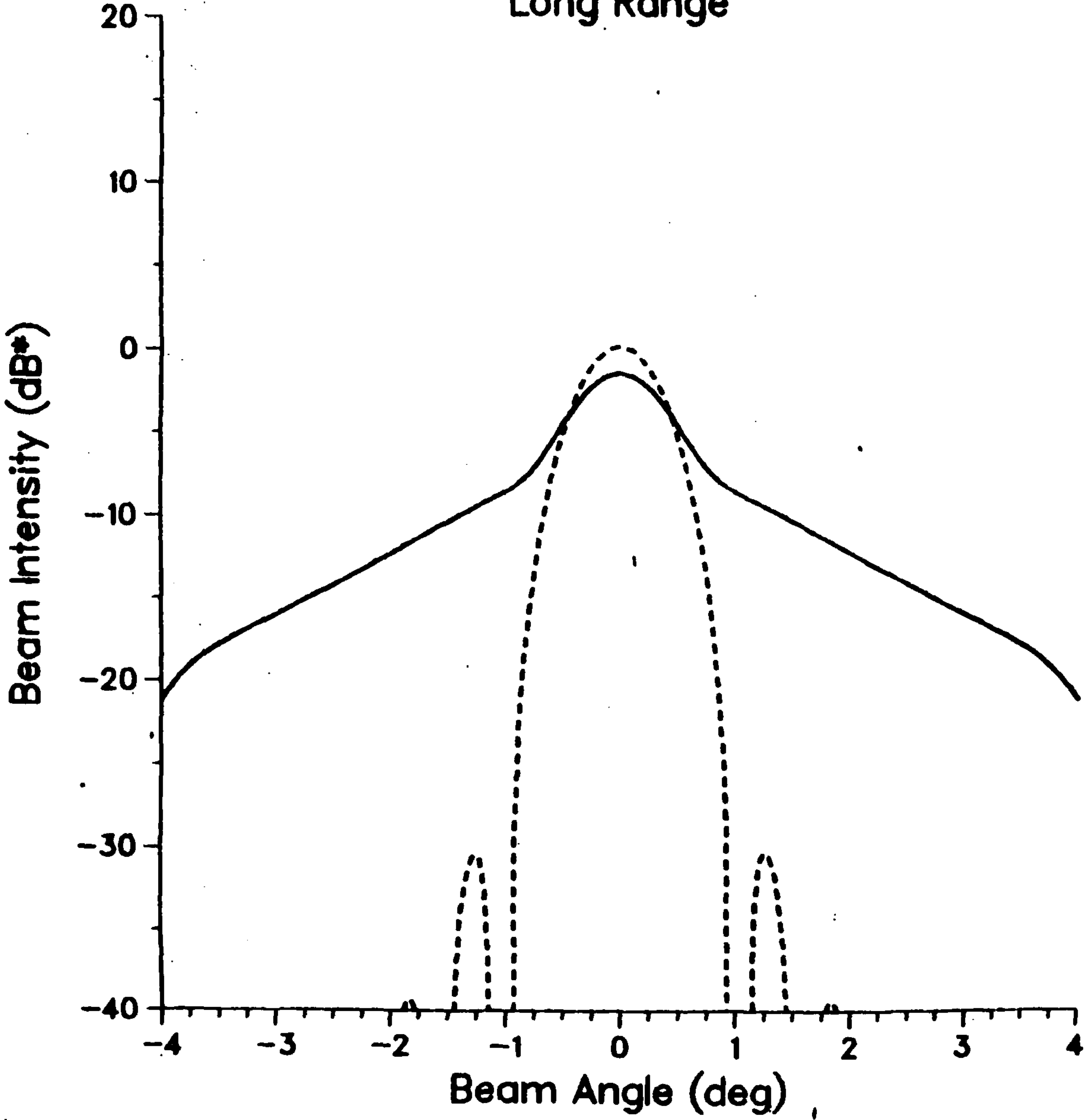

30 Hz

5000–m Array
at 3750 m

Beamwidth 0.5°

Hanning Shading

Focused at 488.5 km

Source Bearing 0.0°
Range 488.5 km

Bottom Slope 15°

σ_1, σ_2 = 20 m, 20 m

L_1, L_2 = 400, 400 m

94 % Scattering
at 20° Grazing

* Direct arrival unperturbed response = 0 dB

NRL

Vertical Array (Rough Slope)

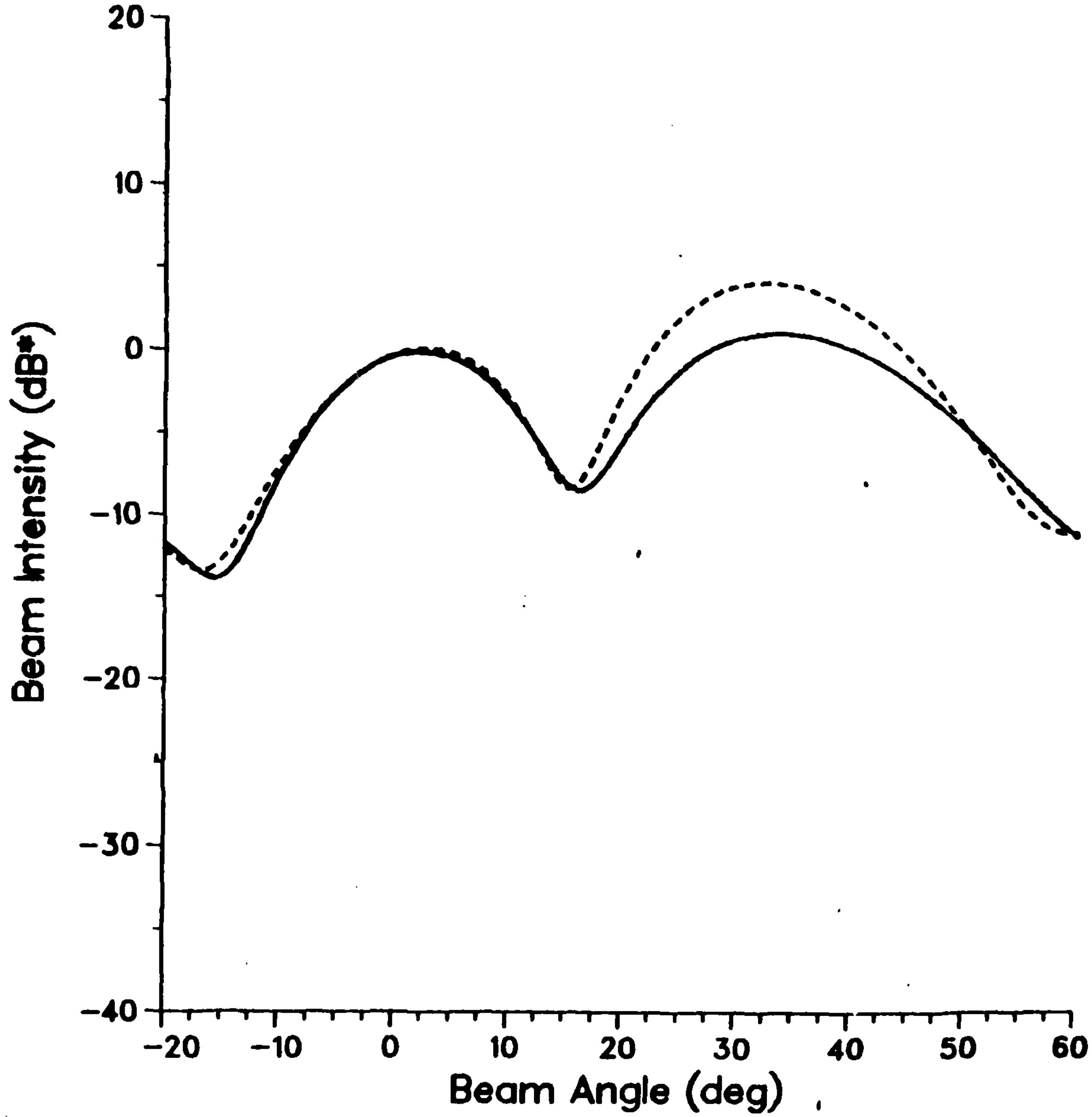

30 Hz

150–m Array
at 3700 m

Beamwidth .17.2°

Uniform Shading

Source Bearing 0.0°
Range 93.0 km

Bottom Slope 15°

σ_1, σ_2 = 20 m, 20 m

L_1, L_2 = 400, 400 m

94 % Scattering
at 20° Grazing

* Direct arrival unperturbed response = 0 dB

NRL

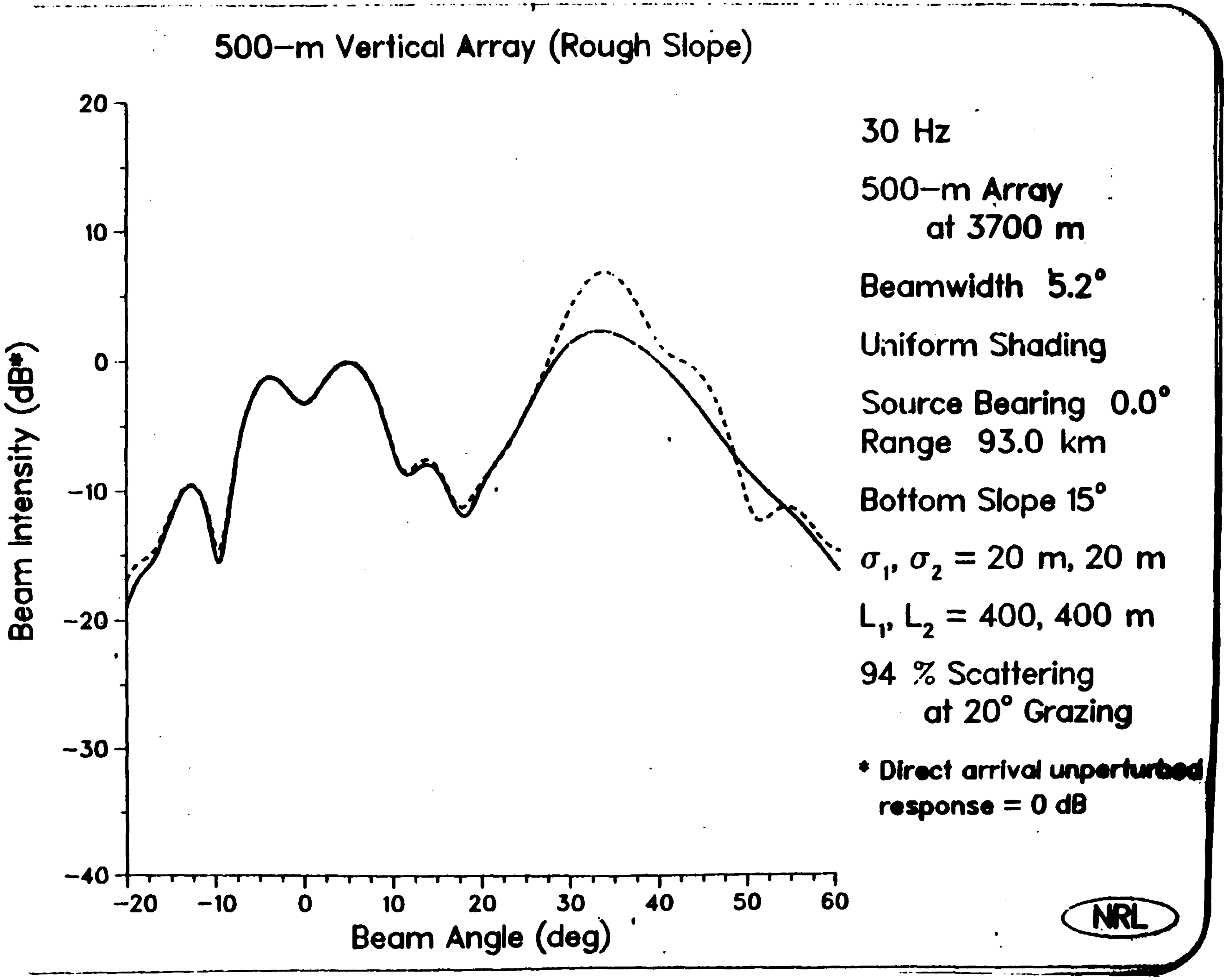
500–m Vertical Array (Rough Slope)
Beam Intensity (dB*)
20
10
0
−10
−20
−30
−40
−20
−10
0
10
20
30
40
50
60
Beam Angle (deg)
30 Hz
500–m Array
at 3700 m
Beamwidth 5.2°
Uniform Shading
Source Bearing 0.0°
Range 93.0 km
Bottom Slope 15°
σ_1, σ_2 = 20 m, 20 m
L_1, L_2 = 400, 400 m
94 % Scattering
at 20° Grazing
* Direct arrival unperturbed
response = 0 dB
NRL

Array Signal Gain of 24-Wavelength Array vs. Roughness and Correlation Length of Isotropic **Bottom**

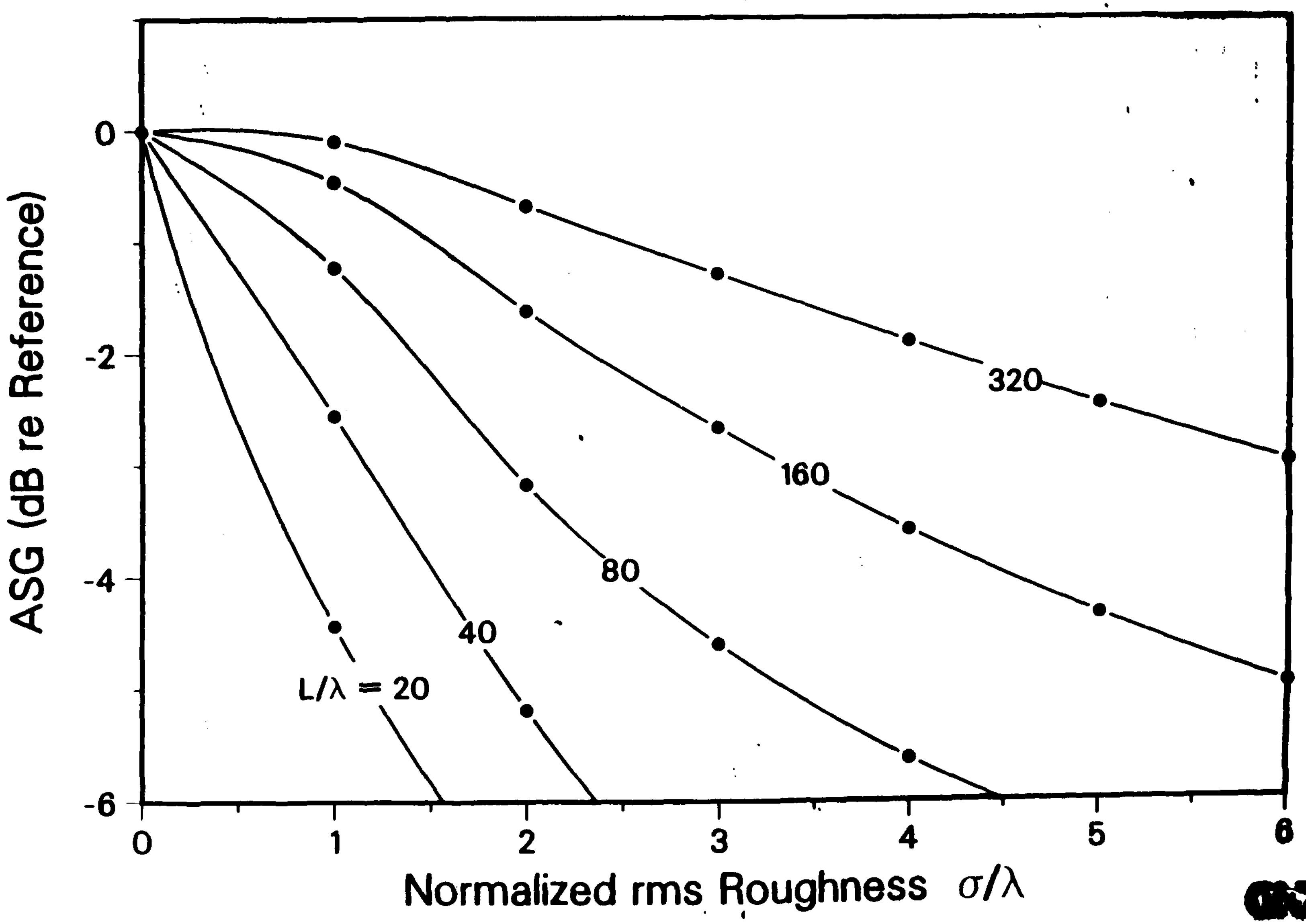

Beam Width of 24-Wavelength Array vs. Roughness and Correlation Length of Isotropic Bottom

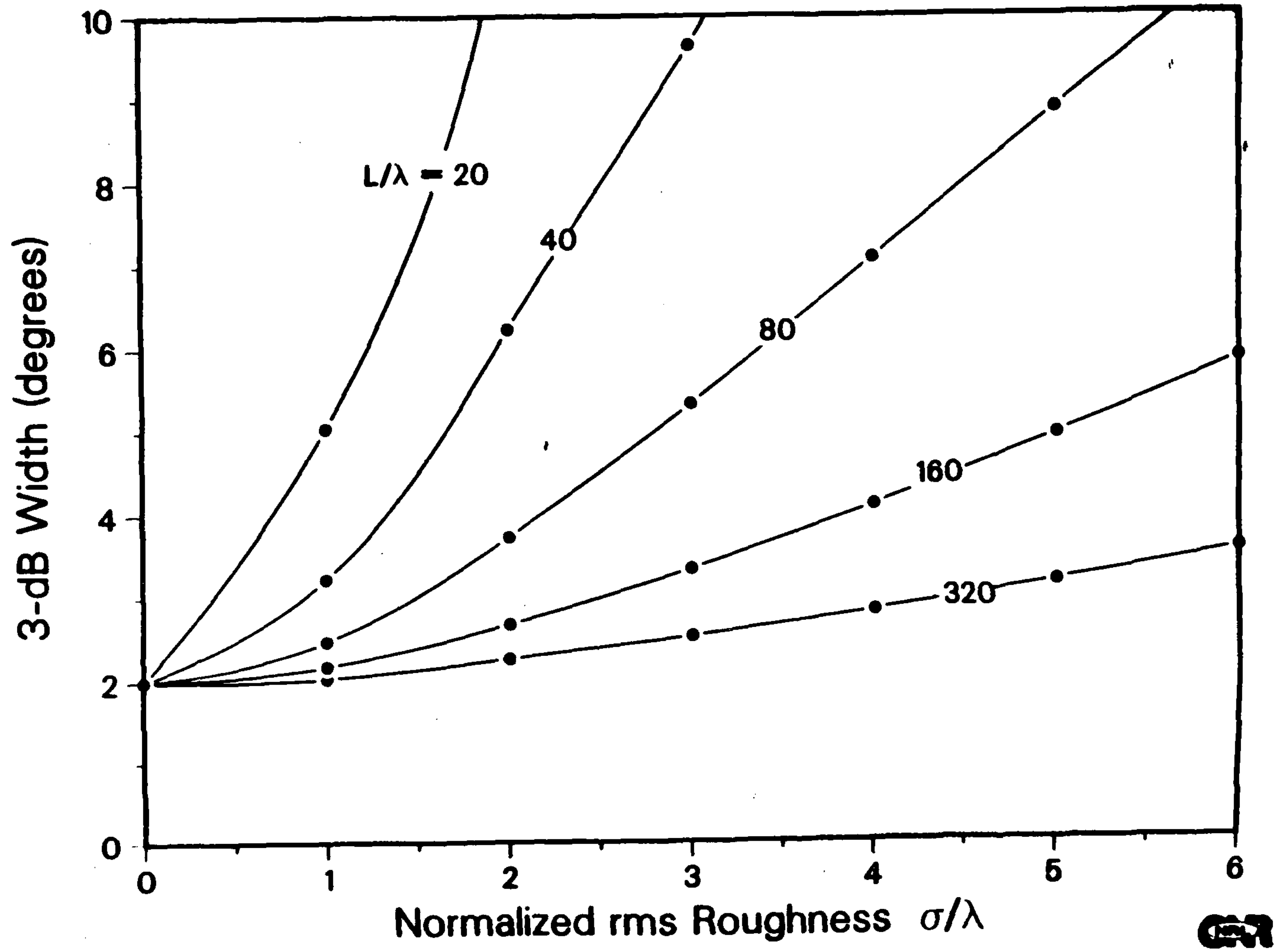

FUTURE DIRECTIONS

MULTIPLE BOUNDARY INTERACTIONS

TIME CONSIDERATIONS:

- MOVING SOURCES
- MOVING RECEIVERS
- PULSED SOURCES

SUBBOTTOM INCORPORATION

HIGHER-ORDER MOMENTS:

- LIKELIHOOD OF TARGET DETECTION
- WHAT MUST BE DONE TO ACHIEVE A GIVEN PROBABILITY OF SUCCESS

:LING SUPPORT FOR CAPE FEAR VLF EXERCISE

W. TUNNELL AND H. F. SCHREINER , JR.
\VAL OCEAN RESEARCH AND DEVELOPMENT ACTIVITY , CODE 240
3TL , MS 39529

1e Cape Fear Very Low Frequency (VLF) Exercise is scheduled off the st at Cape Fear , NC during June 4 to July 1 , 1985 as part of the DA 6.1 Very Low Frequency Acoustic Propagation Special Focus Program. exercise is a cooperative effort between the United States Geological vey at Woods Hole and NORDA. The USNS Lynch one other ship will port the exercise. Data acquisition systems will consist of 12 ocean tom seismometers and a vertical hydrophone array (15 element , 20 m cing) built with the VEKA-II technology. Underwater explosives (~100 /shot) and a Mark 6b sound source (187 dB at 10 Hz) will be used as rces.

he modeling results presented here are the array response predictions culated with the maximum entropy method using the acoustic field dicted by the parabolic equation model solved with the implicit finite ference techniques (IFD). The sound speed profile along a previous S track (USGS MCL 32) and historical water column data are used. ilton's results (E.L. Hamilton, "Geoacoustic modeling of the sea floor" . Acoust. Soc. Am. 68(5), pp. 1313 -1340 , Nov. 1880) for density , pressional attenuation , shear sound speed , and shear attenuation ues are used as input. These inputs are used with Kutschale's version the fast field program to derive an effective compressional attenuation t may be used as input to the IFD (the IFD does not describe shear es in the subbottom). This procedure assumes that the range dependence the enviroment has a greater effect on the propagation than shear waves that shear effects can be approximated by an increase in the value of pressional attenuation. IFD intensity contours are plotted for ranges 100 to 175 km (left to right). The dark line indicates the subottom ch varies from 1800 m deep to 370 m deep left to right. A high amount mode drop out is shown over the 100 to 140 km ranges. The IFD results used in a maxium entropy beamformer and the 3 dB contour intervals obtained for arrival angles (-90 to 90) at ranges from (A) 100 to km , (B) 80 to 155 km , (C) 60 to 135 km , and (D) 40 to 115 km . se four results cover the same portion of USGS MCL 32 as the source moved upslope The results show that the energy in the mode drop out ion is large incoherent and that only two modes survive the mode p out region.

Typical Flow Noise Levels From A 10 CM Diameter Pressure Gradient Hydrophone

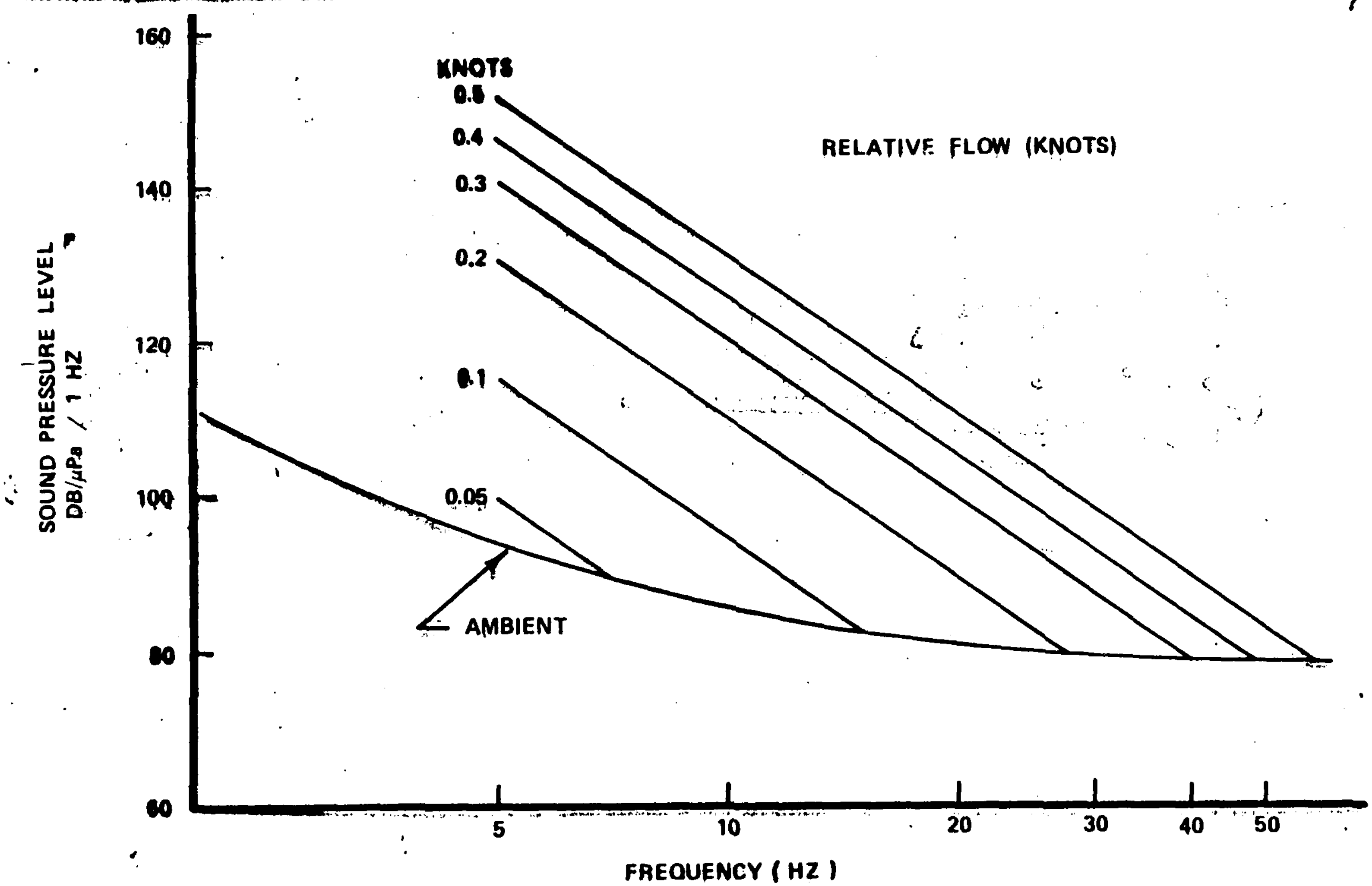

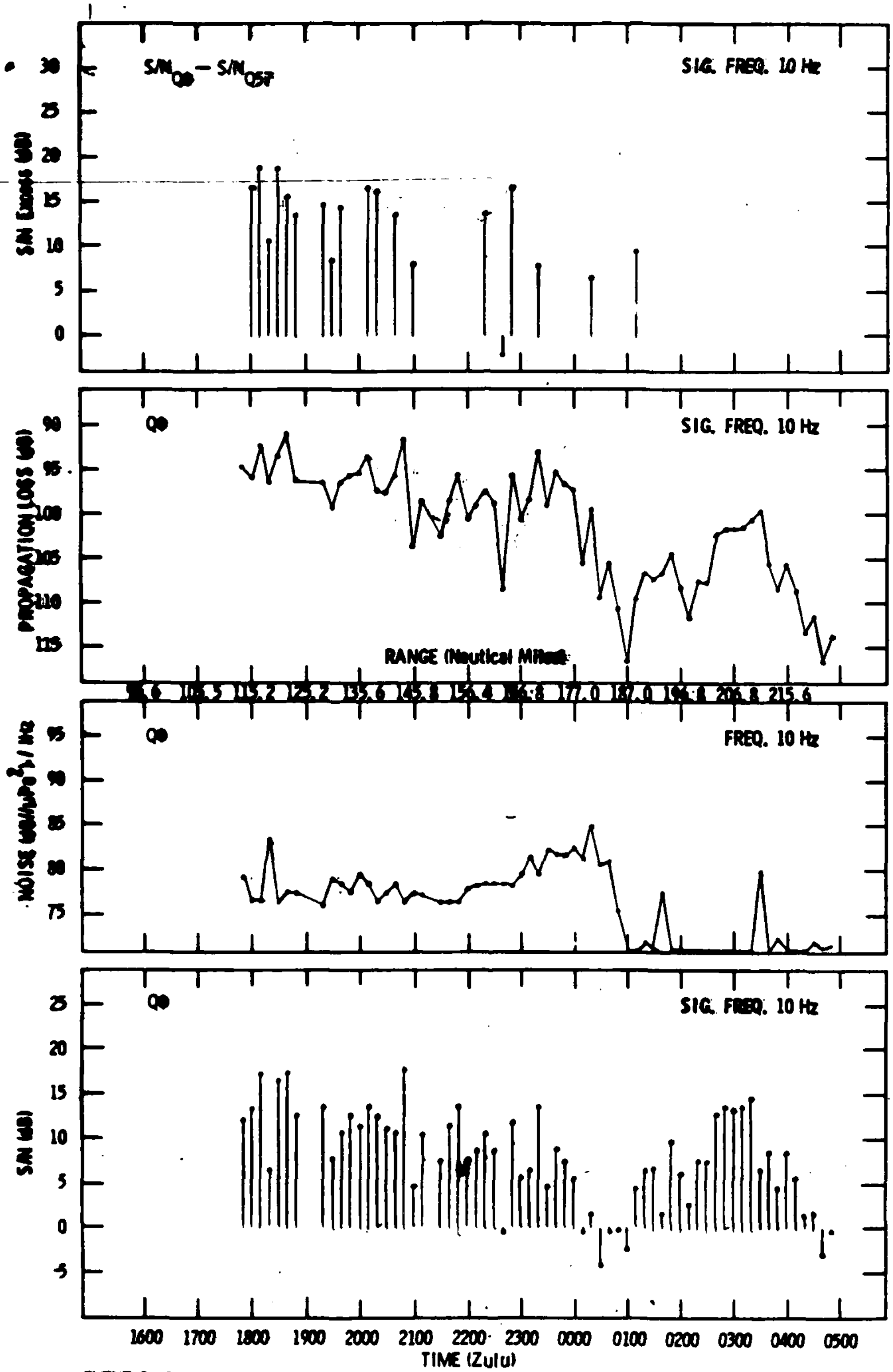

EVENT 2 PLANT A B C

Q0 Chan 26

Q57 Chan 25

a.

Recommended Mechanical/ Flow Noise Limits

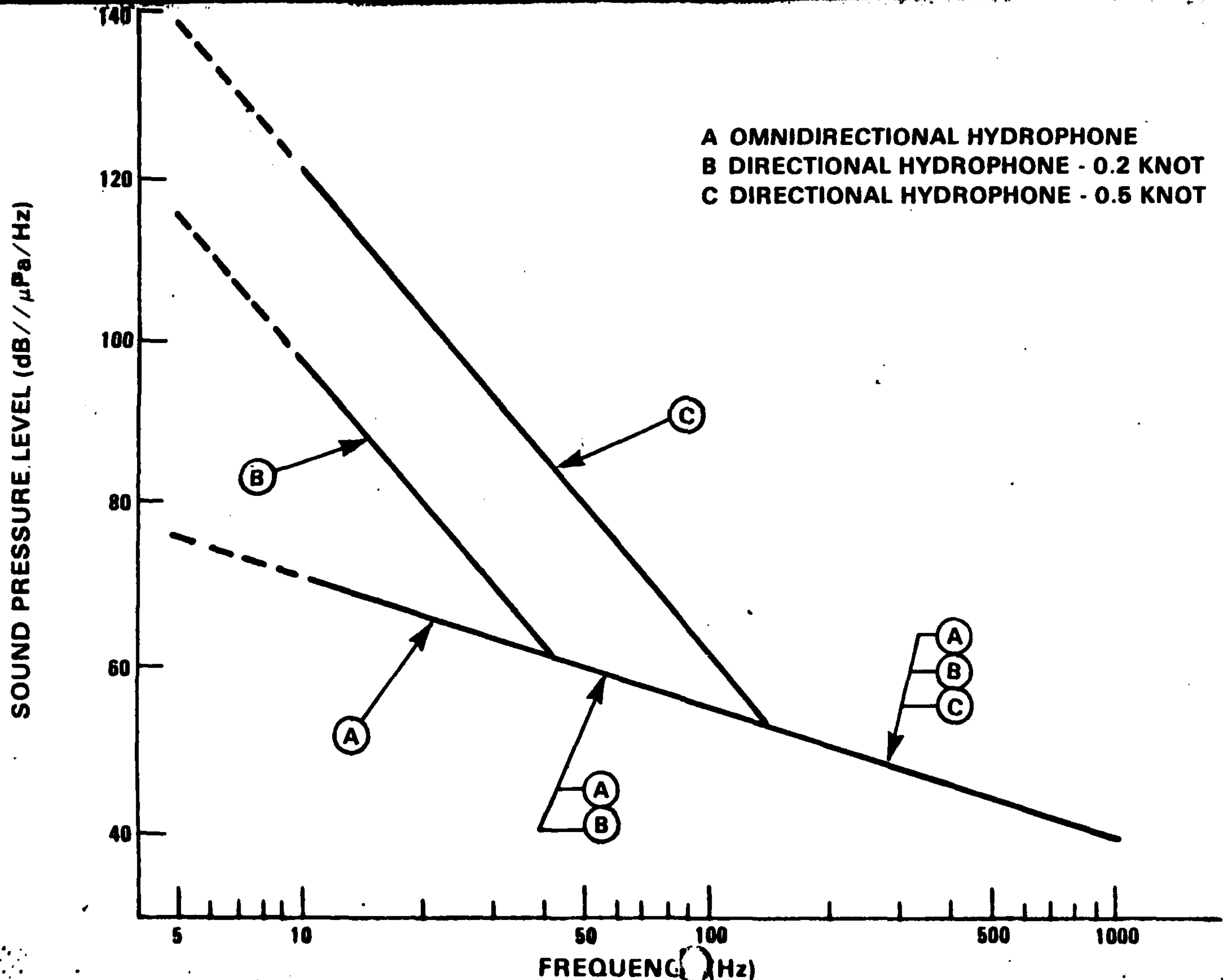

VLF Sonobuoy Development

OBJECTIVE: **IMPROVE PASSIVE SONOBUOY LOW FREQUENCY PERFORMANCE**

* PROVIDE NEAR TERM LOW FREQUENCY IMPROVEMENTS FOR THE AN/SSQ-53B

* ESTABLISH A LONGER TERM DEVELOPMENT PROGRAM TO IMPROVE THE VLF PERFORMANCE OF PASSIVE BUOYS

* DIRECTLY BENEFITS VLF STRAP
  APPLIES TO SSQ-77, RDSS, HLA

Near Term SSQ-53B Improvements

GOAL: 3dB S/N IMPROVEMENT IN [illegible] LF DATA

APPROACH: [illegible]

PAYOFF: Improved LF [illegible]

GOAL: 10 dB IMPROVEMENT IN DIRECTIONAL LF DATA

APPROACH: Velocity [illegible] (Sparton, Hermes)
- Larger Drogue
- Flow Shields, Fairings

[illegible] Reliability
- Larger [illegible]
- [illegible]

PAYOFF: Improved LF [illegible]

O

Long Term VLF Development

GOAL: DIRECTIONAL SENSOR MECHANICAL NOISE EQUAL TO OMNI SENSOR MECHANICAL NOISE

NEED: ON GOING R&D IN FLOW & MECHANICAL NOISE

* NEAR FIELD FLOW INVESTIGATION
  Transition NADC IR flow task
* DIRECTIONAL SENSOR DEVELOPMENT
* GRADIENT ARRAYS, NOISE REJECTION TECHNIQUES
* FLOW SHIELDING TECHNIQUES

ABSTRACT

Summary of VLF Sonobuoy Program at the

Naval Air Development Center

James F. McEachern
Code 3043
Naval Air Development Center
Warminster, PA 18974-5000

NADC's efforts in Very Low Frequency (VLF) sonar evolved out of on going improvement programs in passive sonobuoys. Dual isolation sonobuoy suspensions and research in cable strumming attenuation advanced the state of the art in sonobuoy self noise reduction in the areas of surface wave -induced noise and flow induced vibration noise. A program of low velocity flow noise studies on gradient hydrophones led to the development of an effecive, packageable flow shield for gradient hydrophones.

The Infrasonic Investigation program for target detection and classification drew on NADC's low frequency sonobuoy technology to develop a sonobuoy sensor capable of providing useful submarine detection and classification in the VLF band. Under this program omnidirectional and directional VLF sonobuoys were used to gather target data, ambient noise data and to evaluate VLF propagation models. The impact of VLF technology on all airborne processors and on sonobuoy production and testing was assessed. A recommended self noise limit for VLF sonobuoys was generated.

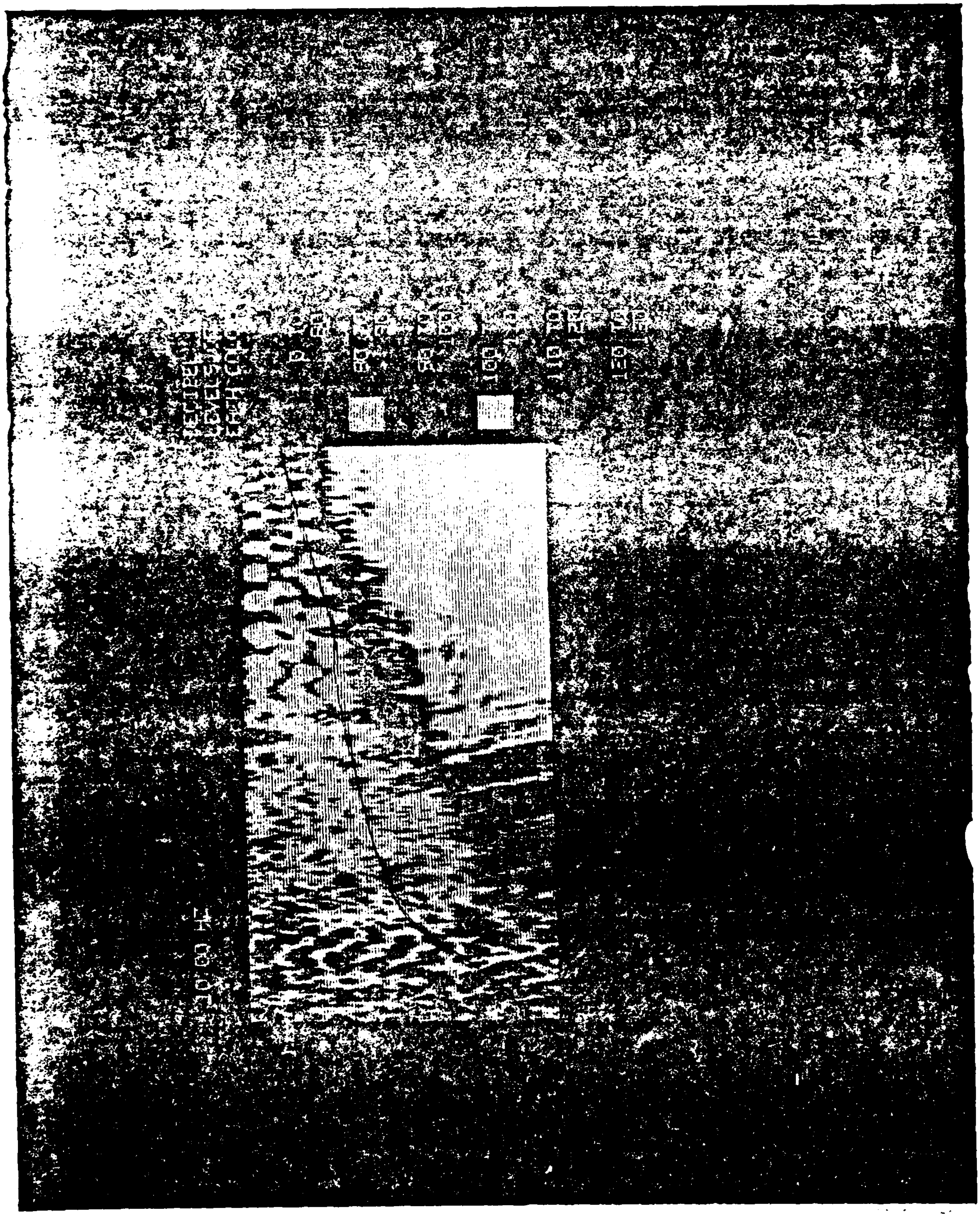

MODELING PROCEDURE

* USGS MCL 32 : COMPRESS. SOUND SPEED

* HAMILTON : DENSITY
  : COMPRESSIONAL ATTEN.
  : SHEAR SOUND SPEED
  : SHEAR ATTENUATION

* FFP: EFFECTIVE COMPRESSIONAL ATTEN.

* USE EFFECTIVE COMPRESSIONAL ATTEN., DENSITY, AND COMPRESSIONAL SOUND SPEED AS INPUT TO PARABOLIC EQ.

MEM ARRAY RESPONSE FOR IFD FIELD; 3 dB INTERVALS

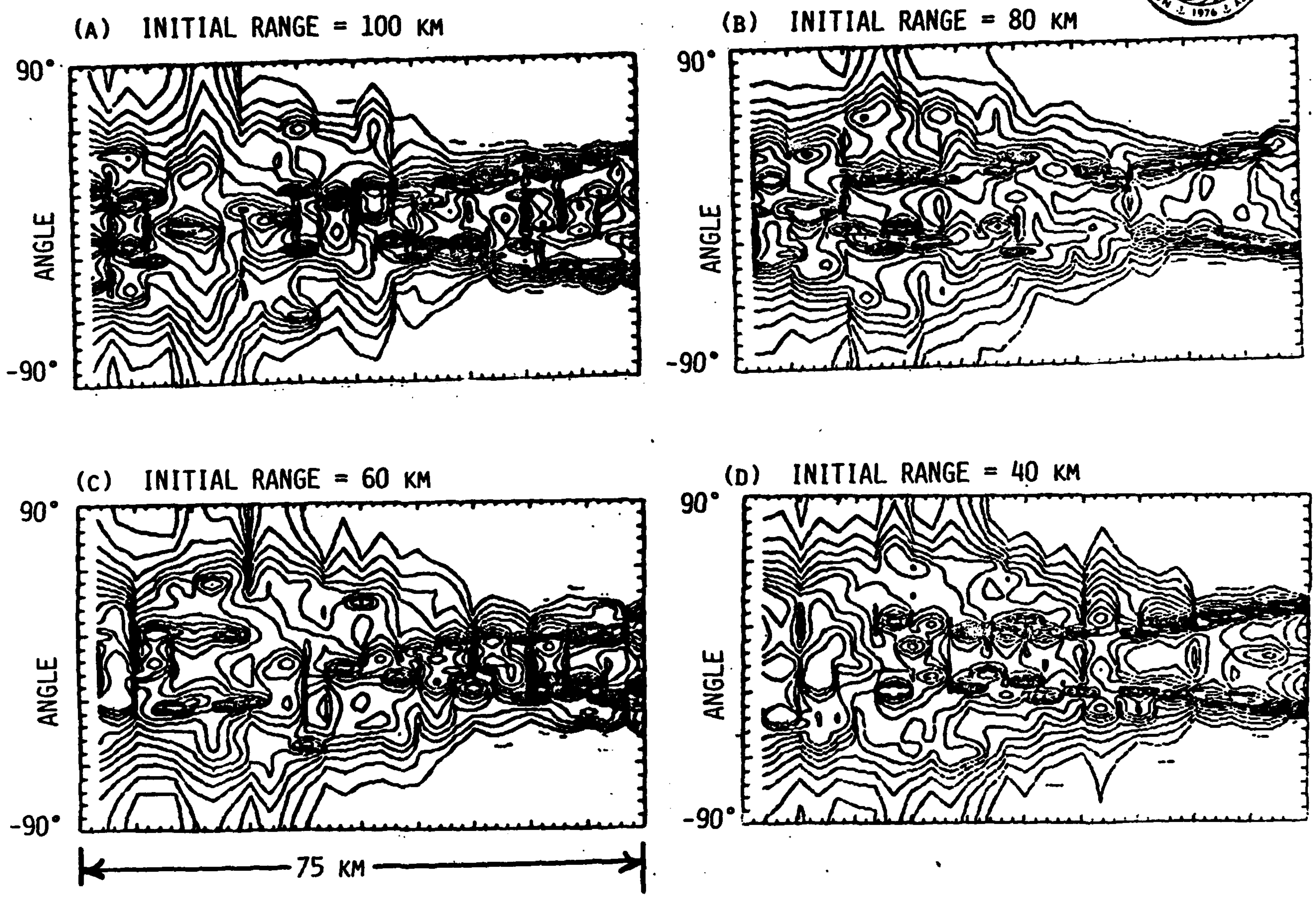

MAXIUM ENTROPY PARAMETERS

* INPUT : 15 ELEMENT ARRAY
  : 20 M
  : 40 M ARRAY DEPTH

* MAXIUM ENTROPY PARAMETERS :
  - 10 TH ORDER
  - 100 AVERAGES (25 M)

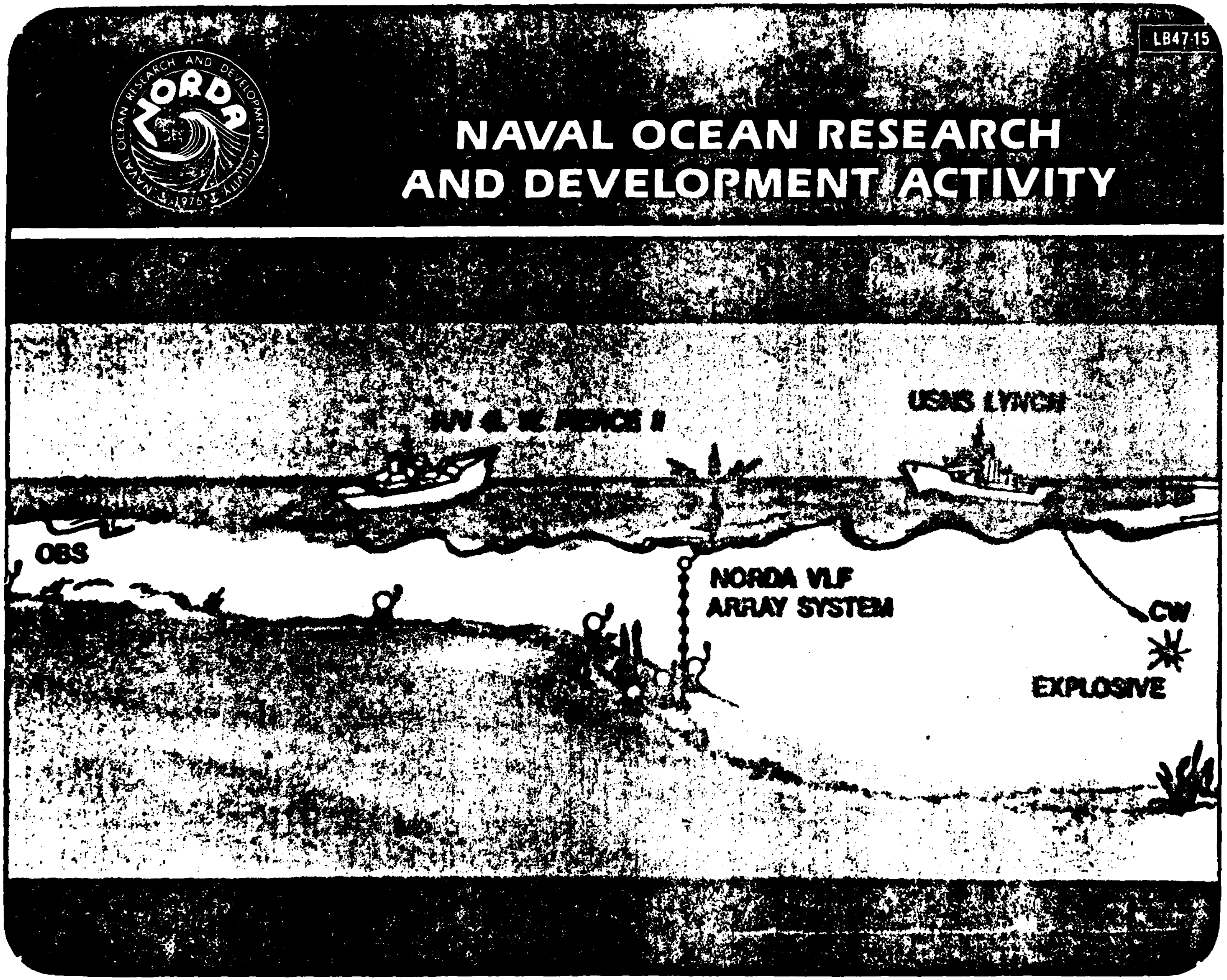
LB47-15
NAVAL OCEAN RESEARCH
AND DEVELOPMENT ACTIVITY
USNS LYNCH
OBS
NORDA VLF
ARRAY SYSTEM
CW
EXPLOSIVE

FIRST FIELD EXERCISE
JUNE 4 - JULY 1, 1985 CAPE FEAR

PARTICIPANTS: USGS AT WOODS HOLE
NORDA (SCRIPPS , NRL)

ASSETS: USNS LYNCH (NORDA)
CONTRACT SHIP (NORDA)
12 OBS UNITS (USGS , NORDA)
VEKA (NORDA)
EXPLOSIVES (NORDA)
CW (NRL , NORDA FUNDS)

6

VERY LOW FREQUENCY ACOUSTIC PROPAGATION (VLF)

A PROGRAM TO DETERMINE THE ACOUSTIC PROPAGATION AND AMBIENT NOISE CHARACTERISTICS IN THE INFRASONIC OR VLF (20 Hz AND LESS) BAND TO ASCERTAIN THE FEASIBILITY AND PERFORMANCE ESTIMATES OF A GENERIC CLASS OF PASSIVE ACOUSTIC SURVEILLANCE SYSTEMS.

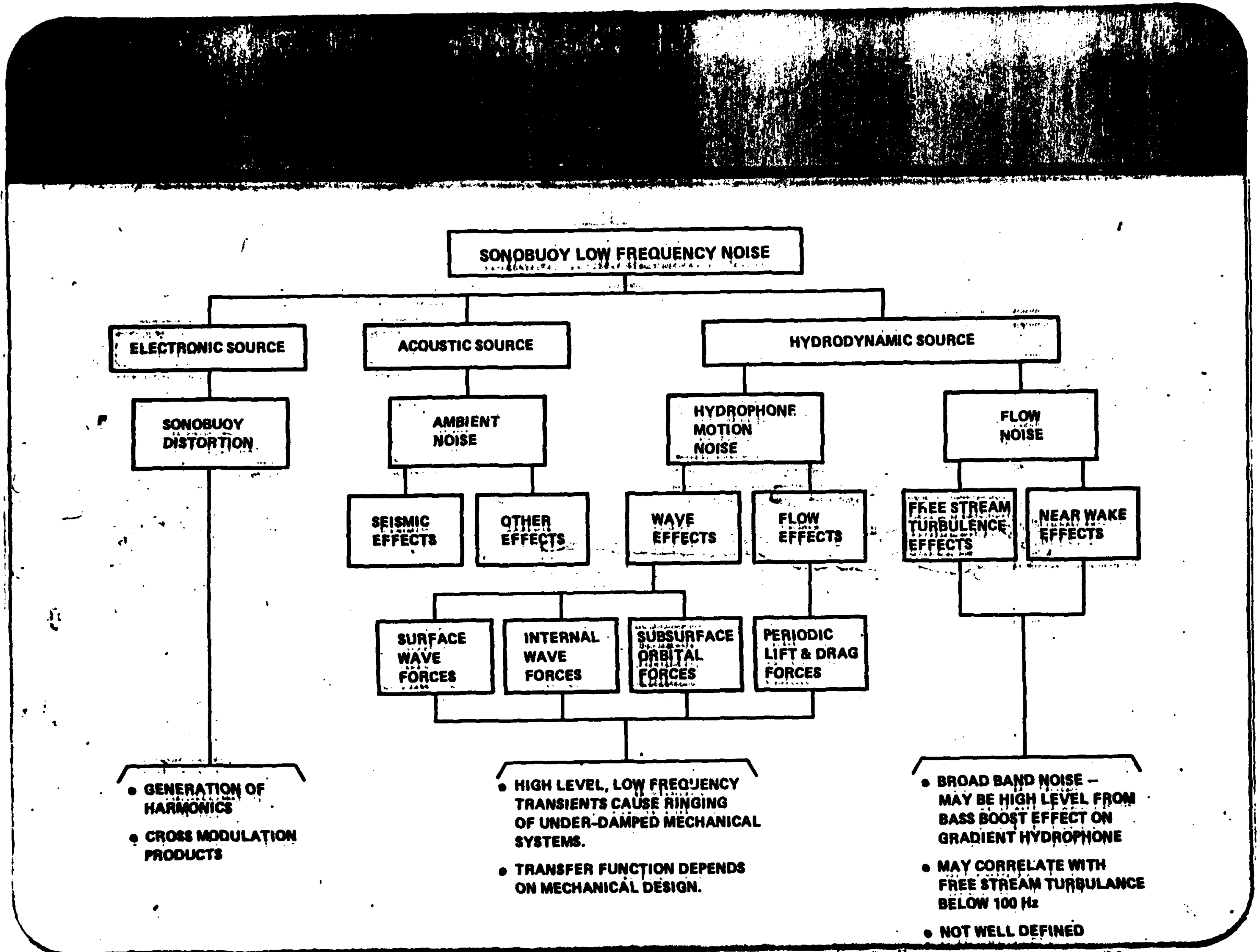
SONOBUOY LOW FREQUENCY NOISE
ELECTRONIC SOURCE
ACOUSTIC SOURCE
HYDRODYNAMIC SOURCE
SONOBUOY DISTORTION
AMBIENT NOISE
HYDROPHONE MOTION NOISE
FLOW NOISE
SEISMIC EFFECTS
OTHER EFFECTS
WAVE EFFECTS
FLOW EFFECTS
FREE STREAM TURBULENCE EFFECTS
NEAR WAKE EFFECTS
SURFACE WAVE FORCES
INTERNAL WAVE FORCES
SUBSURFACE ORBITAL FORCES
PERIODIC LIFT & DRAG FORCES
• GENERATION OF HARMONICS
• CROSS MODULATION PRODUCTS
• HIGH LEVEL, LOW FREQUENCY TRANSIENTS CAUSE RINGING OF UNDER-DAMPED MECHANICAL SYSTEMS.
• TRANSFER FUNCTION DEPENDS ON MECHANICAL DESIGN.
• BROAD BAND NOISE – MAY BE HIGH LEVEL FROM BASS BOOST EFFECT ON GRADIENT HYDROPHONE
• MAY CORRELATE WITH FREE STREAM TURBULANCE BELOW 100 Hz
• NOT WELL DEFINED

V.C. Anderson

Comments on Nearfield Surveillance

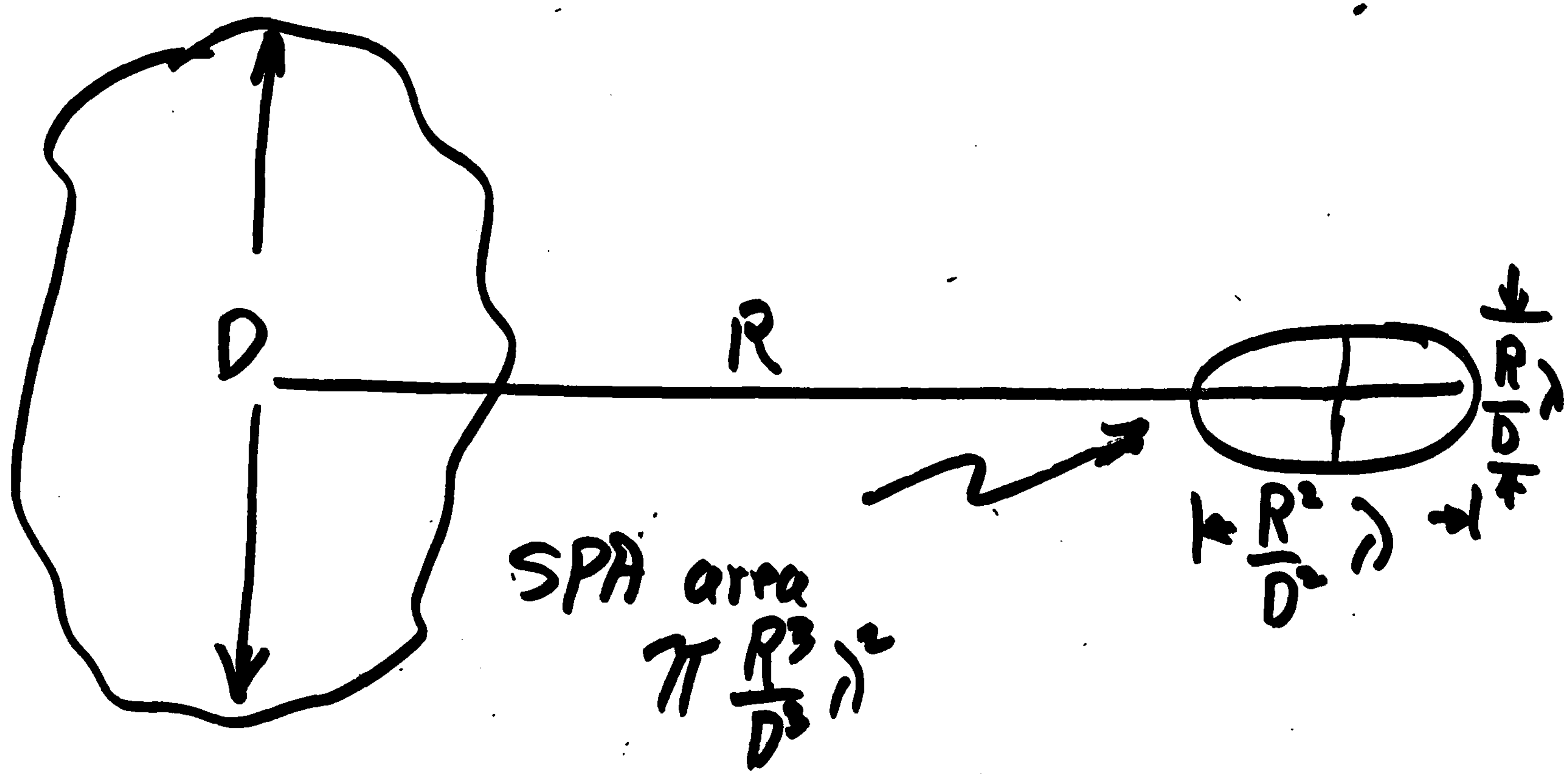
D
R
$\frac{R}{D}\lambda$
$\frac{R^2}{D^2}\lambda$
SPA area
$\pi \frac{R^3}{D^3}\lambda^2$

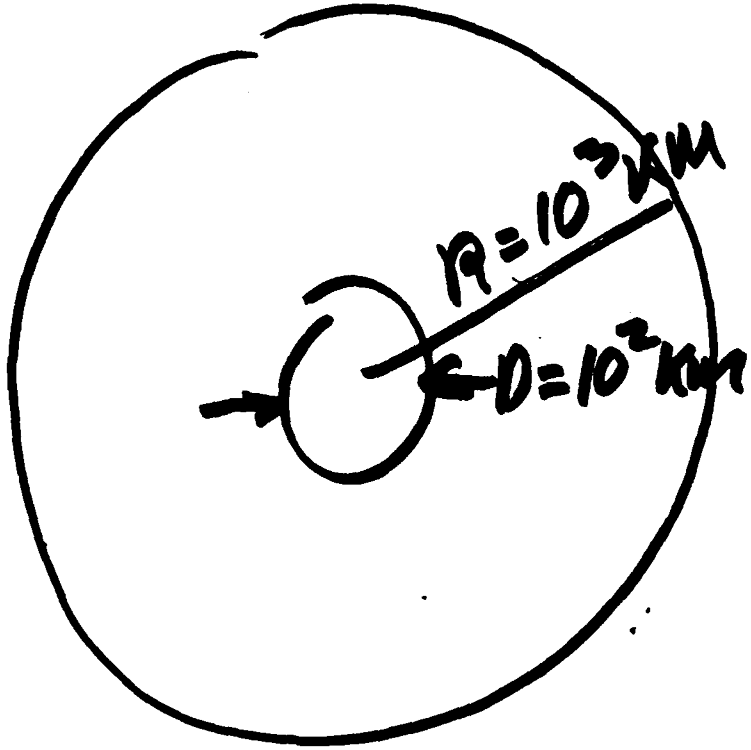

Set $R/D = 10$

$R = 10^3$ Km

$D = 10^2$ Km

Area Coverage

$\simeq 3 \times 10^6$ Km^2

$\simeq$ 1 NAVY ACRE

SPA area $\pi \times 10^3 \lambda^2$

# of resolution cells $N = 3\times10^6/(\pi\times10^3\times1.5^2)f^2$

$$N = \frac{10^3}{2} f^2$$

M = # of elements = 10^4 for 40 dB DI

Sampling rate = $2f$

Data Rate = $N \times M \times 2f$

$= 10^7 f^3$

For 10 Hz = 10^{10} add./sec

ADA Beamformer

$720 \times 1500 \times 10^4 = 10^{10}$ add/sec

(El.) (Beams) (Samplerate)

AT 10 Hz $D = 600\lambda$

(ARTEMIS RECEIVER = 400λ)

AT 10 Hz SPA = 150m × 1500m

ADVANTAGES

- 40 dB DI
- SPATIALLY RESOLVE ALL SHIPPING
- LOCALIZE TARGETS TO WITHIN WEAPON RANGE
- SELF COHERE ARRAY ON HIGH S/N SHIPPING BROADBAND SOURCES
- ROBUST AGAINST TOPOGRAPHIC SHADOWING

TRANSMISSION LOSS TO A SEISMOMETER IN OCEANIC BASEMENT

R. F. HENRICK, J. R. ROTTIER

THE JOHNS HOPKINS UNIVERSITY
APPLIED PHYSICS LABORATORY
LAUREL, MD

TRANSMISSION LOSS TO SEISMOMETER IN OCEANIC BASEMENT

- POSSIBLE ADVANTAGE OVER WATERBORNE HYDROPHONE
- DSDP SITE 581 DATA SET
- FFP MODEL

PNA (T) 24,470 * 1/18/85

SITE 581: SEISMIC PROFILE

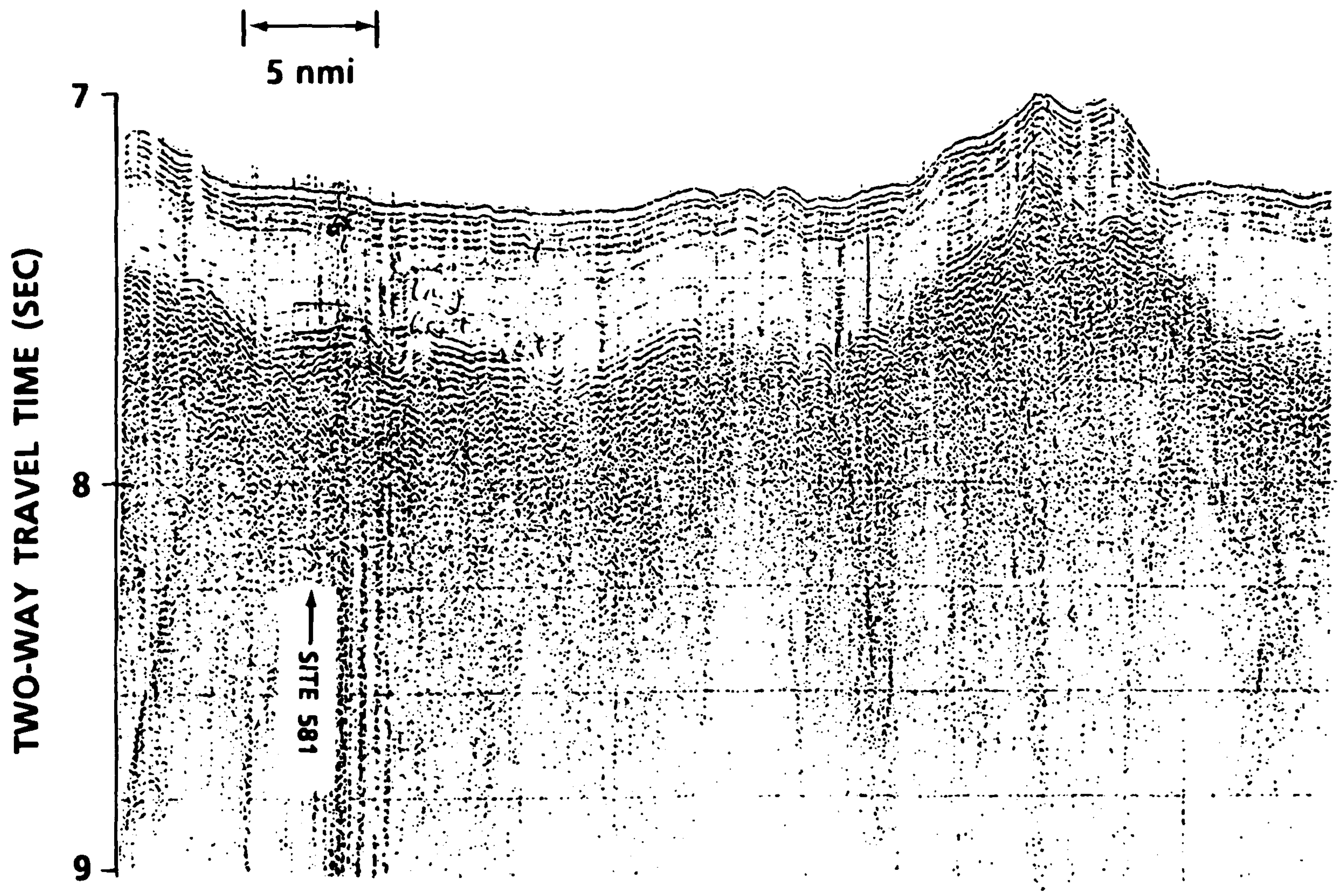

PNA (T) 24,472 * 1/18/85

SITE 581-MEASURED TRANSMISSION LOSS

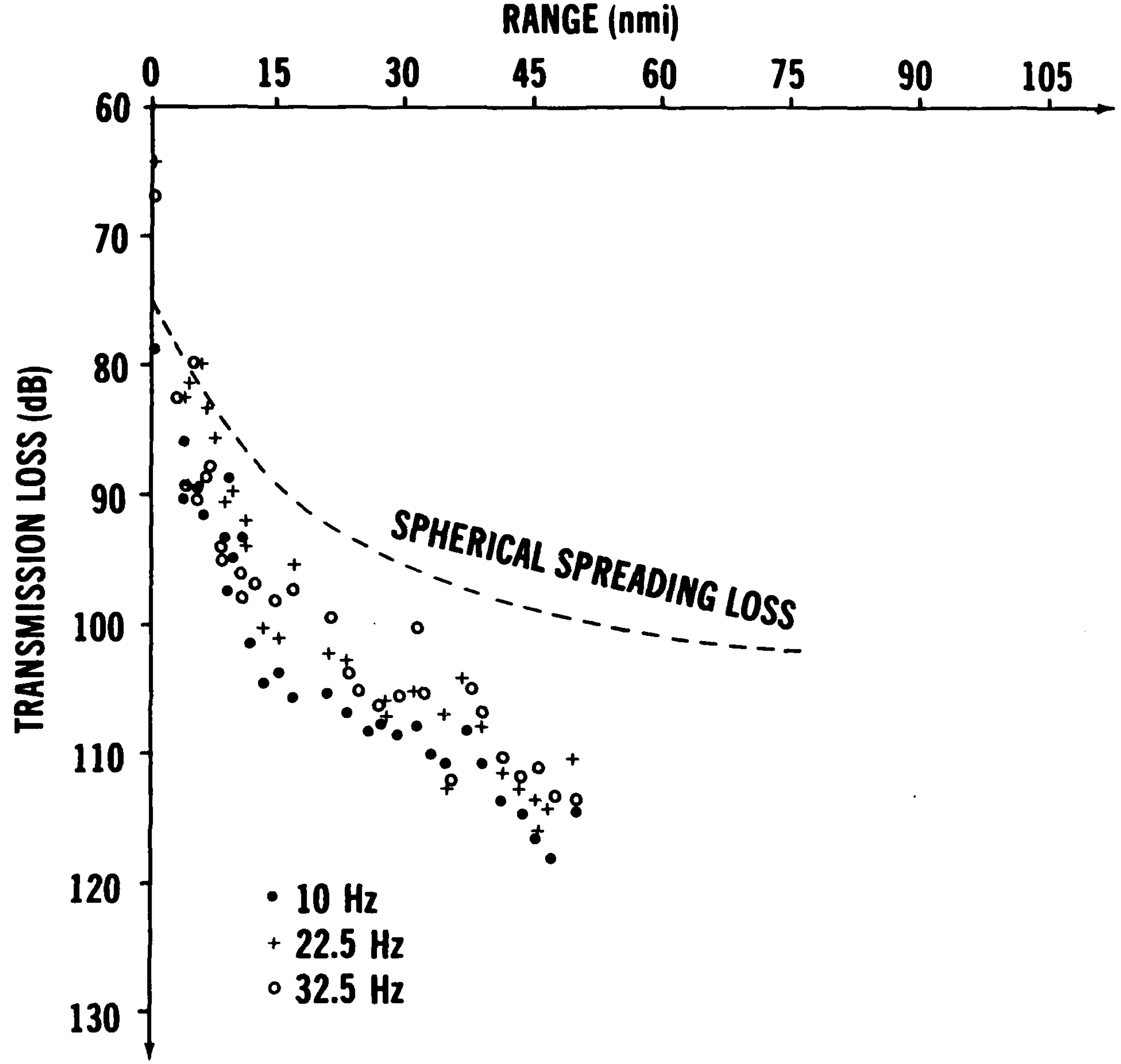

23,448 E208 1/17/85

FFP MODEL

- SOLVE $P = \int G(z, k)/\sqrt{k}\; T e^{-ikr} dk$

- MODELS COMPRESSIONAL AND SHEAR ENERGY

- OUTPUT UNITS OF DISPLACEMENT
  (dB re 1 MILLIMICRON FOR A 1 MICROBAR SOURCE)

SITE 581: GEOACOUSTIC STRUCTURE
FOR FREQUENCY = 22.5 Hz

DEPTH (m)	C_p(m/s)	C_s(m/s)	α_p(dB/m)	α_s(dB/m)	ρ(g/cm3)
0.0	1513.0		.0000001		1.03
15.3	1513.0		.0000001		1.03
18.3	1506.4		.0000001		1.03
30.5	1480.2		.0000001		1.03
45.7	1464.6		.0000001		1.03
50.0	1464.1		.0000001		1.03
60.0	1463.2		.0000001		1.03
106.7	1458.5		.0000001		1.03
152.4	1458.4		.0000001		1.03
304.9	1464.9		.0000001		1.03
457.3	1469.2		.0000001		1.03
686.0	1473.8		.0000001		1.03
1067.1	1479.3		.0000001		1.03
1524.4	1484.8		.0000001		1.03
2134.2	1493.6		.0000001		1.03
2743.9	1503.1		.0000001		1.03
3658.5	1518.0		.0000001		1.03
4573.2	1533.8		.0000001		1.03
5467.0	1550.3		.0000001		1.03
5467.0	1610.0	20.0	.0034	.09	1.35
5517.0	1626.8	100.0	.0034	.09	1.6
5824.0	1730.0	400.0	.0034	.09	1.6
5824.0	4250.0	2450.0	.0002	.0002	2.5
5844.0	4274.7	2464.5	.0002	.0002	2.5
7000.0	5700.0	3300.0	.0002	.0002	2.5
7000.0	6100.0	3500.0	.0002	.0002	2.5
8500.0	6650.0	3840.0	.0002	.0002	2.5
8500.0	6950.0	4000.0	.0002	.0002	2.8
11000.	7350.0	4240.0	.00002	.00002	2.8
11000.	7350.0	3800.0	.00002	.00002	2.9
13500.	7350.0	4700.0	.00002	.00002	2.9
13500.	8100.0	4700.0	.00002	.00002	2.9

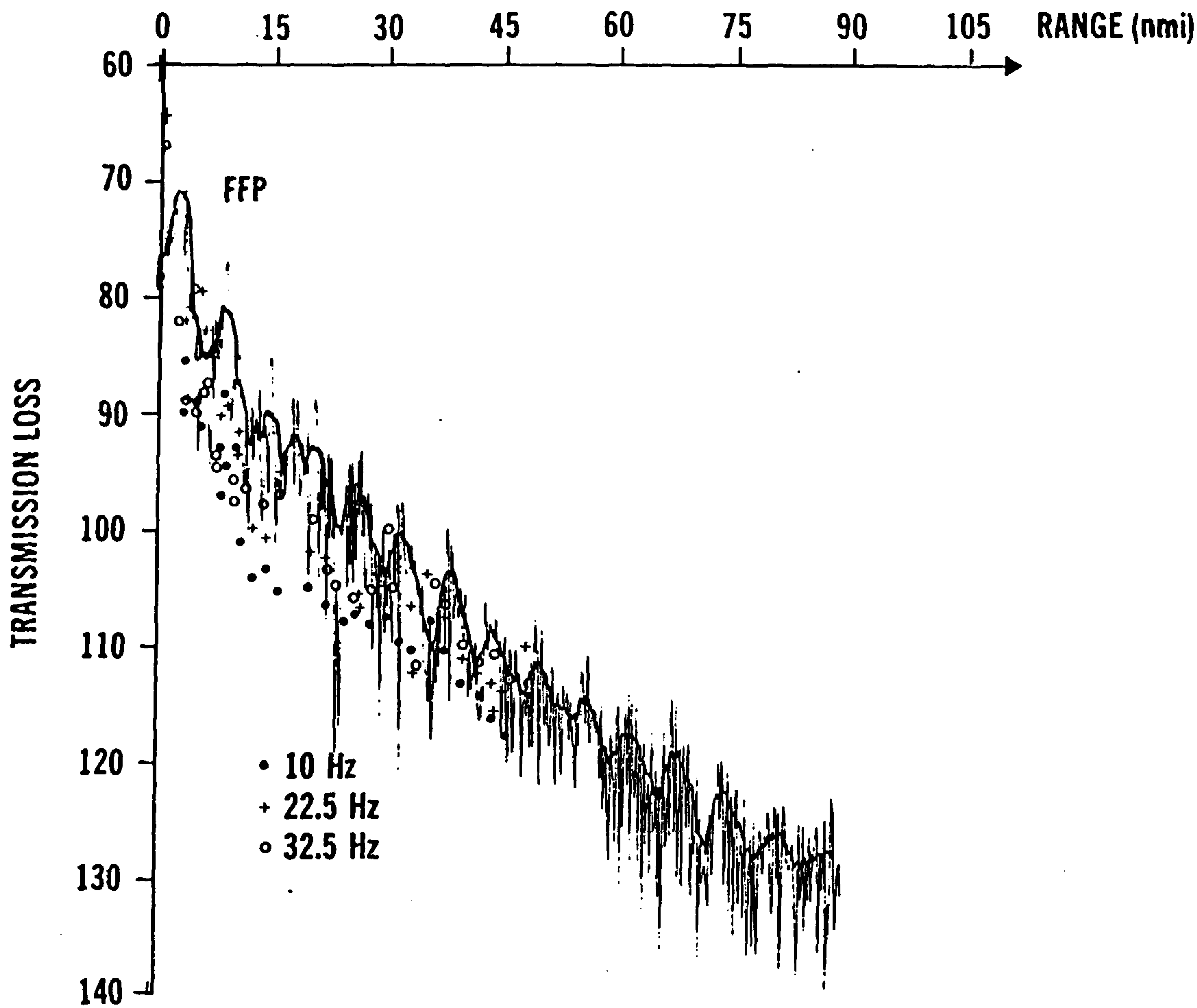

23,449A E2 10/18/84

ISSUES

- ACCURACY OF PROPAGATION MODEL
  - BOREHOLE VS. BOTTOM WATER
  - VS. SOUND CHANNEL
  - SHORT RANGE VS. LONG RANGE
- VALIDITY OF GEOACOUSTIC DESCRIPTION
  - SENSITIVITY TO VERTICAL DETAIL
  - HORIZONTAL ISOTROPY

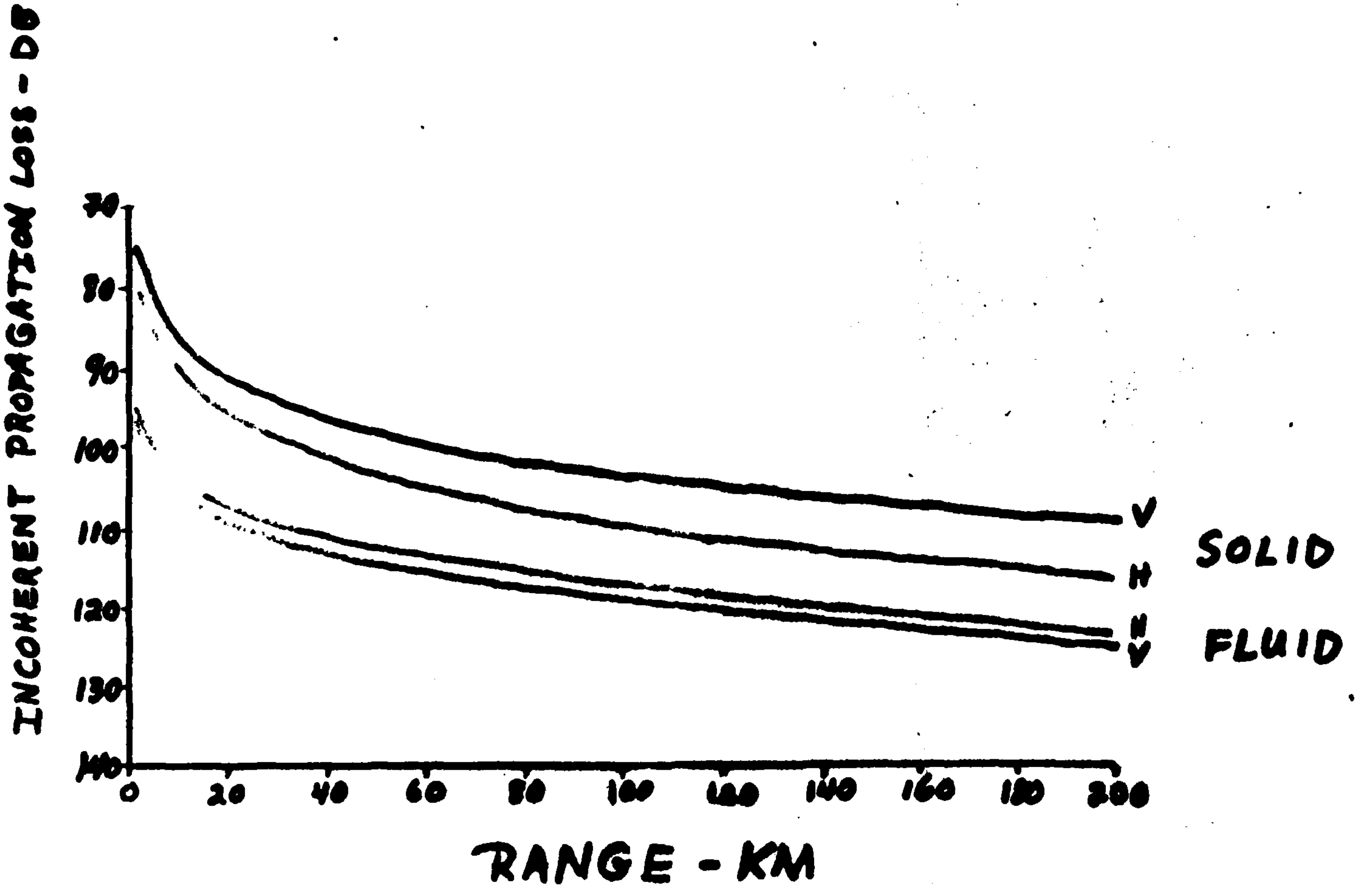

INCOHERENT PROPAGATION LOSS - DB
70
80
90
100
110
120
130
140
0
20
40
60
80
100
120
140
160
180
200
RANGE - KM
V
H
SOLID
H
V
FLUID

RESULTS:

COMPARISON OF MODELED PROPAGATION LOSS AT 15 Hz FOR FLUID VERSUS SOLID SEDIMENT DESCRIPTIONS

- AT WATER-SEDIMENT INTERFACE ONLY VERTICAL DISPLACEMENT STRONGLY AFFECTED

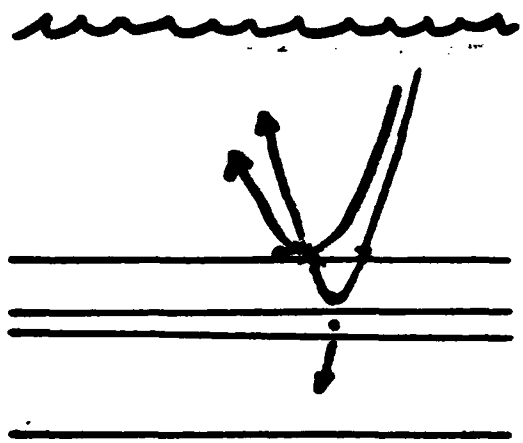

- IN BOREHOLE, SOLID SEDIMENT MODEL GIVES 10 dB OR MORE ENHANCEMENT, AND HORIZONTAL DISPLACEMENT MORE ATTENUATED THAN VERTICAL DISPLACEMENT

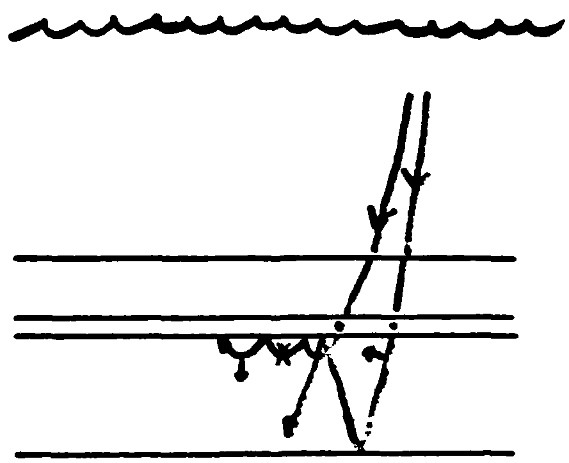

GEOACOUSTIC PROFILE

		DEPTH (M)	C_p (M/SEC)	α_P (dB/M/kHz)	ρ (G/CM^3)	C_s (M/SEC)	α_S (dB/M/kHz)
	WATER	0	1545	0	1.04	0	0
	SEDIMENT	0	1540	.010	1.25	100	4.0
		270	1775	.037	1.50	483	4.0
	CHERT	270	5400	.010	2.60	3150	.010
		340	5400	.010	2.60	3150	.010
RECEIVER AT 360 M	BASALT	340	4420	.010	2.50	2330	.010
		1640	5980	.010	2.50	3370	.010
	SUBSTRATE	1640	6500	.001	2.75	3750	.010

PROBLEM DESCRIPTION:
OCEAN BOREHOLE IMPLANTED SENSORS

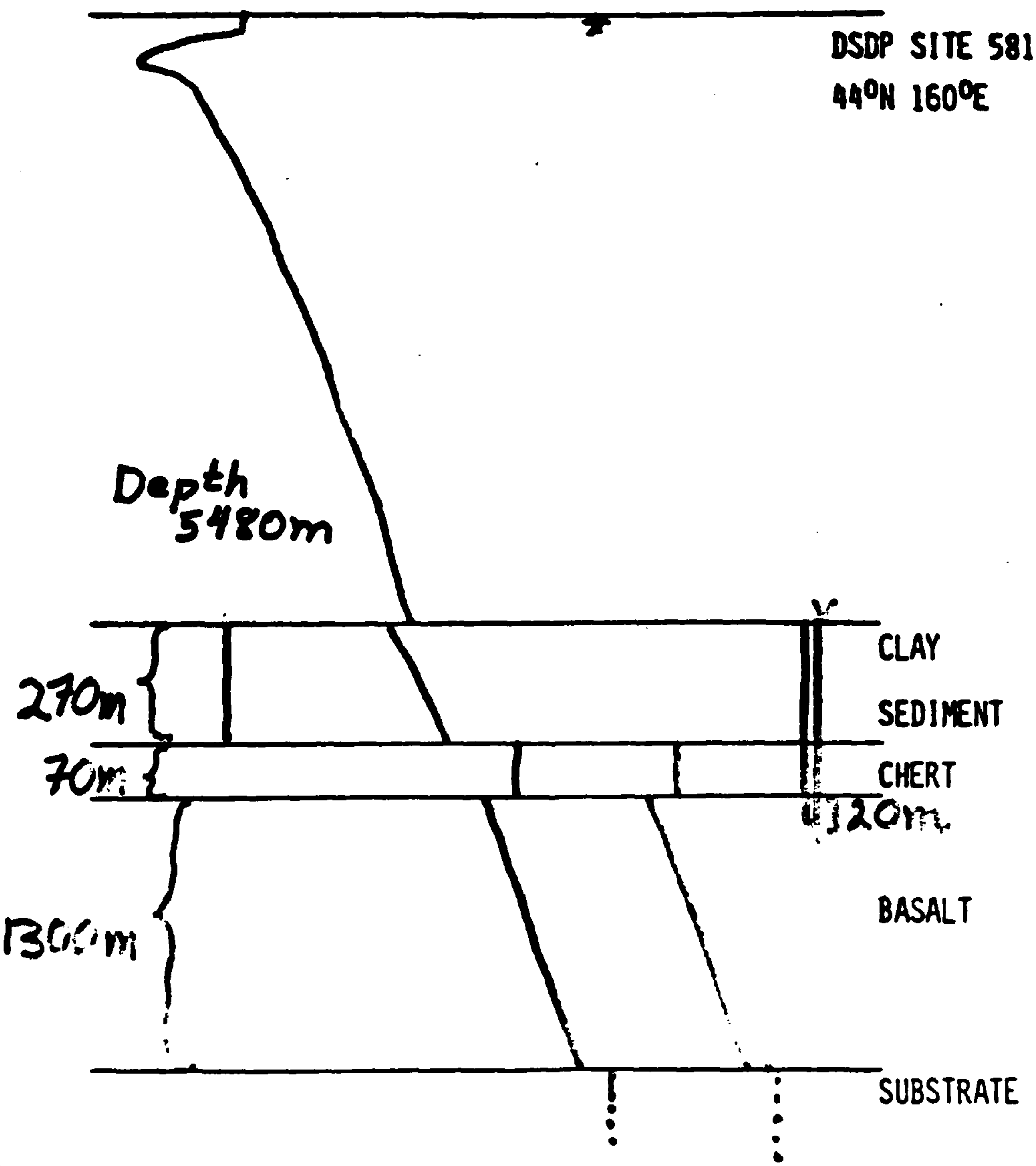

PROBLEM DESCRIPTION:
BOTTOM IMPEDANCE BOUNDARY CONDITION FORMULATION OF NORMAL MODE PROBLEM

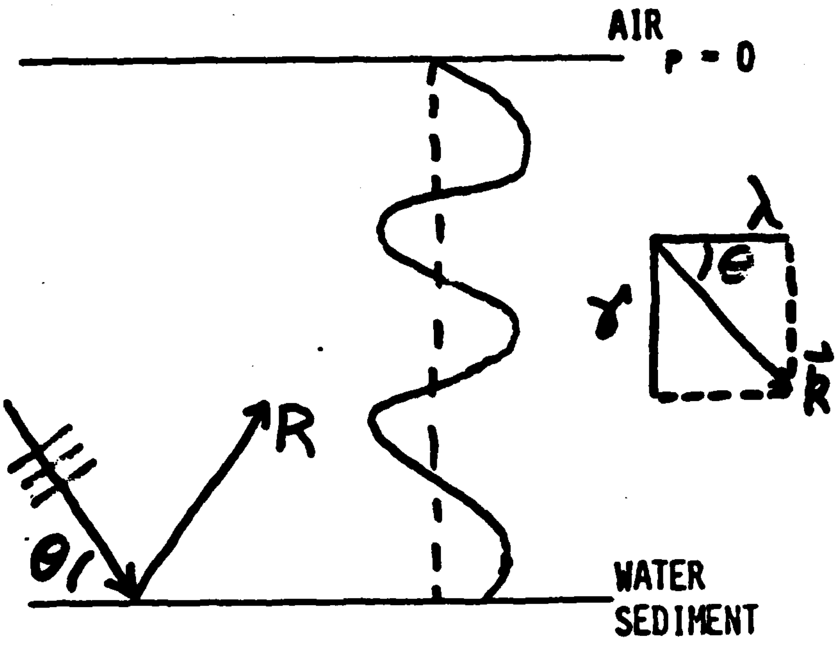

REFLECTION COEFFICIENT R(Θ,ω) DETERMINES BOTTOM BOUNDARY CONDITION FOR NORMAL MODE

OUTLINE

- BOTTOM IMPEDANCE BOUNDARY CONDITION

  NORMAL MODE MODEL
- BOREHOLE GEOACOUSTICS
- IMPORTANT PROPAGATION MECHANISMS
- ISSUES

VLF PROPAGATION

MODELING TO AN

OCEAN BOREHOLE RECEIVER

DR. ROBERT A. KOCH

APPLIED RESEARCH LABORATORIES

UNIVERSITY OF TEXAS AT AUSTIN

ONR, CODE 425 UA

NORDA, CODE 110A

VLF Propagation Modeling to an Ocean Borehole Receiver

Robert A. Koch

Applied Research Laboratories

The University of Texas at Austin

Austin, Texas 78713-8029

ABSTRACT

A normal mode analysis, in which the seafloor is represented by an impedance boundary condition derived from the complex reflection coefficient for a structured solid, is used to predict the dominant features of low frequency propagation from a water column source to near bottom and subbottom receivers. The propagation loss calculations suggest that propagation to a receiver in the basalt is predominately via shear waves. Based upon these and other results, suggestions for future efforts are offered.

SUMMARY

- CAN MODEL TL TO SEISMOMETER WITH FFP
- ATTENUATION FLAT FUNCTION OF FREQUENCY AT LOW FREQUENCY
- SEISMOMETER HAS ADVANTAGE OVER HYDROPHONE AT LOW FREQUENCY, SHORT RANGE

FFP MODEL: PARAMETER SENSITIVITY FOR SITE 581

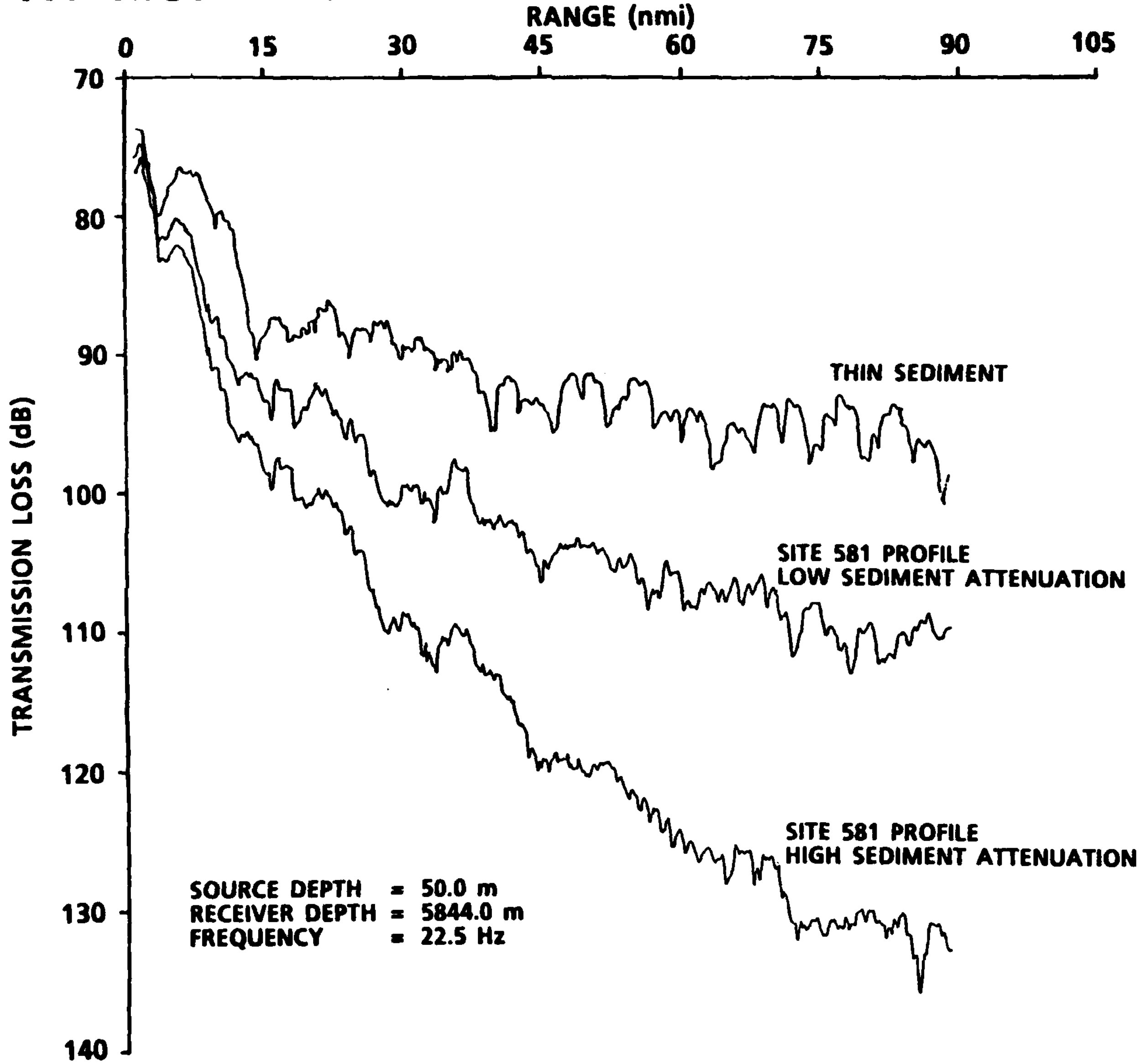

PNA (T) 24,471 * 1 '85

HYDROPHONE/SEISMOMETER PERFORMANCE COMPARISON

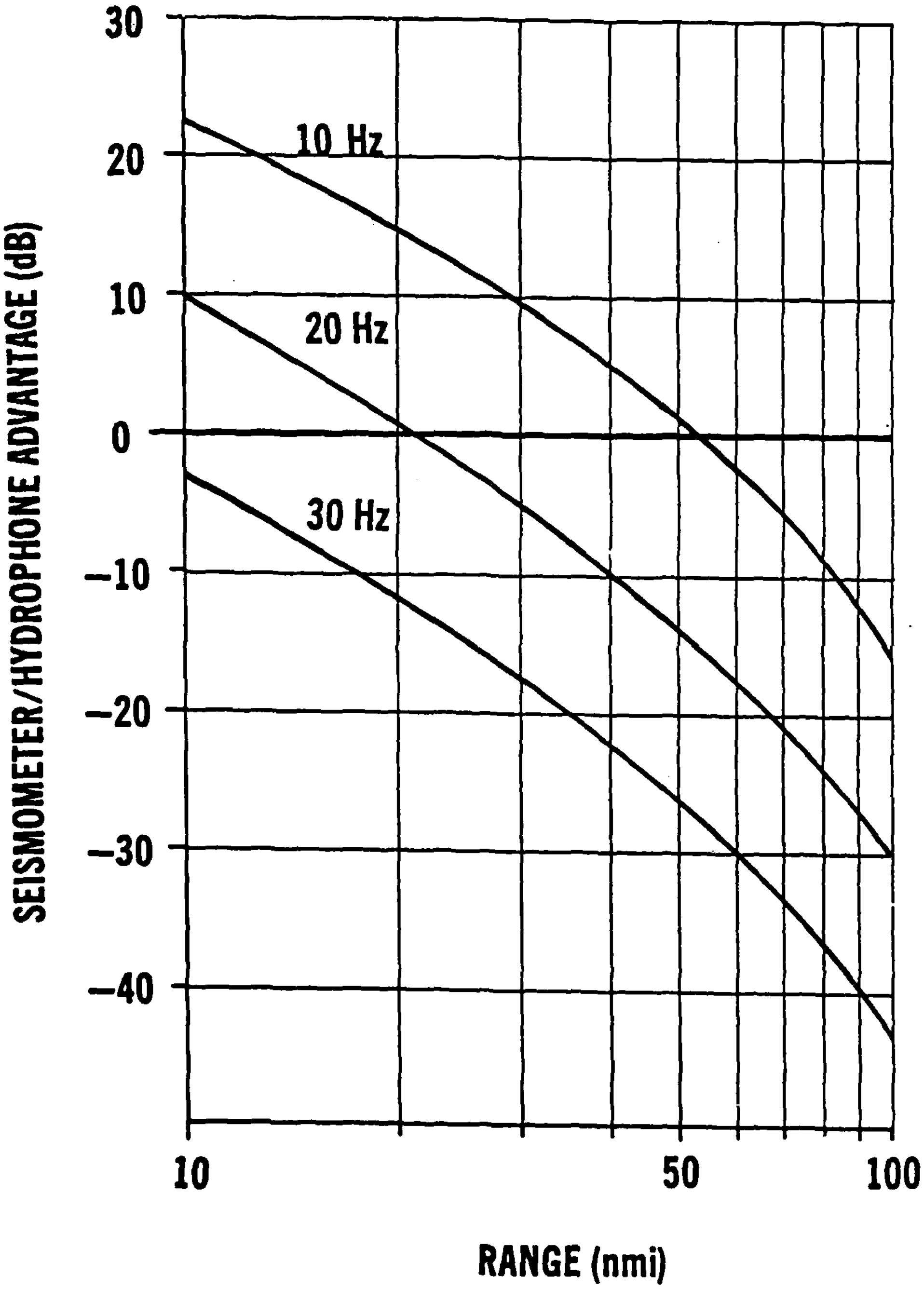

23,459 E208 10/18/84

SITE 581 TL COMPARISON

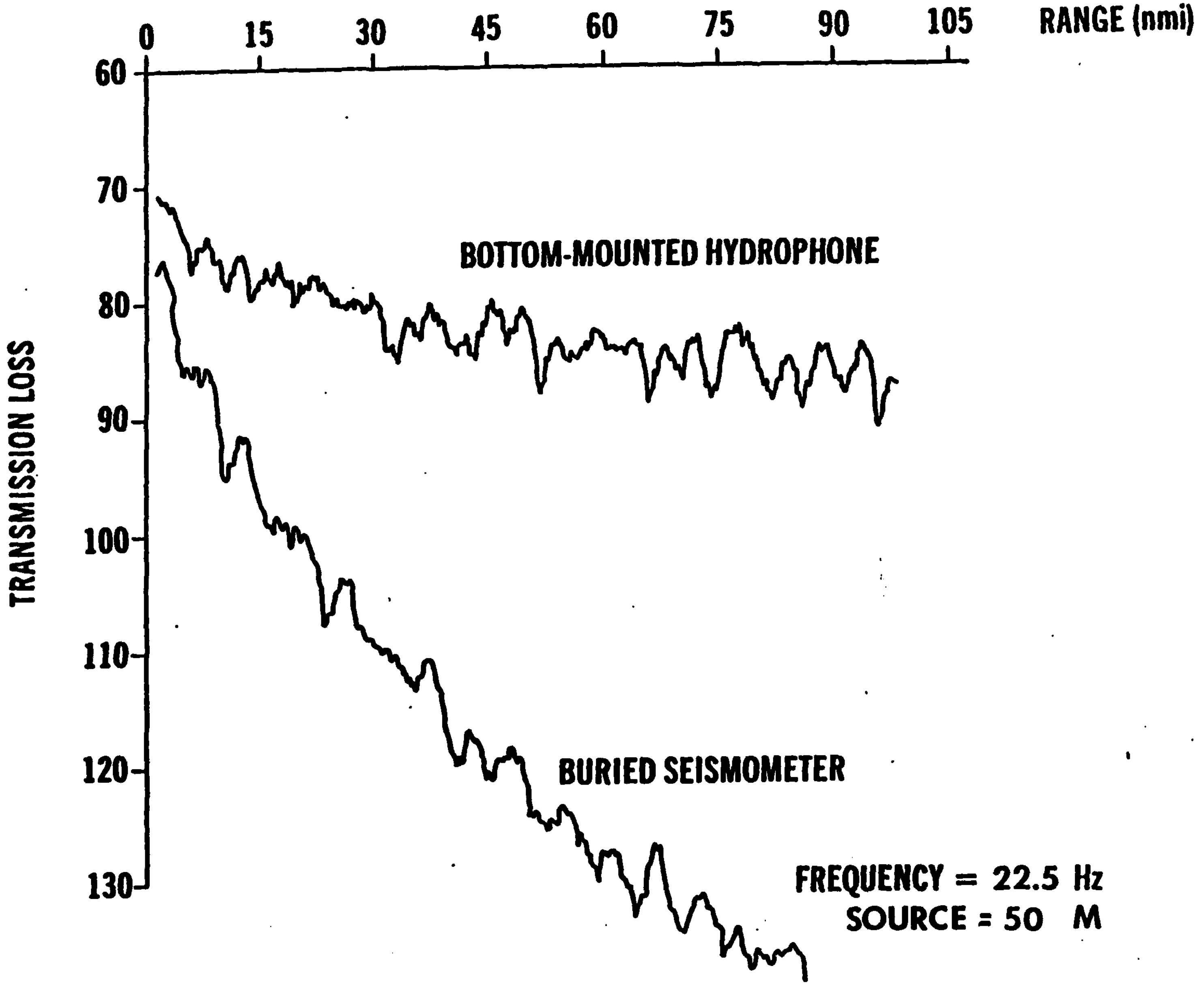

23,453 E2uo .0/22/84

SITE 581 TL COMPARISON

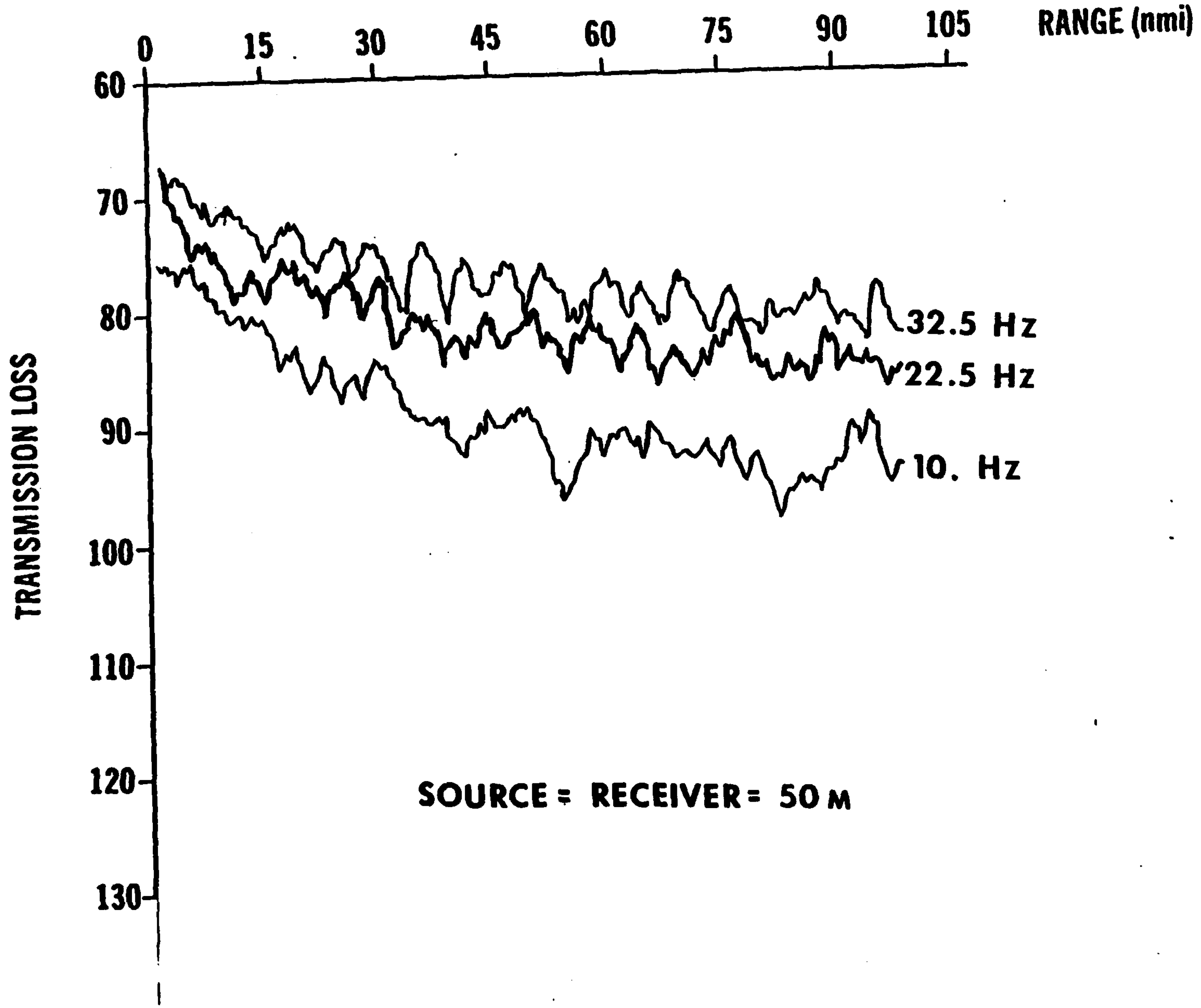

Wm. Carey

VLF Borehole Surveillance Program Requirements

TECHNICAL ISSUES TO BE RESOLVED

- S/N IN THE 3-50 Hz BAND (EMPHASIS BETWEEN 10 AND 20 Hz) FOR BOTTOM AND BURIED SENSORS
- THE FUNDAMENTAL NOISE MECHANISMS FOR SEISMIC NOISE IN THE (1-20 Hz) BAND
- DEPTH DEPENDENCE (IN THE BOTTOM) OF S/N
- HORIZONTAL AND VERTICAL COHERENCE IN THE BOTTOM
- SENSOR DEMONSTRATION AND DEVELOPMENT INCLUDING HYDROPHONE VERSUS GEOPHONE COMPARISONS
- CONFIRMATION OF ANALYTICAL MODELING TECHNIQUES DESCRIBING THE SOUND TRANSMISSION THROUGH THE WATER AND SEDIMENT COLUMN

MILESTONES

Preliminary Analysis and Program Plan	11/84 - 2/85
Sensor Development Plan	2/85
Detailed Experiment Plan	10/85
Sensor Development	4/86
Summer Measurements and Sensor Demonstration	6/86
Measurements Summary Report	8/86
Winter Measurements and Sensor Demonstration	1/87
Measurements Summary Report	3/87
Final Reports	9/87

OBJECTIVE

QUANTIFY THE POTENTIAL GAINS FROM EXPLOITING VLF ACOUSTIC PROPAGATION TO SENSORS BURIES IN SHALLOW WATER

REPRESENTATIVE EXPERIMENT GEOMETRY

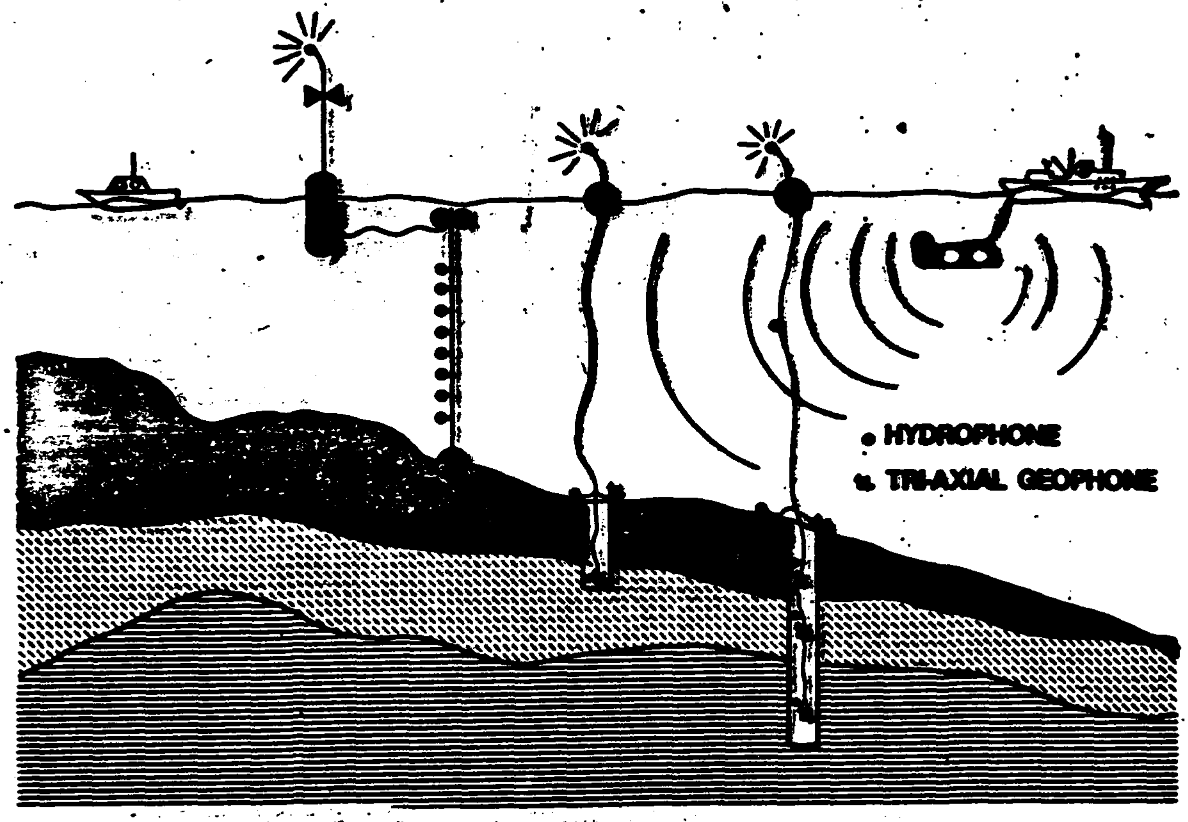

APPROACH

CONDUCT A TWO-SEASON ACOUSTIC/GEOACOUSTIC EXPERIMENTAL INVESTIGATION OF S/N IMPROVEMENT FOR BOREHOLE SENSORS IN SHALLOW WATER, SUPPORTED BY ACOUSTIC AND GEOACOUSTIC MODELING AND GEOPHYSICAL MEASUREMENTS.

FUNDING

	FY 85	FY 86	FY 87
SUBTOTAL	$350K	$1250K	$850K
TOTAL		$2.45M	

OBS Karen vs. MSS

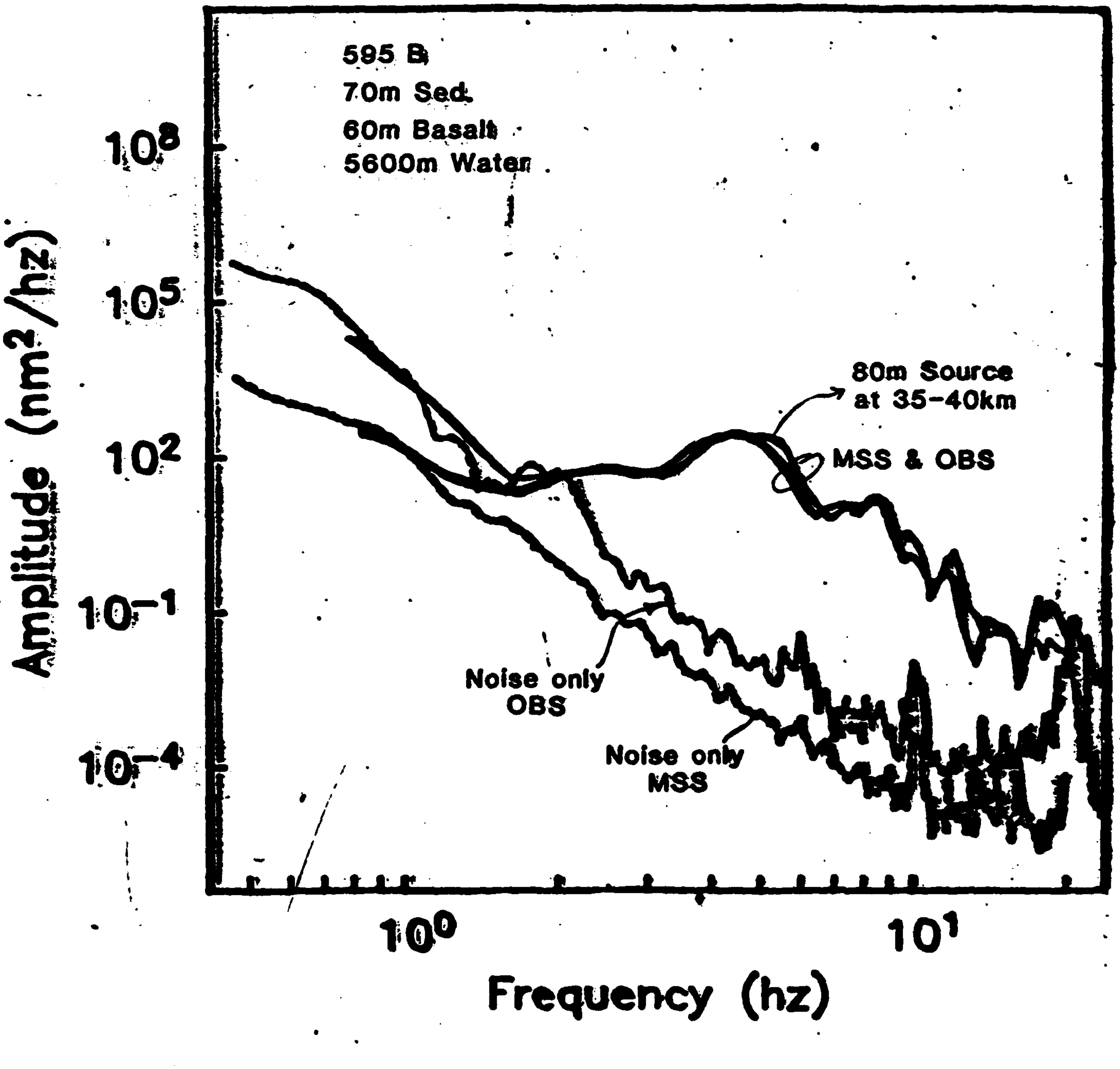

Ref-JOHN ORCUTT-SCRIPPS

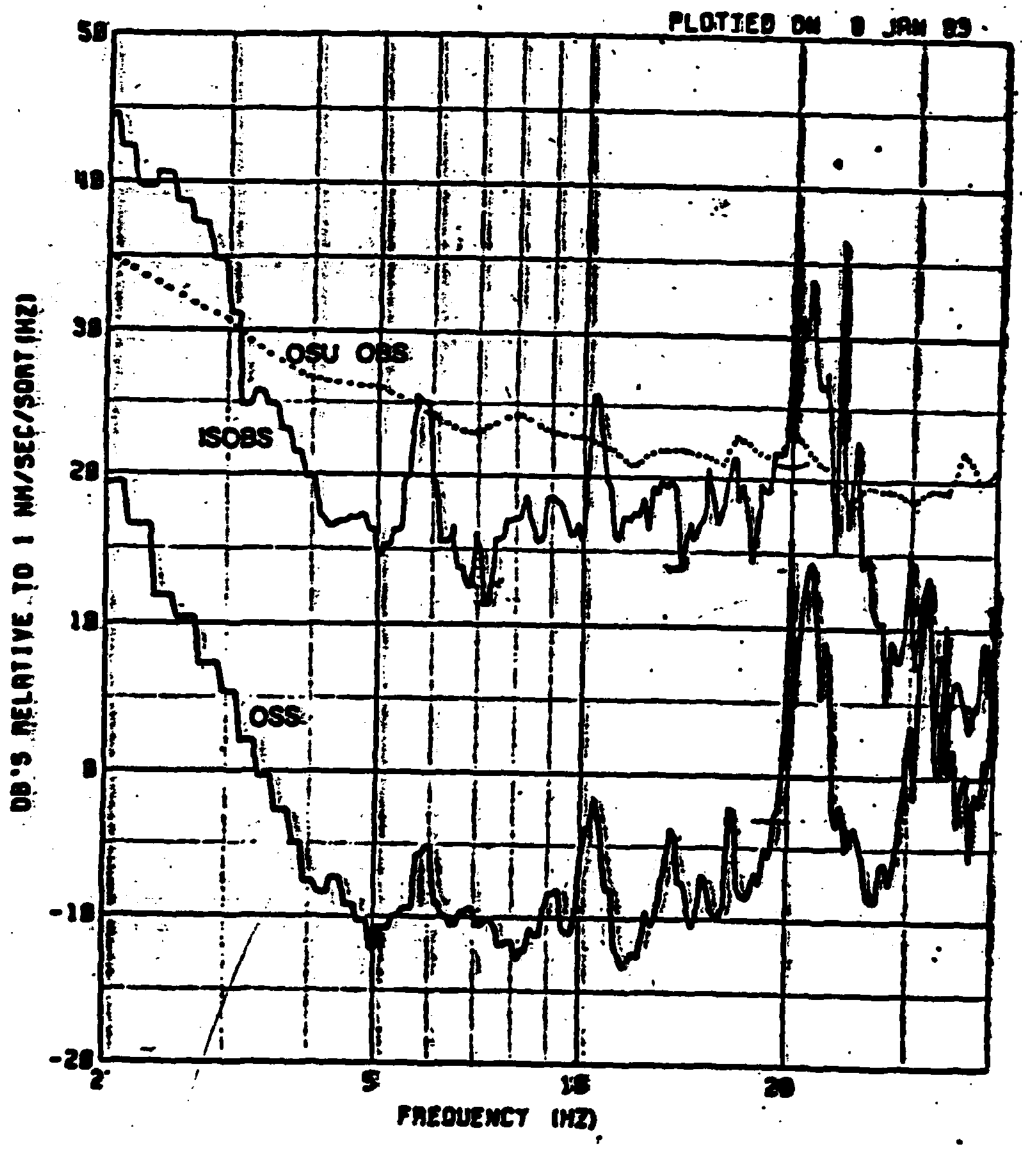

Figure 1. Noise level comparisons. This figure shows the comparison between the OSS vertical geophone and noise on two ocean bottom seismometer vertical geophones during the emplacement phase of OSSIV. Spectra were taken on Day 250, 1982 at 0035Z for a 30-second period.

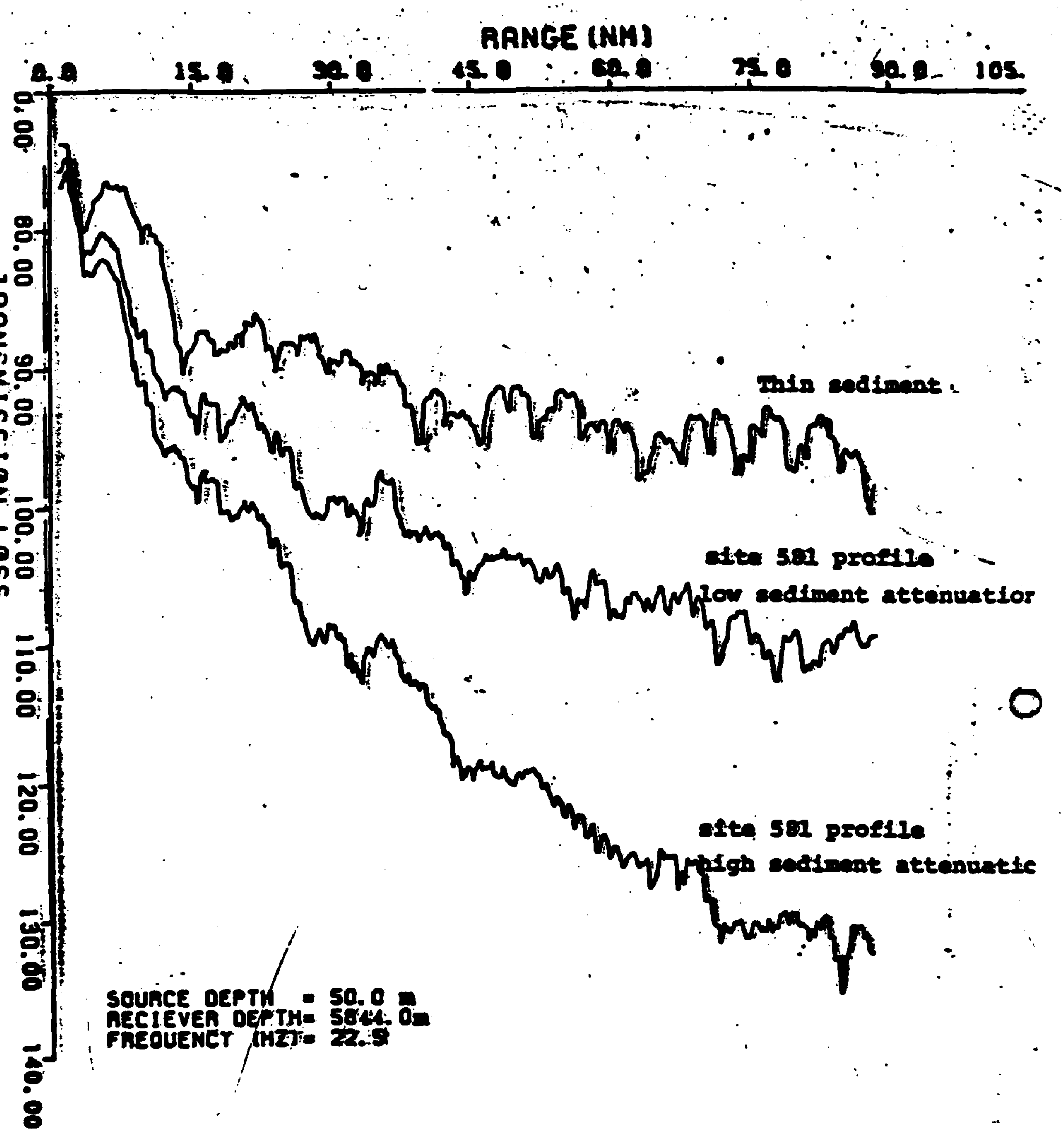

Figure . Transmission Loss vs. Range at 22.5 Hz

σ = seismometer vertical component data at DSDP drillhole site 581. The lines are FFP model output, averaged over 2 nm, for various sediment parameters.

UNCLASSIFIED

TRANSMISSION LOSS

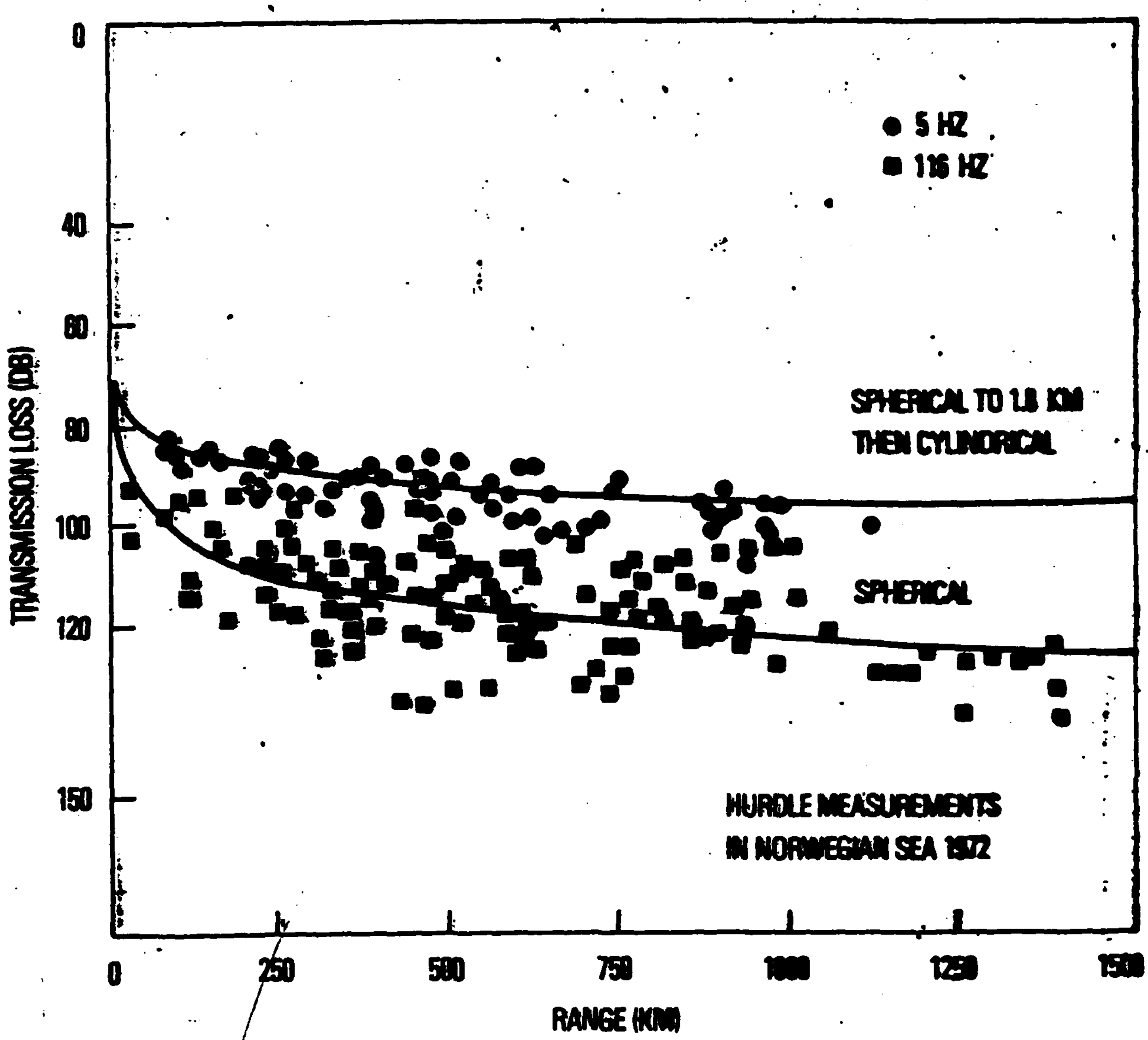

FIGURE 10

UNCLASSIFIED

Measurements of VLF ambient noise

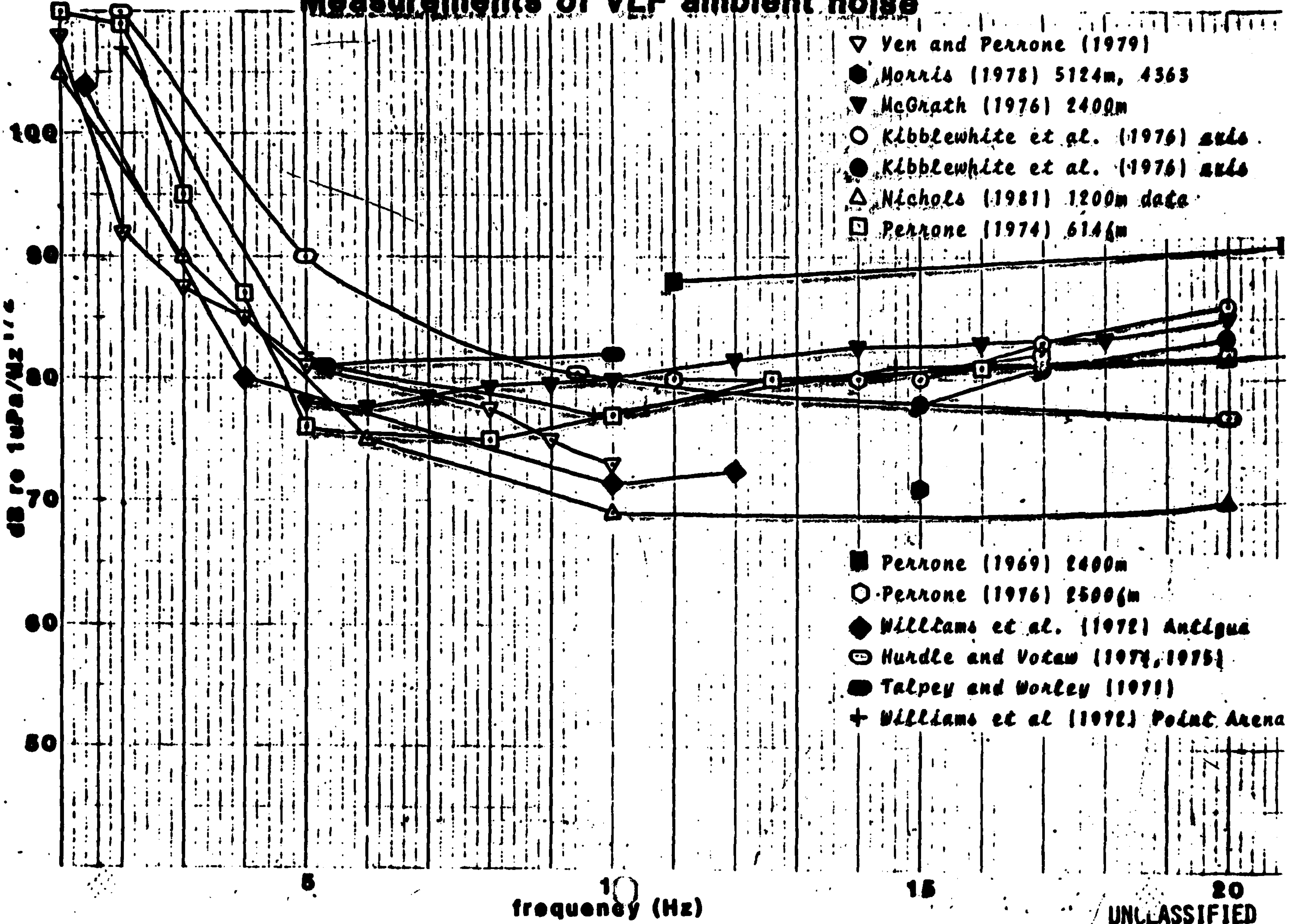

AMBIENT NOISE LEVELS

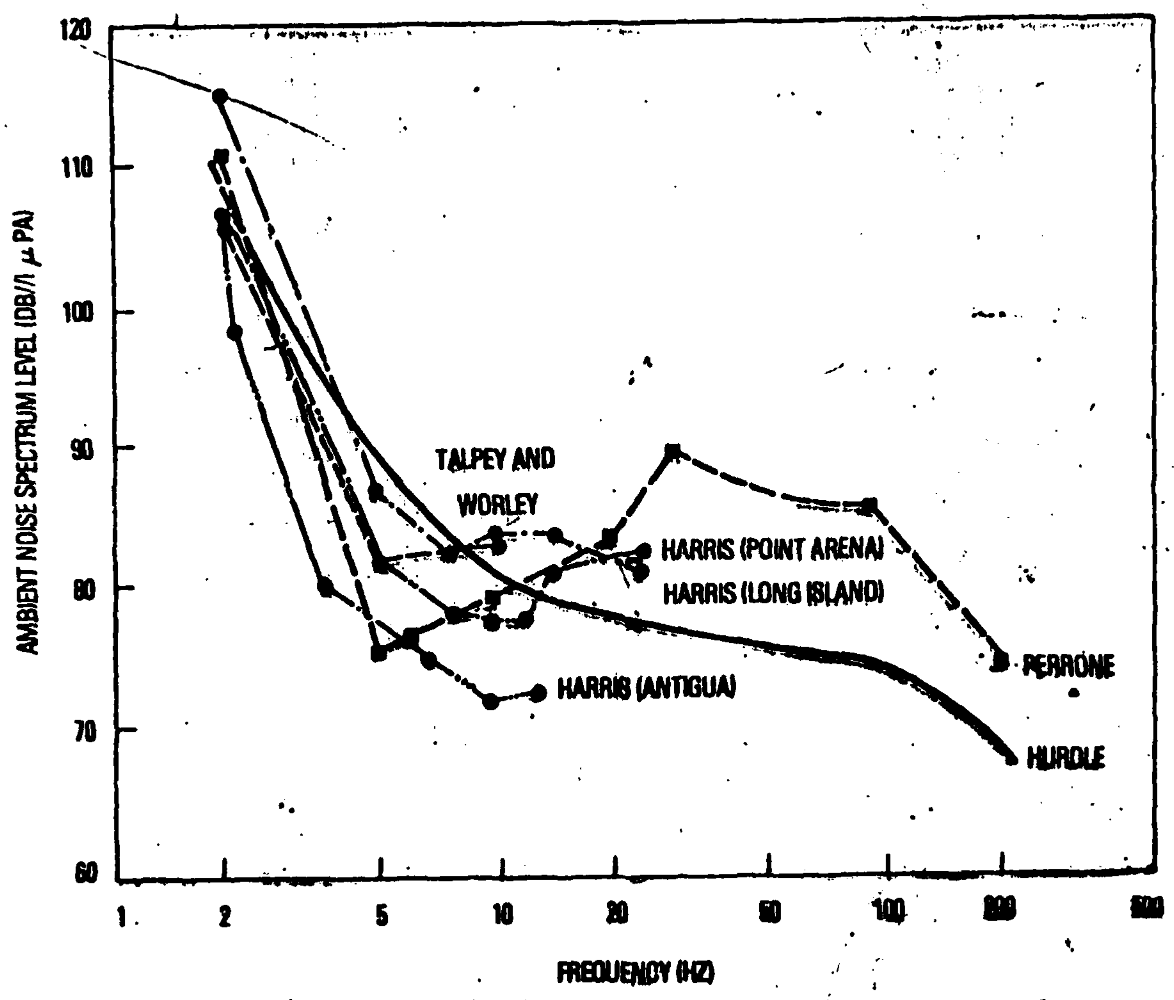

UNCLASSIFIED

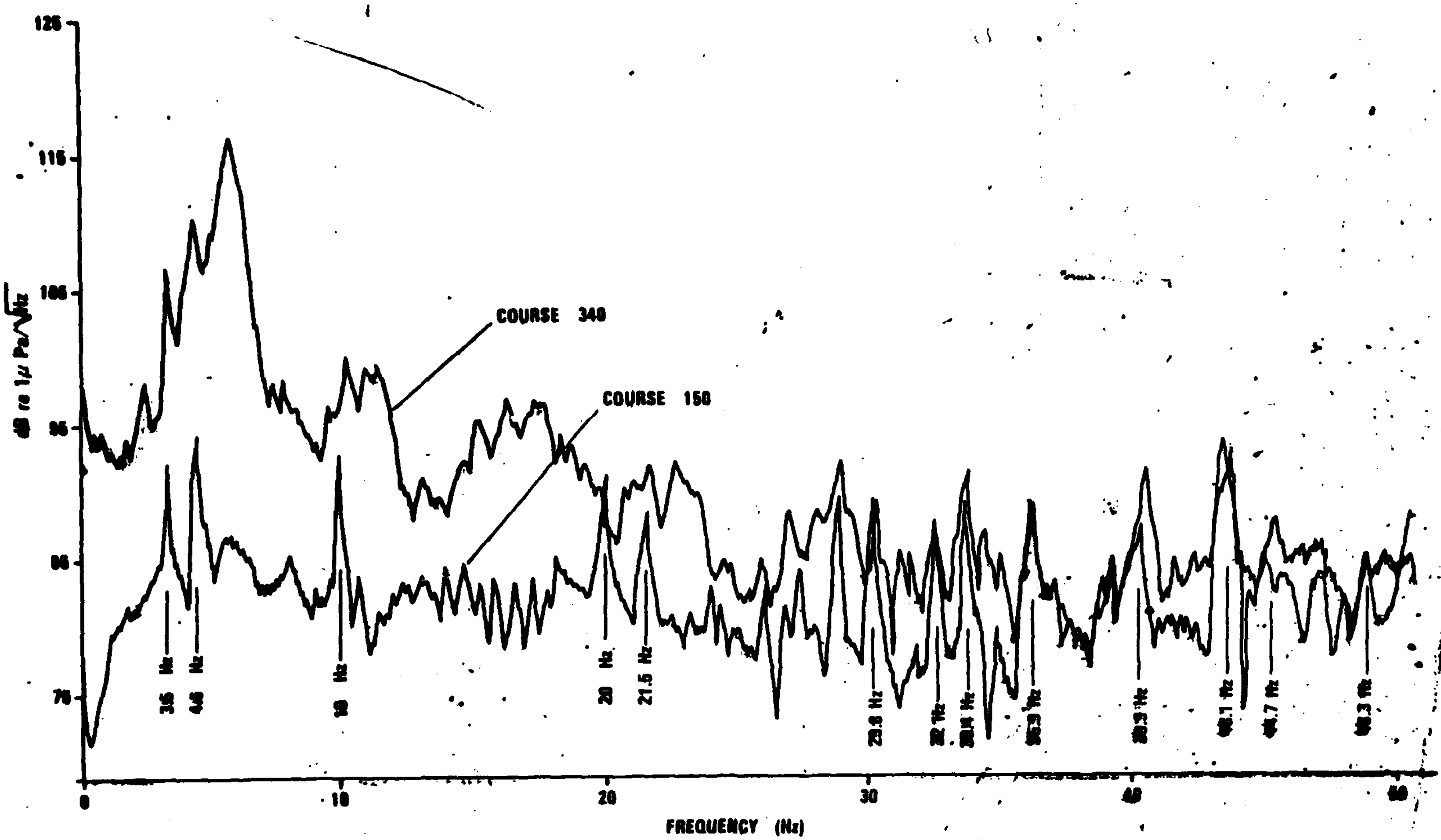

TEST CRUISE NO. 6 FORE H.F. HYDROPHONE GROUP SPECTRA

UNCLASSIFIED

UNCLASSIFIED

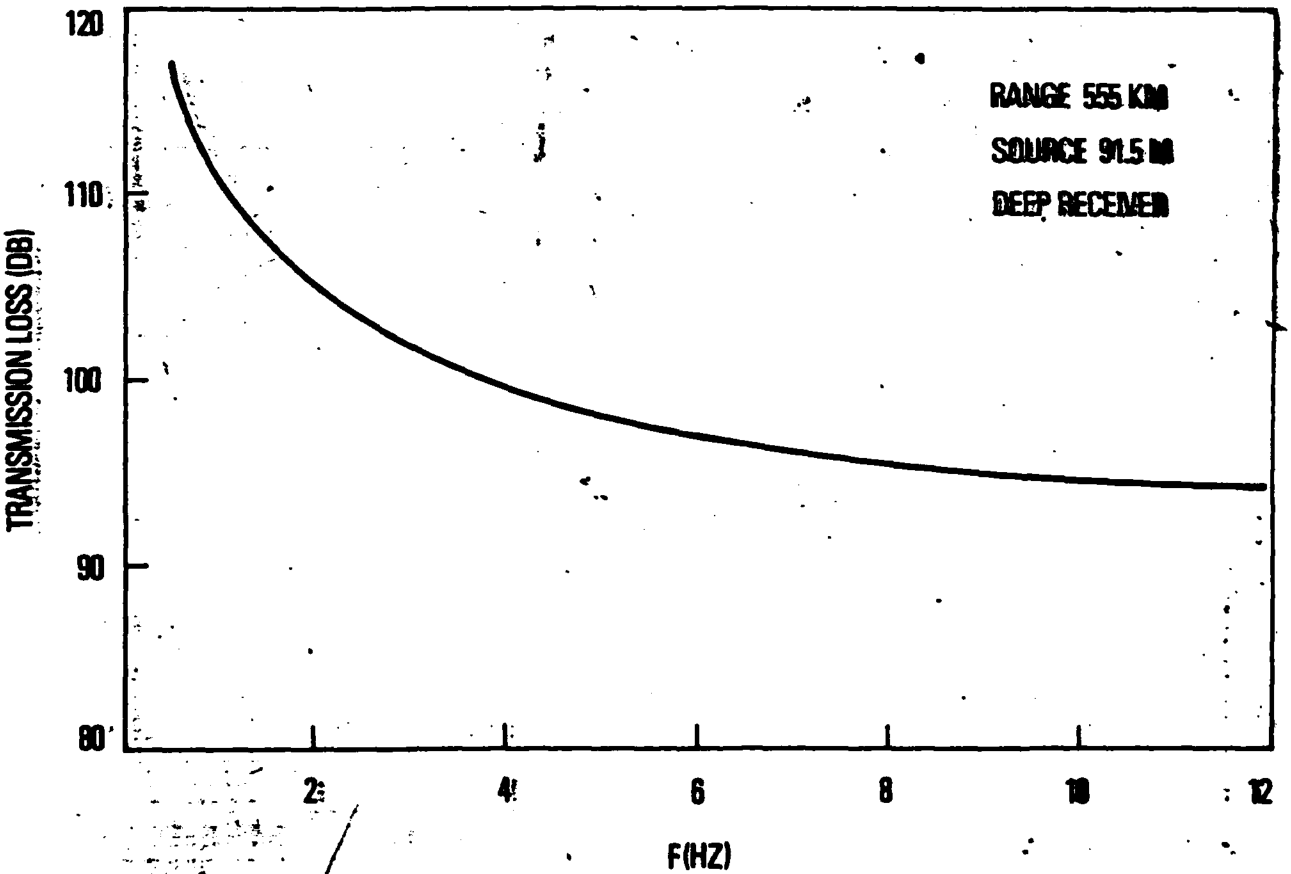

FIGURE 6

FREQUENCY DEPENDENCE OF
PREDICTED VERY LOW FREQUENCY TRANSMISSION LOSS
ACCORDING TO DOLE'S MODEL

UNCLASSIFIED

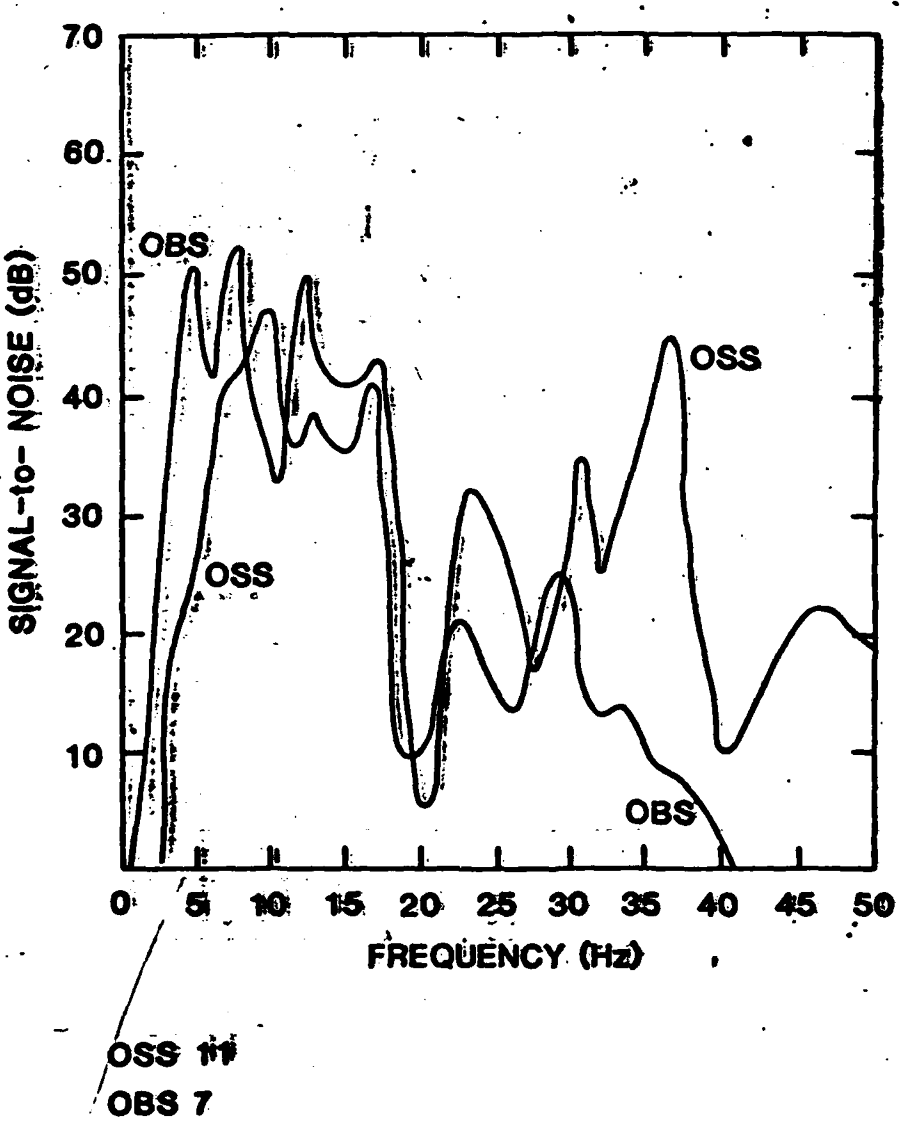

SIGNAL-to- NOISE (dB)
70
60
50
40
30
20
10
0
5
10
15
20
25
30
35
40
45
50
FREQUENCY (Hz)
OBS
OSS
OSS
OBS
OSS 11
OBS 7

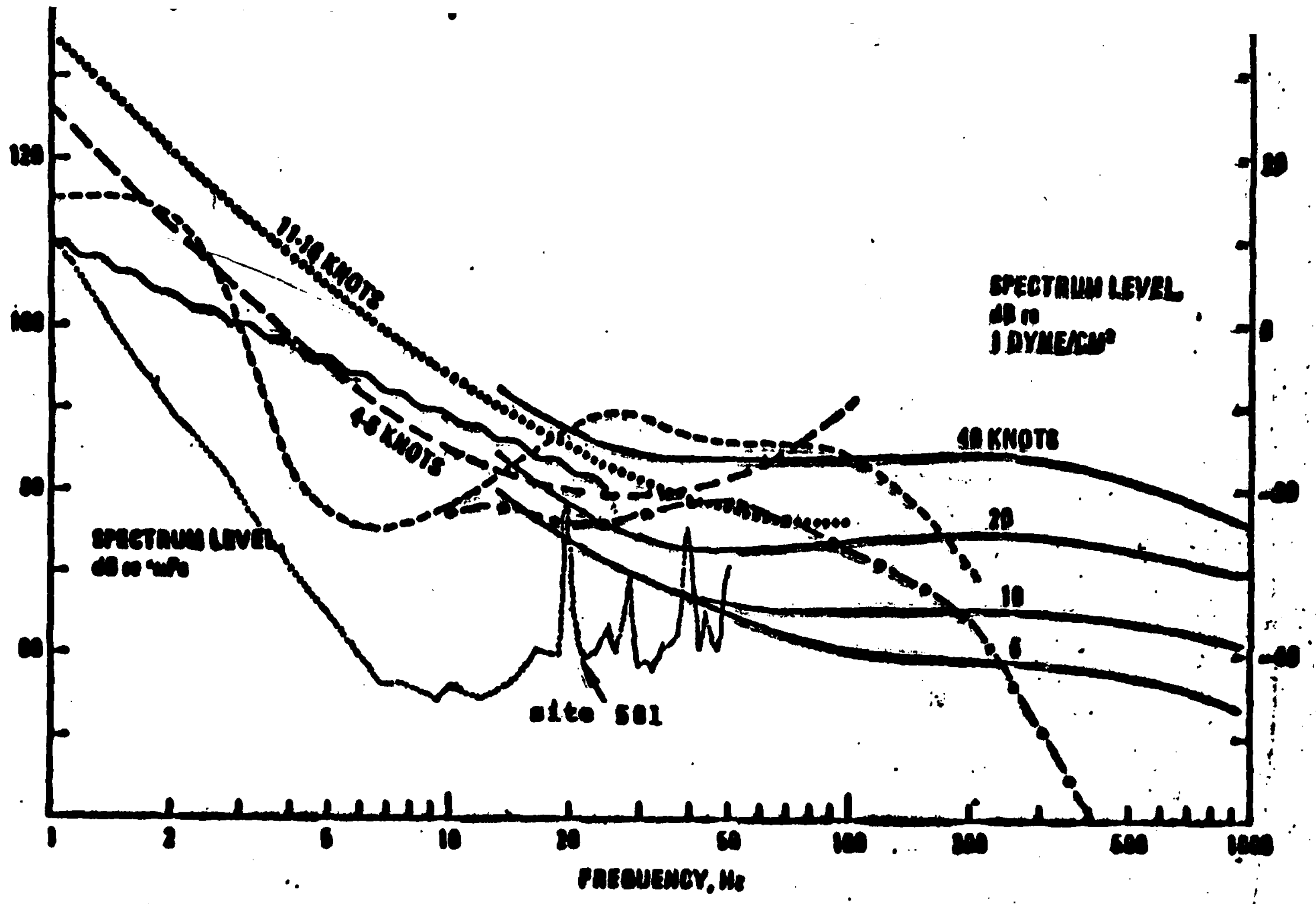

Figure . Ambient Water-noise Spectrum

Solid curves: Scotia shelf 3 mi. offshore, 28 fathams depths for several wind speeds, reference 4 . (••••): mean spectrum on The Grand Banks in 614 fm, reference 5 . (— —): depth = 25 fm, reference 3 . (~~) mean of 25 infrasonic measurements in deep and shallow water, reference 6 . (•—•—): shipping noise in deep water Pacific, reference 8 . Adapted from URICK, reference 1 .

END

FILMED

7-85

DTIC